THE DESIGN, SYNTHESIS, AND CHARACTERIZATION OF AMINOSILICA ADSORBENTS FOR CO_2 CAPTURE FROM DILUTE SOURCES

A Thesis
Presented to
The Academic Faculty

by

Jeffrey Hayden Drese

In Partial Fulfillment
of the Requirements for the Degree
Doctor of Philosophy in the
School of Chemical & Biomolecular Engineering

Georgia Institute of Technology
December, 2010

THE DESIGN, SYNTHESIS, AND CHARACTERIZATION OF AMINOSILICA ADSORBENTS FOR CO_2 CAPTURE FROM DILUTE SOURCES

Approved by:

Dr. Christopher W. Jones, Advisor
School of Chemical & Biomolecular Engineering
Georgia Institute of Technology

Dr. Ronald R. Chance
School of Chemical & Biomolecular Engineering
Georgia Institute of Technology

Dr. William J. Koros
School of Chemical & Biomolecular Engineering
Georgia Institute of Technology

Dr. David S. Sholl
School of Chemical & Biomolecular Engineering
Georgia Institute of Technology

Dr. Jake D. Soper
School of Chemistry
Georgia Institute of Technology

Date Approved: October 14, 2010

ACKNOWLEDGEMENTS

I could not have completed this thesis without the support of many people. I would like to thank my advisor, Professor Chris Jones, for helping me transition from an immature student to a professional researcher. His patience and determination are those of a truly passionate scientist and he has challenged me to go further than I thought possible. Similarly, my committee members, Professors Chance, Koros, Sholl, and Soper, are all sources of professional inspiration to me and their examples will continue to guide me throughout my career.

Special thanks need to be given to two of my co-authors, Dr. Sunho Choi and Ryan Lively. Our work together has enlightened me to the possibilities of collaboration and the power that minds united in friendship can hold. I would also like to thank Dr. Jason Hicks who started this work years ago and instructed me in the art of all things aminosilica with a skill to rival even Socrates. Another group member, Eric Ping, should be acknowledged for constantly poking, prodding, and even shoving me in the direction of excellence with the caring of a true friend.

I thank my parents, John and Linda, for fostering my love of music, math, and science and supporting me through all of life's ups and downs. I would also like to thank my sister, Jenna, for showing me the definitions of courage and kindness.

Most importantly, I thank my fiancée, Roxanne, for everything. Words cannot describe the limits of my gratitude for our relationship, for if they could, the infinite understanding sought by all scientists would have finally been attained.

TABLE OF CONTENTS

LIST OF TABLES

LIST OF FIGURES

Page

LIST OF SYMBOLS AND ABBREVIATIONS

δ	δ Means chemical shift
ΔH_{ads}	heat of adsorption
AEAPTMS	N-(3-(trimethoxysilyl)propyl)ethane-1,2-diamine
ASEC	aqueous size exclusion chromatography
BdB-FHH	Frenkel-Halsey-Hill modified Broekhof-de Boer
BET	Brunauer-Emmet-Teller
BJH	Barret-Joyner-Halenda
Cbz	carbobenzyloxy-protecting group
CCS	carbon capture and sequestration
CTA	covalently-tethered amine
CTAB	cetyltrimethylammonium bromide
DBN	1,5-diazabicyclo[4.3.0]non-5-ene
DBU	1,8-diazabicyclo[5.4.0]undec-7-ene
DCM	dichloromethane
DETA	diethylenetriamine
DI	deionized
di silane	3-(2-aminoethyl)aminopropyltrimethoxysilane
DMA	dimethylacrylamide
DMAPS	3-(dimethyl)aminopropyltrimethoxysilane
DMSO	dimethylsulfoxide
DSC	differential scanning calorimetry
DVB	divinylbenzene
EDA	ethylenediamine

FT	Fourier transform
GC	gas chromatography
HAS	hyperbranched aminosilica
HAS-VLAS	hyperbranched aminosilica varied loading adsorbent set
HMDS	1,1,1,3,3,3-hexamethyldisilazane
HMS	type of ordered amorphous mesoporous silica
IPCC	Intergovernmental Panel on Climate Change
IR	infrared
KIT-6	type of ordered amorphous mesoporous silica
LAS	linear aminosilicas
LPEI	linear poly(ethyleneimine)
MAPS	3-(methyl)aminopropyltrimethoxysilane
MCF	mesocellular foam
MCM-41	type of ordered amorphous mesoporous silica
MCM-48	type of ordered amorphous mesoporous silica
MEA	monoethanolamine
MOF	metal-organic framework
mono silane	3-aminopropyltrimethoxysilane
MS	mass spectroscopy
Mw	molecular weight
NETL	National Energy Technology Laboratory
NMR	nuclear magnetic resonance
N-Z-ethanolamine	benzyl *N*-(2-hydroxyethyl)carbamate
OSA	organically-supported amine
PAN	poly(acrylonitrile)

PAPS	3-(phenyl)aminopropyltrimethoxysilane
PC	pulverized coal-fired power plants
PEG	poly(ethyleneglycol)
PEHA	pentaethylenehexamine
PEHAS	pore-expanded hyperbranched aminosilica
PEI	poly(ethyleneimine)
PESCOM	commercial pore-expanded silica
pK_B	measure of basicity
Pluronic 123	$EO_{20}PO_{70}EO_{20}$ triblock copolymer
PMMA	poly(methylmethacrylate)
ppm	parts per million
PTFE	poly(tetrafluoroethylene)
PVT	pressure-volume-temperature
q	CO_2 capacity
RPV	remaining pore volume
SBA-12	type of ordered amorphous mesoporous silica
SBA-15	type of ordered amorphous mesoporous silica
SBA-16	type of ordered amorphous mesoporous silica
SEM	scanning electron microscopy
SOFC	solid oxide fuel cell
SWNT	single-walled carbon nanotube
TEM	transmission electron microscopy
TEOS	tetraethylorthosilicate
TEPA	tetraethylenepentamine
TFA	trifluoroacetic acid

T_g	glass transition temperature
TGA	thermogravimetric analysis
THF	tetrahydrofuran
TMB	trimethylbenzene
TPD	temperature programmed desorption
tri silane	3-[2-(2-aminoethyl)aminoethyl]aminopropyltrimethoxysilane
VA	volumetric analysis
VBC	vinylbenzylchloride
XPS	X-ray photoelectron spectroscopy
XRD	X-ray diffraction

SUMMARY

The major goals of this thesis were to: (1) investigate the limits of the adsorptive performance of the HAS adsorbent through the preparation of a set of materials with a range of aminopolymer loadings, (2) determine the effect of the silica support by synthesizing HAS adsorbents on several different pore-expanded mesoporous silicas, (3) assess the application of the HAS adsorbent to capturing CO_2 from the ambient air, (4) develop second generation linear aminosilica adsorbents via N-protected-aziridines.

Initially, the large obtainable amine loading in the HAS material made it an attractive candidate for CO_2 adsorption from dilute sources where membrane separation and other technologies are inefficient. The limitations of the HAS adsorbent were found by creating a set of adsorbents with different amine loadings by changing the aziridine to silica reactant ratio. In general, the CO_2 capacities of these adsorbents increased with increasing amine loading. However, it was discovered that at high amine loadings, the aziridine polymerization blocks the pore openings, reducing amine efficiencies and retarding adsorption kinetics. In an attempt to relieve this limitation, the use of several different pore-expanded mesoporous silicas as supports for the aziridine polymerization was investigated. Unfortunately, it was determined that the polymerizations in these materials terminated well before filling the pore spaces, resulting in adsorbents with only moderate amine loadings. Furthermore, it was determined that when normalized by amine loading, the adsorption kinetics of these PEHAS materials were fairly universal and were similar to non-pore-expanded HAS materials with low to moderate amine loadings.

The application of the HAS adsorbent to capturing CO_2 from ambient air was also investigated. In both humid and dry conditions, the HAS adsorbent was found to have a surprisingly large CO_2 capacity in light of the 250-fold reduction in CO_2 partial pressure

from 10% CO_2 (flue gas application) to 400 ppm CO_2 (air capture application), most likely due to the large heat of adsorption associated with the amine-CO_2 interaction.

Finally, a new series of linear aminosilicas was created through the reaction of existing aminosilicas with N-protected-aziridines. Specifically, reaction of aminosilane-functionalized silicas with N-methylaziridine resulted in the linear growth of methylaminoethyl groups, effectively increasing the amine loading of the adsorbent by a stoichiometric amount of an additional amine per attached silane.

CHAPTER 1

INTRODUCTION

Parts of this chapter are reproduced from "Adsorbent materials for carbon dioxide capture from large anthropogenic point sources," by Sunho Choi, Jeffrey H. Drese, and Christopher W. Jones, published in *ChemSusChem*, in 2009, volume 2, pages 796-854.*[1]*

Since the time of the industrial revolution, the atmospheric CO_2 concentration has risen nearly 35% to its current level of 388 ppm.*[1]* Recent consensus in the international scientific community suggests that anthropogenic CO_2 emissions have caused a rise in atmospheric CO_2 concentration and, in turn, a measurable change in the global climate.*[2]* The 2007 Intergovernmental Panel on Climate Change (IPCC) Assessment Report estimated CO_2 concentration to contribute a global radiative forcing of 1.66 W/m^2, which is the most significant of all the Earth's radiative forcing components.*[2]* To slow the increase, reductions in anthropogenic CO_2 emissions are necessary. The largest point sources for these emissions are pulverized coal-fired power plants (PC plants) that account for about a third of all CO_2 emissions in the USA.*[3]* The amount of energy required to operate under the status-quo dictates that, at least for the short to mid-term future, fossil fuel-based electricity generation will be required until alternative energy generation technologies can be adequately developed/scaled to meet the ever-increasing societal demand. Numerous alternative fossil fuel-based power generation schemes that include integrated CO_2 capture have been proposed, such as integrated gasification combined cycle (IGCC), oxycombustion, chemical looping, and membrane-

aided solid oxide fuel cell (SOFC) schemes, but most of these options require the construction of new facilities.*[4-6]*

Post-combustion capture technologies such as absorption with liquid amines or adsorption with solid adsorbents have been proposed as possible retrofits to existing PC plants that are integral to modern power generation infrastructure. Absorption processes involving CO_2 capture by liquid media are widely established. The liquid media are often aqueous amine solutions (e.g. monoethanolamine, MEA) or other fluids with basic character, such as chilled ammonia, that chemically absorb the acid gases.*[7-11]* Commercial processes exist that are based on physical absorption as well, using methanol or poly(ethylene glycol) dimethyl ether as absorbing phases.*[12]* However, these liquid media-based absorption technologies are very energy intensive, particularly in the regeneration stage, and are widely viewed to be cost prohibitive, although several commercial technologies exist.*[4]*

Adsorption processes for gas separation via selective adsorption on solid media are also well known.*[13, 14]* These adsorbents can operate via weak physisorption processes or strong chemisorption interactions. Solid adsorbents are typically employed in cyclic, multi-module processes of adsorption and desorption, with desorption induced by a pressure or temperature swing. Several classes of solid CO_2 adsorbents have been investigated and each class has its own advantages and disadvantages.*[15]* Zeolites and activated carbons capture CO_2 via physical adsorption, and consequently are typically hindered in the presence of water.*[16, 17]* Metal oxides (CaO, MgO, etc.), lithium zirconates, hydrotalcites, and solid-supported amines capture CO_2 via chemical adsorption. Metal oxides and hydrotalcites frequently degrade upon regeneration.*[18, 19]* Many lithium zirconates suffer from slow adsorption kinetics.*[20]* Solid supported amines are susceptible to poisoning by flue gas contaminants such as SO_2 and NO_x.*[21, 22]* Metal-organic frameworks (MOFs) are an emerging class of solid adsorbents that capture CO_2 by physical adsorption except in cases where amines are incorporated into

the structure or, possibly, when open metal coordination sites are generated.*[23, 24]* At this time, most MOFs have relatively low adsorption capacities at low CO_2 partial pressures.*[25]*

Of the many different classes of solid adsorbents, my research has been focused on the use of solid-supported amines for this purpose. Chapter 2 of this doctoral thesis consists of a detailed review of this class of adsorbents that was published in 2009. Chapters 3 and 4 discuss the continued development of a hyperbranched aminosilica (HAS) CO_2 adsorbent with a large amine content per weight and a large CO_2 capacity.*[26]* This organic/inorganic hybrid material is prepared by the ring-opening polymerization of aziridine on mesoporous SBA-15 silica, yielding silica pores functionalized by low molecular weight aminopolymers. Early investigation of the HAS adsorbent revealed a relatively high adsorption capacity of 3.1 mmol CO_2/g at 25 °C from humidified, simulated flue gas, that was fully regenerable over 10 adsorption/desorption cycles.*[26]* Chapters 3 and 4 will describe the effects of modification of certain synthesis parameters, such as solvent and reactant concentration, as well as the use of different silica supports on the HAS structure and adsorption properties. By tuning these parameters, a wide range of capture capacities and adsorption kinetics can be achieved. The effects of these changes on the adsorbent structure, including surface area, pore volume, aminopolymer molecular weight, and ratio of 1°:2°:3° amines play a crucial role in the formulated adsorbent's performance.

Capturing CO_2 from large anthropogenic point sources addresses only a third of global CO_2 emissions. To counteract or offset the effects of the remaining emissions, solid adsorbents could be used as a carbon negative technology to separate CO_2 from ambient air. While historically considered impossible from an energetic standpoint, air capture may be feasible if an adsorbent with a strong chemical affinity for CO_2 and accessible low-grade waste heat are utilized. The application of the HAS adsorbent to this

task is considered in Chapter 5 of this thesis by measuring adsorption capacities at 400 ppm CO_2 in both humid and dry conditions.

In an effort to afford direct control over the adsorption capacities and kinetics of silica-supported amine adsorbents, a new adsorbent formulation consisting of short-chain linear aminopolymers synthesized by a step-wise polymerization scheme via alkylcarboxylate-protected aziridines is considered in Chapter 6 of this thesis. In theory, by controlling the number of polymerization steps, an adsorbent's amine content and thus, CO_2 capacity could be controlled. As an alternative to this time-consuming and experimentally challenging strategy, a more simplified strategy for a single incremental increase in amine content via reaction with N-methylaziridine is also considered.

CHAPTER 2

REVIEW OF ORGANIC AND ORGANIC/INORGANIC HYBRID CO_2 ADSORBENTS

This chapter is largely reproduced from "Adsorbent materials for carbon dioxide capture from large anthropogenic point sources," by Sunho Choi, Jeffrey H. Drese, and Christopher W. Jones, published in *ChemSusChem*, in 2009, volume 2, pages 796-854.*[15]*

Numerous factors describe the quality or utility of CO_2 adsorbents. In general, fast adsorption and desorption kinetics, large adsorption capacity, infinite regenerability and stability, and a wide yet tunable range of operating conditions might define an ideal, hypothetical adsorbent. In reality, all practical adsorbents have trade-offs, and in this work, the array of known CO_2 adsorbents is reviewed in the context of each adsorbent's behavior with regard to several important parameters including: (a) adsorption/desorption kinetics, (b) CO_2 capacity, (c) operating window, including adsorption and desorption temperatures, (d) regenerability and multi-cycle stability, and (e) impact of common flue gas components or contaminants such as H_2O, Hg, SO_2 and NO_x. It should be noted that although a hypothetical, ideal adsorbent is described above, in reality no single ideal adsorbent is likely to be invented. Rather, each adsorbent's strengths and weaknesses must be considered in the context of a practical adsorption process for effective CO_2 separation. Ultimately, winning adsorbents will be those that effectively work within a practical and efficient CO_2 separation process. To this end, the behavior of the various classes of adsorbents used for CO_2 separation are reviewed and classified below.

A logical choice for the composition of a solid adsorbent is a solid analogue of a solution species used in absorption processes. The current benchmark technology being widely considered for post-combustion CO_2 capture is absorption by aqueous solutions of amines. Typically, these amines are alkanolamines such as monoethanolamine (MEA), diethanolamine (DEA), and methyldiethanolamine (MDEA). There have been numerous studies on the use of these and other amines in mixtures to optimize performance (for example see*[7, 8, 27-31]*), however, most of the formulations do not deviate from the classic case using roughly 30 to 40 wt% amine in H_2O.

The interaction of CO_2 with amines can be governed by several different mechanisms. Primary and secondary amines can react directly with CO_2 to produce carbamates through the formation of zwitterionic intermediates. The zwitterionic mechanism for the formation of carbamate from the reaction of CO_2 with a primary amine reported by Caplow*[30]* and later summarized, developed and elaborated in several reviews*[7, 8, 27-29]* is shown in Figure 2.1. The first step proceeds with the lone pair on the amine attacking the carbon from CO_2 to form the zwitterion. Free base then deprotonates the zwitterion to form the carbamate. In an aqueous amine environment, this base can be another amine, H_2O, or OH^-. This mechanism is applicable to secondary and sterically hindered amines as well, where sterically hindered amines are defined structurally as primary amines where the amino group is attached to a tertiary carbon atom, or secondary amines where the amino group is attached to a secondary or a tertiary carbon atom.*[31]* Thus, under dry conditions, where H_2O and OH^- are absent, the maximum amine efficiency of an amine adsorbent is 0.5 mol CO_2/mol N. Amine efficiency, defined here as the moles of CO_2 captured per mass unit divided by the moles of N per mass unit, gives a reflection of the adsorbent's efficacy in perspective with its potential. Under humid conditions, where H_2O can act as a base, the maximum amine efficiency is 1.0 mol CO_2/mol N.

Tertiary amines react with CO_2 through a different mechanism. Instead of reacting directly with CO_2, tertiary amines catalyze the formation of bicarbonate. The mechanism involving the base-catalyzed hydration of CO_2 for the reaction of CO_2 with tertiary amines as first reported by Donaldson*[32]* and later reviewed by Kenig*[29]* is detailed in Figure 2.2. In the first step, the tertiary amine dissociates H_2O to form a quaternary cationic species and OH^-. Hydroxide ion then attacks CO_2 to form the bicarbonate anion. The last step is then the ionic association of the protonated amine and bicarbonate. Primary and secondary amines can also react with H_2O and CO_2 in this manner. While the activation energy for this pathway is lower than for the formation of carbamates, the rate constant is actually smaller. It has been observed for humid CO_2 capture with solid-tethered amines that carbamates form initially and then are converted to carbonates and bicarbonates (see section 2.1.9).

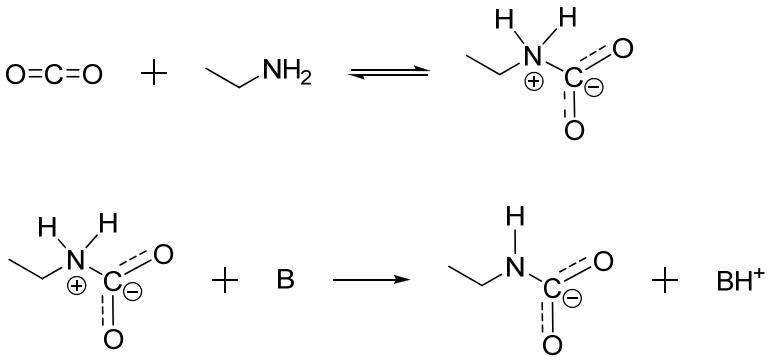

Figure 2.1. Reaction scheme for carbamate formation by reaction of CO_2 with primary, secondary, or hindered amines.

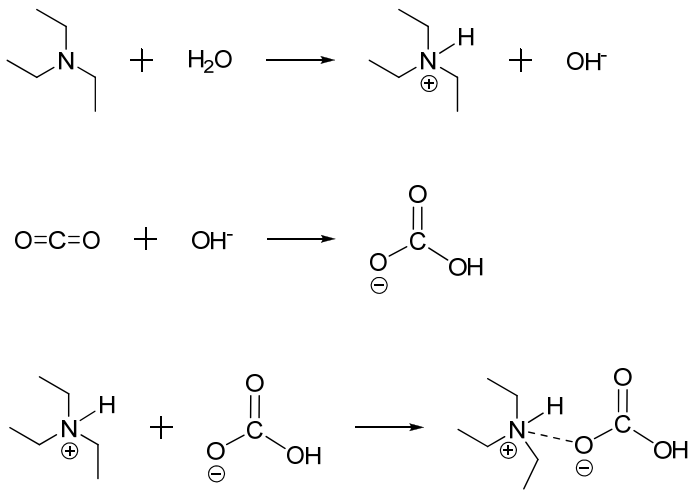

Figure 2.2. Mechanism for the reaction of CO_2 with tertiary amines.

For CO_2 capture applications from flue gas, the immobilization of aqueous amines onto a solid support (e.g. porous silica) could have several advantages. A large energy cost is paid to heat H_2O in the aqueous amine solution during the amine-regenerating, CO_2 stripping step. A portion of this process cost can be avoided by eliminating H_2O in exchange for a solid silica support with lower heat capacity (0.8 kJ/kg*K*[33]* in the case of mesoporous silica SBA-15 vs. 4.19 kJ/kg*K for H_2O). There are additional advantages to the use of supported amine adsorbents. Unlike amine solutions, degradation due to evaporation can be less of an issue for supported amines. Also, because solid-solid contact between silica particles and other solid surfaces is poor, vessel corrosion is less problematic than for an aqueous amine configuration.

Silica supported amines were first used for CO_2 capture by Tsuda in 1992.*[34, 35]* Amorphous silica gels were created by co-condensation of various amine-containing silanes and used for CO_2 capture under dry conditions. Leal reported the first use of amine-functionalized mesoporous silicas for CO_2 adsorption in 1995.*[36]* Silane chemistry was used to immobilize N-propylamine groups onto a commercial, amorphous, mesoporous silica gel. Since then, many groups have investigated the use of supported amines for CO_2 capture. While the adsorption conditions used to measure their

effectiveness are widely varied, there are only two main classes of materials; amines covalently bound to the silica support, and amines physically impregnated into the silica support pore space. The preparation, use, and effectiveness of these adsorbents are described below.

2.1. Amines Physically Adsorbed on Oxide Supports

2.1.1. The "Molecular Basket"

The simplest method of supporting amines on silica or any other support is to physically mix the amines with the support. This method, sometimes described as a "wet impregnation" method, typically involves suspending a support such as porous silica in a solution of the amine of choice and a volatile solvent.*[37]* Amine diffuses into the silica pore space by concentration driving force and in some cases chemical affinity, after which the solvent is removed by evaporation. The amine density of the resulting organic/inorganic composite is controllable through simple reaction stoichiometry, although this does not necessarily translate to the exact density of amines impregnated in the silica pore space since it is possible to deposit amines on the silica particle's exterior or sandwiched in between particles, forming agglomerates. Furthermore, the amine density achieved is not necessarily reflective of the density of "accessible" amines, or those amines that are chemically and sterically free to capture CO_2.

The first amine-impregnated silica used to capture CO_2 was reported by Song*[37]* in 2002. They reported the impregnation of MCM-41, a high surface area mesoporous silica with cylindrical pores of relatively small diameter (2.8 nm, in this case), with low molecular weight poly(ethyleneimine) (PEI) to create an adsorbent they termed a "molecular basket." Subsequently, several groups have reported the use of amine impregnated silicas as CO_2 adsorbents with varying results. The following section highlights several important attributes of these adsorbents.

2.1.2. Amine Type

There have been a number of amines investigated for impregnation into silica supports, but the guiding principle is the use of compounds that maximize the weight percentage of nitrogen. The intent of this principle is to maximize the capture capacity per total weight of adsorbent; however, it is important to note this may not coincide with a corresponding benefit in other important parameters such as adsorption and desorption kinetics or heats of adsorption. The amines investigated so far in the literature range from simple monoamines to aminopolymers, but the most commonly used amine is PEI.

PEI can be either a branched aminopolymer containing a mixture of primary, secondary, and tertiary amines or a linear aminopolymer of secondary amines with primary amine termini. The repeat unit structure of PEI is shown in Figure 2.20. Regardless of linear or branched structure, PEI possesses a high amine content of about 33% nitrogen by weight. The ratio of 1°:2°:3° amines in branched PEI is often assumed to be 1:1:1, however it has been found that substantial deviation can occur depending on molecular weight and synthesis conditions. Specifically, commercial low molecular weight PEI has been reported to have a ratio of 44:33:23 by Jones*[26]* and 42:33:25 by Kissel,*[38]* representing a lower proportion of tertiary amines. An amine ratio of 28:47:25 was measured for low molecular weight polymer synthesized in a confined environment, representing a similarly low proportion of tertiary amines but with a much higher proportion of secondary amines.*[26]* Reduction in the proportion of tertiary amines impacts not only the equilibrium CO_2 capacity of the supported PEI, but also CO_2 capture kinetics, as it has been shown that CO_2 interacts with primary and secondary amines through a different mechanism than with tertiary amines, vide supra.*[29]*

As mentioned above, Song*[22, 37, 39, 40]* has extensively studied the use of low molecular weight, branched PEI-impregnated silicas for CO_2 capture. Ahn*[41]* has used low molecular weight PEI to make similar adsorbents but with various different silica supports (see section 2.3). Drage*[42]* investigated the impregnation of mesoporous silica

by three different samples of low molecular weight PEI; 423 Mw linear, 600 Mw branched, and 1800 Mw branched PEI. The frequent use of low molecular weight PEI over longer polymers is most likely associated with the ease of impregnation into the silica pore space, as longer polymer chains would likely block pore mouths and prevent complete pore penetration.

Another amine, tetraethylenepentamine (TEPA), can be thought of as an ultra-low molecular weight PEI, as it contains only 4 repeat units of PEI (Figure 2.20). TEPA has been impregnated by Zhu*[43-45]* into two different silica supports. Zhu also reported the impregnation of mixtures of TEPA and diethanolamine (DEA, Figure 2.20) into SBA-15 to prepare CO_2 adsorbents. They found a synergistic effect on amine efficiency, and associated the benefit with the interaction of DEA's hydroxyl groups in the formation of bicarbonates. The impregnation of DEA alone was studied by Sayari.*[46]*

2.1.3. Support Structure

The nature of the silica support in these amine impregnated adsorbents impacts their adsorption properties in several ways. In the case of PEI, the high surface areas of mesoporous silicas (500 to 1500 m^2/g) provide an open, accessible backbone for the stabilization of a large number of active adsorption sites. The silica surface has been shown to strongly interact with PEI, which facilitates the distribution of the polymer throughout the pore-space.*[37, 41]* It is assumed that the hydroxyls on the silica surface (silanols) hydrogen bond with the amines, thereby promoting the unraveling and distribution of the polymer chains. This strong interaction with silica has been measured by the decrease in the maximum decomposition temperature of these adsorbents as amine content increases.*[41]* In fact, the maximum decomposition temperature was decreased to 398 K from that of pure PEI (478 K) in one study.*[37]* The hydroxyl groups of DEA also interact with the silica surface,*[46]* again, most likely via hydrogen bonding with silanols.

In some cases, impregnation has been carried out on as-synthesized mesoporous materials, by not removing the organic template used to synthesize the mesoporous silica before impregnation. These materials are referred to here as "as-prepared" or "occluded" silicas. Zhu reported synergistic effects on the adsorption capacities for TEPA impregnated as-prepared silicas versus TEPA impregnated silicas whose templates were removed by calcination or ethanol extraction.*[43-45]* These synergistic effects on adsorption capacity were actually measured for two different as-prepared mesoporous silicas, SBA-15 and MCM-41, which are synthesized from different organic templates, Pluronic 123 ($EO_{20}PO_{70}EO_{20}$) and cetyltrimethylammonium bromide (CTAB), respectively. In one study, the template was removed by calcination, replaced by impregnation and then the final adsorbent was constructed by impregnation with TEPA. This adsorbent actually had a lower equilibrium capacity than the stoichiometrically equivalent impregnated as-prepared support, suggesting that the synergistic effects originate from association of TEPA with the well ordered template micelles. However, it should be recognized that the organic template present in as-prepared silicas reduces gas diffusion through the pores, having a negative impact on adsorption kinetics (see section 2.1.9).

Of course, the type of porous silica support plays an important role in the performance of these adsorbents. The simplest porous silicas are amorphous SiO_2 frameworks with a random array of pore sizes and shapes. These amorphous silicas can in some cases be poor supports for organic material because their entire pore volume may not be accessible to organic functionalizing agents. Also, from a scientific perspective, their disordered structures are difficult to characterize and therefore it is not always easy to understand the adsorbent structure on a molecular level. In contrast, ordered mesoporous silicas are excellent candidates for scientific study because they are easily, reproducibly synthesized, they are easy to characterize and many aspects of their structures are tunable. Ordered mesoporous silicas are generally constructed by forming

an amorphous SiO_2 framework around an organic template, which usually consists of amphiphilic moieties arranged in self-assembled micelles. After condensation of the silica framework in the presence of the template, the organic template is removed either by solvent extraction or calcination, leaving behind pores of defined size and shape. The resulting silica particle size, pore size distribution, pore shape (e.g. cubic or hexagonal), and pore connectivity (one-dimensional vs. multi-dimensional) are all controllable by modern synthetic methods.*[47]* Thus, the effectiveness of adsorbents prepared by impregnation using various ordered mesoporous solids, the maximum organic loading, and the diffusion of CO_2 through the pores can vary widely. To address this problem, Ahn[149] reported a study of the adsorption properties of 5 different mesoporous silica supports all impregnated with 50 wt% PEI. The authors found equilibrium adsorption capacities increased in the order of MCM-41 < MCM-48 < SBA-16 ~ SBA-15 < KIT-6 corresponding to the order of average pore diameter of the bare support (2.8, 3.1, 4.1, 5.5, and 6.5 nm respectively). They also observed the same trend for the time required for each adsorbent to reach 70% of its equilibrium capacity. It is interesting to note that even though MCM-48 and SBA-16 possess three-dimensional pore interconnectivity, neither their kinetics nor capacities were better than those of the one-dimensional SBA-15, in this case. Although it is unclear from this study whether the results are dependent on pore diameter alone, or on a combination of properties unique to each type of silica, there is additional evidence for the important impact of pore diameter; both Sayari*[46]* and Zhu*[44]* report larger capacities for pore-expanded (PE) MCM-41 over typical MCM-41.

2.1.4. Degradation Temperature

There are many factors that contribute to the decomposition temperature of amine impregnated silicas. Typically the temperature at which the onset of degradation begins and the temperature of maximum degradation rate are tracked via thermogravimetric analysis/differential scanning calorimetry (TGA/DSC), where a material is heated at a

constant rate in a controlled atmosphere and the weight loss is measured versus time. From these data, the derivative of the weight loss with respect to time is typically calculated. The maximum absolute value of the derivative of the weight loss with respect to time gives the maximum degradation rate, which is dependent on the heating rate used during the experiment.

Table 2.1. CO_2 capacities and measurement conditions for amine impregnated silicas.

				dry		humid			
		Temp.	pCO_2	q [a]	eff. [b]	q [a]	eff. [b]		
Amine	Support	(K)	(bar)	(mmol/g)	(mol CO_2/mol N)	(mmol/g)	(mol CO_2/mol N)	Method [c]	Ref.
PEI	proprietary inorganic support	348	1	2.4	0.26			TGA	*[48]*
DEA	PE-MCM-41	298	0.05	2.93	0.40			TGA	*[46]*
PEI	MCM-41	348	1	3.02	0.17			TGA	*[37]*
PEI	MCM-41	348	0.15	2.02	0.17	2.97	0.2	GC	*[39]*
PEI	KIT-6	348	1	3.07	0.26			TGA	*[41]*
PEI	MCM-41	348	1	3.02	0.17			TGA	*[40]*
PEI	MCM-41	348	1			2.55	0.22	GC	*[22]*
TEPA	SBA-15	348	1	3.93	0.30			TPD/GC	*[43]*
DEA/TEPA	SBA-15	348	1	4	0.37	3.18	0.3	TPD/GC	*[45]*
TEPA	MCM-41	308	1	5.02	0.32			TPD/GC	*[49]*

[a] Reported CO_2 Capacity
[b] Amine Efficiency
[c] Method of analysis: thermogravimetric analysis (TGA), gas chromatography (GC), temperature programmed desorption (TPD)

The key factor that defines the degradation temperature is the type of amine used. Song measured the maximum degradation rate for pure PEI to be at 478 K.*[37]* The authors also measured a 50 wt% PEI adsorbent to have a maximum degradation rate at 398 K. In disagreement, Ahn reported the maximum degradation rate for pure PEI to occur around 573 K.*[41]* However, like Song, they observed a decrease in degradation temperature as organic loading was increased from 0 to 50 wt%. For materials with

loadings higher than 50 wt%, they observed an increase in decomposition temperature. They attributed this to the hypothesis that the silica support reached its maximum loading at 50 wt% and additional PEI formed films on the silica particle's surface (see section 2.1.5). These films should behave more like bulk PEI and thus, raise the decomposition temperature. Sayari measured two major weight loss peaks for a 66.6 wt% TEPA adsorbent at approximately 473 and 663 K.*[8, 46]* The higher secondary weight loss peak suggested that TEPA has a strong interaction with the silica support.

Degradation temperature was also dependent on the atmosphere under which the degradation experiment occurred. Drage studied the degradation of PEI impregnated adsorbents under CO_2, air, and N_2 atmospheres.*[42]* They found that the adsorbents were stable under N_2 until about 463 K (2% mass loss), and under air until about 423 K (2% mass loss). Under these two atmospheres, loss of mass was attributed to volatilization and evaporation of the amines. Under CO_2, the adsorbents first quickly gained mass as adsorption occurred and then remained constant until about 353 K. The adsorbents lost mass until they reached a minimum at 413 K, at which point they regained mass as temperature increased. The authors attributed this mass gain above 413 K to the formation of secondary adsorption products. They used XPS, solid state ^{13}C NMR, and (Fourier transform-infrared) FT-IR spectroscopy to identify the probable formation of ureas and poly(ureas).

2.1.5. CO_2 Adsorption Capacities Under Dry Conditions

The supported amine literature frequently focuses on equilibrium CO_2 capture capacity as an evaluation of an adsorbent's performance. Although this is only one parameter of many important to practical adsorption processes, equilibrium capacity is certainly critical from the perspective of reducing the amount of adsorbent required to capture a given amount of CO_2, as this has implications for both the capital and operating costs for the CO_2 capture processes. In some cases, adsorption capacities are reported as

working capacities rather than equilibrium capacities, when adsorption is only measured for a predetermined period which is less than the time required to reach equilibrium. Working capacities are also reported in cases where adsorbents are not completely regenerated during the desorption phase of adsorption/desorption cycles. In both these respects, working capacities may be more relevant to an adsorbent's performance, because depending on the process, it may be more economical to shorten the lengths of either the adsorption or desorption cycles or lower the temperature at which desorption is performed if the savings in process costs outweigh the decrease in the amount captured per weight of adsorbent. The capacities of the adsorbents discussed below are listed in Table 2.1 along with their adsorption conditions and methods of measurement.

The theoretical value for the maximum weight percent of amines that can be impregnated into a silica support is equal to the pore volume (cm^3/g) of a given support multiplied by the density of the amine (g/cm^3). Adsorbents prepared with amine weight percents greater than this critical value, therefore, have amines outside of the pore spaces. These amines form an organic film around the silica particle, and these amines should in principle behave as bulk amines. Since impregnated amines interact with the silica support in a synergistic manner, this should result in a decrease of amine efficiency. Sayari reported the capacities and amine efficiencies, measured by TGA, of DEA-impregnated silicas as a function of amine loading.*[46]* Their results verified the hypothesis set above, that as amine loading passed a critical value, in this case about 7 mmol N/g adsorbent, the equilibrium capacity and amine efficiencies reached a maximum and decreased for higher loadings. The authors observed relatively constant amine efficiencies of about 0.37 for materials in the range of 5 to 7 mmol N/g. They explained that this is less than the ideal dry case of 0.5 mol CO_2/mol N because of DEA's strong interaction with the support. They supported this explanation by preparing adsorbents on four supports with increasing surface areas and found that for equivalent amine loadings, amine efficiency decreased as surface area of the support increased. They

reported a maximum equilibrium capacity of 2.93 mmol CO_2/g adsorbent for an adsorbent with 7.31 mmol N/g, which translated to an amine efficiency of 0.40 mol CO_2/mol N.

Zhu has reported the impregnation of TEPA into both SBA-15 and MCM-41 supports.*[43-45]* For as-prepared SBA-15, they prepared adsorbents with varied amine loadings from 0 to 70 wt% and measured CO_2 adsorption by TPD/GC. While the authors measured a continual increase in equilibrium capacity as loading increased, they measured a maximum in amine efficiency of 0.29 mol CO_2/mol N for the 40 wt% adsorbent. This observation can be rationalized by comparing the N_2 physisorption results for the materials. As expected, a reduction in pore diameter and BET surface area was observed for the impregnated, as-prepared SBA-15 materials, as the wt% of TEPA increased. At 50 wt%, there was virtually no measurable pore volume, thus higher loadings resulted in buildup of organic outside of the pores and likely caused added diffusional limitations. The theoretical maximum loading for TEPA inside the pores of their as-prepared SBA-15 material was 42 wt%. This considerably large loading was possible because of the large pore volume of 0.71 cc/g for the as-prepared support. After synthesis, the silica was filtered from solution and washed with H_2O, which removed a sizable fraction of the organic template. It is important to recognize that similar syntheses without extensive washing resulted in far lower pore volumes for as-prepared SBA-15,*[26]* and the theoretical maximum loadings for these materials were reduced accordingly. The equilibrium capacity of 70 wt% impregnated as-prepared SBA-15 was actually higher than that of pure TEPA, further supporting the hypothesis that there was a synergistic effect of the silica and P123 template on the TEPA for capture of CO_2.

As noted above, Zhu also studied the impregnation of TEPA in MCM-41 silica and measured its adsorption of CO_2 with TPD/GC. They prepared adsorbents with varied amine loadings for as-prepared MCM-41 (AM), calcined MCM-41 (CM), MCM-41 with template extracted by ethanol (EM), and as-prepared MCM-41 that had been pore-

expanded with trimethylbenzene (TMB) (PM). As with TEPA impregnated SBA-15, they observed a reduction in amine efficiency at higher loadings; identifying the largest amine efficiency (0.38 mol CO_2/mol N) for 50% loaded PM and the largest equilibrium capacity (5.3 mmol CO_2/g) for 60% loaded PM. All four supports displayed CO_2 capacities higher than pure PEI at certain TEPA loadings, which further indicates that CO_2 capture by impregnated amines is synergistically improved by the presence of the silica support. However, of these four materials, the AM and PM materials, which still had their organic templates in the pores, possessed higher capacities than their template-free equivalents. This also confirms that, in addition to the silica support, the organic template of as-prepared porous silicates can facilitate CO_2 capture.

The impregnation of MCM-41 with a mixture of two amines was also studied by Zhu.*[45]* Sayari*[46]* showed that DEA impregnated silicas displayed relatively high amine efficiencies but strong affinity for the support. Zhu investigated a mixture of TEPA and DEA in as-prepared and calcined MCM-41 to determine whether any synergy existed. For 50 wt% loaded materials, they measured a maximum capacity for as-prepared MCM-41 at a TEPA:DEA of 30:20 and a maximum capacity for calcined MCM-41 at a TEPA:DEA ratio of 20:30, by TPD/GC. Both capacities were larger than those of materials with either TEPA or DEA impregnated alone. Amine efficiencies were also higher for the mixed amine adsorbents than for either TEPA or DEA impregnated alone. The authors obtained higher equilibrium capacities and amine efficiencies for calcined materials than as-prepared materials at modest amine loadings.

The CO_2 capacity of molecular basket adsorbents with varied PEI loadings (0 to 100 wt%), was examined under dry conditions by Song*[22, 37, 39, 40]* with both TGA and GC. The adsorption capacity increased as PEI loadings increased from 0 to 30 wt%, reached a plateau from 30 to 50 wt%, and then decreased to the capacity of pure PEI at 100%. The authors attributed this reduction to a complete filling of the MCM-41 pore space around a weight percent of 50%. As described for the other impregnated amines,

additional PEI beyond the pore capacity incorporated into the composite deposited onto the silica exterior and thus captured CO_2 with the same effectiveness as bulk PEI. This result was echoed by the work from Ahn,*[41]* where maximum CO_2 capacity and amine efficiency were measured for 50 wt% PEI impregnated KIT-6 (55 wt% maximum theoretical loading), by TGA, with higher loadings giving lower values. This pore saturation is displayed in Figure 2.3, where scanning electron micrographs for 50 and 60 wt% PEI-impregnated KIT-6 materials are shown.*[41]* They display a smoothing of the adsorbent surface and the formation of large agglomerates associated with surface bound PEI for the 60 wt% loaded KIT-6.

It is important to note that the amines in the 50 wt% loaded MCM-41 of Song exhibited a higher amine efficiency (0.22 mol CO_2/mol N) than that of bulk PEI (0.11 mol CO_2/mol N), again implying that there was some synergistic effect from the silica support.

2.1.6. CO_2 Adsorption Capacity: Effect of CO_2 Partial Pressure, Adsorption Temperature, and ΔH_{ads}

The equilibrium CO_2 capture capacity of chemisorbents should display saturation dependence on the partial pressure of CO_2 in the feed stream at a given temperature. The isotherm of an adsorbent is useful in the determination of operating parameters and evaluating the effectiveness of an adsorbent. The isotherm usually consists of three regions, a nearly linear region at low pressures called the Henry's Law regime, a nonlinear transition region at moderate pressures, and a saturation region at high pressures, where large changes in CO_2 partial pressure result in small changes in equilibrium capacity.

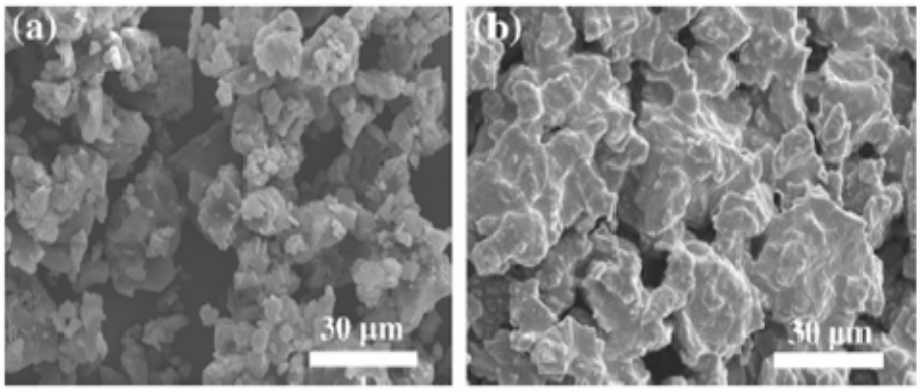

Figure 2.3. Scanning electron micrographs of (a) 50wt% PEI impregnated KIT-6 and (b) 60 wt% PEI impregnated KIT-6 depicting the polymer surface coverage once pore saturation is reached (reprinted with permission from Ref. *[41]*).

Very few papers have reported full adsorption isotherms for amine-impregnated silicas. Song measured an isotherm at 348 K under dry conditions with TGA for a molecular basket adsorbent with 50 wt% PEI impregnated into MCM-41*[37]* (Figure 2.4). They determined that above a CO_2 concentration of about 30% at atmospheric pressure, the molecular basket adsorbent reached a plateau in capacity. Zhu measured the same capacity for TEPA impregnated, as-prepared SBA-15 at 10% CO_2 and 100% CO_2 under dry conditions by TPD/GC.*[43]* Zhu also observed a ~5% loss in capacity as the CO_2 feed concentration was decreased from 100 to 5% for TEPA-impregnated as-prepared MCM-41 by TPD/GC.*[44]* These results show that amine impregnated silicas are very promising candidates for post-combustion CO_2 capture because of their effectiveness at low CO_2 partial pressures.

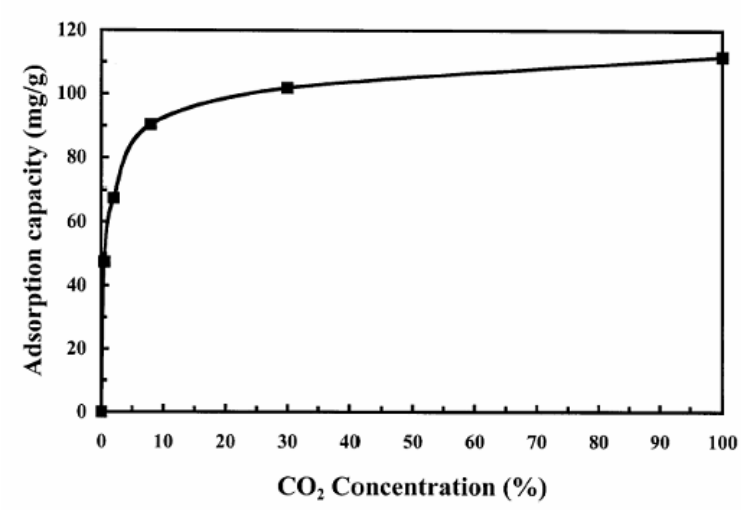

Figure 2.4. Isotherm at 348 K for 50 wt% PEI loaded molecular basket. Concentration is given as percentage of test gas at 1 bar (reprinted with permission from Ref. *[37]*).

According to thermodynamics, equilibrium CO_2 capacity should increase as operating temperature decreases, because both the heat of adsorption and the change in entropy are negative for the adsorption of CO_2 with amines. Interestingly, CO_2 capacities measured by Zhu*[43]* with TGA for the 50 wt% TEPA-impregnated as-prepared SBA-15 adsorbent increased as temperature increased from 308 to 373 K. This result is counter-intuitive for exothermic adsorption, and was explained by the authors as suggesting a strongly diffusion-controlled process. This is a common trend observed in the literature on amine impregnated silicas. Using TGA, Song*[37]* found that the capacity for the molecular basket adsorbent increased as temperature increased from 323 to 348 K, where it displayed a maximum and decreased at 373 K. Like the TEPA-impregnated SBA-15 materials prepared by Zhu, this result is counter-intuitive and suggests diffusion-controlled adsorption. Ahn*[41]* also observed a maximum capacity at 348 K for 50 wt% PEI-impregnated KIT-6 by TGA. When silicas are impregnated with large amounts of amines, effectively eliminating open pore volume, diffusional effects can become more significant than thermodynamic effects on the temperature dependence of their capacities.

2.1.7. Effect of H_2O on CO_2 Capacity

In theory, the presence of H_2O during CO_2 capture should improve the maximum amine efficiency from 0.5 to 1.0 mol CO_2/mol N. This is due to the formation of carbonates and bicarbonates (see Chapter 2 Introduction). In practice, this is not always the case, as it may be that H_2O and CO_2 competitively adsorb on some adsorbents. H_2O also increases the possibility of amine leaching in the case of amine impregnated silicas. This has been observed in a simulated packed-bed flow system where a humid 10% CO_2 stream was used as test gas.*[26]*

There has been limited work reported on the effect of H_2O in a typical flue gas stream on the equilibrium CO_2 capacity of amine impregnated adsorbents. Zhu*[45]* measured a 20% decrease in capacity for TEPA and DEA impregnated SBA-15 when adsorption occurred under humid conditions with TGA. However, it is possible that desorption of H_2O from the pre-hydrated adsorbents went undetected during the gravimetric experiments, which would result in falsely-low capacities. In two different studies,*[22, 39]* one using a continuous CO_2 emission monitor and the other with an online GC, Song measured much longer breakthrough times for humid adsorption experiments versus dry ones for the molecular basket adsorbents. In both studies, they observed a 30% increase in adsorption capacity for the humid case. They also measured substantial H_2O adsorption capacities for the adsorbents by GC. When CO_2 and H_2O were present in the feed stream, the equilibrium capacity of H_2O was 2.63 mmol H_2O/g, but increased to 3.24 mmol H_2O/g when no CO_2 was present, suggesting that, while the presence of H_2O aids CO_2 adsorption, CO_2 competitively adsorbs with H_2O. When the kinetics of the adsorption of H_2O in the presence of CO_2 were measured, very little H_2O adsorbed during the first 30 minutes. However, after about 70 minutes, the amount of H_2O adsorbed became greater than the amount of CO_2 adsorbed. The authors presented this as evidence that CO_2 first adsorbs as carbamate and then reacts with H_2O to form bicarbonate, as has been shown to occur for covalently tethered amines (see section

2.2.7). To further investigate the CO_2-H_2O interdependence, they performed a number of adsorption experiments at different CO_2 and H_2O concentrations. Starting with a H_2O concentration of 0% and CO_2 concentration of 14.8%, several experiments were performed while linearly increasing H_2O concentration and linearly decreasing CO_2 concentration. The last adsorption experiment in this series was done at 16% H_2O and 12.6% CO_2. They found that CO_2 capacity increased along this series with increasing H_2O concentration, despite the decrease in CO_2 partial pressure. There was a dramatic increase in CO_2 capacity when the concentration of H_2O in this series was increased from around 7% to around 9%. Once the partial pressure of H_2O increased past the partial pressure of CO_2, they observed only a very small increase in CO_2 capacity. This suggests that a 1:1 concentration of CO_2 and H_2O may be ideal for maximum equilibrium capacity.

2.1.8. Desorption Temperature, Regeneration, and Effect of Feed Impurities

A solid CO_2 adsorbent must be reused over many adsorption/desorption cycles for practical application. The desorption conditions used in the literature vary, but usually consist of a temperature swing accompanied by an inert gas purge. These conditions shift the CO_2-amine equilibrium in two ways. The decrease in CO_2 concentration in the gas phase shifts the equilibrium towards desorption of CO_2, while the increase in temperature causes a shift to an ultimately net positive Gibb's free energy for the capture of CO_2. This increase in temperature also provides the activation energy required for desorption, as desorption is always an activated process. Zhu*[43]* performed 7 adsorption/desorption cycles with TGA/MS on the 50 wt% TEPA-loaded as-prepared SBA-15 adsorbent by desorbing at 373 K under inert gas flow. They measured about a 4% loss in capacity over these cycles. The authors also investigated the regeneration of 50 wt% TEPA-loaded as-prepared MCM-41 by desorbing under the same conditions.*[49]* They measured about a 9% loss in capacity over 6 adsorption/desorption cycles with TGA/MS. However, Jones

measured a 50% loss in capacity for 50 wt% TEPA-impregnated SBA-15 over 4 adsorption/desorption cycles in a humid flow system monitored by MS, accompanied by visible evidence of amine leaching.*[26]*

Some authors have reported the complete desorption of amine impregnated silicas under inert gas flow only, without temperature swing. Song*[39]* measured fully regenerable capacity over 10 cycles by GC for the molecular basket adsorbent with just an inert purge for the desorption step. Ahn*[149]* measured fully regenerable capacity over 3 cycles by TGA for PEI-impregnated KIT-6 with just an inert purge for the desorption step. From these two reports it seems that PEI-impregnated silicas can be regenerated by inert gas flow alone, as long as the adsorption temperature is sufficiently high to provide the activation energy required for desorption (348 K was used in both studies).

The effect of other contaminants in the flue gas stream on the CO_2 capacity of amine impregnated adsorbents has not been studied in much detail. The only work done in this area is a paper by Song*[22]* that uses gas specific, continuous emission monitors to measure the changes in concentration of CO_2, N_2, O_2, CO, and NO_x during multicomponent adsorption at 353 K from flue gas from a natural gas fired boiler. The authors measured the decrease in CO_2 concentration to almost zero at the start of the experiment, followed by the increase after breakthrough to the starting concentration. The other test gas components were largely unaffected except for NO_x (60 to 70 ppm in feed), which fell to an effluent concentration of almost zero within 100 seconds and remained there for the duration of the adsorption experiment. The NO_x was not liberated during desorption at 353 K under He. This suggests that amine impregnated silicas competitively and irreversibly adsorb NO_x, making its presence potentially detrimental to the equilibrium CO_2 capacity over many adsorption/desorption cycles. For this reason, conceptual US-DOE studies of CO_2 capture using amine processes always include separate SO_x and NO_x removal process(es) upstream of the amine unit.*[21]*

2.1.9. Adsorption and Desorption Kinetics

The kinetics of CO_2 adsorption and desorption are extremely important from a practical perspective. In practical CO_2 capture from a post-combustion flue gas stream, large quantities of CO_2 are required to be captured. The faster an adsorbent can capture CO_2 and be regenerated, the less of it will be required to capture a given quantity of gas. Thus, it is important to investigate and optimize the adsorption kinetics of amine impregnated silicas.

Amine loading, pore diameter of the support, and type of amine have an effect on the rate of CO_2 capture. Sayari*[46]* determined the maximum rate of CO_2 adsorption with TGA by finding the maximum value of the derivative of the weight gain with respect to time. They determined the maximum rate was about the same for amine loadings of 2.74 to 6.34 mmol N/g in DEA impregnated MCM-41 at 0.55 mmol CO_2/g*min. After the theoretical pore saturation point of 6.54 mmol N/g, they measured a sharp increase in maximum CO_2 adsorption rate, the highest value of 0.76 mmol CO_2/g*min occurring at 6.95 mmol N/g, then dropped off sharply at higher loadings due to mass transfer limitations through the thin film of amines deposited outside the silica pores. These experiments suggest that a small amount of amines bound to the outer surface of the silica particle increased the maximum adsorption rate but, at high loadings the diffusional resistance became too large and ultimately retarded the kinetics.

The silica support used in preparation of the adsorbent also affects adsorption kinetics. Ahn*[149]* used TGA to determine the time required for several adsorbents with different supports (50 wt% PEI) to reach 70% of their final equilibrium capacity was MCM-41>MCM-48~SBA-16>SBA-15>KIT-6, which followed the order of increasing average pore diameter. This again is consistent with there being significant diffusional resistance for these materials and showed that a larger pore space, such as in KIT-6, could result in much quicker adsorption kinetics. In fact, impregnated KIT-6 reached 70% of its capacity (1.0 min.) about 6 times faster than impregnated MCM-41 (5.7 min.).

While the exact numbers vary slightly, the common theme for amine impregnated silicas is a quick adsorption phase followed by a slow approach to equilibrium. Zhu*[44]* determined an adsorption halftime (time required to reach half of equilibrium capacity) with TPD/GC for TEPA-impregnated as-prepared MCM-41 of 1.5 minutes, while adsorption still occurred at 140 minutes. Zhu*[43]* observed slightly quicker behavior for TEPA-impregnated as-prepared SBA-15, where it took 2 minutes to reach 75% of its 150 minute capacity. They performed adsorption measurements for 30, 60, 12, 150, and 180 minutes at 348 K for this adsorbent and the capacity increased at every interval, suggesting that full equilibrium was not reached in any case. The time to reach equilibrium is so long for these adsorbents that it likely not practical to refer to equilibrium capacities as performance measures. Rather, working capacities that are defined for short adsorption times or adsorption halftimes may be more useful for evaluation.

2.2. Amines Covalently Tethered to Oxide Supports

The second main class of silica supported amines used as solid CO_2 adsorbents are those in which the amine is covalently bound to the silica support, usually through alkyl–silyl linkages. These adsorbents have a clear advantage over amine impregnated silicas in that they cannot leach amines unless conditions are strong enough to break covalent bonds. This gives covalently tethered amine adsorbents (CTA) the potential to be fully regenerable through repeated adsorption and desorption cycles. The preparation, characterization, and use of CTA adsorbents are described below.

2.2.1. Amine-containing Silanes

The most commonly reported method for synthesizing CTAs is through the use of silane chemistry. A general synthetic scheme is presented in Figure 2.5, where R_1 is often an aminoaklyl group. In it, an aminoalkyltrialkoxysilane is reacted with a silica surface,

typically in an organic solvent. The alkoxysilyl groups condense with surface silanol groups to form new Si-O-Si linkages while liberating alcohols. Trialkoxysilanes are typically used to create as many new linkages to the silica surface as possible. The R_2 groups in the alkoxy functionalities are most often methyls since they have been shown to be more reactive than bulkier groups such as ethyls or propyls.*[50]* The average number of surface bonds actually formed depends on the density of silanols on the silica support, the R_1 and R_2 groups used, and reaction conditions such as silane concentration, temperature, and time.

The choice of amine used for synthesizing CTAs directly impacts the resulting materials' adsorptive properties. Primary and secondary amines have been shown to capture CO_2 more efficiently than tertiary amines, as noted above. As previously discussed, the nitrogen density of supported amines is also critical from a CO_2 capacity per weight perspective. Thus, the logical choice for an amine-containing silane would be one with a maximum density and quantity of accessible primary and secondary amines. However, in practice, the range of choices is usually limited to those silanes that are commercially available, since the end goal of most studies is the preparation of a low cost adsorbent (which may be questionable in any case where expensive silanes are used), rather than one that requires expensive, custom-made reagents. The largest number of primary or secondary amines on a currently commercially available silane is 3, for example with 3-[2-(2-aminoethyl)aminoethyl]aminopropyltrimethoxysilane. A discussion of the different silanes used to produce CTAs is given below.

Figure 2.5. Scheme for the reaction of silane with silica. R_1 can be either alkyl or aminoalkyl group, and R_2 is typically a methyl or ethyl group.

2.2.1.1. Mono, Di, and Tri Aminosilanes

By far, the three most common aminosilanes used in the CTA literature are:

1. 3-aminopropyltrimethoxysilane (mono silane)
2. 3-(2-aminoethyl)aminopropyltrimethoxysilane (di silane)
3. 3-[2-(2-aminoethyl) aminoethyl] aminopropyltrimethoxysilane (tri silane)

These silanes have one, two, and three amines respectively (structures shown in Figure 2.20). Mono*[21, 26, 36, 51-61]* silane only has a primary amine end group, while di*[26, 33, 34, 55, 59, 62-64]* and tri*[34, 55, 59, 65, 66]* aminosilanes have secondary amines in their linkers and are terminated with primary amines.

The amine loading, in terms of number of amines per total weight of material, has a large effect on an adsorbent's performance. Adsorbents with low amine loadings capture too little CO_2 per unit mass to be economically viable. However, the total number of amines present does not directly describe an adsorbent's equilibrium CO_2 capacity or uptake kinetics. When preparing adsorbents via silane chemistry, it is essential to maximize both their amine loadings and amine efficiencies. A discussion of the reported equilibrium capacities and their accompanying amine efficiencies is given in section 2.2.5.

The first use of di and tri aminosilanes for the application of CO_2 capture was reported by Tsuda*[34]* in their work on amorphous silica gel adsorbents. The aminosilanes were condensed in the presence of H_2O to form materials with little or no mesoporosity but large amine content (10.1 mmol N/g for diamine gel). Despite the moderate capacities (e.g. ~1.2 mmol CO_2/g adsorbent) reported for these materials, it is likely that the non-ordered nature of the adsorbents severely hindered adsorption due to poor diffusion of CO_2 to the reactive amine sites. This motivated researchers to pursue adsorbents with large numbers of amines that have favorable diffusional characteristics.

The organic loading achieved from reacting organosilanes with mesoporous silicas is chiefly limited by the surface area and the number of accessible silanols on the

support. The density of silanols on a silica surface changes depending on the method of silica preparation, but generally is between 1 and 5 OH groups/nm^2. Zheng,*[64]* for instance, found 2.3 silanols/nm^2 on SBA-15 by solid state ^{13}C NMR. Van der Voort*[67]* showed that as calcination temperature increased, the density of silanols decreased and that ethanol extracted silicas generally produced larger silanol densities than calcined silicas. The surface areas of mesoporous silicas can vary over a large range, and thus, the morphology of the silica support used is also very important to the total number of silanols present in a material. Furthermore, Chaffee*[56]* found that a smaller degree of support pore curvature resulted in higher silane loadings. Once the total number of silanols was estimated, Chaffee*[55]* found that only a small excess of silane was required to reach a loading near saturation.

The maximum amine loadings reported for CTA's prepared from mono silanes range from 1.27*[36]* to 5.07*[51]* mmol N/g adsorbent. The support used for the material with the lowest amine loading was a 60 to 80 mesh, Davison grade 62 silica gel, while the material with the largest amine loading used an SBA-15 mesoporous silica support. Other mesoporous silica supports such as HMS,*[55]* MCM-41,*[54]* MCM-48,*[61]* and SBA-12*[60]* have been used with varying success in terms of loading.

The maximum amine loadings reported for CTA's prepared from di aminosilanes range from 1.64*[62]* to 5.47*[62]* mmol N/g adsorbent. The support used for the material with the lowest amine loading was an SBA-16 with the organic template removed by extraction, while the material with the largest amine loading used an SBA-16 support with the organic template removed by calcination. Solvent-extracted silicas typically have higher silanol densities than calcined silicas.*[67]* Therefore, this trend is opposite of what may typically be expected for silane functionalization of silica, probably due to incomplete template removal during the extraction process. SBA-15 is the only other mesoporous silica support that has been used with di aminosilanes to make CTA's.

The maximum amine loadings for CTA's prepared from tri aminosilanes range from 4.57*[55]* to 7.98*[65]* mmol N/g adsorbent. The support used for the material with the lowest amine loading was an HMS material, while the material with the largest amine loading used a PE MCM-41 support. Other mesoporous silica supports such as SBA-15,*[59]* and MCM-41*[66]* have been used with varying success in terms of loading.

In view of the loadings given above, the amine loadings of CTA's increase with the silane used, with mono<di<tri silanes. However, when normalized by the number of amines contained in each silane, the actual number of silane molecules that form bonds with the silica surface follows the order of tri<di<mono. This decrease in degree of functionalization can be explained by the size of the silane molecule, which of course is much larger for tri silane than mono silane. During functionalization, steric constraints, imposed by already functionalized regions, can prevent silane molecules from reaching some potentially reactive but sterically inaccessible silanols. Larger silanes provide more steric hindrance, and thus establish a smaller equilibrium degree of surface functionalization. This does not, on average, result in adsorbents with lower amine loadings because of the larger stoichiometric ratio of amine to silane molecule in di and tri aminosilanes. Figure 2.6 displays a histogram of amine loadings averaged for all reported mono, di, and triamine CO_2 adsorbents in the literature. This trend is echoed by the work of Yogo.*[59]* In a series of experiments, they functionalized SBA-15 with mono, di, and tri silanes, obtaining loadings of 2.7, 2.1, and 1.7 mmol silane/g adsorbent.

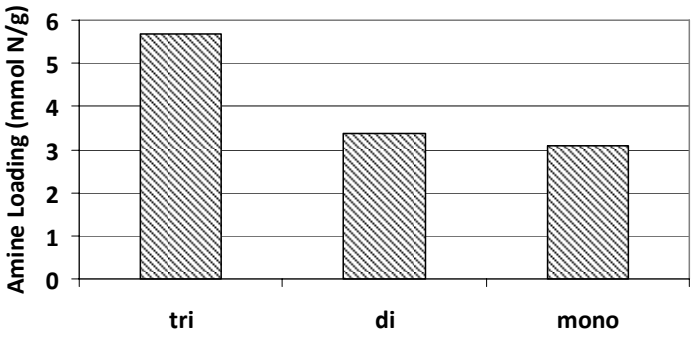

Figure 2.6. Histogram of average amine loading obtained from mono, di, and tri silanes, taken from the reviewed literature.

2.2.1.2. Other Amine-containing Silanes

Other silanes have been used to construct CTA's. Some of these possess amine moieties other than the mono, di, and tri silanes, but still provide a one step route for preparation of an adsorbent. Zelenak studied the capture efficacy of methylaminopropyl and phenylaminopropyl (both secondary amines) functionalized silicas, by using 3-(methyl)aminopropyltrimethoxysilane (MAPS) and 3-(phenyl)aminopropyltrimethoxysilane (PAPS)*[60]* (structures shown in Figure 2.20). Both silanes contain secondary amines, but because of the difference in size and basicity, they have significant differences in reactivity with CO_2. The size of the silane also has an effect on the degree of functionalization, as noted above, and loadings of 2.16 and 1.56 mmol silane/g were found for MAPS and PAPS, respectively.

Yogo studied the differences in CO_2 capture between primary, secondary, and tertiary amines by functionalizing SBA-15 with mono silane, MAPS, and 3-(dimethyl)aminopropyltrimethoxysilane (DMAPS)*[53]* (structure also shown in Figure 2.20). Again, the bulkier silane, DMAPS, resulted in a lower loading of 1.79 mmol silane/g, compared to MAPS, which gave 1.88 mmol silane/g. Many other amine-containing silanes could be studied for the synthesis of CTA's, but as the number of

functionalities on a silane increases, so does the number of synthetic steps and total cost of production, broadly speaking.

A common technique used in the organic functionalization of silica is a two-step process where silica is functionalized with alkylchloride groups and then the desired amine moieties are formed by an S_N2 reaction with amines. Tsuda*[35]* used this strategy to form silica gels from (3-(4-(chloromethyl)phenyl)propyl)trimethoxysilane (Figure 2.20) and PEI. Guliants investigated the functionalization of silica with pyrrolidine and PEI to form adsorbents by employing this strategy.*[61]* The reaction scheme for pyrrolidine is shown in Figure 2.7.

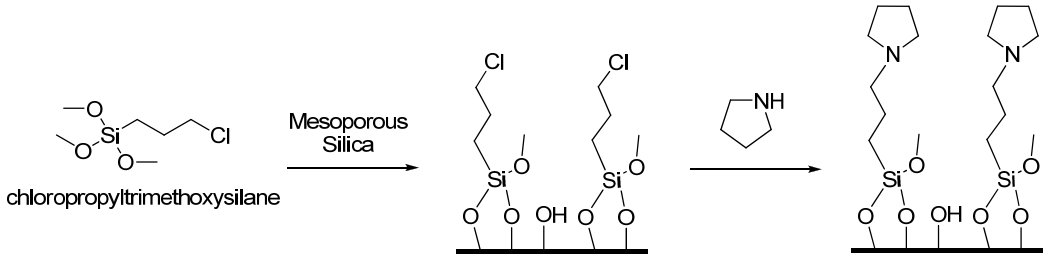

Figure 2.7. Reaction scheme for the two-step functionalization of silica with pyrrolidine.

2.2.2. Incorporation of Amines by Surface Polymerization

Silane condensation is not the only method of functionalizing oxide supports with organic material. The polymerization of reactive small molecules on silica supports has been investigated as a method to obtain organic/inorganic hybrid materials with a substantial loading of organics.

When applied to mesoporous silica, these methods take advantage of the open pore spaces of mesoporous silicas as galleries to constrain the polymerization, which can result in the formation of low molecular weight polymers.*[26]* Since the majority of the introduced organic material is contained within the porous silica, the bulk material remains a free flowing solid, similar to the bare silica support. This is a clear advantage

when compared to the “stickiness” or agglomeration experienced for many polymer resins or amine-impregnated silicas that have been overloaded with organic.

Chaffee*[68]* investigated the step-wise polymerization of melamine dendrons from monoamine SBA-15 for the preparation of CO_2 adsorbents with high amine content. Their synthetic scheme, which was derived from the scheme Shantz first reported for the formation of silica-tethered melamine dendrons,*[69]* (Figure 2.8) illustrates the growth of generational melamine units by the addition of cyanuric chloride and ethylene diamine. They reported the growth of up to 4 generations, labeled G0 through G4, with G0 representing the mono silane functionalized SBA-15 base support. These generations corresponded to amine loadings of 0.52, 2.88, 4.51, 6.75, and 7.49 mmol N/g. The N:C and N:H ratios for these materials were lower than the theoretical values for the ideal dendron structures, suggesting that incomplete growth occurred due to crosslinking or steric interference in the pore space. The authors observed a reduction in surface area and pore volume with successive generational growth, verifying that the majority of functionalization occurred within the silica pores.

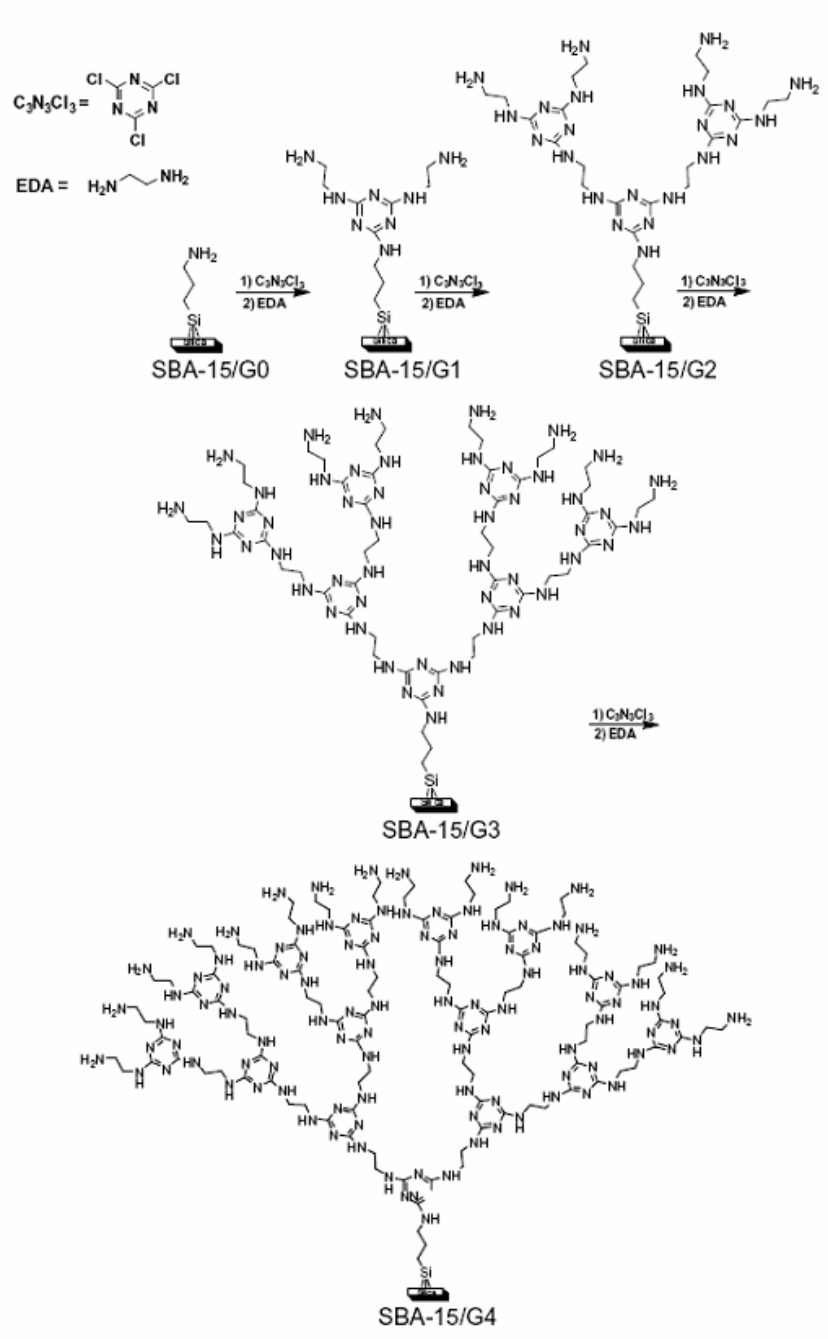

Figure 2.8. Reaction scheme for generational growth of melamine dendrons (reprinted with permission from Ref. *[68]*).

Jones*[26]* prepared adsorbents with high amine content through the polymerization of aziridine from mesoporous silica surface silanols, which they gave the name hyperbranched aminosilica (HAS). Figure 2.9 displays the reaction scheme,

whereby aziridine undergoes ring-opening polymerization in the presence of catalytic amounts of acetic acid to form hyperbranched aminopolymers that were covalently bound to the SBA-15 support. Jones reported an HAS sample to have an amine loading of 7.0 mmol N/g with a pore volume of 0.25 cc/g.

2.2.3. Role of H_2O on Amine Loading

Silanes can polymerize with themselves in the presence of H_2O through condensation of their alkoxy groups. To avoid this, most silane functionalizations of silica are done under anhydrous conditions. However, in some cases, the presence of small amounts of H_2O during silica functionalization results in larger silane loadings. Sayari*[65]* prepared CO_2 adsorbents by functionalizing PE MCM-41 with tri silane with increasing amounts of H_2O. They determined that a ratio of 0.3 mL H_2O/g silica resulted in an adsorbent with maximum equilibrium CO_2 capacity. As the H_2O to silica ratio increased beyond this point, the resulting adsorbents contained similar amine loadings but possessed decreasing equilibrium capacities. At high H_2O to silica ratios, silane polymerization was prevalent, most likely creating inaccessible amines which resulted in the decreased capacities. Adsorbents prepared under anhydrous grafting conditions resulted in about 30% lower loadings. Zheng*[64]* also used a similar ratio of H_2O to silica during silane functionalization (0.32 mL H_2O/g silica) and obtained moderate amine loadings of 2.64 mmol N/g on SBA-15 as a support. Unfortunately, Zheng did not report the preparation of adsorbents under anhydrous grafting conditions to use as comparisons.

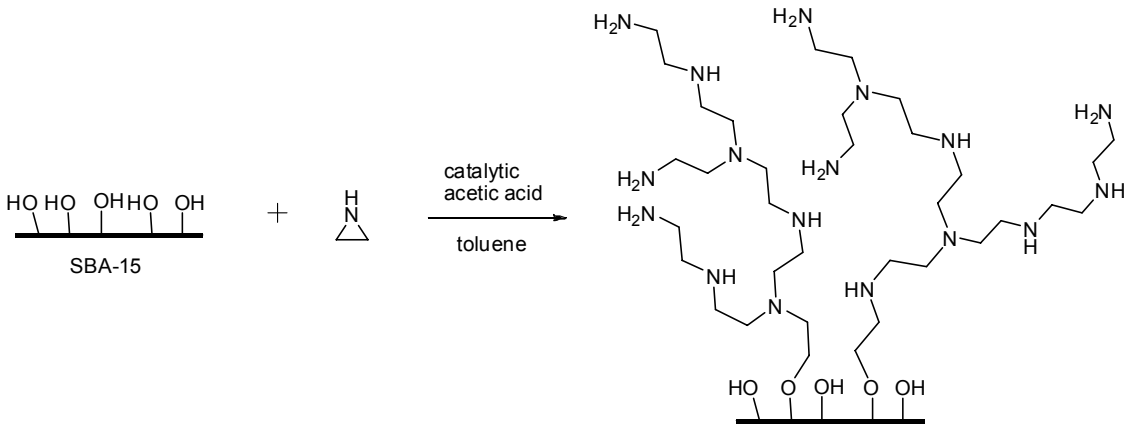

Figure 2.9. Reaction scheme for the polymerization of aziridine to form the HAS adsorbent.

Higher loadings from silane functionalization have also been obtained by hydrothermally modifying silicas. Shi*[63]* modified calcined SBA-16 by dispersing it in boiling H_2O to increase the silanol group density. The hydrothermally modified SBA-16 and unmodified calcined SBA-16 were then functionalized with di aminosilane. The amine loading of the hydrothermally modified silica was 18% higher than for the unmodified silica. The authors indicated that the increase was due to conversion of siloxane bridges on the silica surface to silanols during the hydrolysis process, producing more reactive sites for silane functionalization. To obtain the optimum amine loading from silane functionalization, a combination of hydrothermal modification of the support and H_2O-aided grafting may be used.

2.2.4. Degradation Temperature

The degradation of aminosilane functionalized silicas has been tracked by several authors. The type of amine in the CTA clearly affects the decomposition temperature. The order of stability for the three linear aminosilanes is tri<di<mono. Yang*[57]* measured FT-IR spectra of mono silane functionalized MCM-48 at several temperatures in the range of 298 to 623 K under He. They observed a slight decrease in intensity of

two NH_2 stretches (3368 and 3298 cm^{-1}) at 473 K and a complete disappearance at 623 K. Shi*[63]* determined that di functionalized SBA-16 was stable up to 473 K under N_2 using TGA. Chaffee*[55]* found that triamine functionalized HMS was stable until 443 K under N_2. Sayari*[66]* measured decomposition of triamine functionalized MCM-41 at around 433 K under N_2 but attributed this loss to evolution of methanol from unreacted methoxy groups of partially-condensed silanes. They claimed that decomposition of the amine functionalities did not begin until 523 K. Chaffee*[68]* reported a decomposition temperature of 573 K for melamine dendron functionalized SBA-15 heated under air.

The temperature at which CTA's decompose is dependent on the atmosphere under which they are heated. In highly oxygenated environments, Chaffee*[55]* found that triamine functionalized HMS degraded at 423 K, 20 K lower than in an inert environment. However, mildly oxygenated environments do not drastically affect the decomposition temperature of CTA's. Yogo*[70]* determined that mono silane functionalized SBA-15 was stable in air to 473 K by TGA, and Chuang*[21]* determined mono silane functionalized SBA-15 was stable in a 1:2 mixture of air:He until about 523 K by TGA. Thus CTA's appear to be stable for short to moderate timescales under typical (NO_x and SO_x free) flue gas capture conditions.

2.2.5. CO_2 Adsorption Capacities Under Dry Conditions

The CTA literature frequently focuses on equilibrium CO_2 capture capacity as a key evaluation metric of an adsorbent's performance. As with amine impregnated silicas, this one property does not completely describe an adsorbent's effectiveness, but should be examined along with an adsorbent's reaction kinetics, robustness, flexibility to different operating conditions, and cost.

There are a wide range of reported equilibrium capacities for mono, di, and tri silane functionalized silicas in the literature. There are several reasons for this. First, the maximum amine loadings for these adsorbents vary from 1.3 to 8.0 mmol N/g adsorbent.

If all other factors are taken to be equal, the reported equilibrium capacities should vary by a factor of 6. Secondly, different mesoporous silicas with accompanying differences in pore architecture, diameter, volume, and surface area have been used to support the amines. The resulting adsorbents therefore have different amine loadings and different gas transport properties. Finally, the conditions used to determine equilibrium capacities vary widely. Operating temperatures are reported in the range of 293 to 373 K. CO_2 partial pressures in the feed have been varied from 5 to 100%. Relative humidities in the feed have been varied from 0 to 100%. Additionally, the analytical techniques used to measure capacities at these varied conditions include TPD/MS, TGA, GC, and volumetric analysis (VA).

While measurement conditions do vary widely, certain generalities can be drawn from the literature. Except for a few cases, triamine functionalized silicas have the highest adsorption capacities, largely due to their higher amine loadings, on average. Equilibrium capacities of CTA's increased as operating temperatures decreased, except for cases where diffusion was severely hindered due to pore clogging. Furthermore, the equilibrium capacity displayed saturation dependence on CO_2 partial pressure in the feed, usually reaching a plateau around 0.2 to 0.3 bar CO_2. These dependencies of the equilibrium capacities for CTA's are important because they illustrate that large working capacities can be achieved for typical post-combustion CO_2 capture conditions.

The following discussion describes the range of reported equilibrium capacities and draws comparisons where appropriate. The amine efficiency, or amount of CO_2 captured divided by the amount of amines present for a given weight of adsorbent, is used as a tool to compare adsorbents. The amine efficiency of an adsorbent represents the degree to which it has met its theoretical capacity. Amine efficiencies less than 0.5 for anhydrous conditions and 1.0 for humid conditions reflect either amine inaccessibility or non-ideal adsorption operating conditions. Amine inaccessibility could be due to transport effects caused by material defects, such as pore blockages due to silane

polymerization. The CO_2 capacities and amine efficiencies for the CTA adsorbents are listed in Table 2.2. Identification of ideal operating conditions, which are adsorbent and process specific, are beyond the scope of this review and will not be addressed except for the description of the equilibrium capacity's dependence on temperature and CO_2 partial pressure. For an excellent discussion of the capacities of aminosilane functionalized silicas under both dry and humid conditions see the work of Sayari.*[65, 71]*

The largest reported equilibrium CO_2 capacity for mono silane functionalized silicas at modest CO_2 partial pressures (≤0.15 bar) under dry conditions was 2.05 mmol CO_2/g for a PE MCM-41 support functionalized with mono silane under H_2O-aided grafting conditions.*[71]* Adsorption with this material was measured by Sayari with a combined TGA/MS system, and the adsorbent exhibited an amine efficiency of 0.49 mol CO_2/mol N (hereafter referred to without units for simplicity) which is close to the theoretical maximum value. Large amine efficiencies of 0.39, 0.49, and 0.50, were also measured at modest CO_2 partial pressures for monoamine adsorbents prepared by Gray,*[51]* Zelenak,*[60]* and Yang,*[57]* as measured by TPD/MS, TGA, and TPD/MS, respectively.

The largest reported equilibrium CO_2 capacity for diamine functionalized silicas at modest CO_2 partial pressures (≤0.15 bar) under dry conditions was 0.87 mmol CO_2/g for an SBA-15 support*[59]* measured by GC. This material exhibited an amine efficiency of 0.21, which was slightly less than the highest reported value for diamines of 0.28.*[26]* Larger capacities of 1.95 and 1.40 mmol CO_2/g and their corresponding amine efficiencies of 0.74, and 0.85, were measured at CO_2 partial pressures of 1 bar for diamine adsorbents prepared by Zheng*[64]* and Hornebecq,*[62]* with MS and VA, respectively.

The largest reported equilibrium CO_2 capacity for triamine functionalized silicas at modest CO_2 partial pressures (≤0.15 bar) under dry conditions was 2.65 mmol CO_2/g for a PE MCM-41 support functionalized with tri silane under H_2O-aided grafting

conditions.*[65]* Adsorption was measured with a combined TGA/MS system, and the adsorbent exhibited an amine efficiency of 0.33, which was the highest reported value for triamines. A comparable amine efficiency of 0.29 was measured using TGA at a high CO_2 partial pressure for triamine adsorbents prepared by Chaffee.*[55]*

Zelenak*[60]* studied a set of materials prepared by functionalizing SBA-12 with mono silane, MAP, and PAP to determine the reactivity difference of primary and secondary amines and the effect of amine basicity on CO_2 affinity. Amine efficiencies were measured with TGA in the order of PAP<MAP<mono under dry conditions (0.43, 0.45, and 0.49) which corresponded to capacities of 0.68, 0.98, and 1.04 mmol CO_2/g. These results suggest that supported primary amines were slightly more reactive than secondary amines for CO_2 capture. Under dry conditions, the stronger base should be more efficient at deprotonating the zwitterion and give higher capacity, which is likely what is seen when the capacities of MAP and PAP are compared. Monoamine and MAP have about equal base strength with pK_B ~4, while PAP is a much weaker base with a pK_B = 8.9. Therefore, amine basicity is an important factor to consider when selecting amines for CO_2 adsorbents.

The reactivity of primary, secondary, and tertiary amines was also investigated by Yogo.*[53]* SBA-15 was functionalized with mono silane, MAPS, and DMAPS, obtaining amine loadings of 2.61, 1.88, and 1.79 mmol N/g, respectively. They measured dry capacities of 0.05, 0.25, and 0.66 mmol CO_2/g adsorbent and amine efficiencies of 0.03, 0.13, and 0.25 for DMAPS, MAPS, and mono silane functionalized SBA-15, respectively, by GC. These results further confirm that, in general, the order of reactivity of amine type with CO_2 is primary>secondary>tertiary.

There is evidence in the literature that amine proximity affects the amine efficiency of monoamine adsorbents. For anhydrous capture, the zwitterion mechanism suggests that two amines are required to capture one molecule of CO_2. Yogo reported a slight increase in amine efficiency with an increase in average amine surface density

from 2.5 to 4 amines/nm^2,*[59]* and a near linear increase from about 1 to 3 amines/nm^2*[53]* for monoamine SBA-15. However, for average densities below 1 amine/nm^2, Chaffee*[56]* concluded that there were no significant increases in capture efficiency under anhydrous conditions and a 90% CO_2 feed than from that of the bare solid. This suggests that the amines are too far apart to capture CO_2 at this density and the material instead captures by physisorption, which supports the dual amine capture mechanism.

The remaining pore volume of an adsorbent after functionalization appears to affect the magnitude of its equilibrium capacity. The pores of the adsorbent must be sufficiently large to allow facile diffusion of CO_2. If pores become partially blocked due to dense functionalization and formation of carbamates and carbonates, the diffusion of CO_2 into the interior pore space of an adsorbent will be limited. This effect would result in low amine efficiencies for highly loaded adsorbents with small to medium sized pores. This effect can be seen for adsorbents prepared by Yogo*[59]* where SBA-15 was impregnated with mono silane that polymerized with itself and then formed bonds to the silica surface. This resulted in an adsorbent with a high amine loading of 6.0 mmol N/g but no measurable internal pore volume, presumably due to blocking of the pores with polymerized silane. When measured by GC under anhydrous conditions, this adsorbent had a capacity of 0.16 mmol CO_2/g, which corresponded to an amine efficiency of 0.03. The adsorbents prepared by Tsuda*[34]* were derived from the polymerization of silanes to create amorphous gels. Although no porosity or surface area data were reported for these materials, it is likely that many amines were inaccessible since they obtained an amine efficiency of 0.09 as measured by GC.

Guliants*[61]* determined a CO_2 capacity of 0.42 mmol CO_2/g for PEI substituted, chloropropyl silane functionalized, MCM-48, under dry conditions with GC, which is about half of the capacity measured for monoamine MCM-48 under the same conditions. The amine efficiency for this material was 0.08 and very little pore volume existed after

functionalization (0.02 cc/g), suggesting that many of the amines in the PEI were inaccessible due to nearly complete pore filling. Pyrrolidine substituted, chloropropyl silane functionalized, MCM-48, prepared by Guliants in the same study performed poorly for different reasons. Despite a large existing pore volume of 0.45 cc/g in the tertiary amine functionalized silica, a low adsorption capacity of 0.28 mmol CO_2/g and amine efficiency of 0.19 were measured. This is likely due to the poor reactivity of tertiary amines with CO_2 under the conditions used.

The capacities of adsorbents prepared by polymerization tell a more complicated story. The melamine dendron SBA-15 adsorbents prepared by Chaffee*[68]* possessed dry capacities of 0.45, 0.82, 0.80, 0.77, 0.98, and 0.25 mmol CO_2/g adsorbent for bare SBA-15, G0, G1, G2, G3, and G4 respectively. Under their adsorption conditions (293 K, 90% CO_2/10% Ar, 70 mL/min, measured by TGA), the bare SBA-15 support adsorbed a large amount of CO_2, which makes determining amine efficiency difficult. If 0.45 mmol CO_2/g adsorbent is subtracted from the reported values and the remainder divided by the amine loading for each generation, the amine efficiencies are calculated to be 0.70, 0.12, 0.07, 0.08, and -0.03 mol CO_2/mol N for G0 through G4 adsorbents. An amine efficiency of 0.70 is unrealistic for dry conditions and a negative amine efficiency is unrealistic for any situation. These inconsistencies suggest that different proportions of the total reported capacities are due to physisorption of CO_2 rather than chemisorption by amines. Thus, while it is impossible to accurately assess the efficiency of the amines in the melamine dendron adsorbents from the reported values, it is reasonable to state that the efficiency decreases markedly from the base G0 material to the later generations. The reduction in pore volume of the successive generations is likely a contributing factor to this decrease in amine efficiency, as G2 through G4 materials have pore volumes below 0.2 cc/g. Another possible reason for poor amine efficiency of the higher generations is the estimated reduced basicity of the secondary amines present in the adsorbents due to their conjugation with neighboring triazine rings.

2.2.6. CO_2 Adsorption Capacity: Effect of CO_2 Partial Pressure, Adsorption Temperature, and ΔH_{ads}

At typical flue gas CO_2 partial pressures of 0.10 to 0.15 bar, most CTA's exhibit sufficiently high capacities to adsorb CO_2 efficiently. Many researchers have determined adsorption isotherms for CTA's. Leal,*[36]* Yang,*[57]* Guliants,*[61]* and Sayari*[54]* have all reported isotherms for monoamine silicas as measured by VA, GC, TGA, and TGA/MS, respectively (Figures 2.10-2.12). Zheng,*[64]* Chuang,*[33]* and Hornebecq*[62]* have all reported isotherms for silica supported diamines as measured by TGA/MS, MS, and VA, respectively (Figures 2.12 and 2.13). There have not been any isotherms reported for triamine silicas. The isotherms typically transition from the Henry's Law regime to a region of smaller changes in capacity with changing pressure around 0.1 to 0.2 bar partial pressure of CO_2. Most of the isotherms are reported for CO_2 partial pressures in the range of 0 to 1 bar, but Hornebecq*[62]* reported the partial pressure dependence of capacity for two diamine silicas in the range of 1 to 30 bar. He compared these isotherms with those of the unfunctionalized support and found that at partial pressures above 2 to 5 bar, the bare supports had larger capacities. At high pressures, bare silica captured CO_2 through physisorption onto the silica framework, while CTA's captured via physisorption on any bare framework and chemisorption by the amines. The functionalization of silica with amines reduced the number of physisorption sites and the pore volume of the support. Therefore, at high pressures, physisorption was hindered by the presence of amines in CTA's, which caused a reduction in the total adsorption capacity at high pressures.

Table 2.2. CO_2 capacities and measurement conditions for CTA adsorbents.

				dry		humid			
Silane	Support	T (K)	pCO_2 (bar)	q [a] (mmol/g)	eff. [b] (mol CO_2/mol N)	q [a] (mmol/g)	eff. [b] (mol CO_2/mol N)	Method [c]	ref.
di	SBA-15	295	0.15	0.57	0.22			MS	*[64]*
di	SBA-15	295	1	1.95	0.74			MS	*[64]*
di	SBA-15	303	0.1			0.79		MS	*[33]*
di	SBA-15	333	0.15	0.87	0.21	0.9	0.21	GC	*[59]*
di	SBA-16 (hydrothermally modified)	333	0.15	0.73	0.24			TGA	*[63]*
di	SBA-16	333	0.15	0.59	0.23			TGA	*[63]*
di	SBA-16 (solvent extracted)	300	1	1.4	0.85			VA	*[62]*
di	SBA-16	300	1	0.8	0.15			VA	*[62]*
di	SBA-15	333	0.15	0.66	0.14	0.65	0.14	GC	*[53]*
di	silanes	303	0.67	1.2	0.12	1.47	0.15	GC	*[34]*
mono	SBA-15	298	0.1	2.01	0.40	2.01	0.40	TPD/MS	*[51]*
mono	HMS	293	0.9	1.59	0.65			TGA	*[56]*
mono	davison 62	300	1	0.41	0.32	0.93	0.73	GC	*[36]*
mono	MCM-48	298	0.05	1.14	0.50			TPD/MS	*[57]*
mono	MCM-48	298	1	0.8	0.33			TGA	*[61]*
mono	SBA-15	333	0.15	0.52	0.19	0.5	0.19	GC	*[59]*
mono	SBA-15	298	0.1			0.73		MS	*[21]*
mono	SBA-12	298	0.1	1.04	0.49			TGA	*[60]*
mono	PE-MCM-41	298	0.05	2.05	0.49	3.27	0.78	TGA/MS	*[71]*
mono	SBA-15	333	0.15	0.25	0.10	0.25	0.10	GC	*[53]*
mono	SBA-15	298	0.04	0.33	0.09	0.36	0.09	TPD/MS	*[58]*
tri	SBA-15	333	0.15	1.1	0.22	1.21	0.24	GC	*[59]*
tri	HMS	293	0.9	1.34	0.29	0.95	0.21	TGA	*[55]*
tri	HMS	348	0.9	0.45	0.10			TGA	*[55]*
tri	MCM-41	298	0.05	0.97	0.17	1.01	0.18	TGA/MS	*[66]*
tri	PE-MCM-41	298	0.05	1.41	0.24	1.52	0.25	TGA/MS	*[66]*
tri	PE-MCM-41	298	0.05	2.65	0.33	2.94	0.37	TGA/MS	*[65]*
tri	SBA-15	333	0.15	1.36	0.23	1.51	0.26	GC	*[53]*
tri	silanes	303	0.67	0.72	0.05			GC	*[34]*
MAP	SBA-12	298	0.1	0.98	0.45			TGA	*[60]*
PAP	SBA-12	298	0.1	0.68	0.44			TGA	*[60]*
MAP	SBA-15	333	0.15	0.25	0.13	0.25	0.13	GC	*[53]*
DMAP	SBA-15	333	0.15	0.05	0.03	0.05	0.03	GC	*[53]*
cl-PEI	MCM-48	298	1	0.40	0.08			TGA	*[72]*
cl-pyr	MCM-48	298	1	0.30	0.20			TGA	*[72]*
melamine dendrons	SBA-15	293	0.9	0.98	0.41			TGA	*[68]*
HAS	SBA-15	298	0.1			3.11	0.44	MS	*[26]*

[a] Reported CO_2 capacity
[b] Amine efficiency
[c] Method of analysis: thermogravimetric analysis (TGA), gas chromatography (GC), temperature programmed desorption (TPD), mass spectrometry (MS), and volumetric apparatus (VA).

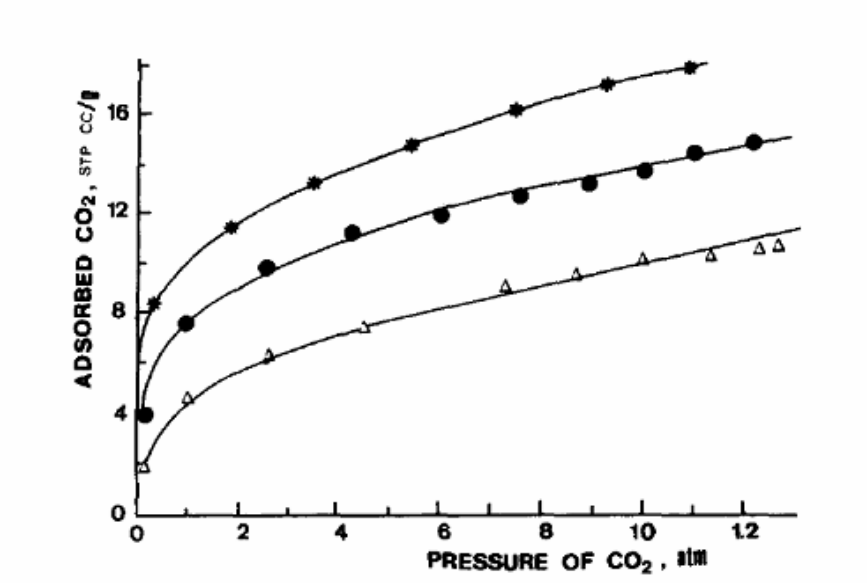

Figure 2.10. CO_2 adsorption isotherms for mono silane functionalized Davison grade 62 silica gel at three temperatures: ⁕, 273; ●, 296; and Δ, 323 K (reprinted with permission from Ref. *[36]*).

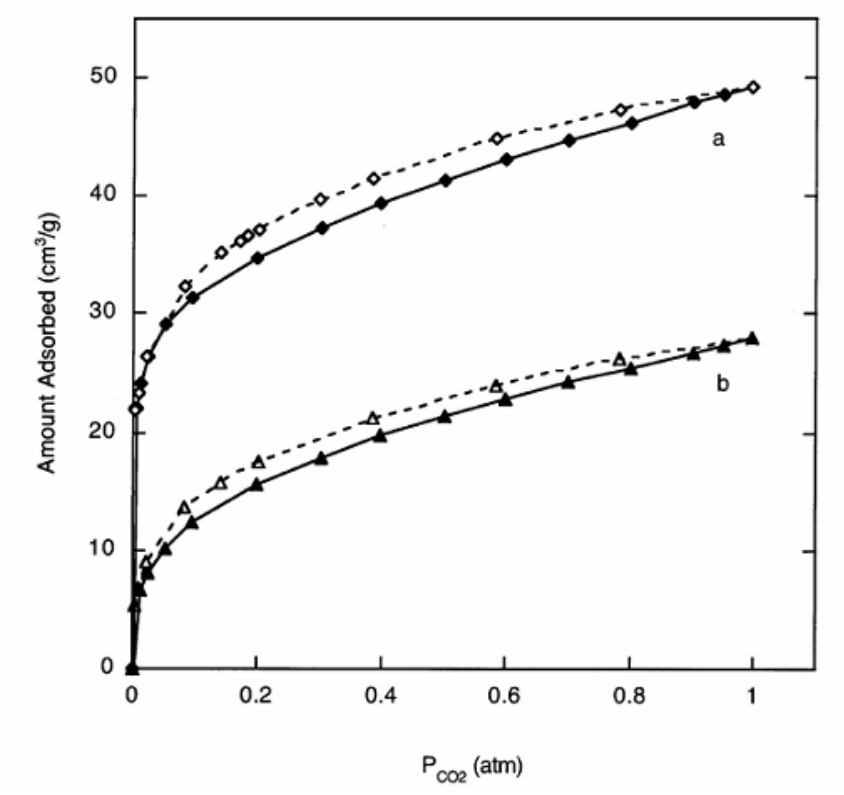

Figure 2.11. CO_2 adsorption/desorption isotherms for mono silane functionalized (a) MCM-48 and (b) xerogel at 298 K. Open symbols are for desorption and solid symbols are for adsorption (reprinted with permission from Ref. *[57]*).

Larger amine efficiencies have been reported for CTA's than are physically possible considering only a chemisorption mechanism at amine sites. Chaffee*[56]* measured a capacity of 1.59 mmol CO_2/g with TGA for monoamine HMS, which corresponds to an amine efficiency of 0.65 at a CO_2 partial pressure of 0.90 bar. Zheng*[64]* and Hornebecq*[62]* reported similar results at a partial pressure of 1 bar. It is likely that at these moderate pressures, the silica support physically adsorbs a substantial amount of CO_2. The resulting equilibrium capacity would be a combination of physical and chemical adsorption, leading to higher perceived amine efficiencies. Indeed, Sayari*[54]* reported this phenomenon for bare PE MCM-41 at a CO_2 partial pressure of 1 bar by measuring a capacity of 0.65 mmol CO_2/g with TGA/MS. Therefore, capacities of CTA's at moderate to high partial pressures of CO_2 should be interpreted with the knowledge that physisorption by the support is important.

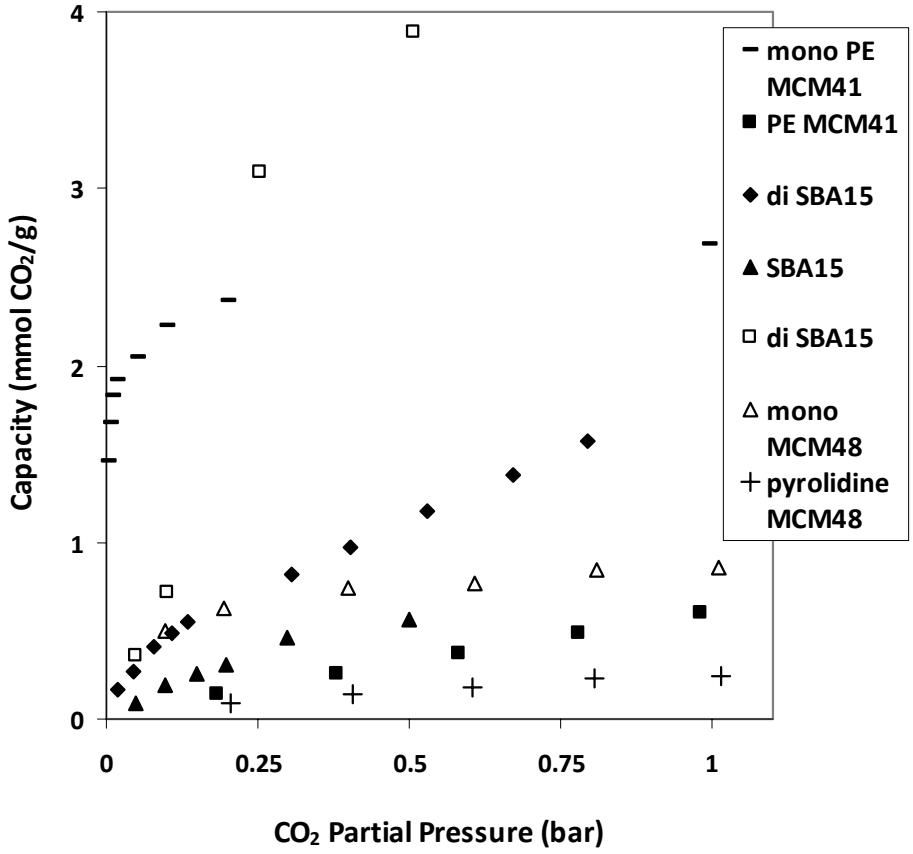

Figure 2.12. Adsorption isotherms of mono silane and pyrolidine functionalized MCM-48 at 298 K (dry, open triangles and crosses, respectively),*[61]* unfunctionalized and mono silane functionalized PE MCM-41 (dry, closed squares and dashes, respectively) at 298 K,*[71]* unfunctionalized and di silane functionalized SBA-15 (dry, closed triangles and diamonds, respectively) at room temp.,*[64]* and di silane functionalized SBA-15 (wet, open squares).*[33]*

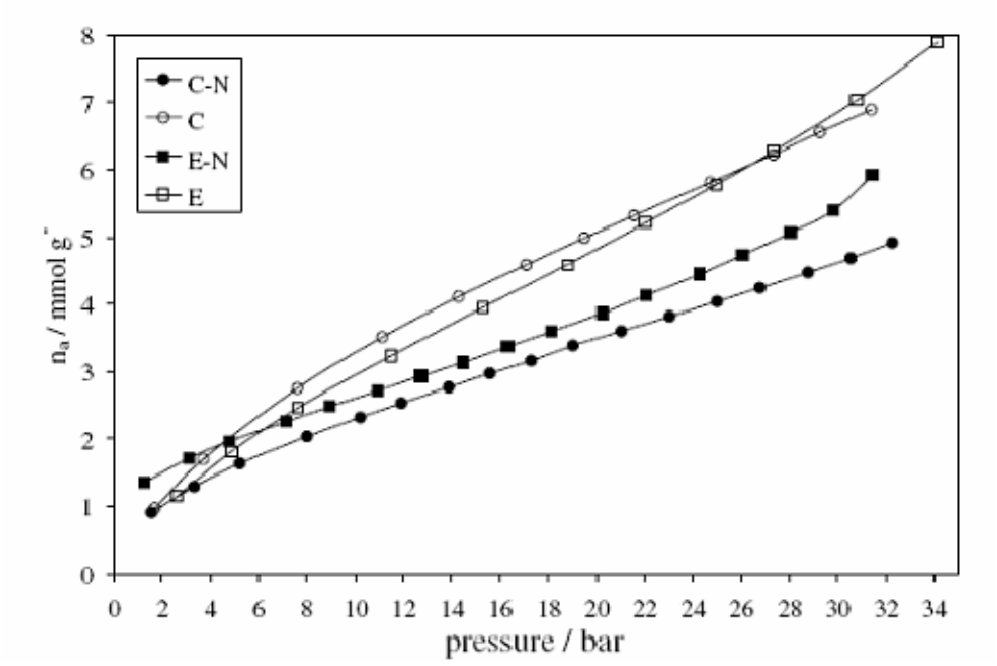

Figure 2.13. Adsorption isotherms at 300 K for calcined SBA-16 (C), solvent-extracted SBA-16 (E), di silane functionalized C (C-N), and di silane functionalized E (E-N) (reprinted with permission from Ref. *[62]*).

According to thermodynamics, equilibrium CO_2 capacity should increase as operating temperature decreases, because both the heat of adsorption and the change in entropy are negative for adsorption. Yogo*[53]* measured a linear decrease in capacity as a function of temperature from 333 to 373 K for triamine functionalized SBA-15 at three different CO_2 partial pressures (15%, 5%, and 1%) with GC. Leal*[36]*, Chaffee*[55]*, and Jones*[26]* measured similar decreases in capacities, albeit with different magnitudes. For adsorbents with hindered diffusion, an increase in operating temperature can cause an increase in CO_2 capacity. Guliants*[61]* used TGA to measure a 67% higher capacity for PEI functionalized MCM-48 when the operating temperature was increased from 323 to 373 K. Similar behavior has been observed for amine-impregnated silicas whose pores were mostly filled with organic material (see section 2.1.5).

The heat of adsorption of CO_2 by amines dissolved in aqueous solution has been reported to be in the range of -48 to -84 kJ/mol.*[73]* The reported values for CTA's

largely fit in this range. The highest heat of adsorption of -73 kJ/mol was reported by Shi*[63]* for di silane functionalized, hydrothermally-modified, SBA-16, by DSC analysis at 333 K. The lowest heat of adsorption reported, -48 kJ/mol, was also reported for diamine silica (SBA-15).*[33]* However, this value was estimated by FT-IR spectrum analysis by subtracting desorption spectra from adsorption spectra and inferring CO_2 capacities, and should be considered a lower bound on the binding energy. Heats of adsorption for monoamine and triamine silicas have been reported between these two values. Shi observed an increase in the heat of adsorption of diamine functionalized SBA-16 as amine loading increased*[63]* and Chaffee*[55]* observed a similar increase as the number of tethers/nm^2 increased for triamine functionalized HMS. The heat of adsorption for bare silica has been measured to be in the range of -20 to -35 kJ/mol.[163, 169, 170, 173] Thus, as amines are added to the material, the heat of adsorption should increase from that of the bare silica and approach that of bulk amines in solution, corresponding to a change from physical to chemical adsorption. This trend is shown in Figure 2.14 for literature reported values.*[36, 55, 56, 62, 63]*

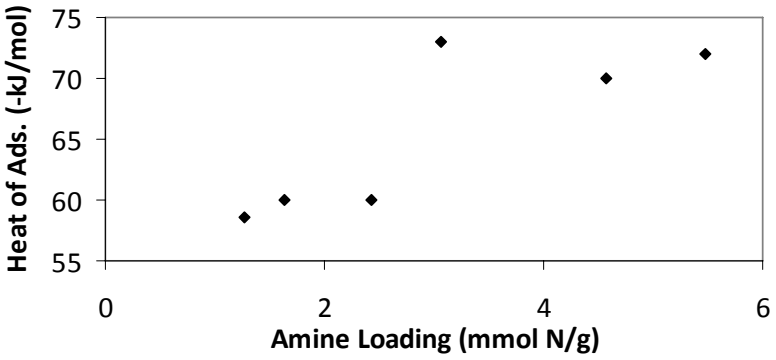

Figure 2.14. Increase of heat of adsorption for covalently-tethered amines as a function of amine loading; from literature values. *[36, 55, 56, 62, 63]*

Hornebecq*[62]* used VA to determine the CO_2 partial pressure dependence of the heat of adsorption for diamine SBA-16 (Figure 2.15). Starting at values between -70 to -

80 kJ/mol at CO_2 partial pressures below 0.5 bar, the heats of adsorption sharply decrease to ~-30 kJ/mol at 1.5 bar, and become approximately constant (within 10 kJ/mol) at higher pressures; reaching -20 to -25 kJ/mol at nearly 6 bar.

2.2.7. Effect of H_2O on CO_2 Capacity

As previously discussed, under humid conditions, amines can capture CO_2 through the formation of carbonates and bicarbonates in addition to the carbamates usually formed under dry conditions. Several reports have verified the formation of these structures by FT-IR spectroscopy and are discussed in section 2.1.10. There was an average increase of 15% in the capacities and amine efficiencies of CTA's under humid conditions where both dry and humid adsorption was reported.*[34, 36, 51, 53-55, 58, 59, 65, 66]* In fact, the largest capacities reported in the literature for CTA's have been under humid conditions. The largest reported capacities for mono, di, and triamine silicas were 3.27, 1.47, and 2.94 mmol CO_2/g, respectively. They were reported by Sayari,*[54]* Tsuda,*[34]* and Sayari*[65]* and measured by TGA/MS, GC, and TGA/MS, respectively. Jones*[26]* measured by MS the largest capacity of 3.1 mmol CO_2/g for CTA's prepared by polymerization for the HAS adsorbent.

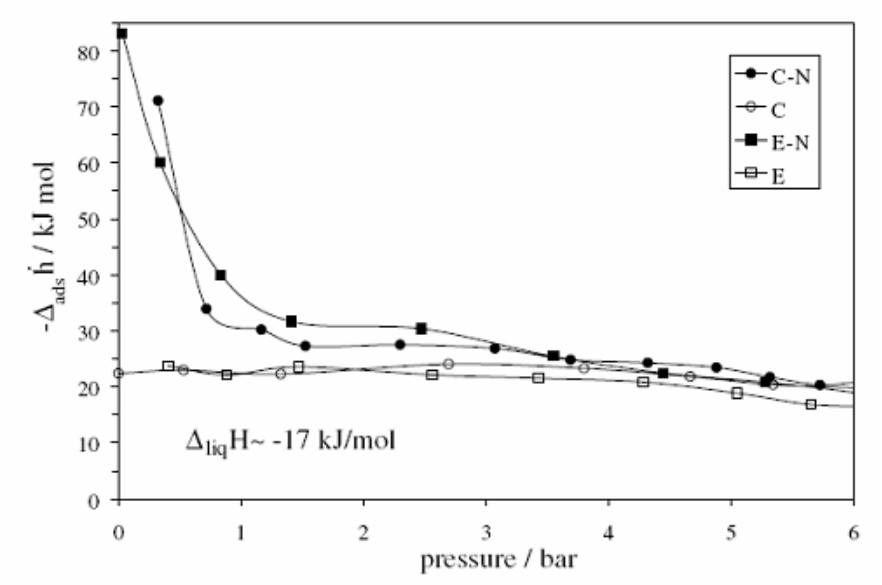

Figure 2.15. Pressure dependencies of the heats of adsorption of calcined SBA-16 (C), solvent-extracted SBA-16 (E), di silane functionalized C (C-N), and di silane functionalized E (E-N) (reprinted with permission from Ref. *[62]*).

Zheng*[64]* and Yogo*[53, 59, 70]* both reported either small or no gains in CO_2 capacity using CTAs in the presence of H_2O by MS and GC. Both groups studied multiamine (di and tri) functionalized SBA-15 with relatively short (less than 20 minutes) adsorption measurements. Chaffee*[56]* observed two phases during adsorption with monoamine silica with TGA. They attributed the first phase, which was rapid, to the formation of carbamates, due to the similarity in rate to that of dry adsorption, for which mechanism was clear. The second adsorption phase was much slower and was postulated by the authors to be due to the formation of carbonates and bicarbonates. Indeed, Kenig*[29]* found that the rate of carbamate formation was much faster than the rate of carbonate formation for CO_2 adsorption with aqueous amines. Yogo*[53]* tracked humid adsorption with mono, di, and triamine silicas by FT-IR spectroscopy and only detected formation of carbamates (3300 to 3370 cm^{-1}) over the 5 minute length of the adsorption experiment. This supported the hypothesis that humid adsorption by CTA's occurs by the

quick formation of carbamates followed by the slow conversion to carbonates and bicarbonates.

A number of different experimental procedures and apparatuses have been used to measure CO_2 capacity in the literature. When adsorption was measured under humid conditions, it has sometimes been the practice to pre-hydrate the adsorbent by exposing it to humid inert gas before switching to humid CO_2. However, when this process is monitored by gravimetric methods, it can be difficult to discern the difference between weight gain solely due to CO_2 adsorption or due to simultaneous desorption of H_2O and adsorption of CO_2. Indeed, Sayari*[54]* measured comparable dry CO_2 capacities by MS and TGA, but found that TGA under-predicted the capacity for humid adsorption by pre-hydrated adsorbents. Therefore, it is possible that the effect of H_2O on CO_2 adsorption capacity has been missed or underestimated in some reports.

The concentration of H_2O during adsorption affects the synergistic increase in capacity compared to the dry case. Sayari*[54]* measured an increase in capacity of 20 to 79% for prehydrated monoamine silica when the relative humidity was increased from 27 to 74%. Higher relative humidity was not studied because above 74%, capillary condensation was detected in the pores of the adsorbent. At this level of wetting, the amines were in a partially solvated environment and adsorption most likely occurred in a similar manner to adsorption with aqueous amines. It is possible that many adsorbents used under humid conditions have reached this partially solvated state, which may lead to misleading conclusions about their adsorption and desorption kinetics.

2.2.8. Desorption Temperature, Regeneration, and Feed Impurities

The capacities of CTA's are generally considered to be fully regenerable, provided desorption is performed under sufficient conditions. Zheng*[64]* found diamine SBA-15 to have a fully regenerable humid capacity when the adsorbent was desorbed by inert purge under heating from 408 to 423 K. Yogo*[59, 70]* determined a fully

regenerable humid capacity for mono and triamine SBA-15 when the adsorbent was desorbed by inert purge under heating to 423 K. Chaffee*[56]* determined a fully regenerable dry capacity for monoamine HMS when the adsorbent was desorbed by inert purge at 293 K. This is the only case in the CTA literature suggesting complete regeneration without significant heating. However, there are a number of reports of incomplete desorption when only an inert purge was used.*[52, 58, 60]* Chaffee*[68]* reported incomplete desorption (30% loss in capacity) of melamine dendron silicas with only an inert purge but complete regeneration when the adsorbents were heated to 378 K under an inert gas flow. Therefore, it can be concluded that for most CTA's, regeneration must be performed at a moderately elevated temperature. The exact temperature at which desorption should be performed is adsorbent specific, but most reports use at least 373 K. Zheng*[64]* observed the main weight loss peak (temperature at which the absolute value of the first derivative of the weight loss was greatest) from CO_2 desorption with diamine SBA-15 in He at 372 K by TGA. The main weight loss peak from CO_2 desorption in air occurred at 387 K. In an actual industrial process however, it is likely impractical to desorb with an inert purge. However, to our knowledge, desorption of CTA adsorbents with steam or vacuum has not been studied. Such studies are critically important, as practical desorption for carbon capture and sequestration (CCS) will likely not involve inert purging.

The temperature at which desorption occurs depends on the type of amine used and the structure formed with CO_2. Yogo*[70]* measured the decomposition of the CO_2-amine complex formed by adsorption with mono, di, and tri silane functionalized SBA-15 by TGA under He. They determined that the temperature at which the derivative of the weight loss was maximum increased in the order of mono<di<tri silane functionalized SBA-15, suggesting that triamine more strongly interacted with CO_2 than monoamine, possibly because of the potential formation of intramolecular bidentate species. Guliants*[61]* observed a lower desorption temperature for pyrrolidine MCM-48 than for

monoamine MCM-48, giving further evidence that the interaction of CO_2 with tertiary amines is of lower energy than that with primary and secondary amines.

There are a number of different structures that can be formed when CO_2 adsorbs in the presence of multiple amines, including the formation of bidentate species that have stronger binding energies than monodentate species. The number of bidentate species formed during adsorption can change over adsorption/desorption cycles. Chuang*[58]* observed a decrease in the heat of desorption accompanied with an increase in the formation of bidentate carbonate species over several regeneration cycles when the adsorbents were desorbed with helium and H_2O. Since carbonates are only formed in the presence of H_2O, this suggested that humid desorption results in the displacement of CO_2 by H_2O that hydrogen bonds with the amines. Subsequent adsorption resulted in the formation of carbonates due to the close proximity of H_2O and amines.

The additional components of flue gas such as NO_x, SO_x, and O_2 have been shown to adversely affect adsorption with aqueous amines under certain conditions.*[74]* It is therefore reasonable to expect that these components will also hinder CO_2 adsorption with CTA's. Unfortunately, not much work has been done to explore this hypothesis, or to quantify the interaction strengths of these contaminants with supported amine sites. Chuang*[21]* tracked the humid adsorption of SO_2 by FT-IR spectroscopy and observed reductions in N-H stretches in the presence and absence of H_2O. TPD resulted in a negligible change to these bands and minor changes in the sulfate/sulfite bands, suggesting irreversible bonding of SO_2 with amines. Subsequent attempts to capture CO_2 with these adsorbents were unsuccessful, further supporting the conclusion that the adsorbents were irreversibly poisoned with SO_2. In addition to interactions with NO_x and SO_x present in flue gas, there is the potential for amines to be oxidized by O_2 present in the gas, especially at elevated temperatures. Indeed, Zheng*[64]* observed oxidation of diamine SBA-15 during TGA under air at 473 K. This oxidation is likely irreversible.

2.2.9. Adsorption and Desorption Kinetics

The kinetics of CO_2 adsorption and desorption with CTA's is just as important a measure of performance as equilibrium capacity. For CTA's to be used in practical applications, adsorption/desorption cycles most likely have to be completed on the order of minutes. CTA's seem promising candidates to meet this goal. However, the method of measurement appears to make a large difference in the measured kinetics. Several authors have measured kinetics with the adsorbent in a packed bed configuration where the effluent CO_2 concentration was measured with MS or GC. Yogo*[59]* measured the breakthrough kinetics of mono silane impregnated SBA-15 and triamine SBA-15 in a flow system connected to a GC. Monoamine impregnated SBA-15 had a breakthrough time of almost zero when 1.5 g of the adsorbent was exposed to 30 mL/min of 15% CO_2, 12% H_2O, and balance N_2 at 333 K. This adsorbent had no measurable pore volume, possibly due to silane condensation at the pore mouths of the silica, thus, the kinetics of adsorption were severely reduced. By contrast, a triamine SBA-15 with a pore volume of 0.37 cc/g displayed a breakthrough time of 8 minutes. In a later report,*[53]* Yogo measured the humid adsorption kinetics of mono, di, and triamine SBA-15 in a flow system by GC. They measured breakthrough times of 4, 11, and 13 minutes, respectively, under a flow of 15% CO_2, 12% H_2O, and balance N_2 at 30 mL/min, which corresponded to 82, 97, and 97% of their equilibrium capacities.

Other authors have measured kinetics by gravimetric methods such as TGA. Chaffee*[56]* observed near complete uptake for mono silane functionalized HMS after 10 minutes for dry conditions, with an adsorption halftime of about 1.5 minutes. Yang*[57]* determined that 80% of its equilibrium capacity was reached after 30 minutes under dry conditions, with an adsorption halftime of around 5 minutes. Sayari*[66]* measured an adsorption halftime of about 1.5 minutes for triamine functionalized PE MCM-41 under dry conditions. They also determined that the maximum adsorption rate for a range of materials synthesized with different silane concentrations (which resulted in a range of

final amine loadings) displayed a saturation dependence. In a later study,*[65]* Sayari examined the effect on adsorption rate of other changes in the synthesis, such as synthesis temperature and amount of H_2O added to the adsorbent synthesis. They obtained a maximum adsorption rate of 1.79 mmol CO_2/g*min for triamine silica prepared at 358 K with the addition of 0.3 ml H_2O/g silica. This adsorbent reached 80% of full capacity in 1.5 minutes under dry conditions. Zelenak*[60]* measured a slower maximum uptake rate of 0.24 mmol CO_2/g*min for monoamine SBA-12 under dry conditions. This may be due to the four-fold lower number of amines contained in the Zelenak adsorbent compared to the Sayari adsorbent or it may be reflective of the difference in silica support or analysis conditions. This example illustrates the need for consistency when comparing not only the capacity of adsorbents but also the adsorption kinetics.

2.2.10. Structure of Adsorbed CO_2

The adsorption of CO_2 with CTA's has been monitored with FT-IR spectroscopy by several researchers. When CO_2 reacts with amines under anhydrous conditions, only the formation of carbamate is considered possible. Under humid conditions, four additional species can form: monodentate carbonate, bidentate carbonate, monodentate bicarbonate, and bidentate bicarbonate. There is some disagreement regarding the FT-IR spectroscopy assignment of some of these species. Chuang*[58]* assigns the carbamic acid species to bands at 1595, 1441, and 1330 cm^{-1}, while Yogo*[53, 70]* assigns the bands at 1628, 1563, and 1488 cm^{-1}. Zheng*[64]* only reported one band at 1576 cm^{-1} for the formation of carbamate. Lastly, Tsuda*[34]* observed an increase of two bands assigned to ammonium carbamates at 1580 and 1330 cm^{-1}.

Chuang*[21, 33, 58]* reported the formation of monodentate carbonate from 1337-1363 cm^{-1}, bidentate carbonate from 1541-1575 cm^{-1} and 1390 cm^{-1}, monodentate bicarbonate from 1470-1493 cm^{-1} and 1422-1432 cm^{-1}, and bidentate bicarbonate from 1628-1634 cm^{-1}. These carbonate species were assigned during humid CO_2 capture, but

Yogo did not observe these species during humid runs. In fact, Yogo reported almost no change in the FT-IR spectra taken from dry and humid runs. It is important to note that these spectra were taken after 5 minutes of exposure to CO_2. It has been theorized that humid adsorption first occurs by the formation of carbamate species followed by conversion to carbonates. Therefore, it is possible that adsorption was not monitored for a sufficient length of time to observe this conversion. However, Chuang,*[58]* with a different adsorbent and a different experimental setup, measured spectra at 0.06, 0.31, 0.49, 0.68, and 4.01 minutes during humid CO_2 adsorption and observed an increase in intensity for all species, not a transition from carbamates to carbonates. Again, it may be that adsorption was not monitored for a sufficient length of time to see conversion to carbonates. Alternatively, the adsorbed species formed may vary greatly with different adsorbents and adsorption conditions. Further investigations with different types of aminosilicas need to be conducted to ascertain the nature of the products formed from these reactions.

Chuang*[33]* performed several FT-IR spectroscopy studies to determine the relative strengths of these carbonate species. Concentration swing experiments showed that bidentate carbonates, and to a lesser extent monodentate bicarbonates, were weakly bound and could be desorbed by partial pressure driving force. TPD experiments suggested that bidentate bicarbonates and bidentate carbonates were efficiently desorbed by temperature swing. Similar results were obtained when these studies were performed on mono and diamine SBA-15, suggesting that bidentate species were mainly intermolecular and not intramolecular. In a later report,*[21]* Chuang observed a decrease in the formation of carbonate and bicarbonate species as adsorption temperature increased.

2.3. Amines Supported on Solid Organic Materials

There have been a number of organically-supported amines (OSA) investigated in the literature as CO_2 adsorbents. There are several different configurations of these adsorbents, including amine-functionalized porous carbons, organic resins, and polymers. However, they are all similar in that they rely on chemisorption with amines, at least in part, as the mechanism of capture. Although realistic process configurations are not often investigated for these adsorbents, as materials, they offer promising alternatives to other adsorbents that primarily have been tested in fixed bed configurations. Descriptions of these adsorbents and their properties are given in the following sections.

2.3.1. Carbon-supported Amines

Carbon is available in several commercially available forms, such as porous activated carbon, fly ash, graphite, diamond, graphene and carbon nanotubes. By themselves, carbonaceous solids have been shown to capture CO_2, especially under moderate to high pressures.*[15]* However, when functionalized by amines, these carbons can be capable of both chemical and physical adsorption. One way of incorporating amines into carbons is to apply simple impregnation methods. Pis*[75]* employed a wet impregnation method similar to those reported for amine-impregnated silicas*[40]* to impregnate commercial activated carbon with diethylenetriamine (DETA), pentaethylenehexamine (PEHA), and PEI (shown in Figure 2.20). The wet impregnation of amines leads to a physical mixture of amine and support, and results in a non-covalent incorporation of organic into the pore spaces or onto surfaces. Pis supported 7.86, 8.05, and 6.98 mmol N/g in the materials impregnated with DETA, PEHA, and PEI, respectively.

The functionalization of carbons with amines by the formation of covalent bonds can also be accomplished through reaction with surface functionalities. The surfaces of carbons are easily modified to include reactive functionalities. Barron*[76]* reacted

fluorinated single-walled carbon nanotubes (SWNT) with PEI of different molecular weights (600, 1800, 10000, and 25000) to create aminopolymer functionalized SWNT's capable of CO_2 capture. In some cases, the surface of carbons already contains reactive surface functionalities. Gray*[77]* reported the amination (Figure 2.16) of fly ash carbons possessing alcoholic and carboxylic acid moieties on the surface with chloropropylamine (Figure 2.20). They evaluated the oxidation of the carbon surface with KOH in an effort to create more sites for amine anchoring; however, this resulted in an adsorbent with a surface amine density of 0.79 mmol N/g, which was lower than the non-oxidized case (0.92 mmol N/g).

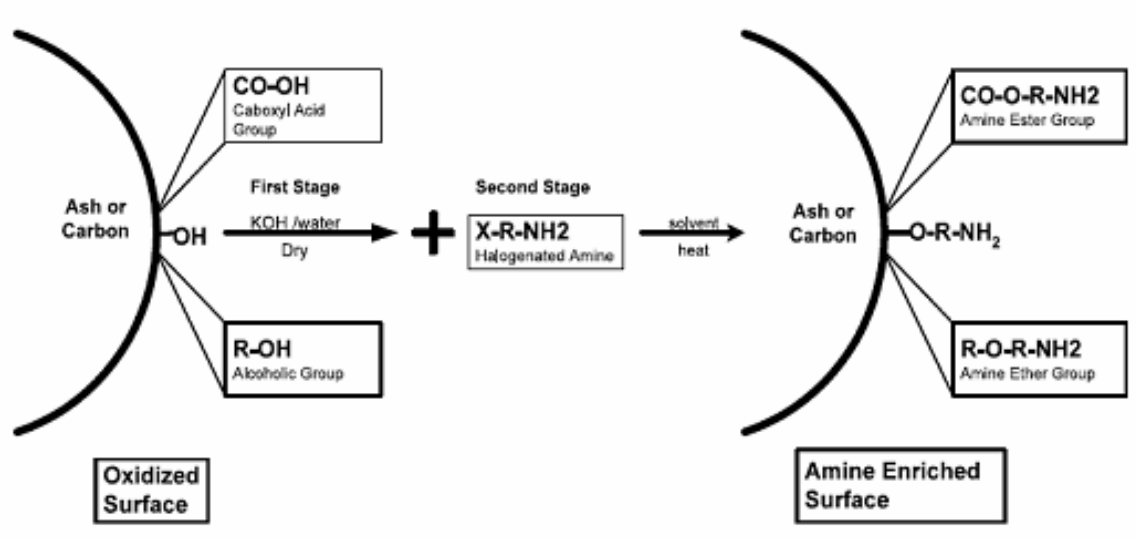

Figure 2.16. Synthetic scheme for the amination of fly ash by reaction of halogenated alkylamines with surface carboxylic acid or alcoholic groups to form aminoesters or aminoethers, respectively (reprinted with permission from Ref. *[77]*).

2.3.2. Polymer-supported Amines

Polymeric amine adsorbents have been studied by several authors in the literature. Two general strategies have been employed to create polymeric amine adsorbents. The first is to incorporate polymers or oligomers with high amine content into polymer supports either by impregnation or covalent functionalization by chemical reaction.

Filburn*[48]* reported the use of a proprietary adsorbent consisting of PEI bonded to a high surface area poly(methylmethacrylate) (PMMA, Figure 2.20) support and coated with PEG (Figure 2.20) layer. Helble*[78]* also supported amines on PMMA by impregnating the support with both acrylonitrile modified tetraethylenepentamine (TEPA, Figure 2.20) and a commercial mixture of oligomeric ethyleneimines (E-100) also modified with acrylonitrile (ME-100). Chanda*[79]* bonded PEI to a poly(acrylonitrile) (PAN, Figure 2.20) support through a multiple-step process. PAN was carboxylated with a basic ethanol solution and then ion exchanged with copper. The copper sites bound to added PEI, which was then crosslinked with glutaraldehyde (Figure 2.20). The nitrogen content of the base PAN fiber was 17.21 mmol N/g, but these nitrogen species were not capable of CO_2 capture because of their triple bond to carbon. The PEI functionalized, glutaraldehyde cross-linked, PAN adsorbent had an overall lower amine content of 14.71 mmol N/g, but contained a large number of active amines capable of capture. This modified adsorbent contained 5% H_2O and possessed a pore volume of 0.53 cc/g.

The second strategy employed to create polymeric amine adsorbents is to synthesize copolymers with amine-containing monomers or monomers that are easily derivatized to incorporate amines. Chen*[80]* reported the synthesis of a cross-linked copolymer of PEI and epichlorohydrin (ECH, Figure 2.20) that was coated onto commercial glass fibers with high surface areas. Coating layer weight percentages of 31 to 76% (% of the total weight of adsorbent) were used to prepare the composites. The weight ratio of PEI to ECH in the coating layer was varied from 5:1 to 30:1, resulting in composites with amine loadings of 7.22 to 17.61 mmol N/g. Beckman*[81, 82]* reported the synthesis of copolymers made from styrene, vinylbenzylchloride (VBC), and in some cases, divinylbenzene (DVB) (structures shown in Figure 2.20). These copolymers were then modified with amines through reaction of the chloride functionalities in the VBC units, akin to Tsuda's*[140, 141]* modification of chloride functionalities in silica gels

with PEI. In their first report,*[81]* the authors synthesized linear copolymers from styrene and VBC that were subsequently aminated with ethylenediamine (EDA, Figure 2.20). Cross-linked copolymer beads were synthesized from styrene, VBC, and DVB, and after modification with EDA, had amine loadings ranging from 2.57 to 5.57 mmol N/g. In a later report,*[82]* copolymers of 89 mol% styrene and 11 mol% VBC were aminated with diamines containing alkyl spacers of length n = 2 to 10 to investigate the effect of the alkyl spacer length on the glass transition temperature (T_g) of the copolymer, which the authors hypothesized would track with adsorption capacity.

Endo*[83]* used a similar approach as Beckman to prepare amine containing copolymers. They synthesized copolymers from VBC and either styrene or dimethylacrylamide (DMA). The alkylchloride functional groups in the VBC units were then aminated with either lithium salts of 1,8-diazabicyclo[5.4.0]undec-7-ene (DBU), or lithium salts of 1,5-diazabicyclo[4.3.0]non-5-ene (DBN). The structures for these compounds are given in Figure 2.20. The amine loadings of these copolymers ranged from 3.88 to 8.46 mmol N/g.

2.3.3. Incorporation of Amines into Solid Resins

The formation of amine containing solid organic resins is also a possible method of preparing CO_2 adsorbents. Drage*[84]* investigated the formation of solid organic resins from potassium carbonate, formaldehyde, and either melamine or urea, which were termed MF or UF resins (Figure 2.20). Activation of the potassium carbonate resins at elevated temperature increased the surface area of the resin by introducing porosity. The MF resins were activated at 773, 873, and 973 K, resulting in amine loadings of 7.20, 6.95, and 6.89 mmol N/g and BET surface areas of 12, 23, and 56 m^2/g. The UF resins were activated at 673, 773, 873, and 973 K, resulting in amine loadings of 2.80, 2.36, 1.93, and 0.70 mmol N/g and BET surface areas of 25, 365, 910, and 2479 m^2/g. Thus, for both resins, increasing the activation temperature resulted in resins with increasing

surface area but decreasing amine content, albeit to a much greater extent for the UF resin.

2.3.4. Degradation Temperature

As with any organic compound, OSA adsorbents degrade at elevated temperatures. Adsorbent degradation can be manifested in several ways, such as the loss of surface area or porosity caused by phase transition, oxidation of amines, combustion, or even evaporation of low molecular weight amines. Unfortunately, there have not been many investigations of the thermal stability of OSA's, so it is difficult to give a general description of safe operating temperature ranges. Rather, it is appropriate to characterize the thermal stability of OSA's on an individual basis, as their chemical makeup varies over such a wide range.

An important factor in the degradation of polymeric amines is the polymer support's glass transition temperature, above which, the polymer undergoes conformational changes that may be detrimental to gas diffusion. Beckman*[82]* synthesized copolymers with 11 mol% diamines containing alkyl spacers of length n = 2 to 10 to investigate the effect of the alkyl spacer length on the glass transition temperature (T_g) of the copolymer, which the authors hypothesized would track with adsorption capacity. They measured a linear decrease in T_g from 374 to 338 K of diamine copolymers with increasing alkyl chain length of n = 0 to 8.

Other forms of degradation are usually tracked by gravimetry. Chen*[80]* observed the degradation onset of PEI and ECH copolymers coated on glass fibers around 473 K, which is consistent with what was observed for PEI impregnated or functionalized silicas (see section 2.1.4). Pis*[75]* observed the decomposition of carbons impregnated with DETA, PEHA, and PEI at 373, 503, and 543 K, respectively, which correlated roughly with increasing molecular weight and boiling point.

2.3.5. CO_2 Adsorption Capacities Under Dry Conditions

The equilibrium CO_2 capture capacities of OSA's are important measures for comparison. The capacities of the adsorbents discussed below are listed in Table 2.3 along with their adsorption conditions and methods of measurement. However, just as important to process considerations are the permeability and selectivity of the polymeric amines. Beckman*[81]* measured the diffusion coefficient of CO_2 through cross-linked copolymers of EDA modified VBC, DVB, and styrene as a function of the EDA-VBC functional comonomer mole fraction. They observed over an order of magnitude difference in the diffusion coefficient for copolymers with functional comonomer mole fractions over the range of 0.24 to 0.75, reaching a maximum of D*c = 3.6 e-5 g/cm*s for a functional comonomer mole fraction of 0.4, where D is the diffusion coefficient in cm^2/s and c is the concentration of CO_2 in g/cm^3.

Some carbonaceous species simply act as high surface area supports for active capture agents. Barron*[76]* determined CO_2 capacities of 0.93, 1.09, 1.18, and 1.64 mmol CO_2/g at 348 K for SWNT's functionalized with PEI of different molecular weights (600, 1800, 10000, 25000) by TGA. At first glance, the differences in capacities do not seem very large; however, the SWNT-supported PEI adsorbents did not have equal amine loadings. The amine efficiencies of these four adsorbents were 0.02, 0.08, 0.14, and 0.16 mol CO_2/mol N, which suggests that high molecular weight PEI more efficiently captures CO_2 than low molecular weight PEI in this configuration. This trend may be partially explained by relative ratios of tertiary amines present in the different commercial polymers (not reported), which are not as reactive as primary or secondary amines. However, it is unlikely that the eight-fold increase in efficiency corresponds to an eight-fold decrease in the tertiary amine ratio.

Table 2.3. CO_2 capacities and measurement conditions for amines supported on solid organic materials.

				dry		humid			
		T	pCO_2	q [a]	eff. [b]	q [a]	eff. [b]		
Amine	Support	(K)	(bar)	(mmol/g)	(mol CO_2/mol N)	(mmol/g)	(mol CO_2/mol N)	Method [c]	ref.
DETA	carbon	298	1	0.91	0.12			TGA	*[85]*
PEHA	carbon	298	1	1.09	0.14			TGA	*[85]*
PEI	carbon	298	1	1.11	0.16			TGA	*[85]*
PEI	SWNT	348	1	1.64	0.16			TGA	*[76]*
CPA	fly ash	298	0.1			0.17		TPD/MS	*[77]*
PEI	PMMA	298	0.02	0.91				IR	*[48]*
PEI	PAN	303	0.01			3.4	0.71	VA	*[79]*
PEI/ECH	glass fiber	303	0.16	0.26	0.04	3.98	0.56	GC	*[80]*
EDA	crosslinked VBC/DVB	298	0.14	2.16				TGA	*[81]*
EDA	linear VBC	298	0.14	2.62				TGA	*[81]*
diamine	linear VBC/styrene	298	1	0.67				TGA	*[82]*
DBN	styrene	298	1	0.76				TGA	*[83]*
DBN	DMA	298	1	0.39				TGA	*[83]*
UF	resin	298	1	1.86				TGA	*[84]*
MF	resin	298	1	1.03				TGA	*[84]*

[a] Reported CO_2 capacity
[b] Amine efficiency
[c] Method of analysis: thermogravimetric analysis (TGA), gas chromatography (GC), temperature programmed desorption (TPD), mass spectrometry (MS), volumetric apparatus (VA), and infrared spectroscopy (IR)

In some carbon supported amines, physical and chemical adsorption of CO_2 were both significant because the carbonaceous supports were fairly effective physical adsorbents by themselves.*[15]* As a result, interpreting reported CO_2 capacities in terms of amine efficiencies is sometimes misleading and can result in falsely high values (see section 2.2.6). It is also not sufficient to simply subtract out the physical adsorption capacity of the bare support because the inclusion of amines into carbonaceous supports causes a reduction in porosity and surface area, reducing the number of physical

adsorption sites. Pis*[75]* found capacities of 0.91, 1.09, and 1.11 mmol CO_2/g for DETA, PEHA, and PEI impregnated commercial activated carbon, while the bare support had a capacity of 1.66 mmol CO_2/g. These values were measured at 298 K and a CO_2 partial pressure of 1 bar by TGA. The physical adsorption capacity of the bare support was greater than the combination of the chemical adsorption capacity of the added amines plus the remaining physical adsorption capacity of the carbon, due to the significantly reduced physical adsorption capacity due to amine impregnation.

Like the carbon supported amines described above, amine containing solid organic resins also displayed both physical and chemical adsorption. The syntheses used yielded amine functionalized carbonaceous supports that themselves were capable of capture. The resins made by Drage*[84]* displayed moderate CO_2 capacities of 1.86 and 1.03 mmol CO_2/g for UF and MF resins, respectively. These values were measured by TGA at 298 K under pure CO_2. The activation of the resins containing potassium carbonate generated inorganic potassium derived adsorption sites. For a discussion of adsorption with metal carbonate derived adsorbents alone, see our full review paper on solid adsorbents.*[15]* It is unclear whether adsorption with these resins occurs on the amines, these basic metal oxide sites, or a combination of both. However, changes in the resin activation procedure do result in changes in capacity. A study was conducted to determine the effect of activation temperature on CO_2 capacity and it was determined that 773 K was the optimal temperature for both resins. They observed decreasing capacities but increasing surface areas for both resins as their activation temperature increased. These results suggest adsorption on the inorganic sites plays a role.

The CO_2 capacities of polymeric amines vary over a large range. This is not only due to differences in analysis conditions and adsorption apparatuses, but also to the large differences between the materials themselves. The PMMA/PEI/PEG composites reported by Filburn*[48]* displayed a maximum CO_2 capacity of 0.91 mmol CO_2/g at 298 K using isothermal flow microcalorimetry with 2% CO_2 feed. Beckman*[81]* measured CO_2

capacities of 2.16 and 2.62 mmol CO_2/g for a cross-linked copolymer of EDA-modified VBC, and DVB and a linear polymer of EDA-modified VBC and styrene using TGA with a 14% CO_2 feed. Endo*[83]* measured CO_2 capacities of 0.76 and 0.39 mmol CO_2/g for a copolymer of styrene and DBN and a copolymer of DMA and DBN, respectively, at 298 K using TGA with a 100% CO_2 feed. Beckman*[82]* also reported the capacity as a function of alkyl chain length of styrene and VBC copolymers aminated with diamines containing alkyl spacers of length n = 2 to 10. They observed a maximum in capacity of 0.67 mmol CO_2/g for an alkyl chain length of n = 4.

2.3.6. CO_2 Adsorption Capacity: Effect of CO_2 Partial Pressure, Adsorption Temperature, and ΔH_{ads}

As with most inorganically-supported amines, the CO_2 adsorption capacities of OSA adsorbents displayed strong dependence on the feed concentration of CO_2. Isotherms have been determined for several of the reported OSA adsorbents. Chanda*[79]* determined a humid isotherm by VA for a PEI and glutaraldehyde copolymer coated on PAN at 303 K for CO_2 partial pressures in the range of 0 to 11 mm Hg. Transition from the Henry's Law regime occurred around a partial pressure of 6 mm Hg, but saturation had not yet occurred at 11 mm Hg. Chen*[80]* also measured humid isotherms for PEI and ECH copolymers coated onto glass fibers by GC, and determined that at CO_2 feed concentrations above 12% CO_2, the adsorbent was in the saturation region (Figure 2.17). Pis*[75]* used TGA to find dry isotherms for DETA, PEHA, and PEI impregnated activated carbon as well as the bare support at 273 K for a CO_2 partial pressure range of 0 to 0.035 bar (Figure 2.18). At very low partial pressures, PEHA-impregnated activated carbon had the highest capacity. At partial pressures above 0.005 bar, the bare activated carbon displayed higher capacity than any of the amine-impregnated carbons, whose isotherms had already reached saturation dependence.

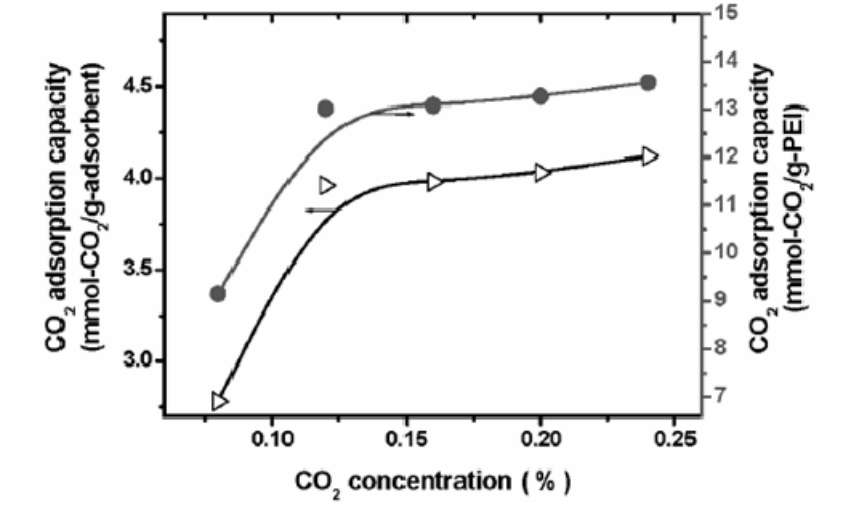

Figure 2.17. Adsorption isotherms for PEI and ECH copolymers coated on glass fibers at 353 K. Concentration is given as percentage of test gas at 1 bar (reprinted with permission from Ref. *[80]*).

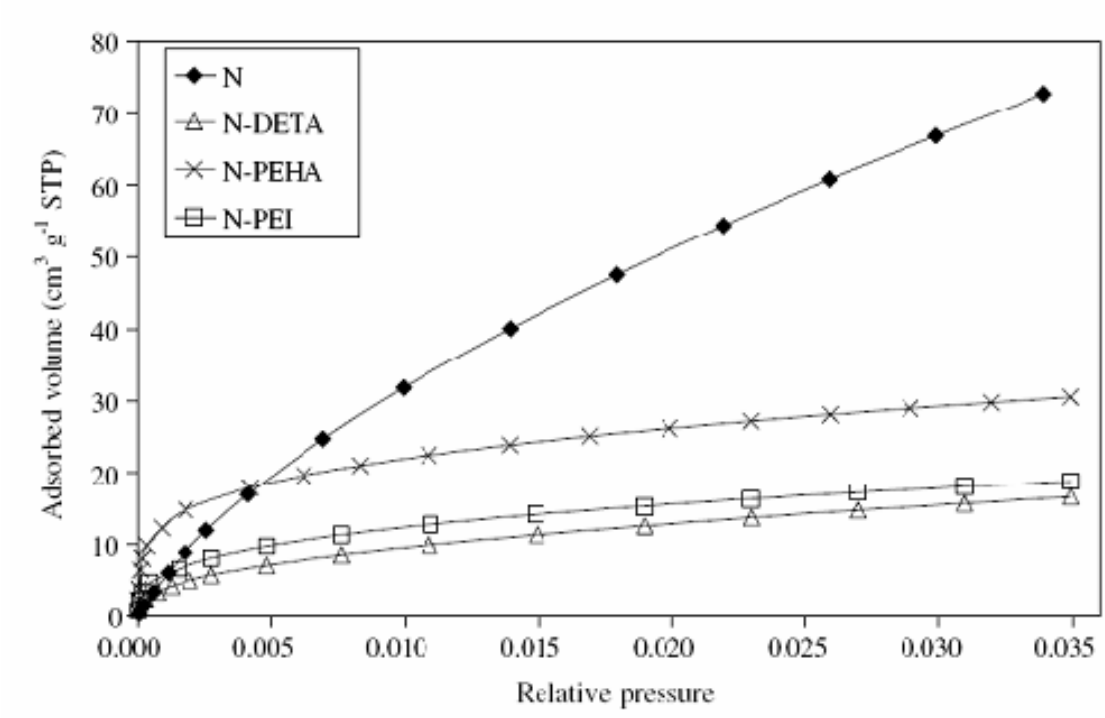

Figure 2.18. Adsorption isotherms for activated carbon (N) impregnated with DETA, PEHA, and PEI at 273 K (reprinted with permission from Ref. *[75]*).

The CO_2 capacities of OSA's are also strongly dependent on operating temperature. Thermodynamics predict an increase in capacity with a decrease in

temperature for the amine-CO_2 interaction. Several authors have observed this trend. Beckman,*[81]* Barron,*[76]* and Pis*[75]* observed linear decreases in the capacities of their adsorbents as operating temperature increased from room temperature to moderately elevated temperatures. Drage*[84]* measured a 56% decrease in capacities of UF and MF resins when the operating temperature was increased from 298 to 348 K. Endo*[83]* measured a 35% decrease in the capacity of a styrene and DBN copolymer when the operating temperature was increased from 298 K to 338 K. Li*[80]* determined the capacity of PEI and ECH copolymer to have a non-linear temperature dependence from 303 to 363 K, with the capacity leveling off at temperatures above 328 K. This suggests that diffusion limitations existed in the adsorbent, because at higher temperatures the increased diffusion of CO_2 would cause a higher adsorption capacity, as often seen for amine-impregnated silicas (see section 2.1.6).

The proposed operating temperature for post-combustion CO_2 adsorption with amine-based adsorbents is from approximately 298 to 373 K. Even in this small range, the relative order of adsorption capacities of these adsorbents is not constant. Pis*[75]* performed TPD on four different adsorbents under anhydrous conditions with 1 bar CO_2 and found that from 298 to 333 K commercial activated carbon had the highest capacity, but from 333 to 373 K, DETA-impregnated activated carbon had the highest capacity (Figure 2.19). This highlights the importance of determining a given adsorbent's capacity as a function of temperature, since the operating cost of an adsorption process can change drastically with operating temperature, and the attractiveness of certain adsorbents may be different in different temperature ranges.

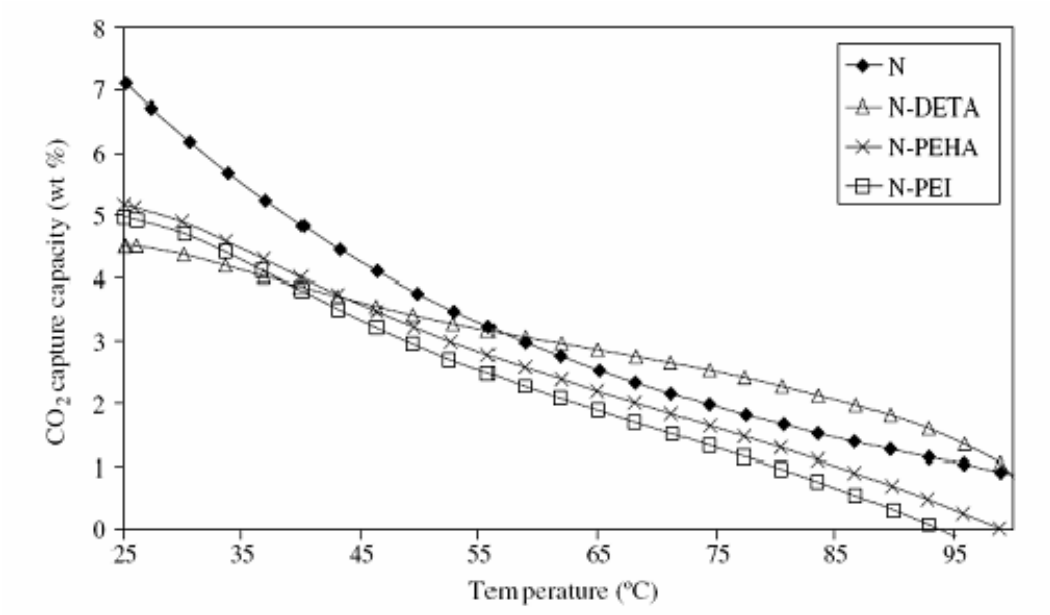

Figure 2.19. Temperature dependencies of CO_2 capacities under 1 bar CO_2 for activated carbon (N) impregnated with DETA, PEHA, and PEI (reprinted with permission from Ref. *[75]*).

The heats of adsorption of CO_2 by amines dissolved in aqueous solution have been reported to be in the range of -48 to -84 kJ/mol.*[73]* Most silica-supported amines also fall within this range, however, the two reports of heats of adsorption for OSA's lie outside. Filburn*[48]* reported a heat of adsorption of -94 kJ/mol for PEI coated PMMA, but explained the larger than expected value by incomplete desorption of CO_2 and H_2O. A heat of adsorption of -30 kJ/mol for the PEI and ECH copolymer coated on a glass fiber was estimated from figures reported by Chen*[80]* in a temperature range of 303 to 328 K. This low value suggests that some physical adsorption occurred on these adsorbents since the heats of adsorption for bare silica are typically around -20 to -35 kJ/mol.*[56, 62, 63, 66]*

2.3.7. Effect of H_2O on CO_2 Capacity

Under humid conditions, amines can capture CO_2 through the formation of carbonates and bicarbonates in addition to the carbamates usually formed in dry conditions, as noted above. This positive influence was obvious in Chen's*[80]* report of humid adsorption tests (GC) conducted on PEI/ECH copolymers coated on glass fibers, as they observed 15 times larger capacity under humid conditions than in a dry state, resulting in the largest capacity reported for OSA's of 3.98 mmol CO_2/g. However, physical adsorption has been shown to be important for many OSA's, and the physical adsorption of CO_2 is hindered in the presence of H_2O for some physical adsorbents, such as zeolites.*[15]* Since it is difficult to quantify the relative contributions of physical and chemical adsorption for some of these materials, the direct effect of H_2O on adsorption capacity is not easily defined. It may be that the presence of H_2O decreases physical adsorption of CO_2, such as seen in zeolites, but increases chemical adsorption, such as seen in silica-supported amines. Some of these materials do display large H_2O adsorption capacities. Chen*[80]* reported increasing H_2O adsorption capacities from 4.5 to 8.0 mmol H_2O/g for PEI and ECH copolymers of increasing molar ratios from 5:1 to 30:1. Filburn*[48]* reported a weight gain of 16.8% for the adsorption of H_2O on PEI coated PMMA. They measured a 27.3% weight gain from CO_2 adsorption under humid conditions, but only a 3.7% weight gain from CO_2 adsorption under dry conditions. The net increase in the mass adsorbed during humid CO_2 adsorption indicated that a synergy exists between CO_2 and H_2O adsorption, although it is impossible to define the exact increase in CO_2 capacity from their experiments. Chanda*[79]* measured a high capacity of 3.4 mmol CO_2/g when adsorption was performed with PEI functionalized PAN from a humid feed with a CO_2 partial pressure of 11 mm Hg.

2.3.8. Desorption Temperature, Regeneration, and Feed Impurities

Unfortunately, the varied composition of OSA's prevents a broad characterization of their heat capacities. Filburn*[48]* measured heat capacities of 1.73 to 1.81 J/g*°C for a PEI coated PMMA adsorbent from 298 to 323 K by differential scanning calorimetry. The heat capacities of other OSA adsorbents have not been reported but their importance should not be overlooked. Another factor in the energy cost of regeneration is the desorption temperature required to sufficiently regenerate a given adsorbent. Most solid amine adsorbents cannot be regenerated solely by concentration swing. Pis*[75]* observed capacity losses of 15.0, 27.1, and 18.4% after 3 vacuum swing adsorption cycles for DETA, PEHA, and PEI-impregnated activated carbons, respectively. Instead, elevated temperature is required to fully regenerate most amine-based adsorbents. Barron*[76]* determined a regenerable capacity for PEI functionalized SWNT's at 348 K under flowing argon. However, it is possible to damage adsorbents by regenerating at too high a temperature. Beckman*[82]* observed slower kinetics and a reduction in capacity for styrene and EDA-modified VBC copolymers when regeneration was performed above their glass transition temperatures; possibly due to the observed loss in porosity.

On the other hand, elevated temperature is sometimes still not sufficient to fully regenerate OSA adsorbents. Like many inorganic adsorbents, the inorganic adsorption sites of OSA's can undergo irreversible changes due to either physical rearrangement or chemical alteration.*[15]* Beckman*[81]* measured a 20% decrease in capacity after 4 adsorption/desorption cycles for a copolymer adsorbent regenerated at 278 K below its glass transition temperature. Amine-functionalized fly ash was found by Gray*[77]* to lose about 20% of its capacity when regenerated at 393 K, while PEI and ECH copolymers were found by Chen*[80]* to lose 6% capacity at the same temperature.

There are other relevant factors in the performance of adsorption/desorption cycles with solid adsorbents. Helble*[78]* employed a statistical design method called a Taguchi fractional factorial method to identify the variables most important to a packed

bed TSA capture system with amine-impregnated PMMA adsorbents for use in the International Space Station. They considered eight variables: adsorption/desorption cycle time (15 to 20 min.), feed CO_2 partial pressure (6 to 9 mm Hg), feed dew point (saturated at 273 to 298 K), gas residence time (1.7 to 3 sec.), adsorption temperature (298 to 303 K), desorption temperature (323 to 333 K), desorption pressure (26 to 93 mm Hg), and TEPA vs. ME-100 amine type. For the TEPA amine, desorption pressure contributed to 61% of the overall system variance, while the desorption temperature and feed CO_2 partial pressure only contributed 19 and 12% of the variance. For the ME-100 amine, 94% of the variance was due to the desorption pressure. This study was performed over a fairly narrow parameter range, and it remains to be seen if the relative importance of these variables changes when they are extended over a wider parameter space. Regardless, under these conditions, changes in desorption pressure accounted for the most influence on system performance for both types of adsorbents, which highlights the importance of efficient removal of CO_2 from the adsorbent bed during desorption.

Impurities in the feed stream of an adsorption process have the potential to hinder adsorbent regeneration and adversely affect equilibrium adsorption capacity. Acid gases, such as SO_x and NO_x, can react with amines in a similar manner to CO_2, sometimes irreversibly. Unfortunately, this has not been examined in much depth in the OSA adsorbent literature. Only Beckman*[81]* has performed an extensive investigation of the affect of impurities. Beckman observed a linear increase in the SO_2 capacity of an EDA-modified copolymer as the ratio of functional comonomer was increased, reaching a capacity of about 4.5 mmol SO_2/g with a 1% SO_2 balance N_2 stream. They reported reversible SO_2 adsorption for copolymers modified by tertiary amines, and "nearly complete" reversibility of the EDA-modified copolymers. In the same report, Beckman found the copolymer adsorbents were unaffected by a 2% N_2O feed stream, but did adsorb when fed streams with either 0.5% NO or 0.5% NO_2. Attempts to regenerate the adsorbents after NO_x adsorption were unsuccessful, resulting in an 80% reduction in

capacity after one cycle for the case of NO. Analysis of the adsorbents with FT-IR spectroscopy suggested the loss in capacity was due to amine oxidation. Although these results are adsorbent specific, and should not be taken to apply to all OSA adsorbents, the underlying chemistry applies to most supported amines, and should be expected to occur in most systems.

2.3.9. Adsorption and Desorption Kinetics

As with most solid amine adsorbents, OSA's generally have shown quick adsorption halftimes on the order of minutes, followed by prolonged shoulders of slower uptake rates. Drage*[84]* determined that full equilibrium was reached by UF and MF resins in about 20 and 40 minutes, respectively. Pis*[75]* determined that amine-impregnated activated carbons reached equilibrium in approximately 40 minutes. Measurements by Endo*[83]* indicated that styrene and DBN copolymers did not reach equilibrium for hundreds of minutes. These results were all measured by TGA and may be inapplicable to most process configurations where gas is fed through adsorbents and not past or around them.

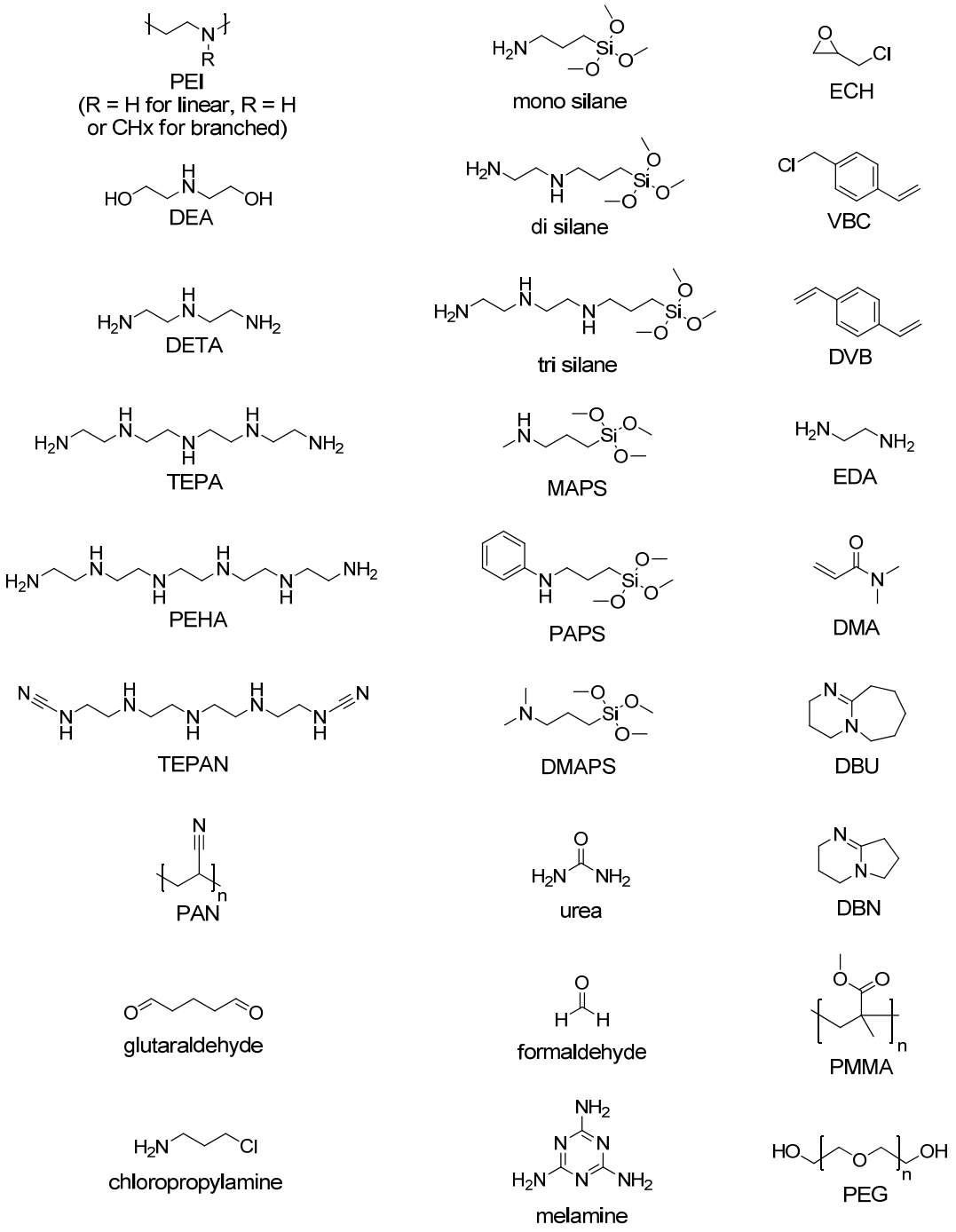

Figure 2.20. Amines, silanes, monomers, and polymers used in the synthesis of solid supported amine adsorbents.

Changes in process conditions also affect adsorption kinetics. Chanda*[79]* measured initial uptake rates as a function of initial CO_2 partial pressure for PEI functionalized PAN fibers. At low partial pressures (<15 mm Hg) there was a nearly linear relationship with a slope of $9.7*10^{-3}$ mmol CO_2/min*g*mm Hg. Beckman*[82]* determined that copolymer adsorbents regenerated above their glass transition temperatures displayed slower adsorption kinetics, most likely due to decreased mass transfer induced by a loss in porosity.

Adsorption kinetics for polymeric amines can vary with changes in adsorbent structure. Endo*[83]* observed a decrease in adsorption halftime for styrene and DBN copolymers made with decreasing DBN contents of 100, 51, and 30 mol%. This increase in kinetics is likely due to increased accessibility afforded to the DBN polymer units by the styrene spacers. However, lower amine content usually translates into lower CO_2 capacity per weight of any adsorbent, so a tradeoff between capacity and kinetics would have to be considered in the ultimate design of any process.

2.3.10. Structure of Adsorbed CO_2

The formation of CO_2-amine adducts during adsorption with OSA's can be tracked by FT-IR spectroscopy. Under dry conditions, carbamates are the expected structures, while under humid conditions, carbonates and bicarbonates can also form. Under dry conditions, Beckman*[81]* and Endo*[83]* both observed the formation of carbamates at 1650 cm^{-1}. Gray*[77]* observed peaks from 2400-2300 cm^{-1} for adsorption under dry conditions with amine-functionalized fly ash due to the adsorption of CO_2. Then under humid conditions they observed the appearance of two additional signals at 1148 and 1087 cm^{-1}, most likely due to the formation of carbonates.

2.4 Concluding Remarks and Outlook

The removal of anthropogenic CO_2 from the post-combustion flue gas at large point sources has been spotlighted in recent years as a potential way to reduce greenhouse gas emissions. Among a range of separation technologies including membrane separation, absorption, cryogenic distillation, and others, adsorption with solids appears to be one of the most promising CO_2 capture strategies. Of the adsorption processes studied over the past decades, adsorptive separation of CO_2 by PSA techniques has been most extensively studied. However, a temperature swing process is often envisioned for post-combustion capture of flue gas from existing coal-fired power plants, owing to the low pressure of most flue gas streams.

This work does not seek to suggest that adsorption is the ideal way to achieve efficient CCS. Rather, if adsorption is to be used for large scale implementation of CCS, the physical and chemical properties of the adsorbent must be well understood. To this end, this review categorizes the available adsorbent materials that have been reported to date and enumerates the important adsorption properties and operating conditions for each class of adsorbent materials.

Selection of the proper adsorbent is a critical step in retrofitting the current power generation infrastructure with CO_2 capture processes, but it is not straightforward to simply choose the most promising adsorbent a priori because multiple parameters affect the overall process performance and economics. Indeed, there is and will be no single, ideal adsorbent. Instead, adsorbents need to be compared in light of the specific process they will be adapted to, ranking the importance of adsorbent parameters as they apply to the specific constraints of the system. However, some generalizations can be drawn from the reviewed literature.

The adsorptive properties of organic and organic/inorganic hybrid adsorbents depend on both the composition and geometry of the chemisorptive moieties and their solid supports. Amine-impregnated silicas have high CO_2 capacities but because the

amines are not covalently bound to the silica support, they have the potential to leach under humid flow conditions. Organically-supported amines display relatively low adsorption capacities, in some cases due to amine inaccessibility, but are generally considered to be fully regenerable using a temperature swing process. Covalently-tethered amines have large, fully regenerable capacities, and while adsorption halftimes are typically fast, they require a long time to reach full equilibrium, possibly because of reduced diffusion through the porous support at high CO_2 and amine loadings.

Figure 2.21 displays the dry adsorption capacities of the three types of supported amine adsorbents at different temperatures and shows that, generally speaking, amine-impregnated adsorbents have the highest capacities among the organic chemisorbants. The adsorption capacities of supported amine adsorbents are not negatively affected and in many cases are actually aided by the presence of moisture, unlike the inorganic physisorbents. However, their operating conditions are inherently limited to the low temperature regime due to their significant organic content. Figure 2.22 displays the humid adsorption capacities for supported amine adsorbents at different temperatures.

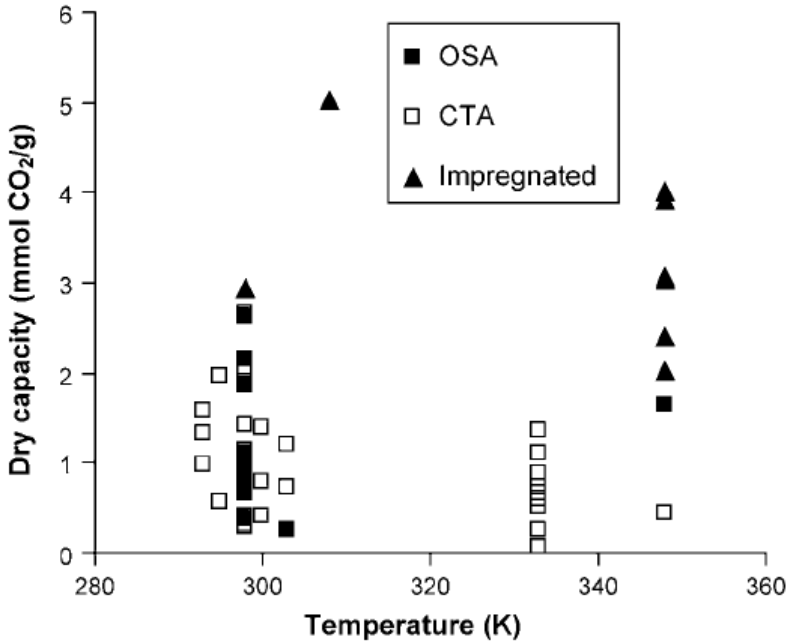

Figure 2.21. CO_2 capacities of organic and organic/inorganic hybrid adsorbents at various temperatures under dry conditions.

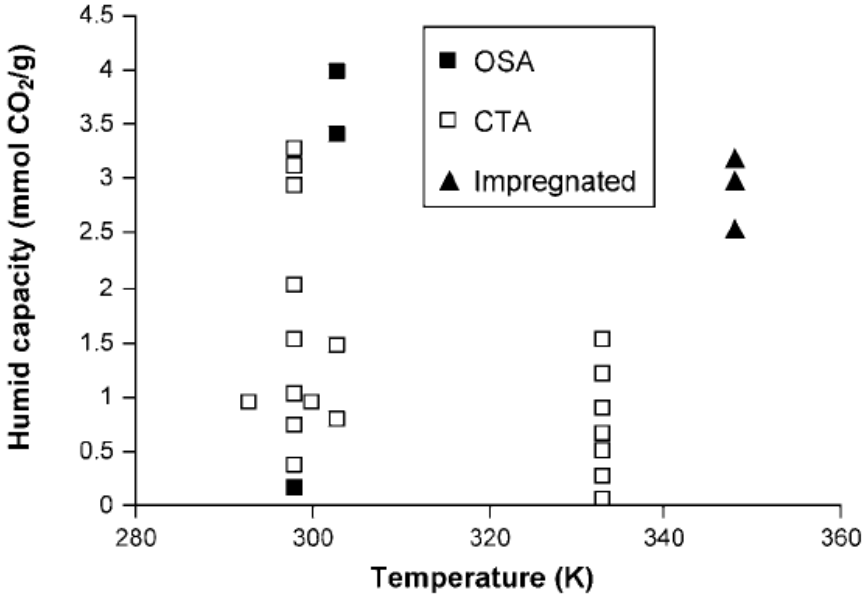

Figure 2.22. CO_2 capacities of organic and organic/inorganic hybrid adsorbents at various temperatures under humid conditions.

Supported amine adsorbents have relatively large CO_2 capacities at low CO_2 partial pressures (Figure 2.23) compared to other adsorbent types. In addition, they can be designed to have excellent amine efficiencies. Figure 2.24 shows that amine-impregnated adsorbents have high capacities but low amine efficiencies, while covalently-tethered amine adsorbents have lower capacities but higher amine efficiencies, with organically-supported amine adsorbents falling in between.

The selection of the optimum CO_2 adsorbent for capture of power plant flue gas will depend on the process used, the adsorbent performance, adsorbent lifetime and adsorbent cost, among other factors. Although in the scientific literature authors most often focus on adsorbent capacity as a design metric, in this work we bring out and review the multitude of technical parameters that need to be considered for any adsorbent that will be utilized in post-combustion flue gas capture.

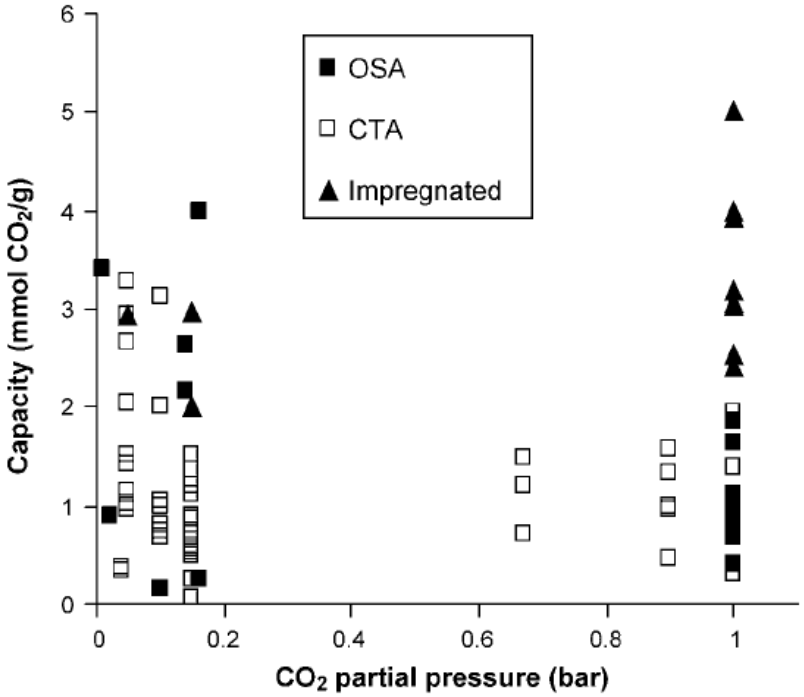

Figure 2.23. CO_2 capacity vs. CO_2 partial pressure for organic and organic/inorganic hybrid adsorbents.

Improved, next generation adsorbents are clearly needed. Among the categories of the supported organic adsorbents, covalently-tethered amines show the potential to be outstanding adsorbents in cases where adsorption capacity and adsorption kinetics can be productively balanced. Overall, further understanding of adsorbent structure-property relationships and the subsequent improvement of adsorbent performance under realistic operating conditions will likely allow for the implementation of some solid adsorbents in practical post-combustion CO_2 capture processes in the near future.

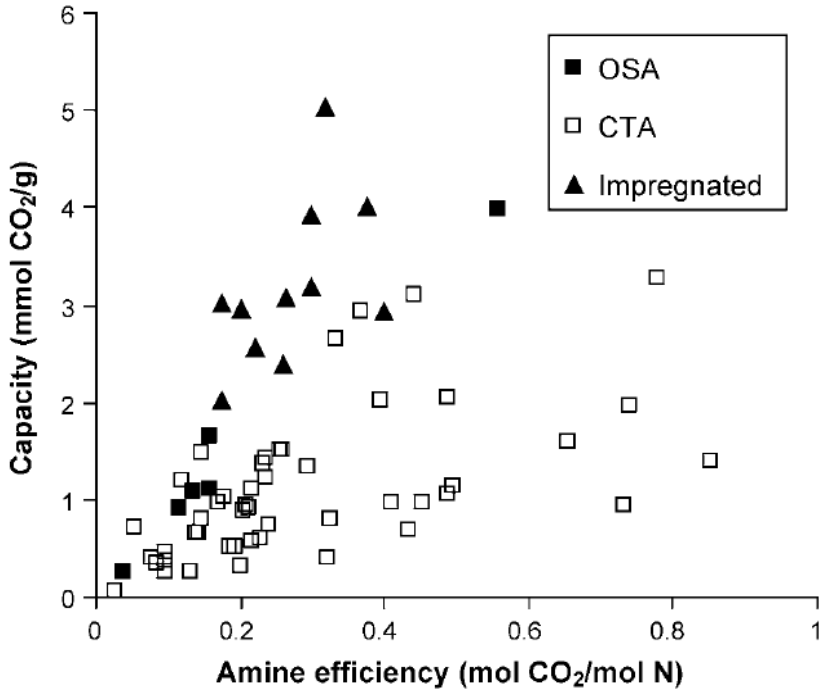

Figure 2.24. CO_2 capacity vs. amine efficiency for organic and organic/inorganic hybrid adsorbents.

CHAPTER 3

SYNTHESIS-STRUCTURE-PROPERTY RELATIONSHIPS FOR HYPERBRANCHED AMINOSILICA CO_2 ADSORBENTS

This chapter is largely reproduced from "Synthesis-Structure-Property Relationships for Hyperbranched Aminosilica CO_2 Adsorbents" by Jeffrey H. Drese, Sunho Choi, Ryan P. Lively, William J. Koros, Daniel J. Fauth, McMahan L. Gray, and Christopher W. Jones, published by *Advanced Functional Materials*, in 2009, volume 19, pages 3821-3832.*[86]*

3.1 Introduction

A key objective in the design of a solid adsorbent is to increase the available adsorption sites per mass of material to reduce the size of the required process equipment and the associated operating cost. In a previous report, we described the synthesis of a silica-supported amine adsorbent with a very high loading of amine adsorption sites compared to previous covalently-attached amine adsorbents.*[26]* This adsorbent, called a hyperbranched aminosilica (HAS), was prepared by the acid-catalyzed, ring-opening polymerization of aziridine from a mesoporous silica (SBA-15) support. The HAS adsorbent displayed superior CO_2 adsorption capacities from humid simulated flue gas compared to other types of silica-supported amine adsorbents. The adsorption capacity was fully regenerable over 11 adsorption/desorption cycles.

Here, we describe the range of material characteristics and adsorptive properties attainable with HAS adsorbents by modifying certain synthesis conditions, such as reaction solvent and aziridine to silica weight ratio. An analysis of the aminopolymers formed in these reactions and the behavior of the HAS materials in dry and humid CO_2

adsorption follows with the intent of developing synthesis-structure-property relationships for this class of adsorbents.

3.2. Results and Discussion

3.2.1. Synthesis and Characterization HAS Adsorbents with Varied Loadings

The equilibrium CO_2 capacities of solid amine-based adsorbents are often used as the primary metric to evaluate their performance.*[15, 37, 71]* This is because the higher the capacity of a given adsorbent, the lower the quantity of adsorbent that is required to capture a given amount of CO_2 from a flue gas stream. Intuition suggests that the higher the equilibrium adsorption capacity the better; however, the importance of the other characteristics of an adsorbent should not be overlooked. For instance, an adsorbent with very high capacity but very slow adsorption kinetics would likely be useless for capturing CO_2 from flue gas in a practical way, where flow rates are high and fast adsorption cycle times are required. For this reason, it is sometimes more useful to discuss capture capacities in terms of working capacities that are achievable in a fixed amount of time.

For the silica-supported amine class of adsorbents, it has been shown that there is indeed a tradeoff between capacity and kinetics, especially in cases where the silica supports are so highly loaded that there is little or no remaining pore volume.*[15, 46, 59]* Diffusion of CO_2 into the interior of the adsorbent can be blocked or retarded by organic functionalities that have drastically reduced the open pore space. A set of HAS adsorbents possessing a range of organic loadings were synthesized to investigate these issues. These adsorbents consisted of a mesoporous silica support (SBA-15) covalently functionalized with a hyperbranched aminopolymer with ethyleneamine repeat units, achieved by the acid-catalyzed ring-opening polymerization of aziridine from silanol groups on the silica surface. It should be noted that a silicon-based material was first functionalized with aminopolymer in this manner by Park, although they worked on flat

siliceous substrates.*[87]* Subsequently, SBA-15 was also functionalized with aminopolymers by aziridine polymerization in the works of Linden for a different application,*[88-92]* and by our group for CO_2 capture.*[26]*

The functionalization of ordered mesoporous silicas through reaction with surface silanols has been extensively studied.*[93, 94]* Typically, these grafting reactions involve the use of silane chemistry where alkoxy groups from a silane condense with the surface silanols to form covalent tethers to the silica surface through Si-O-Si bonds, incorporating organic functionalities through substituents on the silane molecule.*[93]* The HAS synthesis directly incorporates organic functionalities to the silica surface by forming Si-O-C bonds through ring-opening polymerization with surface OH groups, if the polymerization is carried out on a bare silica surface. Alternately, aziridine can be polymerized from silane-functionalized surfaces that contain nucleophilic reactive centers, such as amines.

HAS adsorbents with varied amine loadings (hereafter referred to as the HAS varied loading adsorbent set, or HAS-VLAS) were prepared similar to reported procedures*[26, 87]* by varying the weight ratio of aziridine to SBA-15 used in the synthesis. Table 3.1 displays the amine loadings, pore volumes, pore diameters, and surface areas of the HAS adsorbents prepared as well as the aziridine to SBA-15 weight ratios used in their syntheses and the resulting yields. The yields were reported as the percent of aziridine that remained attached to the silica support after the synthesis relative to the amount added to the solution. The organic loadings were assessed by TGA and the amine loadings were stoichiometrically estimated from this value. The BET surface areas were determined at 77 K by N_2 physisorption (isotherms shown in Appendix A). The spatial characteristics of the porosity were determined from the N_2 physisorption data interpreted by the Frenkel-Halsey-Hill modified Broekhof-de Boer method (BdB-FHH), which has been shown to be more accurate than the Barrett-Joyner-Halenda method (BJH) for practical application to mesoporous materials.*[95-100]* Confirmation of

organic functionalization with aliphatic amines was determined for the HAS-VLAS by FT-IR spectroscopy (Appendix A).

HAS adsorbents in the VLAS were prepared with amine loadings as low as ~ 2 mmol N g^{-1} adsorbent and as high as ~ 10 mmol N g^{-1} adsorbent, by adjusting the aziridine to silica weight ratio in the synthesis (Table 3.1). Thus, the amine loading of the HAS adsorbent is tunable and controllable within these limits. However, as with all silica supported amine adsorbents, there is a physical upper-bound to the amount of amines that can be loaded into the pores of the support that is equal to its total pore volume. The SBA-15 used for this study had a pore volume of ~ 0.78 cc g^{-1}, thus the theoretical maximum amount of aminopolymer that could be loaded into the pore space is ~ 0.84 g organic g^{-1} silica, which translates to ~ 10.6 mmol N g^{-1} adsorbent. To put this into perspective, pure PEI, an aminopolymer widely used in constructing effective adsorbents, has an amine loading of ~ 23 mmol N g^{-1} polymer.*[35, 37, 41, 42, 61, 75, 76]* However, pure PEI is a viscous liquid and thus, a poor candidate as a single component liquid absorbent. Nevertheless, it is important to note that, unless another polymer with higher amine content is used, the maximum amine loading for an amine based solid adsorbent is just under 23 mmol N g^{-1}, regardless of the type of solid support.

As the aziridine to SBA-15 reactant ratio was increased from values below 1 to about 3, the HAS amine loading obtained increased in a roughly linear fashion, as shown in Figure 3.1. When a very large reactant ratio of 5 was used, the amine loading decreased to a value below the maximum, suggesting that a large amount of aziridine may have polymerized in solution before it could diffuse into the pores of the silica particles. Aminopolymer formed in solution in this manner was washed away from the silica particles during workup.

Table 3.1. Compositions and physical characteristics of HAS adsorbents.

Sample	Amine Loading [mmol N/g]	Reactant Ratio [w/w]	Yield [a] [mol N/mol aziridine]	Pore Dia. [nm]	BET Surface Area [m^2/g]	Pore Vol. [cc/g]	Pore Vol. [cc/ g SiO_2]	Micropore Vol. [cc/g]	Polymer Vol. [b] [cc polymer/ g SiO_2]	Remaining Pore Vol. [c] [cc/g SiO_2]
HAS1 [d]	9.78	2.65	0.29	4.9	45	0.11	0.20	0.00	0.72	-0.11
HAS2 [d]	8.30	2.03	0.30	5.0	71	0.15	0.25	0.00	0.56	-0.01
HAS3 [d]	7.25	1.33	0.37	4.9	119	0.25	0.38	0.00	0.46	-0.03
HAS11 [e]	5.27	5.01	0.06	5.4	234	0.39	0.55	0.01	0.30	-0.07
HAS13 [f]	3.65	0.53	0.38	5.9	278	0.49	0.64	0.02	0.19	-0.02
HAS10 [e]	2.84	0.33	0.43	6.4	314	0.51	0.61	0.03	0.14	0.04
HAS14 [f]	2.27	0.13	0.86	6.3	579	0.69	0.81	0.08	0.11	-0.11
SBA1	0			6.2	865	0.81	0.81	0.08		
SBA2	0			5.9	840	0.78	0.78	0.06		
SBA3	0			6.3	870	0.81	0.81	0.09		

[a] Calculated as mol N g^{-1} SiO_2 in the prepared HAS divided by the reactant ratio [mol N g^{-1} SiO_2]
[b] Calculated as aminopolymer loading obtained from TGA divided by the density of commercial PEI (1.07 g cc^{-1})
[c] Theoretical unaccounted for pore volume, calculated by subtracting the adsorbent pore volume and calculated aminopolymer volume from the pore volume of unfunctionalized SBA-15
[d] SBA1 used as silica support in synthesis
[e] SBA2 used as silica support in synthesis
[f] SBA3 used as silica support in synthesis

The BET surface areas, BdB-FHH pore volumes, and pore diameters were calculated from N_2 physisorption data to determine the HAS-VLAS's pore characteristics (Table 3.1). When the organic loadings of the HAS materials increased, the BET surface areas and pore volumes decreased. A plot of surface area and pore volume vs. amine loading is shown in Figure 3.1. There was a sharp decrease in both characteristics as amine loading increased at low values. Surface area and pore volume linearly decreased at increasing amine loadings, eventually reaching plateaus with the highest loaded materials. The three unfunctionalized SBA-15 silicas used for these syntheses had BET surface areas of 840 to 870 m^2 g^{-1} and total pore volumes of 0.78 to 0.81 cc g^{-1}, including micropore volumes from 0.06 to 0.09 cc g^{-1}. Linden claimed that aminopolymer-functionalized SBA-15 first filled the silica micropores and subsequently the mesopores.*[90, 92]* They also suggested that the nitrogen adsorption isotherms indicated

that no partial pore blocking occurred after functionalization, as the adsorption and desorption branches were essentially parallel and exhibited a narrow hysteresis.*[90]* Unfortunately, the authors did not report the aziridine to silica ratios used in their syntheses so a direct comparison to the work here is somewhat difficult. The results from Table 1 indicate that micropore volume does not disappear in the HAS materials described here until relatively high amine loadings are obtained, higher than those reported for aminopolymer-functionalized, calcined SBA-15 prepared by Linden.*[90]* It should be noted that SBA-15 materials prepared under slightly different conditions may have significantly different amounts of micropores and micropore size distributions, and this may account for the differences seen in these studies.

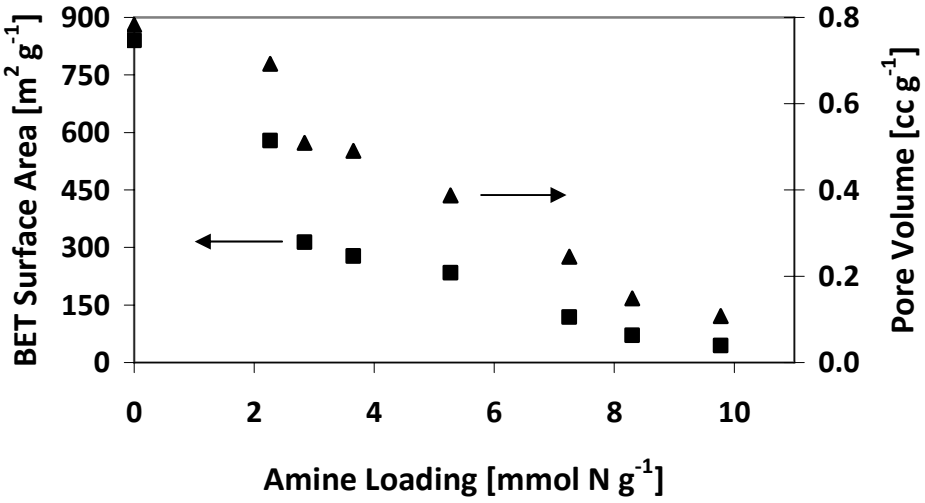

Figure 3.1. BET surface area and pore volume vs. amine loading of the parent HAS adsorbent.

The average pore diameters found for the HAS-VLAS also decreased as the amine loading of the HAS material increased from low to moderate loadings (Figure 3.2). However, at higher loadings, the pore diameters remained at ~ 5 nm and there was little or no adsorption from pores below 4.5 nm in size. This trend was also observed for the

polymerization of isopropylacrylamide monomers on SBA-15, where substantial inclusion of polymer (27.5 wt%) resulted in only a 1 nm reduction in pore diameter.*[101]* If increasing organic inclusion into the silica pores occurred evenly by layer-by-layer growth of aminopolymer on the pore walls, the pore diameters of highly loaded materials where the pores are almost filled, but not blocked, should continue to decrease in approximately a linear fashion approaching zero. Instead, it appears that as pores were filled with aminopolymer, functionalization occurred in the majority of the pores until a critical diameter of ~ 5 nm was reached. Past this point, the data suggest additional polymer inclusion occurred as pores were closed or blocked by additional aziridine polymerization, leaving the average pore diameter (of the remaining unblocked pores) unchanged at the critical diameter. This hypothesis is consistent with the observation of there being a critical pore diameter, after which the pore size does not decrease further but the number of pores of this size decreases as loading increases (see Figure 3.2). The location where a pore closes due to polymerization is unknown, but likely occurs at or near the pore mouth because of the high reactivity of aziridine.*[102]* Partially blocked pores have been suggested to have an inkbottle effect on the desorption branch of the N_2 adsorption isotherm,*[101]* deviating from the parallel adsorption and desorption branches observed for open cylindrical pores with small deviations in pore diameter.*[92, 103]* It is likely that the fraction of pores of the HAS-VLAS materials that are blocked are completely or nearly completely blocked because the adsorption and desorption branches of the N_2 adsorption isotherms are relatively parallel.

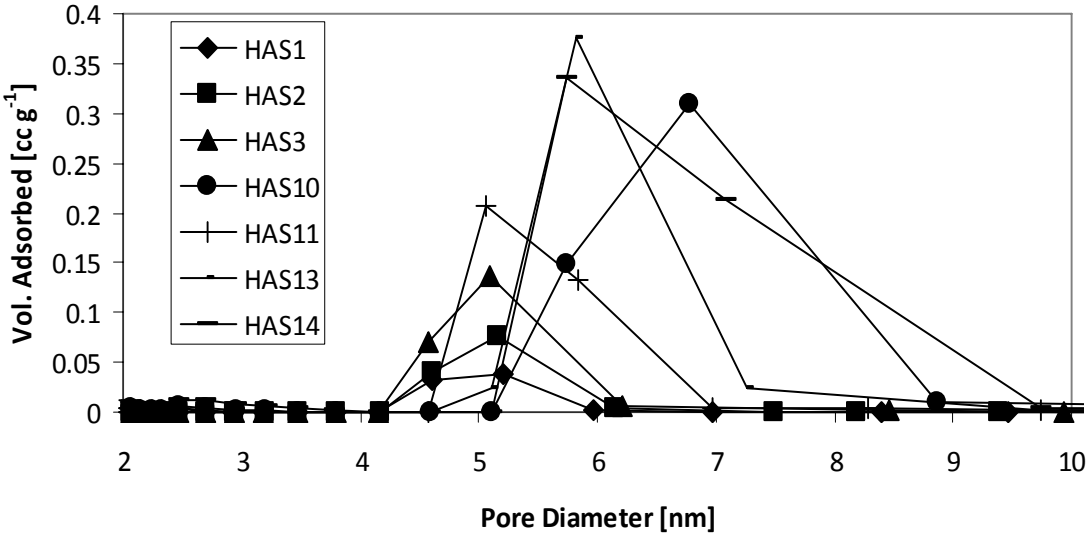

Figure 3.2. Pore diameter distributions from N_2 physisorption at 77 K for the HAS-VLAS. A possible consequence of this pore blocking phenomenon is the increased likelihood of polymerization occurring outside of the pore spaces.

To further investigate this, a simple calculation was performed to reconcile the N_2 adsorption results with the TGA results for these materials (Table 3.1, columns 10 and 11). In the ideal case of an HAS material with all of the aminopolymer located inside the pores, the sum of the estimated volume of added aminopolymer per weight of silica and pore volume of the HAS material per weight of silica, subtracted from the original pore volume of the unfunctionalized SBA-15 should equal zero. A negative value of this parameter (Remaining Pore Volume or RPV) suggests that aminopolymer is located outside of the pores, while a positive value suggests that there exists some pore volume that is inaccessible to N_2 adsorption. Similarly, it is possible to have both inaccessible pore volume and aminopolymer outside of the pores that could result in positive or negative values, depending on the relative magnitudes. Table 3.1 shows that for all the HAS-VLAS except for HAS10, the sums of the pore volumes and aminopolymer volumes (assuming a density of 1.07 g cc^{-1} for commercial PEI) are greater than the pore volume of the bare support and thus, some aminopolymer is likely located on the particle

exterior. Though there is not a trend in the RPV vs. amine loading or any of the pore characteristics, the two most negative values were observed for the highest and lowest loaded materials. The pore volume and pore diameter of the lowest loaded HAS material (HAS14) are very near those of the silica support. This negative value for the RPV suggests that aziridine initially preferentially reacts with the silica surface (including the particle exterior). This supports the hypothesis that the majority of the silica pores are functionalized with aminopolymer until a critical radius is reached, which may coincide with a nearly complete coverage of the silica surface by a thin layer of aminopolymer.

Indeed, it is possible to selectively functionalize the exterior silica surface with aminopolymer. Linden achieved a loading of 1.7 mmol N g^{-1} material for aminopolymer-functionalized nonporous silica nanoparticles.*[88]* In a separate work, Linden claimed to preferentially functionalize the exterior of SBA-15 particles with 6.55 mmol N g^{-1} material by performing aziridine polymerization on as-prepared SBA-15 and later removing the pore-forming organic template via solvent-aided extraction.*[89]* After extraction of the template, this material had a pore volume of 0.99 cc g^{-1} SiO_2, compared to a pore volume of 1.16 cc g^{-1} SiO_2 for unfunctionalized, template-extracted SBA-15. The authors claimed that because the two materials possessed the same average pore diameters, at least a portion of the added polymer was located outside of the pores. It is also possible that some of the organic template of the as-prepared silica was displaced during aziridine polymerization and that the difference between pore volumes of the two materials represents the incorporation of some aminopolymer inside the pores. In fact, the volume of aminopolymer present in the functionalized material was 0.37 cc g^{-1} SiO_2, whereas the difference in pore volume was 0.17 cc g^{-1} SiO_2, meaning that potentially 46 % of the added polymer was actually located in the pores. These examples illustrate that under certain conditions, large amounts of aminopolymer can be grown from the silica particle exterior, but that the aziridine molecule may be small enough to access and

polymerize in the pores even in situations where the pores are partially filled with organic material.

The reaction yield over the series of HAS-VLAS syntheses decreased as the reactant ratio increased (Table 3.1, Figure 3.3). At low reactant ratios the yield decreased sharply as the ratio increased, but then followed a roughly linear behavior thereafter. This suggests that the functionalization of SBA-15 with aziridine is diffusion controlled under these conditions, since materials at low reactant ratios had low amine loadings and high pore volumes, making them more accessible to entering reactants. For materials with higher reactant ratios and smaller resultant pore volumes, increasing quantities of aziridine remained unreacted or polymerized in solution to form aminopolymer that was removed during workup.

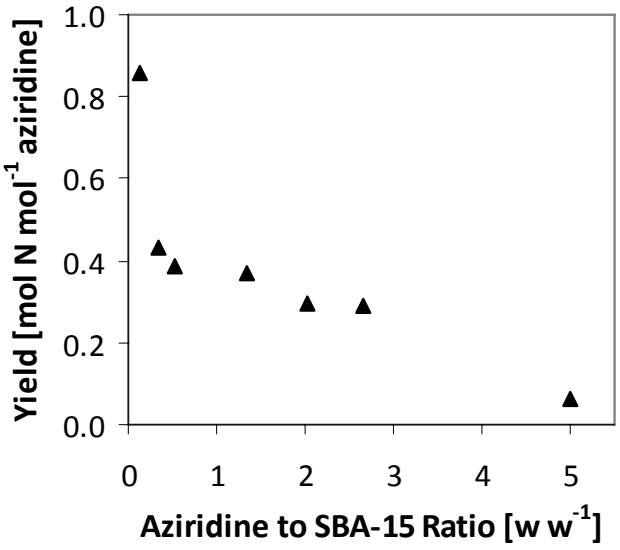

Figure 3.3. Reaction yield for the HAS-VLAS (calculated as moles N in prepared HAS material per moles aziridine used in reaction) vs. the aziridine to SBA-15 weight ratio used in the synthesis.

3.2.2. Aminopolymer Characterization: Degree of Branching and Molecular Weight

In addition to the amine loading and pore characteristics of a given HAS adsorbent, it is also important to know the distribution of amine types (primary, secondary, and tertiary). In the HAS synthesis, aziridine polymerizes from the silica support, forming a hyperbranched aminopolymer that contains a mixture of primary, secondary, and tertiary amines (hereafter referred to as 1°, 2°, and 3°, respectively). The 1°:2°:3° ratio of PEI synthesized in solution can vary over a range depending on synthesis conditions and molecular weight. For example, Kissel determined that the 1°:2°:3° amine ratios for eight commercial PEI's fell inside of a range of 31-42:33-39:25-31.*[38]* As previously discussed, amine type is important to the efficacy of CO_2 adsorbents because the reaction of CO_2 with 1°, 2°, and sterically hindered amines is usually described by a zwitterionic mechanism, whereas the reaction with 3° amines is governed by the base-catalyzed hydration of CO_2 (see CH2, Introduction).*[29]* Since the different amine types react with CO_2 in different ways, especially in the presence of water, it is important to determine the relative amounts of each contained in the HAS adsorbent, if adsorption capacities and kinetics are to be optimized.

Our first report on the HAS adsorbent identified an amine ratio of 28:47:25 for a moderately loaded adsorbent.*[26]* However, for differently loaded HAS adsorbents it was hypothesized that the aminopolymer structure could vary in its degree of branching and polymer chain length as the available pore space in the silica support changed. To investigate this possibility, the aminopolymers of the HAS-VLAS had to be separated from their silica supports so that traditional polymer characterization techniques could be used. This was accomplished by dissolving the mesoporous silica in strong base, effectively cleaving the aminopolymer from its support. The aminopolymer was then recovered by phase separation after partial solvent removal and a subsequent physical separation. To characterize these materials, aqueous size exclusion chromatography

(ASEC) was used to assess the aminopolymer molecular weight and inversely-gated ^{13}C solution NMR was used to measure the 1°:2°:3° amine ratio.

The inversely-gated ^{13}C NMR experiments were conducted on all adsorbents from the HAS-VLAS. This proton-decoupled technique produced quantitative ^{13}C spectra. For commercial PEI, the spectrum consisted of eight shifts between 40-60 ppm that corresponded to carbons in slightly different environments within the polymer chain. The 1°:2°:3° amine ratios were then found by peak integration and are shown in Table 3.2. Additional details regarding the carbonaceous environments and the 1°:2°:3° amine ratio calculations are described in the Appendix A. The cleaved aminopolymers (Table 3.2, rows 2 through 7) do not significantly differ from each other in terms of their degree of branching. They have an average 1°:2°:3° amine ratio of 28:46:26. The error in the analysis was estimated from three repeated runs with sample 6. Indeed, the ratios of the cleaved samples do not change very much outside of this error. However, the cleaved aminopolymers are distinctly different from the two commercial PEI's (Table 3.2, rows 1 and 9). These data suggest that the degree of branching of the HAS aminopolymer is affected by the reaction conditions, and perhaps by the pore diameter of the silica support (roughly the same in all cases) and not as affected by the polymer loading of the parent material or the concentration of aziridine used in the material's synthesis.

The cleaved aminopolymers were also analyzed by ASEC to determine their average molecular weights. In this technique, molecules are eluted from the column in decreasing order of their molecular weight, usually with the small molecular weight mobile phase components eluting last. Figure 3.4 shows the molecular weights of the cleaved aminopolymers as a function of the amine loading of the parent HAS material from which the polymers were obtained. At low HAS amine loadings the retention times decreased as amine loading increased, reflecting increasing aminopolymer molecular weight. However, at higher amine loadings the retention times leveled off, suggesting that the molecular weights were all similar among the materials with high loadings. The

relative molecular weights of the cleaved aminopolymers (Table 3.2) were determined by comparing their retention times to a calibration curve constructed from commercial PEI samples (Appendix A).

Table 3.2. Retention times of cleaved aminopolymers and calculated molecular weights relative to commercial PEI standards.

Sample	Amine Loading [mmol N g^{-1}]	Amine Ratio [a] [%]			Avg. Mw [Daltons]	Avg. Repeat Units [number]
		1º	2º	3º		
Low Mw PEI	N/A	44	33	23	800	19
HAS1	9.78	29	43	28	5695	132
HAS2	8.30	24	49	27	5695	132
HAS8	7.89	31	42	27	6577	153
HAS11	5.27	29	50	22	5383	125
HAS13	3.65	26	47	27	4814	112
HAS10	2.84	31	44	25	2140	50
HAS14	2.27	N/M	N/M	N/M	661	15
High Mw PEI	N/A	25	41	34	60000	1395

[a] Calculated amine ratio error was estimated by triplicate analysis of HAS13. This error applied to the calculated average over the HAS-VLAS is given by the range, 1°:2°:3° = 27.9-29.2 : 45.1-46 : 25.7-26.3.

One might hypothesize that at high amine loadings, polymerization occurred on the particle exterior instead of inside the pores, resulting in comparably high molecular weight surface-bound polymers. These ASEC results seem to contradict that hypothesis because molecular weight would increase with amine loading throughout the data series, not just at low amine loadings, and there would likely be a bimodal distribution to the data, although admittedly, bimodal distributions at very low molecular weights may be difficult to resolve with typical ASEC techniques. However, the collected data are consistent with the hypothesis that the aminopolymers grow in the silica pores and eventually block the pore mouths once a critical radius is reached. As an increasing number of pores in the SBA-15 particle become blocked, the average molecular weight would then approach the chain length required to block a pore.

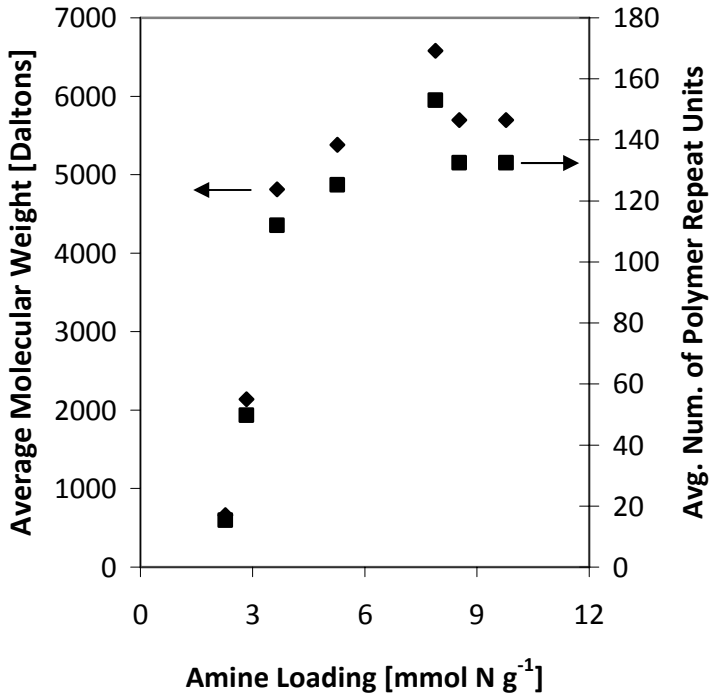

Figure 3.4. ASEC retention times for aminopolymers cleaved from HAS adsorbents with different amine loadings.

3.2.3. Modification of the HAS Adsorbent Synthesis

Small changes to the HAS synthesis were made to determine their effect on the resulting material's aminopolymer loading. The first experiment was to examine the catalytic effect of the acetic acid in the HAS synthesis. The first mechanistic step of the ring-opening polymerization reaction is suggested to be the protonation of aziridine by acid in solution when acetic acid is present. However, the silica surface silanols are mildly Brønsted acidic, and thus acetic acid may not be needed in this synthesis. HAS9 was synthesized without the addition of acetic acid, and it was determined that added acid had little or no effect on the final aminopolymer loading, resulting in 7.37 mmol N g^{-1} at an aziridine to silica ratio of 2. Therefore, the acidity of the SBA-15's surface silanol groups is sufficiently strong to catalyze the aziridine ring-opening reaction, as expected.

The ring-opening polymerization is a fast reaction and thus can create aminopolymers uncontrollably, sometimes to the detriment of material properties such as gas diffusion when the polymerization occurs rapidly enough that it may block pores. In an effort to affect the reaction rate, HAS12 was synthesized by the dropwise addition of aziridine to the reaction environment over 90 minutes without the addition of a catalytic amount of acetic acid. The obtained organic loading is lower than expected for the aziridine to silica ratio used (~ 3). This unexpected result suggests that a concentration gradient from the bulk solution to the interior pore space may be crucial for aziridine diffusion into the pore space and subsequent productive reaction in the pore system.

Another important aspect in the preparation of any complex material is synthetic reproducibility. To investigate whether the uncontrolled but constrained polymerization was reproducible, two HAS materials were synthesized side by side with the same quantities of aziridine, mesoporous silica, and acetic acid from the same batches. They were reacted for the same length of time in glass pressure vessels of the same size and shape and were stirred at the same rate with stir bars of the same size and shape. The nitrogen loadings of the two materials were 7.58 and 7.89 mmol N g^{-1} and the surface areas were 47 and 60 m^2 g^{-1}, respectively, indicating that the two materials were very similar (Table 3.3, HAS7 and HAS8). However, it should be noted that these materials do not fit exactly into the trends in composition and pore characteristics described for the HAS-VLAS. Instead, it appears that while the HAS synthesis is reproducible with the same batch of materials, the use of different batches of aziridine, SBA-15, toluene, as well as small variations in laboratory conditions such as humidity and temperature, may make it difficult to exactly reproduce HAS adsorbents with specific loadings and pore characteristics.

Table 3.3. Compositions and physical characteristics of HAS adsorbents prepared through various synthesis modifications.

Sample	Amine Loading [mmol N/g]	Aziridine to SBA-15 Ratio [w/w]	Yield [a] [mol N/mol aziridine]	Pore Dia. [nm]	BET Surface Area [m^2/g]	Pore Vol. [cc/g]	Pore Vol. [cc/g SiO_2]	Micropore Vol. [cc/g]
HAS7 [b]	7.58	2.00	0.29	4.5	47	0.09	0.16	0.00
HAS8 [b]	7.89	2.00	0.30	4.7	60	0.12	0.20	0.00
HAS9 [b, c]	7.37	2.01	0.27	4.9	68	0.12	0.21	0.00
HAS12 [d, e]	4.46	3.10	0.08	5.1	245	0.38	0.50	0.01
SBA2	0			6.2	865	0.81	0.81	0.06
SBA4	0			5.9	774	0.74	0.74	0.05

[a] Calculated as mol N g^{-1} SiO_2 in the prepared HAS divided by the reactant ratio [mol N g^{-1} SiO_2]
[b] SBA2 used as silica support in synthesis
[c] Synthesis performed without the addition of acetic acid
[d] SBA4 used as silica support in synthesis
[e] Synthesis performed without the addition of acetic acid and with aziridine added dropwise to the reaction over a period of 90 minutes

The role of solvent in the HAS synthesis is complex. First, the solvent must be capable of dispersing the mesoporous silica adequately under stirring so that the reaction environment is well-mixed and the mass transfer of aziridine to the particle surface is minimized. Second, aziridine must be soluble in the reaction solvent, again for the reaction environment to be well-mixed. Third, the solvent must be non-reactive to the mesoporous silica and the aziridine molecule, which excludes all protic solvents. However, several common organic solvents meet these criteria while still displaying different physical characteristics, such as dipole moment and dielectric constant.

To understand the effect of reaction solvent on the resulting HAS material, reactions were run with an aziridine to SBA-15 reactant ratio of 2 in diethyl ether, tetrahydrofuran (THF), dichloromethane (DCM), and acetonitrile. A small amount of glacial acetic acid was added to catalyze the reactions and the reaction mixtures were left overnight at room temperature under vigorous stirring in glass pressure vessels. In a typical synthesis using toluene, considerable amounts of product fell out of dispersion and built up in the form of white gel on the wall of the pressure vessel during reaction.

This is likely due to the highly hydrophilic character of the aminopolymer, in that once a sufficient quantity of the polymer forms on the silica support, the particles agglomerated due to repulsion from the surrounding organic solvent. However, this effect was not observed in the reactions performed in THF, DCM, and acetonitrile, while the reaction with diethyl ether showed a small amount of gel-like agglomeration, albeit much less than was observed in toluene. The organic loadings of the resulting HAS materials were all substantially lower than those obtained from reaction in toluene (Table 3.4). These observations are possibly related to the polarity or hydrogen-bonding nature of the various organic solvents disrupting the polymerization of amines or preventing the fixation of organics on the silica surface. It may be that these forces provide a driving force for aziridine to diffuse to the relatively hydrophilic environment of the silica pore surface.

Table 3.4. Organic contents and pore properties of various samples synthesized in different reaction solvents.

Sample	Solvent Used	Dipole Moment [debye]	Dielectric Constant	Amine Loading [mmol N/g]	Pore Dia. [nm]	BET Surface Area [m^2/g]	Pore Vol. [cc/g]
HAS8	Toluene	0.37	2.4	7.98	4.6	61	0.09
SCHAS1	Diethyl Ether	1.15	4.3	5.19	5.4	284	0.44
SCHAS2	THF	1.75	7.5	5.49	5.3	302	0.48
SCHAS3	DCM	1.6	9.1	5.60	5.4	233	0.38
SCHAS4	ACN	3.92	37	5.07	5.5	270	0.43

3.2.4. Adsorption Capacities of the HAS-VLAS

The equilibrium CO_2 adsorption capacity of a solid adsorbent is often used as the primary measure of its performance. The amount of CO_2 an adsorbent can adsorb per unit mass has a direct effect on the amount of adsorbent needed to capture CO_2 from a given process. Raising an adsorbent's capacity could drastically reduce the capital and

operating costs of a CO_2 capture process. However, it is important to note that equilibrium capacity is not the only important parameter in evaluating an adsorbent's performance. Adsorption and desorption kinetics, heats of adsorption, attrition, regenerability, operating temperature range, and reaction with contaminants are all important characteristics that need to be determined and then weighted properly for the specific application (e.g., a 500 MW coal-fired power plant) to effectively measure an adsorbent's performance. Adsorption capacities are sometimes reported as working capacities rather than equilibrium capacities, when adsorption is measured for a shorter time than required to reach equilibrium. Working capacities may also be reported when an incomplete desorption step is performed, leaving part of an adsorbent's capacity inaccessible for subsequent adsorption steps. In either instance, working capacities are perhaps more relevant to an adsorbent's performance in a real CO_2 capture process where cycle times will likely be short and temperature swings performed as narrowly as possible to reduce energy costs. Typically, cycle times in a practical adsorption process will be significantly shorter than those used here, where relatively long cycle times were used to generate working capacities. Again, all these factors must be evaluated, and the tradeoff between amount of adsorbent and process costs for that adsorbent considered, for a specific local application, to determine an adsorbent's efficacy.

The first report on HAS adsorbents described a sample with a CO_2 capacity of 3.11 mmol CO_2 g^{-1} adsorbent (hereafter shortened to mmol g^{-1}) for a moderately loaded adsorbent with a humidified 10% CO_2 test gas to simulate flue gas capture.*[26]* However, the capacities reported here are slightly higher than those reported previously for similar materials. The experiments discussed in this paper were conducted with similar parameters and equipment (see Experimental section), but the step size between scans in the MS was decreased from 7 to 0.7 seconds. This increases the number of data points by a factor of ten and substantially reduces the error obtained from numerical integration. Additionally, the data was analyzed in a slightly different manner; adsorption was

measured from the time CO_2 was first introduced to the adsorbent bed, not from the time the first CO_2 signal was detected with the MS (breakthrough time). For more information on the data analysis, please see the Appendix A. In most cases, this distinction did not have a great effect on the final determined capacity because of the relatively small size of the adsorbent bed and the minimal pressure drop experienced across it. Nevertheless, the effect was noticeable over the range of adsorbents prepared.

The CO_2 working capacities of the HAS-VLAS were measured at 25 and 75 °C under humid conditions via methodology described in the Experimental section and Appendix A and are summarized in Figure 3.5. The working capacities increased as amine loading increased in a roughly linear manner. This result was expected because a sufficiently long adsorption time was chosen (200 minutes) rendering kinetic effects less important, leaving the measured capacity mainly a function of the accessible adsorption sites. This trend was observed for both operating temperatures that were investigated, where the capacity at 25 °C was 1.1 mmol g^{-1} higher than the capacity at 75 °C, averaged over the data set, a trend that is in good agreement with the previously reported results.*[26]* The highest capacity measured was 5.55 mmol g^{-1} for an HAS adsorbent with an amine loading of 9.78 mmol N g^{-1}. It should be noted that since these working capacities do not represent full equilibrium capacities and were measured over a temperature range of 50 °C, they should not be used for the calculation of fundamental constants such as heats of adsorption.

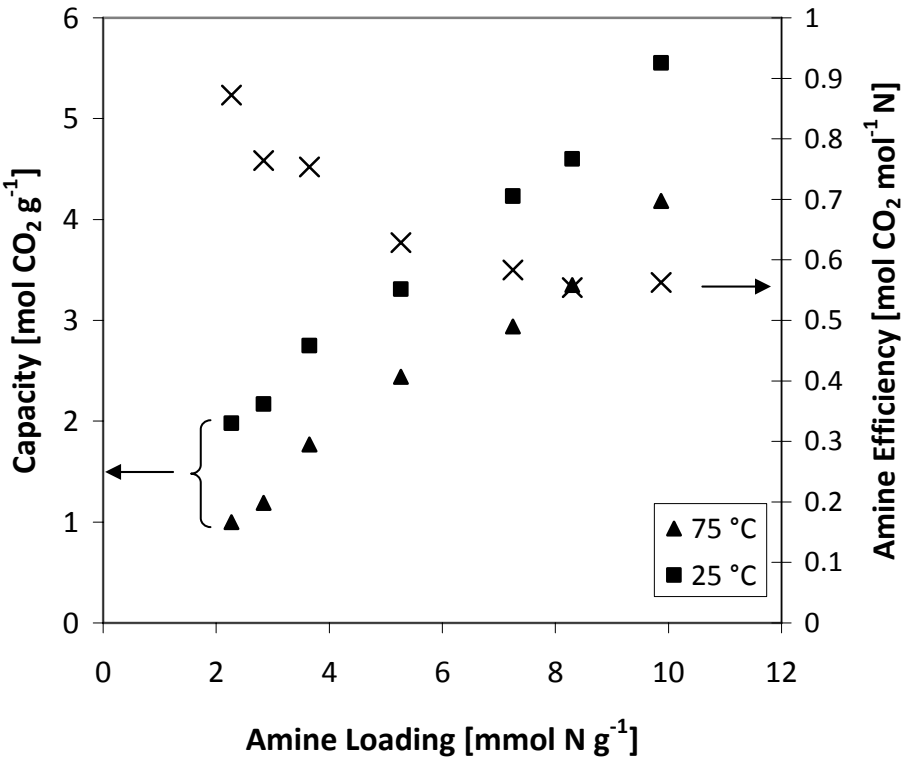

Figure 3.5. CO_2 capture working capacities at 25 and 75 °C and associated amine efficiency vs. HAS amine loading for the HAS-VLAS.

Another important measure of an amine-based adsorbent's performance is its amine efficiency, or the ratio of the moles of CO_2 captured to the moles of nitrogen present in the material. The maximum amine efficiency of an adsorbent depends on the amine type and the presence or absence of water. Under dry conditions, 1° and 2° amines react with CO_2 to form carbamates through a zwitterionic mechanism.*[7, 8, 27-30]* This mechanism requires free base to deprotonate the zwitterion to form the carbamate. Thus, under dry conditions, two moles of amines are required to capture one mole of CO_2, reducing the maximum amine efficiency to 0.5 mol CO_2 mol^{-1} N. In humid conditions, H_2O or OH^- can act as free base, raising the maximum amine efficiency to 1.0 mol CO_2 mol^{-1} N as long as stoichiometric quantities of H_2O are present. 3º amines are not suggested to react directly with CO_2, rather they catalyze the formation of bicarbonate in

the presence of water.*[29, 32, 104]* The first step in this mechanism is the dissociation of H_2O to form a cationic quanternary amine and OH^-, which then reacts with CO_2 to form the bicarbonate anion. Therefore, the maximum amine efficiency for 3º amines is 1.0 in the presence of water but the expected value is close to 0 under dry conditions. 1º and 2º amines may also react via this mechanism, however, the reaction rate for the formation of carbonates in solution by this mechanism is generally much lower than for the zwitterionic mechanism.*[7, 29]* Taking both of these reaction mechanisms into consideration, the maximum amine efficiency for the HAS adsorbent is 1.0 under humid conditions and 0.37 under dry conditions, assuming an average amine ratio of 1º:2º:3º = 28:46:26. Clearly, the performance of the HAS adsorbent is fundamentally aided by the presence of water, unlike other types of solid adsorbents, such as zeolites, activated carbons, and MOFs.*[15-17]*

Several additional factors can cause a decrease in amine efficiency. Amines can be inaccessible to entering CO_2 due to pore blockage, location within micropores, or steric hindrance from neighboring species, especially after long adsorption periods where equilibrium is nearly reached and almost every amine has captured a CO_2 molecule. Amine efficiency can be reduced if, in spite of the presence of water, CO_2 reacts with the amines to form carbamates. There is some evidence in the literature that suggests that at early adsorption times, the formation of carbamates is kinetically favored, although it is unclear whether this is an inherent characteristic of supported amines or due to other factors such as accessibility and amine type.*[39, 53, 58, 70, 71]* Amine efficiency may also be reduced when CO_2 adsorbs in the form of bidentate species. Chuang observed the formation of bidentate carbonate (1575,1390 cm^{-1}) and bidentate bicarbonate (1634 cm^{-1}) for CO_2 adsorption with primary amine-functionalized SBA-15 under dry conditions.*[58]*

Figure 3.5 shows the amine efficiencies for the HAS-VLAS at 25 °C. At low loadings, the amine efficiency decreased as amine loading increased and reached a plateau at higher loadings. Since these measurements were made after 200 minutes of

adsorption, these amine efficiencies are somewhat lower than they would be at full equilibrium. Nevertheless, they exhibit the fact that HAS adsorbents with high loadings do not take full advantage of their high amine density. Since the highly loaded adsorbents displayed low pore volumes and likely possessed blocked pores, the reduced amine efficiencies were probably due to limited mass transfer or steric constraints.

The above discussion described experiments designed to investigate CO_2 capture from a simulated flue gas consisting of humidified 10 % CO_2 in Ar. An alternative way to describe an adsorbent's performance is to measure its adsorption isotherm over a broad range of CO_2 partial pressures, since flue gases vary slightly in CO_2 concentration and other alternative power-generation strategies may produce process streams in need of CO_2 separation that vary over a wide concentration range. Additionally, isotherms are often used to extract information on key physical constants of an adsorbent, such as heats of adsorption and Henry's Law constants.

Single component isotherms for a highly loaded HAS adsorbent (HAS2) were measured at 35 and 75 °C (Figure 3.6) using pressure-volume-temperature (PVT) techniques. In these measurements, a small amount of sample (0.8 g) was exposed to a known volume of CO_2 and allowed to reach equilibrium. The moles of CO_2 adsorbed at a given pressure were then calculated and the experiment repeated at an increased pressure, assembling the isotherm. In some cases, single expansions took several weeks to reach equilibrium, so it is likely that heat transfer and reaction rate effects, which have timescales on the order of minutes or less, were not relevant to the measured equilibrium. However, it is interesting to note that the results indicate a higher dry capacity at 75 °C than at 35 °C. This goes against intuition since the adsorption of CO_2 with amines is an exothermic process with a negative change in entropy. Fundamentally, thermodynamics suggests that capacity should decrease with increasing temperature. Hence, this observation is probably associated with severely hindered diffusion at the 35 °C adsorption condition. Similar results have been observed for solid amine-impregnated

silica adsorbents possessing large amine loadings with little or no remaining pore volume.*[37, 41, 43]* This result again fits with the hypothesis that nearly complete pore blockage occurs at or near the pore mouths of the HAS adsorbent, effectively blocking off access to amines already in the pores.

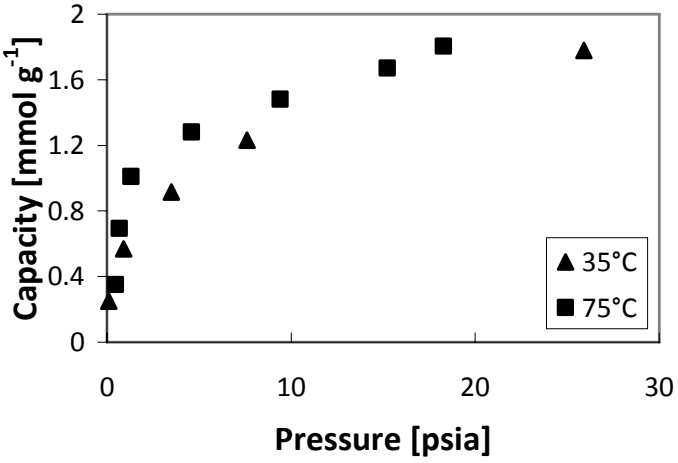

Figure 3.6. Single component CO_2 adsorption isotherm for a highly-loaded HAS adsorbent at 35 and 75 °C.

3.2.5. Adsorption Kinetics

The kinetics of adsorption and desorption are also important in assessing an adsorbent's performance. The application of capturing CO_2 from flue gas requires that adsorbents capture CO_2 as quickly as possible to shorten adsorption/desorption cycle times and to reduce the total quantity of adsorbent required to reduce CO_2 concentration to a required level. A general theme in the silica-supported amine literature is a fast initial adsorption step followed by a much slower approach to equilibrium,*[49]* which may be so gradual as to cause most researchers to simply end the experiment before true equilibrium is reached.*[15]* In addition to obvious material characteristics, such as the density of adsorption sites a material possesses, there is also a strong link between the open pore volume of the adsorbent and adsorption kinetics.*[41, 59]* This is related to the

mass transfer of CO_2 through the pores to the adsorption sites and illustrates the importance of amine accessibility.

The adsorption kinetics of the HAS-VLAS measured in the packed bed flow system and reported below are not true adsorption kinetics, but rather, a combination of process related effects (adsorbent bed bypass, gas mixing, etc.), internal mass transfer effects, and intrinsic chemical reaction rates. They should be interpreted as being experiment dependent and not necessarily scalable. However, the results do highlight physical differences in the adsorbents and support hypotheses drawn in the materials characterization sections.

The MS at the outlet of the packed bed flow system collects transient concentration data as adsorption occurs. With the assumption that deviation from the value at 200 minutes is attributed to active adsorption, the amount adsorbed at a certain time is the integral of the concentration differences from the start of the experiment to that given time. This translates to an uptake curve of the mass adsorbed (Mt, here normalized by weight of adsorbent used) versus square root time (to highlight the large changes in early times). Uptake plots for the HAS-VLAS are given in the Appendix A for adsorption temperatures of 25 and 75 ºC, respectively.

Given the long times required for some of these adsorbents to approach equilibrium, it is perhaps more reasonable to discuss their kinetics in terms of working capacities that are reported for some time less than the time required to reach full capacity. It is common practice to use the measure of adsorption halftime (the time where the adsorbent reaches half of its capacity at the end of the experiment) for this purpose.*[103]* Figure 3.7 shows the adsorption halftimes for the HAS-VLAS at 25 and 75 ºC. At room temperature, the adsorption halftimes of the HAS materials with high loadings were significantly longer than those of adsorbents with lower loadings. Since process and measurement variables were all similar for these measurements, these data show that mass transfer limitations of the highly loaded adsorbents had a significant

detrimental effect on the adsorption kinetics, despite the presence of a larger number of potential adsorption sites. Again, this fits our hypothesis that highly loaded HAS materials likely have a large number of their pores blocked at or near the pore mouths, dramatically reducing mass transfer. The data set obtained at 75 ºC also displayed this trend, albeit to a lesser degree. This is expected since diffusional resistances will be less significant at higher temperatures. The variation in adsorption capacity and kinetics show that these HAS materials can be tuned to have different adsorption rates and capacities which, coupled with process variations (fixed-bed, fluidized-bed, fibers*[105]*) can enable the scientist or engineer significant leeway in designing an optimized CO_2 capture process.

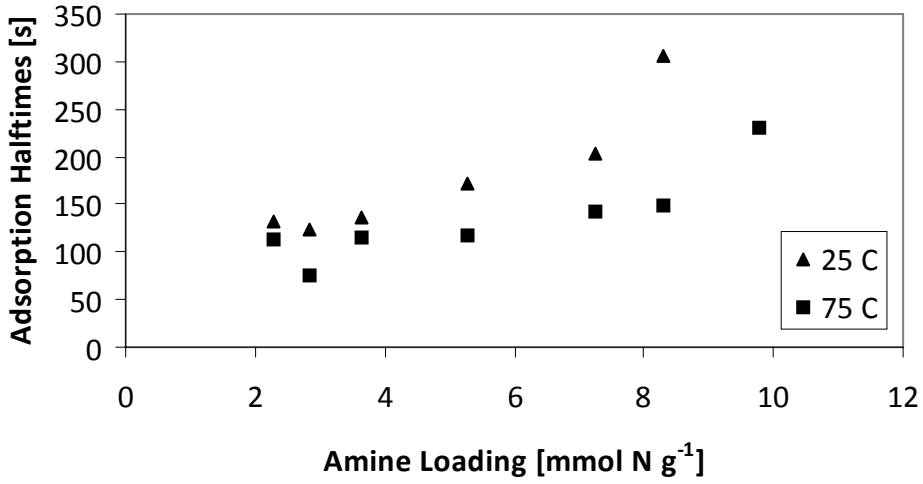

Figure 3.7. Adsorption halftimes of the HAS-VLAS at operating temperatures of 25 and 75 °C. The halftime at 25 ºC for an amine loading of 10 mmol N g^{-1} was omitted because it was off the scale of the plot, with a value of 2300 seconds.

3.3. Conclusions

We have investigated the degree of control that can be exerted on the HAS synthesis to tune the adsorbent's composition, adsorption capacity, and adsorption

kinetics. Specifically, it was found that by simply adjusting the aziridine to silica reactant ratio, materials with a wide range of characteristics were prepared. Amine loadings, and therefore, potential active adsorption sites ranged from 2 to 10 mmol N g^{-1} adsorbent, resulting in working adsorption capacities ranging from 2.0 to 5.6 mmol g^{-1} at 25 °C. As adsorbent organic content increased, pore volume and surface area decreased. At high loading levels, N_2 physisorption data and ASEC data indicated that polymer growing inside the silica pores reached a critical density and then caused pore blocking, likely at or near the pore mouths. This inferred physical characteristic was likely the cause of the HAS-VLAS's observed decline in amine efficiencies and adsorption kinetics at high amine loadings. It is important to note that the pore characteristics of the parent SBA-15 support were the physical boundaries that limited the amount of amines that were incorporated into the adsorbent and also the mass transfer to those amines. Future research will investigate the variation of the silica support to further increase the performance of HAS adsorbents.

Despite the tunability of the HAS amine loading and the following predictability of the adsorption behavior, the aminopolymer growth was still the result of an uncontrolled polymerization. However, it appears that the polymerization may have been constrained by the silica support, as evident by in the similar degree of branching of the aminopolymer (1°:2°:3° amines = 28:46:26) and an upper bound in the molecular weight (approximately 6500 Daltons). Efforts to further constrain the polymerization by changing reaction conditions or adding inhibitors may be successful, but it is unlikely that the degree of branching or molecular weight will ever be controlled using this monomer. Nevertheless, the outcome of the HAS synthesis is fairly predictable and, to that end, makes the HAS adsorbent a promising candidate for CO_2 capture process technologies where the balance between desired adsorption capacities, kinetics, and operating temperature (among others) will likely be decided on a local application specific basis.

3.4. Experimental

All chemicals were purchased from Sigma-Aldrich and used without modification. Single component gases were purchased from Airgas, Inc. Custom gas mixtures were purchased from Matheson Tri-Gas, Inc.

3.4.1. SBA-15 Synthesis

Mesoporous SBA-15 was synthesized similar to previously reported methods.*[106-108]* In a typical synthesis, 17.9 g P123 (EO-PO-EO block copolymer), 99.4 g HCl, and 561 g H_2O were stirred overnight in a 1 L Erlenmeyer flask. To the micellular solution, 39.6 g tetraethylorthosilicate (TEOS) was added and stirred for 5 minutes. The solution was transferred to an oven and stirred at 35 ºC for 20 h. Stirring was then terminated and the solution was post-treated at 80 ºC for 24 h. The white solid was filtered and washed with copious amounts of DI H_2O and dried overnight at 75 ºC. The organic template was removed by calcination using the following temperature program: (1) ramping the temperature to 200 ºC at a rate of 1.2 ºC $min.^{-1}$, (2) holding at 200 ºC for 1 h., (3) ramping the temperature to 550 ºC at a rate of 1.2 ºC $min.^{-1}$, (4) holding at 550 ºC for 6 h. The calcined SBA-15 was then dried at 200 ºC under vacuum overnight.

3.4.2. Aziridine Synthesis

Aziridine was synthesized and purified similar to reported methods.*[26, 87]* In a typical synthesis, 34.5 g 2-chloroethylamine hydrochloride was added to a solution of 34.1 g KOH in 200 g DI H_2O. The solution was stirred at 50 ºC for 2 h. Aziridine was then distilled from solution under a partial static vacuum of 530 mm Hg and collected in a cold trap. The collection flask was sealed and then stored at 0 ºC. ^{1}H NMR (400 MHz, D_2O, δ): 1.56 (s); ^{13}C NMR (400 MHz, CD_2Cl_2, δ): 18.1. Aziridine is toxic if swallowed, inhaled, or absorbed through the skin. *Caution: Aziridine is a carcinogen and*

reproductive hazard. Use extreme caution when handling aziridine. Only handle aziridine in a ventilated fume hood and always wear proper personal protection equipment.

3.4.3. HAS synthesis

The HAS synthesis has been reported elsewhere.*[26]* Variations of the syntheses with different aminopolymer loadings are reported here (Table 3.1). In a generalized synthesis, a predetermined amount of aziridine was added to a suspension of a measured amount of SBA-15 in toluene. Approximately 4 drops of glacial acetic acid were added to catalyze the ring-opening polymerization. The mixture was stirred overnight at room temperature in a glass pressure vessel, sealed with a PTFE cap. The solid was filtered and washed with copious amounts of toluene and methanol and then dried at 50 ºC under vacuum.

3.4.4. Removal of Aminopolymer from Silica Support

For a given reaction targeted at cleaving the aminopolymer from the inorganic support, approximately 500 mg of HAS adsorbent was stirred in a basic solution of 33 g KOH in 100 g DI H_2O at 50 ºC overnight, after which the silica support was degraded into soluble species. About half of the H_2O was removed by vacuum distillation at 75 ºC and the remaining solution was stored in a freezer overnight. The aminopolymer phase separated and was recovered by decanting/physical separation. To ensure that this process did not damage or alter the aminopolymer, commercial low molecular weight PEI was subjected to the same cleavage conditions and workup. The recovered polymer was found to have the same degree of branching by inversely-gated ^{13}C NMR before and after this cleavage treatment.

3.4.5. Characterization

Pore characteristics of the bare silica support and the HAS adsorbents were assessed via N_2 physisorption analysis at 77 K using a Micromeritics ASAP 2010. Amine loadings were determined by TGA using a Netzsch STA409. Total organic loading was estimated as the weight loss from 160 to 760 °C, followed by inference of a stoichiometric ratio of ethyleneimine units (molecular weight of 43 Daltons) after accounting for silica surface silanol condensation (~ 1 wt%). FT-IR spectroscopy using KBr pellets and FT-Raman spectroscopy were obtained on a Bruker Vertex 80v optical bench with a RAMII Raman module. ^{1}H solution NMR experiments were conducted on a Varian Mercury Vx 400. Inversely-gated ^{13}C solution NMR experiments were conducted on a Bruker DRX 500. Samples were prepared with D_2O and a single drop of $Cr(acac)_2$ in deuterated dimethylsulfoxide (DMSO) to aid relaxation and minimize interference from possible residual silica or base salts. Typically, 6000 to 10000 scans were gathered with a relaxation time of 4 seconds in the experiments using an inversely-gated pulse sequence. This relaxation time is in excess of the 3.3 seconds required for quantitative analysis determined in a full T1 study by Geckle for branched PEI.*[109]* Molecular weights of PEI and cleaved aminopolymer were determined by ASEC at 30 °C. The ASEC system was comprised of a Shimadzu LC-20AD pump, a Shimadzu RID-10A RI detector, a Shimadzu SPD-20A UV detector, a Shimadzu CTO-20A column oven, and Viscotek TSK Viscogel PWXL Guard, G3000, G4000 and G6000 columns mounted in series. The mobile phase consisted of 0.5 M acetic acid and 0.3 M Na_2SO_4 and the flow rate was maintained at 0.5 mL $min.^{-1}$ Commercial PEI's of a range of molecular weights from 800 to 10000 Daltons were used to generate a calibration curve.

3.4.6. Adsorption

Humid adsorption capacities and apparent adsorption kinetics were measured with a packed bed flow reactor with an online mass spectrometer (MS) as described in a

previous report.*[26]* Briefly, approximately 60 to 80 mg of adsorbent was dispersed in 300 mg of sieved sand (250 to 425 micron) and loaded into a pyrex tubular reactor (1/4 in. O.D.). The assembly was then placed in a temperature controlled tube furnace. Before an experiment was started, desorption was performed for at least 3 h at 110 ºC under flowing Ar. Also, before an adsorption experiment, test gas (10 % CO_2 balance Ar) was pre-humidified to a steady state by flowing through two glass water bubblers at room temperature. To begin an experiment, the inlet to the reactor was switched from desorption gas to test gas and the time was noted. Adsorption was then performed at a test gas flow rate of 20 mL min^{-1} for 200 minutes at the desired temperature. The CO_2 concentration at the reactor outlet was measured with a Pfeiffer Vacuum QMS 200 Prisma Quadrupole MS. The mass of CO_2 adsorbed was calculated from the MS output as described in the Appendix A.

CHAPTER 4

EFFECT OF SUPPORT STRUCTURE ON CO_2 ADSORPTION PROPERTIES OF PORE-EXPANDED HYPERBRANCHED AMINOSILICAS

This chapter is largely reproduced from "Effect of Support Structure on CO_2 Adsorption Properties of Pore-expanded Hyperbranched Aminosilicas" by Jeffrey H. Drese, Sunho Choi, Stephanie A. Didas, Praveen Bollini, McMahan L. Gray, and Christopher W. Jones, submitted to Langmuir for publication.*[110]*

4.1. Introduction

Growing concern over the increasing atmospheric CO_2 concentration has driven focused research to the development of new processes and technologies for CO_2 separation from dilute sources, such as flue gas from power generation facilities. Of the many technologies and strategies that have been considered for this application, CO_2 absorption with aqueous solutions of amines is the most established and mature. However, several aspects of the aqueous amine process detract from its cost-effectiveness, including the large energy penalty for regeneration associated with the solution's substantial composition of water and the corrosion of process equipment from contact with the caustic liquid. As an alternative, solid-supported amines have been considered for this application because of their lower heat capacity and reduced potential for corrosion from solid-solid contact.

Several solid materials have been used to support amine-containing organic moieties, such as activated carbons, carbon nanotubes, and various polymers, but the bulk of the supported-amine literature focuses on the use of mesoporous silica.*[15, 69, 111,*

112] The amorphous SiO_2 structure of mesoporous silica can be synthesized to include ordered pore spaces with different geometries (e.g. 2-D cylindrical: MCM-41, SBA-15; 3-D interconnected: MCM-48, SBA-16, KIT-6), or non-ordered pore spaces with a distribution of sizes and connectivities (e.g. mesocellular foam (MCF), various commercial materials).*[93, 108, 113-115]* These materials are attractive from the mass transfer perspective because their pore diameters and pore volumes are larger than comparable microporous supports, such as carbons or zeolites, while still retaining high surface areas.

There are three classes of aminosilica adsorbents that are distinguished by their method of preparation.*[116]* Class 1 adsorbents are prepared through the physical impregnation of a mesoporous silica support with amine-containing organic moieties, the most commonly used being PEI.*[37, 41, 43]* Since nearly the entire pore volume of the support can be filled with amines, class 1 adsorbents generally have large amine loadings, but under certain conditions may be susceptible to leaching because they are not covalently bound to the support through a chemical bond.*[26]* Class 2 adsorbents are prepared through the reaction of amine-containing silanes with the silica support's surface silanol groups.*[34, 66]* While the amine moieties in these materials are covalently tethered to the support, their functionalized density is limited to a degree by the support's surface area and the stoichiometric ratio of amines per silane molecule. Class 3 adsorbents are prepared through polymerization of an amine-containing reactive species, such as aziridine, from the surface silanols of the support, creating covalently bound aminopolymers in the pore space.*[26, 86]*

The inclusion of organic species into the pore space of mesoporous silica results in the reduction of surface area, pore diameter, and pore volume of the composites for all adsorbent classes, but to varying degrees. Typically, only the pore walls of class 2 adsorbents are functionalized with organic groups if the grafting synthesis is done in the absence of added water, leaving the centers of the pores open for gas to diffuse

through.*[17]* In contrast, class 1 adsorbents prepared with PEI, a hyperbranched polymer, may have much of their pore space filled, depending on the ratio of organic to silica used in the synthesis. In this way, if enough organic is impregnated into the support, the resulting composite may show little or no measurable pore volume.*[40]* Thus, the pore volume of the bare silica support establishes a practical limit to the amine loading of a class 1 adsorbent, where the further addition of organic will accumulate on the particle exterior.*[41]* Diffusion of gas through this extra layer will behave as diffusion through bulk organic, providing additional mass transfer resistance. Therefore, the structure of the mesoporous silica support, in terms of average pore diameter and pore volume, defines the maximum amine loading and mass transfer characteristics of a class 1 adsorbent. Illustrating this point, Ahn synthesized several class 1 adsorbents with 50% organic content with five different mesoporous silica supports: MCM-41, MCM-48, SBA-15, SBA-16, and KIT-6.*[41]* The equilibrium adsorption capacities of the five materials with equal amine loadings varied over a small range from 2.52 to 3.07 mmol CO_2/g adsorbent (hereafter referred to as mmol/g) suggesting only a small fraction of amine sites were inaccessible. However, the time required for the 50% PEI loaded KIT-6 adsorbent to reach 90% of its equilibrium capacity was almost an order of magnitude faster than for adsorbents prepared from the other four silica supports. This is likely because of the moderate remaining pore volume of the KIT-6 adsorbent (0.18 cc/g) compared to the other composites, which were all below 0.10 cc/g. Large differences in the particle sizes of different materials may also affect adsorption kinetics, but the particle sizes of these materials were not reported.

Class 3 adsorbents, such as the HAS adsorbents previously reported by our research group, consist of organic polymers chemically tethered to the walls of the silica support, typically being prepared via in-situ polymerization.*[26]* Although the location of the polymer in the pore space cannot always be precisely identified, it was suggested that at low polymer loadings, most of the pore surface was functionalized with small

molecular weight polymers, perhaps preferentially at or near the pore openings.*[86]* However, at higher amine loadings, polymerization was suggested to propagate axially into the pore space and in some cases the polymerization blocked the pores, again perhaps preferentially at or near the pore openings. In a previous study using SBA-15 as the mesoporous silica, a set of HAS adsorbents was synthesized with a range of organic loadings by adjusting the aziridine to silica weight ratio used in the synthesis. Characterization of the adsorbents revealed that below a critical radius of ~5 nm, the aziridine polymerization blocked the silica pores, severely hindering mass transfer and resulting in reduced amine efficiencies (mol CO_2/mol N) over the course of the adsorption experiment. Analysis of the HAS aminopolymer formed in these materials showed that the molecular weight remained nearly constant at these higher loadings, supporting the hypothesis that polymerization propagated until the pore was blocked.*[86]*

In this contribution, the synthesis and characterization of HAS adsorbents prepared using several different mesoporous silicas (pore diameters >10 nm) as the solid supports are described. The use of PE MCM-41 as a support was shown to improve the adsorption performance of a class 2 adsorbent.*[66]* This strategy was applied to the HAS synthesis to minimize pore blocking from polymerization and improve adsorption performance in CO_2 capture experiments using simulated flue gas.

4.2. Experimental Methods

PESCOM silica was acquired from a commercial vendor. Cab-O-Sil fumed silica was purchased from Cabot Corp. All other chemicals were purchased from Sigma-Aldrich and used without modification. Single component gases were purchased from Airgas, Inc. 10% CO_2 balance Ar mixed gas was purchased from Matheson Tri-Gas, Inc.

4.2.1. Pore-expanded SBA-15 Synthesis

The synthesis of mesoporous PE SBA-15 was adapted from a previously reported method. In a typical synthesis, 13.2 g Pluronic 123 (EO-PO-EO block copolymer), 79.4 g HCl, and 343.7 g DI H_2O were stirred in a 1 L Erlenmeyer flask at room temperature. After 5 min, 13.2 g TMB was added to the solution as a swelling agent. After an hour of stirring, 28.3 g TEOS was added to the micellular solution and stirred for another 5 minutes. The solution was transferred to a sealed autoclave and stirred at 35 ºC for 24 h. Stirring was then terminated and the solution was post-treated at the desired temperature (100, 110, or 120 ºC) for 72 h. The white solid was filtered, washed with copious amounts of DI H_2O, and dried overnight at 75 ºC. The organic template was removed by calcination in air using the following temperature program: (1) ramping the temperature to 200 ºC at a rate of 1.2 ºC $min.^{-1}$, (2) holding at 200 ºC for 1 h., (3) ramping the temperature to 550 ºC at a rate of 1.2 ºC $min.^{-1}$, (4) holding at 550 ºC for 6 h. The calcined SBA-15 was then dried at 200 ºC under vacuum overnight.

4.2.2. Mesocellular Foam Synthesis

The synthesis of MCF was adapted from previously reported methods.*[117, 118]* In a typical synthesis, a solution of 16.0 g P123, 47.4 g HCl, and 260 g DI H_2O was stirred at room temperature in a 500 mL Erlenmeyer flask until complete dissolution of the polymer. Then 16.0 g of TMB was added and the solution was stirred at 39 ºC for 2 hours. 34.6 g TEOS was added to the solution and stirred for 5 minutes before the mixture was transferred to an oven at 40 ºC and heated without stirring for 20 hours. A solution of 184 mg NH_4F in 20 mL DI H_2O was added as a mineralization agent to the siliceous mixture, briefly stirred, and then post-treated at 100 ºC for 24 hours. The white solid was filtered, washed with copious amounts of DI H_2O, and dried overnight at 75 ºC. The organic template was removed by calcination in air using the following temperature

program: (1) ramping the temperature to 550 ºC at a rate of 1.2 ºC/min., (2) holding at 550 ºC for 6 h. The calcined MCF was then dried at 200 ºC under vacuum overnight.

4.2.3. Non-Pore-Expanded SBA-15 Synthesis

The synthesis of SBA-15 was adapted from previously reported methods.*[86, 108]* In a typical synthesis, a solution of 17.9 g P123, 99.4 g HCl, and 561 g H_2O was stirred overnight in a 1 L Erlenmeyer flask at room temperature. 39.6 g TEOS was added to the micellular solution and stirred for 5 min. The mixture was transferred to an oven and stirred at 35 ºC for 20 h. Then the mixture was post-treated at 80 ºC without stirring for 24 h. The white solid was filtered and washed with copious amounts of DI H_2O and dried overnight at 75 ºC. The organic template was removed by calcination in air using the following temperature program: 1) ramping the temperature to 200 ºC at a rate of 1.2 ºC/min., (2) holding at 200 ºC for 1 h., (3) ramping the temperature to 550 ºC at a rate of 1.2 ºC/min., (4) holding at 550 ºC for 6 h. The calcined SBA-15 was then dried at 200 ºC under vacuum overnight.

4.2.4. MCM-41 Synthesis

The synthesis of MCM-41 was adapted from a previously reported method.*[40]* In a typical synthesis, 4.0 g Cab-O-Sil was dispersed in 25.7 g DI H_2O. Separately, 14.0 g tetramethylammonium silicate solution was added to 5.74 g sodium silicate solution and stirred for 10 min. Both mixtures were then combined and stirred for 15 min. A separate solution of 12.9 g CTAB and 87 g DI H_2O was added and stirred for 20 min. The mixture was transferred to a sealed autoclave and heated at 100 ºC for 16 h. The white solid was filtered, washed with copious amounts of DI H_2O, and dried overnight at 75 ºC. The organic template was removed by calcination using the following temperature program: (1) ramping the temperature to 550 ºC under N_2 at a rate of 5 ºC/min., (2) holding at 550

ºC for 1 h., (3) switched atmosphere to air and continued heating at 550 ºC for 5 h. The calcined MCM-41 was then dried at 200 ºC under vacuum overnight.

4.2.5. Aziridine Synthesis

The synthesis and purification of aziridine was similarly conducted to reported methods.*[26]* In a typical synthesis, a basic solution of 35 g KOH in 200 g DI H_2O was poured into a round-bottom flask containing 35 g 2-chloroethylamine. The solution was stirred at 50 ºC for 2 h. The temperature of the flask was raised to 75 ºC and aziridine was then distilled from solution under a partial static vacuum of 530 mm Hg and collected in a cold trap. The collection flask was sealed and then stored at 0 ºC. ^{1}H NMR (400 MHz, D_2O, δ): 1.56 (s); ^{13}C NMR (400 MHz, CD_2Cl_2, δ): 18.1. *Caution: Aziridine is toxic if swallowed, inhaled, or absorbed through the skin. Aziridine is a carcinogen and reproductive hazard. Use extreme caution when handling aziridine. Only handle aziridine in a ventilated fume hood and always wear proper personal protection equipment.*

4.2.6. PEHAS Synthesis

The HAS synthesis has been reported elsewhere.*[26, 86]* The PEHAS adsorbents were synthesized accordingly, except without the use of acetic acid as a catalyst. In a generalized synthesis, a given weight of aziridine (calculated from a predetermined weight ratio of aziridine to pore-expanded mesoporous silica support) was added to a suspension of the corresponding amount of silica in toluene. The mixture was stirred overnight at room temperature in a glass pressure vessel, sealed with a PTFE cap. The solid adsorbent was recovered by filtration and washed with copious amounts of toluene and methanol and then dried at 50 ºC under vacuum.

4.2.7. Removal of Aminopolymer from Silica Support

The method of cleavage and recovery of aminopolymer from the inorganic support of HAS adsorbents has been reported elsewhere and was applied to the PEHAS adsorbents.*[86]* In a typical cleavage reaction, approximately 500 mg of PEHAS adsorbent was stirred in a basic solution of 33 g KOH in 100 g DI H_2O at 50 ºC overnight. About half of the H_2O was removed from the solution of soluble species and base by vacuum distillation at 75 ºC and the remaining solution was stored in a freezer overnight. The aminopolymer phase-separated and was recovered by decanting/physical separation.

4.2.8. Characterization

The pore diameters, volumes, and BET surface areas of the bare silica supports and the PEHAS adsorbents were determined via N_2 physisorption analysis at 77 K using a Micromeritics ASAP 2010. Amine loadings were determined by TGA using a Netzsch STA409. Total organic loading was estimated as the weight loss from 160 to 760 °C, and the adsorbent's amine loading was determined by applying a stoichiometric ratio of ethyleneimine units (molecular weight of 43 Daltons) after accounting for silica surface silanol condensation (~ 1 wt%). FT-Raman spectra were obtained on a Bruker Vertex 80v optical bench with a RAMII Raman module. ^{1}H solution NMR experiments were conducted on a Varian Mercury Vx 400. Inversely-gated ^{13}C solution NMR experiments were conducted on a Bruker DRX 500 and samples were prepared with D_2O and a single drop of $Cr(acac)_2$ in deuterated DMSO to aid relaxation and minimize interference from possible residual silica or base salts. Approximately 10000 scans with an inversely-gated pulse sequence were gathered with a relaxation time of 4 seconds. This relaxation time is in excess of the 3.3 seconds required for quantitative analysis determined in a full T1 study by Geckle for branched PEI.*[109]* Molecular weights of cleaved aminopolymer were determined by ASEC at 30 °C using a system comprised of a Shimadzu LC-20AD

pump, a Shimadzu RID-10A RI detector, a Shimadzu SPD-20A UV detector, a Shimadzu CTO-20A column oven, and Viscotek TSK Viscogel PWXL Guard, G3000, G4000 and G6000 columns mounted in series. The mobile phase consisted of 0.5 M acetic acid and 0.3 M Na_2SO_4 and the flow rate was maintained at 0.5 mL/min. Commercial PEI's of a range of molecular weights from 800 to 10000 Daltons were used to generate a calibration curve.

4.2.9. Adsorption

The amounts of CO_2 adsorbed and apparent adsorption kinetics under humid conditions were measured with a packed bed flow reactor with an online MS as described in a previous report.*[26]* Approximately 70 to 90 mg of adsorbent was dispersed in ~3 g of sieved sand (250 to 425 micron) and poured into a Pyrex tubular reactor (1/4 in. O.D.). The reactor tube was then placed in a temperature controlled tube furnace. Before an adsorption experiment, the adsorbents were desorbed for at least 3 h at 110 ºC under flowing Ar. Separately, during the desorption phase, test gas (10 % CO_2 balance Ar) was pre-humidified to 100% water saturation by flowing through two glass water bubblers at room temperature. Adsorption was started by switching the reactor inlet from desorption gas to test gas and the time was noted. Adsorption was then performed at a test gas flow rate of 20 mL/min for 200 min. at the desired temperature. The CO_2 concentration at the reactor outlet was measured with a Pfeiffer Vacuum QMS 200 Prisma Quadrupole MS. The mass of CO_2 adsorbed was calculated by integration of the MS output to a certain time-point determined as described in the Results and Discussion section.

4.3. Results and Discussion

4.3.1. Synthesis and Characterization of Large-pore Mesoporous Silicas

Mesoporous silicas with large pore diameters were used in this study as supports for aziridine polymerization in an attempt to prevent the blocking of pores observed in a

previous report.*[86]* Using a smaller-pored SBA-15 as a support, it was determined that, despite an approximately linear dependence of the final amine loading on the aziridine/silica ratio used in the synthesis, the pore diameter reached a critical radius of ~5 nm, below which aziridine polymerization quickly blocked pore openings. To avoid this phenomenon, several large-pore mesoporous silicas were synthesized or obtained for use as supports for the aziridine polymerization in this work.

A series of PE SBA-15 materials (PESBA1, 2, and 3) with increasing pore sizes and pore volumes were synthesized according to a method adapted from Katiyar, et al.*[119]* The post-synthesis heat treatment step was conducted at 100, 110, and 120°C for 72 hours, resulting in decreasing average pore diameters and pore volumes (Table 4.1) by nitrogen physisorption at 77 K. Further analysis of the nitrogen physisorption isotherms (Appendix B, Figures B.1-B.5) by the Frankel-Halsey-Hill modified Broekhoff de Boer method revealed an increasing separation in the average pore diameters obtained from the adsorption and desorption branches of the silicas as the heat treatment temperature decreased, suggesting deviation from uniform cylindrical pores. The BET surface areas of these materials were in the range of 560-710 m^2/g, but did not correlate with the heat treatment temperature. The particle sizes for all three materials were determined to be within the range of 1-10 μm by analysis of scanning electron microscopy (SEM) images (Appendix B, Figures B.6-B.8), with the larger particles being aggregates of smaller primary particles. These values are slightly larger and more widely distributed than the particle sizes of 1-2 μm observed for the non-pore-expanded SBA-15 used in previous reports of the HAS material.*[26, 86]*

MCF was synthesized according to a method adapted from Ping, et al.*[117]* Like the PE SBA-15 silicas, this material possesses large pore diameters and large pore volumes, however, the structure consists of non-ordered arrays of 24.4 nm diameter spherical cages connected randomly by slightly smaller 15.0 nm diameter windows, providing three-dimensional connectivity that is very attractive from a mass transfer

perspective. The MCF particle sizes were determined to be within the range of 3-10 μm by analysis of SEM images (Appendix B, Figure B.9).

The above pore-expanded mesoporous silicas were synthesized in-house at the multi-gram scale. However, mesoporous silicas are also available commercially on the kilogram scale. One such silica, hereafter referred to as PESCOM, was acquired for this study to provide a comparison to an industrially relevant support. Nitrogen adsorption analysis at 77 K showed that the PESCOM silica had mesopores with average pore diameter of 21.6 nm and a pore volume of 1.78 cc/g. Despite its comparable pore characteristics, the BET surface area (332 m^2/g) of PESCOM was much lower than the surface areas of the in-house synthesized silicas, suggesting the presence of large non-porous regions in the SiO_2 framework or thicker pore walls. The PESCOM particle size was determined to be within the range of 4-10 μm by analysis of SEM images (Appendix B, Figure B.10). The presence of smaller amorphous non-ordered regions was also detected.

4.3.2. Synthesis and Characterization of HAS Adsorbents with Pore-expanded Mesoporous Silicas

A set of pore-expanded HAS (PEHAS) adsorbents was synthesized using aziridine to silica weight ratios of 0.13, 0.53, and 2.65 for each pore-expanded silica support. The addition of the aminopolymers to the silica supports was verified using FT-Raman spectroscopy (Appendix B, Figures B.11-B.15). The amine loadings of these materials were determined by TGA and are summarized in Table 4.1 and Figure 4.1. As expected, the amine loadings increased with increasing aziridine to silica reactant ratios. However, contrary to the HAS materials synthesized from non-pore-expanded SBA-15 (reported elsewhere*[86]*, hereafter referred to as HAS materials, Appendix B, Table B.1), some materials displayed a non-linear trend relating final polymer loading and mass of aziridine added to the synthesis. This result can be rationalized from the perspective of

the surface area available for functionalization and the fact that the parent supports possess pores substantially larger than 5 nm, so diffusion of aziridine monomers into the pore space should not be hindered. One interesting case is the similar amine loadings achieved in the PEHAS14 and PEHAS15 materials despite different reactant ratios of 0.13 and 0.53, respectively. The PESCOM support for these materials had a much smaller surface area than the other pore-expanded supports, and therefore, less accessible silanol groups. Thus it is possible that at the lower reactant ratio, more aziridine monomers react with growing polymer chains on or near the particle surface than silanols deep inside the pores, and this effect is enhanced by the lower surface area of the PESCOM support, thus explaining the similar amine loadings achieved.

Given the lower than expected amine loadings, in an attempt to increase amine loading, PEHAS materials were prepared with larger aziridine to silica ratios than previously used for the HAS materials.*[86]* PEHAS9 and PEHAS10 were prepared from the PESBA3 support with aziridine to silica ratios of 3.29 and 5.00, respectively, resulting in amine loadings of 5.16 and 4.44 mmol N/g. Although it is unclear why the incremental degree of functionalization decreased at higher reactant ratios, this result is likely not due to the hindered diffusion of aziridine into the pores, because each material possessed pores much larger than 5 nm, the limit below which polymerization blocked the pores of HAS materials synthesized from non-pore-expanded SBA-15.*[86]*

Table 4.1. Synthesis parameters, amine loadings, and pore characteristics of pore-expanded mesoporous silica supports, PEHAS adsorbents, a typical class 1 adsorbent, and a typical class 2 adsorbent.

Material	Silica Support	Reactant Ratio[a]	Amine Loading (mmol N/g)	Pore Dia. (nm)[b]	Pore Vol. (cc/g)	Surf. Area (m^2/g)	Norm. Pore Vol.[c]	Norm. Surf. Area[d]
PESBA1				18.2	2.47	569		
PESBA2				11.4	2.05	658		
PESBA3				13.2	2.32	709		
PESCOM				21.6	1.78	332		
MCF				15	2.98	652		
SBA-15				63	0.73	802		
MCM-41				35	1.01	1203		
PEHAS1	PESBA1	0.13	2.35	18.1	2.03	396	0.82	0.70
PEHAS2	PESBA1	2.65	4.41	16.7	1.55	274	0.63	0.48
PEHAS3	PESBA2	0.13	2.61	11.6	1.88	430	0.92	0.65
PEHAS4	PESBA2	0.53	2.92	13	1.53	308	0.75	0.47
PEHAS5	PESBA2	2.65	5.17	11.1	1.41	288	0.69	0.44
PEHAS6	PESBA3	0.13	1.55	13.1	2.21	476	0.95	0.67
PEHAS7	PESBA3	0.53	3.90	13.5	1.84	354	0.79	0.50
PEHAS8	PESBA3	2.65	4.63	12.8	1.51	294	0.65	0.41
PEHAS9	PESBA3	3.29	5.16	12	1.33	285	0.57	0.40
PEHAS10	PESBA3	5.00	4.44	13.6	1.59	312	0.69	0.44
PEHAS11	MCF	0.13	1.83	15.6	2.61	421	0.88	0.65
PEHAS12	MCF	0.53	3.48	15.9	2.12	350	0.71	0.54
PEHAS13	MCF	2.65	4.49	14.3	1.97	320	0.66	0.49
PEHAS14	PESCOM	0.13	1.78	20.8	1.67	283	0.94	0.85
PEHAS15	PESCOM	0.53	1.78	20.5	1.62	278	0.91	0.84
PEHAS16	PESCOM	2.00	2.49	20.4	1.58	260	0.89	0.78
PEHAS17	PESCOM	3.00	3.00	20.1	1.40	238	0.79	0.72
class 2	SBA-15	N/A	3.65	5.1	0.36	245	0.52	0.31
class 1	MCM-41	N/A	6.36	--	0.01	1	0.01	0.00

[a] Ratio of aziridine to silica used in the adsorbent synthesis.
[b] Calculated by taking an average of the pore size distribution obtained from the desorption branch of the N_2 isotherm.
[c] Calculated by dividing the adsorbent pore volume by the pore volume of the parent silica support.
[d] Calculated by dividing the adsorbent surface area by the surface area of the parent silica support.

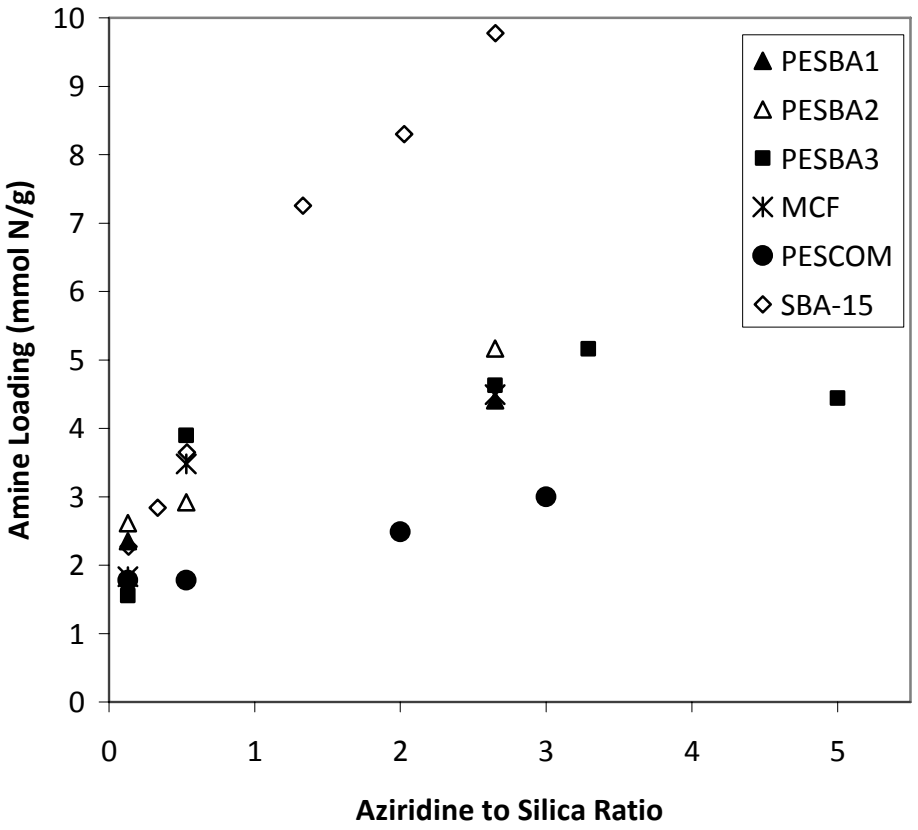

Figure 4.1. Amine loadings of HAS adsorbents on different silica supports prepared at varying aziridine to silica weight ratios. SBA-15 HAS materials were reported elsewhere.*[86]*

The pore volumes, average pore diameters, BET surface areas, and amine densities for the PEHAS materials are shown in Table 4.1. At reactant ratios shown to produce blocked pores and substantially reduced pore volumes in non-pore-expanded SBA-15 (<20% of initial pore volume), the PEHAS materials possess >57% of their initial pore volume. A similar trend was observed for the BET surface areas of the PEHAS materials. Accordingly, the average pore diameter of these materials decreases with increasing amine loading, albeit only slightly in most cases, and never more than 10%. Thus, it appears that the functionalization of pore-expanded silicas with aziridine does not exhibit the same pore blocking phenomenon observed with SBA-15. Figure 4.2 highlights this observation. For each PEHAS adsorbent, as well as non-pore-expanded

HAS adsorbents with low to moderate amine loadings (≤5.3 mmol N/g), the amine densities of the composites are all below 0.025 mmol N/m^2 (15 amine sites/nm^2), consistent with uniform polymerization orthogonal to the pore surface throughout the pore space.*[53]*

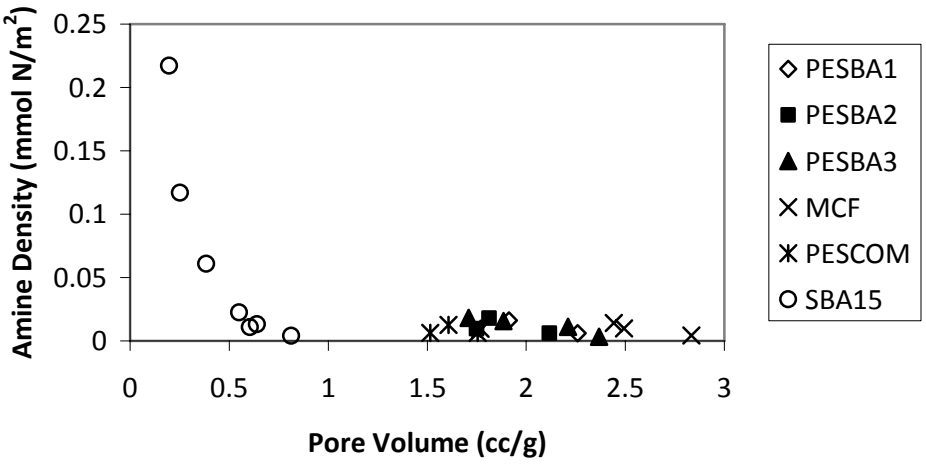

Figure 4.2. Amine density as a function of pore volume for HAS adsorbents with different silica supports. SBA-15 HAS materials were reported elsewhere.*[86]*

The aminopolymers of selected PEHAS materials were separated from their respective silica supports according to a base catalyzed polymer cleavage method reported elsewhere.*[86]* The nine PEHAS materials were selected because they were prepared with varying amine loadings from three different types of pore-expanded silicas (PESBA, MCF, and PESCOM). The molecular weights of these aminopolymers were determined from aqueous size exclusion chromatography and are reported in Table 4.2. Although there was not a clear trend correlating the molecular weight and the aziridine to silica ratio, the largest observed molecular weight of 6378 Daltons for PEHAS5 was within the range previously reported for highly loaded HAS materials (5500-6500 Daltons). This gives further evidence that the aziridine polymerization in PEHAS supports terminates before the entire pore space is filled because similar molecular

weights were obtained for polymerizations conducted in pore environments 2 to 3 times larger than SBA-15. In our previous report on the HAS material, we concluded that the aziridine polymerization was constrained by the pore walls because similar aminopolymer molecular weights were obtained from HAS adsorbents with moderate to high amine loadings.*[86]* In light of the results presented here, an as yet unknown termination mechanism that leads to molecular weights in the range reported here may have contributed to the plateau in molecular weights observed in our previous report.

The degrees of branching or ratio of primary (1°), to secondary (2°), to tertiary (3°) amines of the aminopolymers cleaved from selected PEHAS materials were found by inversely-gated ^{13}C solution NMR experiments (Table 4.2). The aminopolymers from the HAS materials prepared from SBA-15 were previously found to have an average degree of branching that produced an amine distribution of 1°:2°:3° = 28:46:26, with little variation with changes in the amine loadings of the parent materials.*[86]* The PEHAS materials synthesized from PESCOM had similar degrees of branching to the HAS materials. However, the PEHAS materials prepared from PESBA2 and MCF displayed different degrees of branching at different amine loadings. The highest loaded materials (PEHAS5, PEHAS13) had similar degrees of branching of approximately 1°:2°:3° = 20:50:30. However, the aminopolymers of moderately-loaded materials (PEHAS4, PEHAS12) were less hyperbranched with degrees of branching of approximately 1°:2°:3° = 40:40:20.

Surprisingly, it appears that the materials with large amine densities (highly loaded HAS materials with non-pore-expanded SBA-15) are those where polymerization blocked pores.*[86]* Using supports with expanded pore volumes and pore diameters, as shown here, did not significantly allow for higher loadings of aminopolymer. Therefore, it may be difficult to prepare HAS adsorbents with both high amine loadings (>~6 mmol N/g) and unblocked pores using current aziridine synthesis methods, and future work should seek to address this issue.

Table 4.2. Molecular weights and degrees of branching for cleaved aminopolymers from selected PEHAS materials.

Material	Amine Loading (mmol N/g)	Molecular Weight (Daltons)	Amine Ratio (%)		
			1°	2°	3°
PEHAS3	2.61	5639	ND[a]	ND[a]	ND[a]
PEHAS4	2.92	2794	38	41	21
PEHAS5	5.17	6378	23	46	30
PEHAS12	3.48	3335	42	38	20
PEHAS13	4.49	6179	18	52	30
PEHAS14	1.78	6293	ND[a]	ND[a]	ND[a]
PEHAS15	1.78	4330	ND[a]	ND[a]	ND[a]
PEHAS16	2.49	4842	29	47	24
PEHAS17	3.00	6350	29	46	25

[a] The degree of branching was not determined (ND) because of poor NMR signal intensity.

4.3.3. Effect of Catalytic Acid on PEHAS Synthesis

In the experiments discussed above, PEHAS adsorbents with large amine loadings (>6 mmol N/g) could not be prepared using the typical synthesis procedure of changing the aziridine to silica ratio in the synthesis without the presence of acid. Theoretically, if the entire pore spaces of PESBA-15, MCF, and PESCOM were filled with aminopolymer, the amine loadings of the resulting materials would be 16.87, 17.70, and 15.25 mmol N/g, respectively, assuming the standard bulk density of PEI. The lower than expected amine loadings achieved above indicate that the aziridine polymerization terminated before the aminopolymers filled the pore space. In an effort to improve the degree of amine functionalization and probe this polymerization termination, the effect of catalytic acid addition on the PEHAS synthesis was explored.

In a previous report on the HAS series of adsorbents, the use of a catalytic amount of acetic acid resulted in only a small increase in amine loading (~7%), giving evidence that the silanols of the silica support were sufficiently acidic to initiate the aziridine polymerization.*[86]* To probe the effect of acid on the PEHAS synthesis, the synthesis of PEHAS8 was repeated three times with the addition of 0.1, 0.4, and 0.8 mL of acetic acid

at the start of the reaction. The amine loadings of these materials (PEHAS18, PEHAS19, and PEHAS20, Appendix B, Table B.2) ranged from 12% higher to 23% lower than that of PEHAS8. Thus, the addition of a catalytic amount of acid at the start of aziridine polymerization does not greatly increase the degree of functionalization, regardless of the pore space characteristics of the silica support. It is possible that the addition of acid to the reaction environment increases the reaction rates both on the silica support surface and in solution, in some cases negatively impacting the degree of polymerization on the solid support.

Another experiment was performed to probe the effect of acid on the PEHAS reaction and reduce the reaction of aziridine in solution. Before reaction with aziridine, PESBA3 was pretreated with a solution of 5 mL acetic acid in toluene for 1 hour, where it was presumed that the acetic acid would adsorb to the hydrophilic silica surface. The solid was filtered and washed once with toluene, then dispersed in fresh toluene. Aziridine was added almost immediately at an aziridine to silica ratio of 3 and the reaction was stirred overnight at room temperature. The reaction was worked up according to the standard PEHAS procedure. The amine loading of the resulting composite (PEHAS21, Appendix B, Table B.2) was only 3.13 mmol N/g, ~30% lower than the amine loading of PEHAS8, which was prepared with a lower reactant ratio of 2.65. Despite the efforts to pre-adsorb the acetic acid and locate it primarily inside the silica pores, it is likely that once the pretreated silica was added to the fresh toluene solution, acetic acid desorbed from the silica into solution by concentration driving force, and led to an increase in the amount of aziridine polymerized in solution.

Further experiments were performed to determine if sequential additions of the aziridine monomer to the PEHAS reaction environment could increase the composite's amine loading. Aziridine aliquots at an aziridine to silica ratio of 0.5 were successively added at 0, 30, 60, 85, 105, and 120 minutes after the start of reaction with PESBA3, summing to a final aziridine to silica ratio of 3. The amine loading of this material

(PEHAS22, Appendix B, Table B.2) was 4.73 mmol N/g, falling in between the amine loadings of PEHAS materials prepared according to the un-modified synthesis method with aziridine to silica ratios of 2.65 and 3.29, and implying that the degree of functionalization is primarily dependent on the final concentration of aziridine in the reaction environment. The effect of acid in this process was also probed in a similar experiment. PESBA3 was reacted with aziridine at an aziridine to silica ratio of 2.65 in the presence of 4 drops of acetic acid overnight then additional equal portions of aziridine and acid were added the next day for a total aziridine to silica ratio of 5.3 and 8 drops acetic acid. The reaction was stirred for another 12 hours and then worked up according to the non-modified PEHAS synthesis method. The amine loading of the resulting composite (PEHAS23, Appendix B, Table B.2) was 5.68 mmol N/g, just 0.64 mmol N/g larger than the amine loading of the PEHAS18 material that was prepared with only one of these aliquots. Assuming that the degree of competition between polymerization of the first aziridine aliquot in solution and on the particle surface was similar to PEHAS18 (5.04 mmol N/g) and the polymerization reached completion/equilibrium before the second aliquot was added, again, it appears that the amine loading mainly depends on the sum total of aziridine added to the reaction environment, because otherwise the amine loading should be twice as large as that of PEHAS18. These experiments illustrate that the aminopolymer loading could not be significantly enhanced on these large pore supports by addition of extra aziridine or catalytic acid. In addition, it appears the role of acid in the PEHAS synthesis is a complicated one and may require a detailed, systematic study to completely describe the coupled reaction kinetics, reactant diffusion and thermodynamic equilibria of the aziridine polymerizations in solution and at the solid liquid interface.

4.3.4. CO_2 Adsorption Performance

Previous reports have shown that the uptake curves of aminosilica adsorbents with high amine loadings often display two phases; a fast initial uptake phase followed by a slow secondary phase.*[49, 53, 57, 86]* The slow secondary phase has been attributed to different phenomenon such as heat transfer effects, hindered diffusion, and the rearrangement of the chemisorbed species from carbamates to carbonates.*[39, 71]* Although very little research has been done on the heat transfer effects of aminosilicas in packed-bed adsorption systems, they could be important due to the supported amine materials' large heats of adsorption. However, in materials with little remaining pore volume after functionalization, both diffusional and chemical rearrangement effects are also likely present, and may be difficult to decouple. In a competitive adsorption study of H_2O and CO_2, Song showed that for a PEI-impregnated class 1 adsorbent, there was an initial fast uptake of CO_2 and an induction period for the uptake of H_2O. Only after a certain uptake of H_2O was reached did the CO_2 uptake plateau, suggesting this rearrangement of chemisorbed species from carbamates to carbonates.*[39]* Regardless of the contribution of chemical rearrangement effects to adsorption kinetics, the powerful influence of hindered mass transfer due to pore blockages has been illustrated in our previous work, and marks a significant hurdle for class 1 and 3 adsorbents to overcome.

The large pore spaces of the pore-expanded silicas remained unblocked after the synthesis of the PEHAS materials. Thus, mass transfer through the pores should be relatively unaffected by the inclusion of the HAS aminopolymers. For adsorbents with similar mass transfer characteristics and different amine loadings, the CO_2 uptake rates should be proportional to the amine loading of the adsorbent. However, the time required for adsorbents of similar porosity to reach a certain percentage of their uptake should be equal.*[41]*

The adsorption performance of the PEHAS materials was measured in a packed-bed flow system monitored by MS under simulated flue gas conditions. Adsorption experiments were performed at 75 °C with a test gas concentration of 10% CO_2, balance

Ar, saturated with water vapor. Completion of the adsorption experiments was determined to be when the uptake rates became less than 0.2 μmol CO_2/min and the amount of CO_2 adsorbed during that period was calculated accordingly (Table 4.3). Although obviously linked to the time of breakthrough, this method takes the slope of the breakthrough curve into account, therefore giving more insight into the behavior of the adsorbent. Of course this is not the only way to examine adsorption kinetics. An alternate analysis of these adsorption experiments is given in the Appendix B (Section B.6) where the completion of the adsorption experiment was determined by when the CO_2 outlet concentration of the breakthrough curve reached 95% of the initial CO_2 feed concentration. While this method gives more insight into the early, fast adsorption stage of the experiment, the relationships between the performances of different adsorbents are similar to those drawn below and point to the same conclusions.

The amounts of CO_2 adsorbed by the PEHAS materials shown in Table 4.3 increased with increasing amine loading of the composites for both measurement methods. For comparison, the data from adsorption measurements for HAS materials with different amine loadings (reported elsewhere*[86]*) were reprocessed with the analysis method described above and are also reported here (Appendix B, Table B.5). Figure 4.3 shows the amount of CO_2 adsorbed by the PEHAS and HAS materials with different amine loadings. The amounts of CO_2 adsorbed by pore-expanded and non-pore-expanded HAS materials follow essentially the same linear trend with increasing amine loading. The data in Table 4.3 show that the amine efficiencies for the PEHAS adsorbents were all below 0.26 mol CO_2/mol N, indicating that, at least in this packed-bed configuration, a large portion of the adsorbent's equilibrium capacity is captured at a rate smaller than 0.2 μmol CO_2/min. There is no clear trend in the amine efficiencies of the PEHAS adsorbents in terms of the different pore-expanded silica supports used in the synthesis, simply a slight decrease with increasing amine loading.

Table 4.3. Amounts of CO_2 adsorbed, amine efficiencies, and uptake kinetics for PEHAS adsorbents. Completion of uptake measurement determined when differential uptake was less than 0.2 μmol CO_2/min.

Material	Silica Support	CO_2 Uptake (mmol CO2/g)	Amine Efficiency (mol CO_2/mol N)	μmol CO_2/min = 0.2	
				50% Uptake (min)	98% Uptake (min)
PEHAS1	PESBA1	0.56	0.24	2.6	20.0
PEHAS2	PESBA1	0.61	0.14	2.7	19.6
PEHAS3	PESBA2	0.52	0.20	2.5	17.9
PEHAS4	PESBA2	0.57	0.20	2.6	19.0
PEHAS5	PESBA2	0.63	0.12	2.7	18.0
PEHAS6	PESBA3	0.40	0.26	2.5	13.7
PEHAS7	PESBA3	0.59	0.15	2.5	14.6
PEHAS8	PESBA3	0.71	0.15	2.7	19.8
PEHAS11	MCF	0.38	0.21	2.4	13.5
PEHAS12	MCF	0.51	0.15	2.7	24.3
PEHAS13	MCF	0.85	0.19	2.7	22.3
PEHAS14	PESCOM	0.28	0.16	2.6	13.6
PEHAS15	PESCOM	0.34	0.19	2.5	14.5
PEHAS16	PESCOM	0.41	0.17	2.6	17.5
PEHAS17	PESCOM	0.43	0.14	2.6	15.0
class 2	SBA-15	0.80	0.22	2.7	14.5
class 1	MCM-41	1.2	0.19	3.1	51.5

There are slight differences in the amounts of CO_2 adsorbed by the various PEHAS adsorbents. Figure 4.4 shows the amounts of CO_2 adsorbed by the PEHAS adsorbents as a function of their pore volume. While there is a fair amount of scatter in the data, the PESCOM adsorbents generally adsorb lower amounts of CO_2 owing to their lower degrees of functionalization. The adsorbents prepared from the three PESBA-15 materials follow essentially the same trend, despite the differences in pore volumes of the unfunctionalized supports.

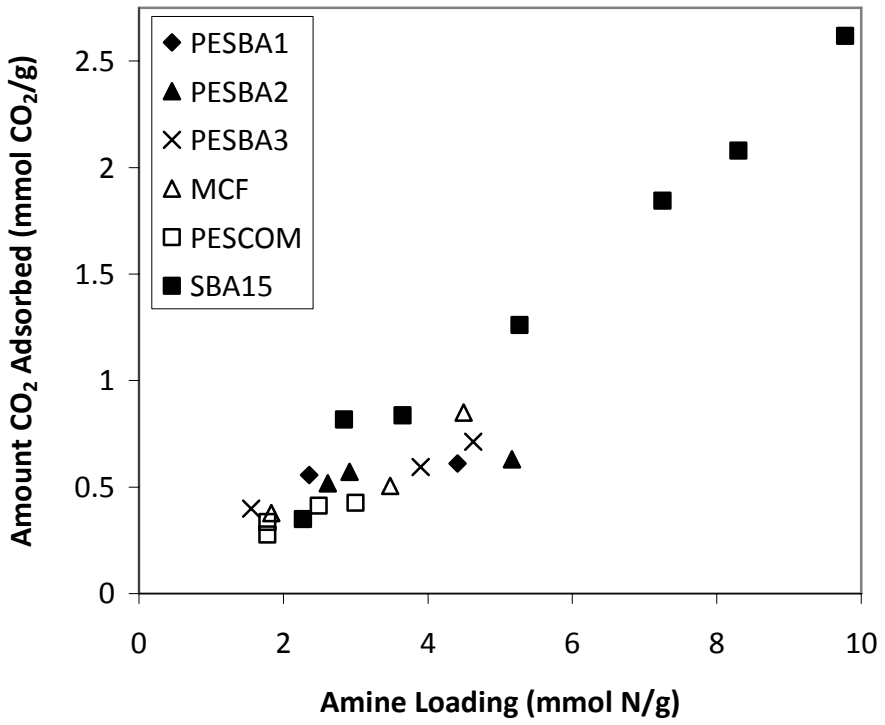

Figure 4.3. Amounts of CO_2 adsorbed by PEHAS and HAS adsorbents with different amine loadings. Completion of uptake measurement determined by a method described in Appendix B. SBA-15 HAS materials were previously reported elsewhere.*[86]*

The uptake kinetics of the PEHAS adsorbents were characterized by the time required to reach 50% and 98% of the total amount adsorbed for each sample (Table 4.3). Reporting uptake kinetics in this manner is convenient because the values are normalized by the amount of CO_2 adsorbed, making it possible to compare the uptakes of the adsorbents with different amine loadings at certain points in their measurement. Each material had essentially the same 50% uptake time (from 2.4 to 2.7 minutes), illustrating that the fast initial uptake phase for aminosilicas is fairly universal. Although there is a slightly larger spread in the PEHAS 98% uptake times (13.6 to 24.3 min), they are much shorter than the 98% uptake times for the HAS adsorbents with blocked pores (up to 4 times longer), showing the detrimental effect that blocked pores have on adsorption kinetics.

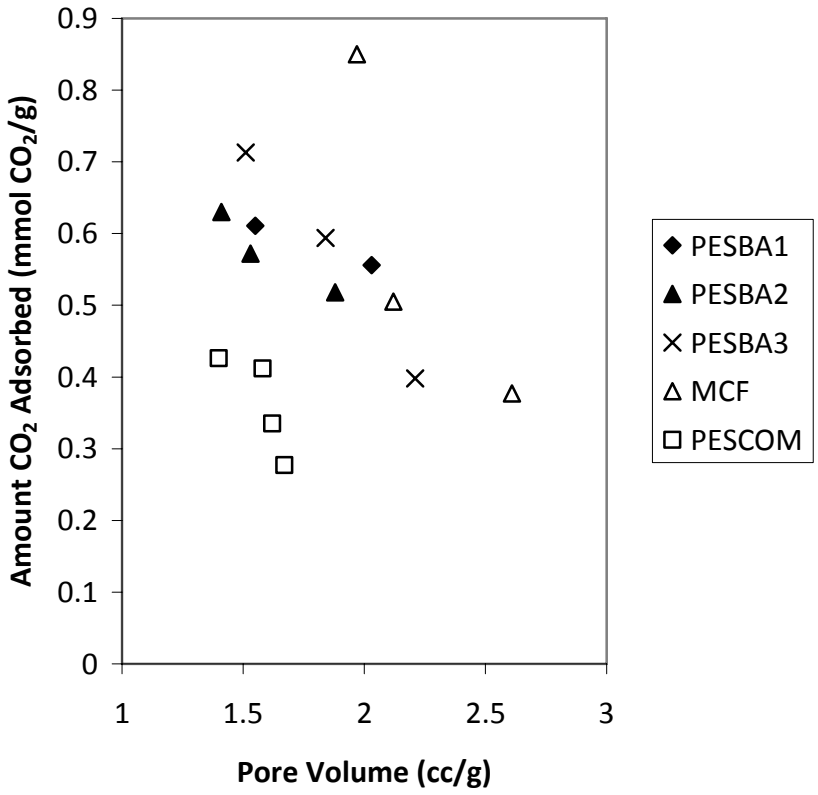

Figure 4.4. Amount of CO_2 adsorbed by PEHAS adsorbents as a function of adsorbent pore volume.

The data and analysis above show that PEHAS adsorbents prepared from pore-expanded silica supports exhibited adsorption kinetics similar to HAS adsorbents without blocked pores. It is also useful to compare their performance to the other aminosilica adsorbent classes. A typical class 1 adsorbent was prepared through the impregnation of MCM-41 mesoporous silica with low molecular weight PEI at a moderate loading of 27 wt%. A typical class 2 adsorbent was prepared through the functionalization of a non-pore-expanded SBA-15 mesoporous silica with 3-[2-(2-aminoethylamino)ethylamino]propyltrimethoxysilane (Tri silane). The pore characteristics and amine loadings of these materials are given in Table 4.1 and their adsorption performances are given in Tables 4.3. The 50% and 98% uptake times for the

class 2 adsorbent were similar to those of the PEHAS adsorbents, indicating similar adsorption kinetics. In contrast, the class 1 adsorbent showed hindered adsorption kinetics similar to highly loaded HAS adsorbents prepared from non-pore-expanded silica. The 98% uptake time for this material was twice as long as the longest time observed for any of the PEHAS adsorbents. Therefore, the pore-expanded class 3 adsorbents presented here exhibit adsorption kinetics more similar to class 2 adsorbents than the hindered adsorption kinetics of class 1 and highly-loaded HAS adsorbents with blocked pores. Under these adsorption conditions, the adsorption kinetics of aminosilicas are seemingly universal when normalized by amine loading except when the composite material's porosity is reduced enough to significantly hinder diffusion.

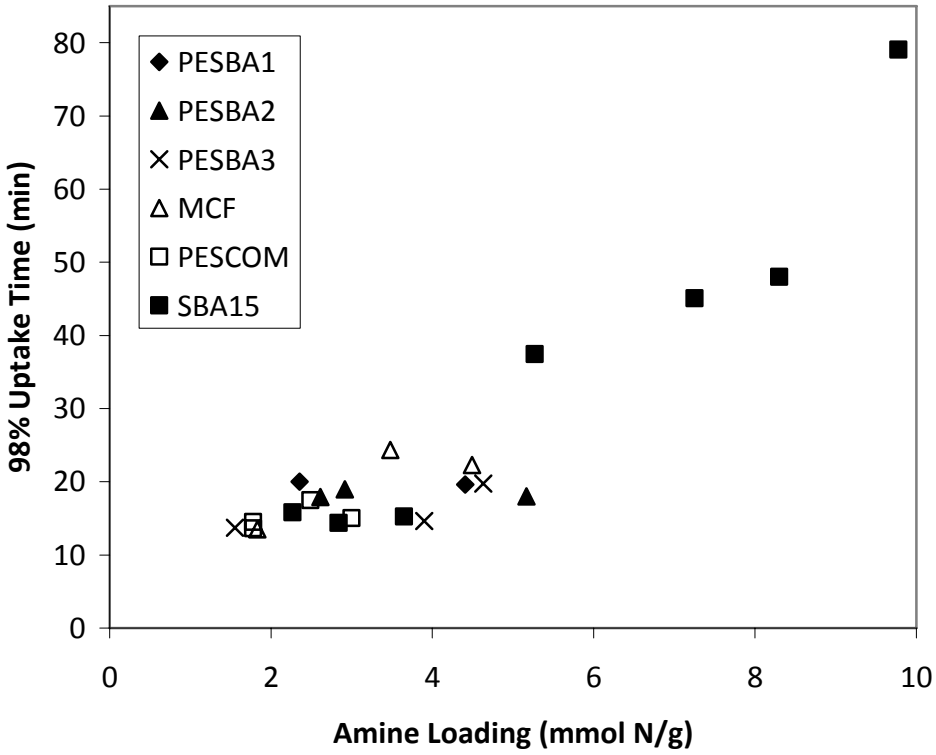

Figure 4.5. 98% uptake times for PEHAS and HAS adsorbents with different amine loadings. SBA-15 HAS materials were previously reported elsewhere.*[86]*

4.4. Conclusions

To investigate the effect of using porous silica supports with larger pore spaces in the synthesis of HAS CO_2 adsorbents, several class 3 aminosilica materials were prepared with aziridine polymerization from PESBA-15, MCF, and PESCOM pore-expanded mesoporous silicas with different aziridine to silica ratios. The amine loadings of these PEHAS adsorbents increased with increasing reactant ratio up to a certain point where polymerization terminated, significantly differing from HAS adsorbents prepared from non-pore-expanded SBA-15. While the pores of the PEHAS adsorbents remained unblocked by polymerization, it is likely that the large amine loadings observed in the HAS adsorbents resulted from this blocking phenomenon. Efforts to circumvent this tradeoff by using acid catalysis during the PEHAS adsorbent synthesis to drive the polymerization process were largely unsuccessful.

The amounts of CO_2 adsorbed by the PEHAS adsorbents scaled approximately linearly with increasing amine loading. Although there was no observable trend in the amine efficiencies, the dependence of the amounts of CO_2 adsorbed on the adsorbent pore volume showed that the PESCOM adsorbents underperformed the other pore-expanded materials. The uptake kinetics of the PEHAS materials were similar and displayed the quick initial adsorption phase followed by a slow secondary phase, characteristic to most aminosilica adsorbents. When compared to HAS adsorbents prepared from non-pore-expanded SBA-15, as well as typical class 1 and class 2 adsorbents, the uptake kinetics of the PEHAS adsorbents did not show the effects of hindered diffusion due to pore blocking. These results indicate that adsorbents prepared from aziridine polymerization on/in pore-expanded silicas are capable of possessing moderate amine loadings without sacrificing large open pore spaces capable of fast mass transfer, improving their potential utility as successful industrial CO_2 adsorbents.

CHAPTER 5

APPLICATION OF AMINE-TETHERED SOLID SORBENTS FOR DIRECT CO_2 CAPTURE FROM THE AMBIENT AIR

Parts of this chapter are reproduced from "Application of Amine-Tethered Solid Sorbents for Direct CO_2 Capture from the Ambient Air" by Sunho Choi, Jeffrey H. Drese, Peter M. Eisenberger, and Christopher W. Jones, submitted to Environmental Science and Technology for publication.

5.1. Introduction

Given the scale of society's energy needs, it will be many decades before renewable energy sources, such as wind, solar, geothermal, and biomass, can bear the majority of the burden of powering our planet. Until then, fossil fuels will continue to be consumed for energy, producing CO_2 in the process. The application of the experiments discussed above was targeted towards relatively concentrated CO_2 sources, such as flue gases generated from large point sources, including electricity generating power plants. However, roughly one third of global carbon emissions are associated with distributed sources such as transportation fuels.*[120]* Thus, large-scale deployment of CCS technologies at point sources can at best slow the rate of increase of the atmospheric CO_2 concentration. A carbon-negative technology, one that actually reduces the concentration of CO_2 in the atmosphere, could become an important tool for environmental control if effects of global climate change become catastrophic. In light of this, direct CO_2 capture from the ambient air ("air capture") shows promise. Lackner proposed the use of air capture as a climate mitigation option in 1999.*[121, 122]* Since then, a number of

scientists have demonstrated methods to extract CO_2 from the ambient air and evaluated, to different extents, different process designs that might be used.*[123-142]*

The ultra-dilute conditions for air capture likely make established CO_2 separation processes that rely on partial pressure differences, such as cryogenic distillation and membrane separation, too energy intensive to be feasible. Fortunately, many adsorption processes provide the large CO_2 affinity required under these dilute conditions. The most well-studied adsorption processes utilize metal hydroxides or oxides (Ca, Na, etc.) and their conversion into metal carbonates, either in solution or as solids. In general, the regeneration of the carbonate into the original oxide or hydroxide has also proven to be quite energy intensive, resulting in high projected energy use and process costs.*[123, 129, 133, 134, 139]* More recently, we,*[143, 144]* Lackner,*[138]* and others*[142]* have focused on the use of solid adsorbents for air capture. While most solid adsorbents that separate CO_2 by physical adsorption (zeolites and carbons) do not perform well at low partial pressures, others that adsorb CO_2 chemically via moderate to high heats of adsorption could be feasible.*[15]* However, some of these types of adsorbents suffer from overwhelming competitive adsorption of water over CO_2, so process designs that use them must practice careful humidity control.*[15]* Lackner's work suggests that use of adsorbents that weakly bind CO_2 (in that case, weak chemisorbents) but show controllable, competitive binding of water may be interesting materials for practical capture processes with suitable process control of humidity. Calcium *[131, 133]* and sodium based oxides *[130]* or lithium zirconates *[145]* are expected to offer considerable adsorption capacities under high temperature conditions, but air capture processes are expected to be most economically favorable when operating near ambient conditions. Solid-supported amine adsorbents effectively adsorb under near ambient conditions, are tolerant to water vapor and can be regenerated by mild temperature swings, making them potentially attractive for this application.*[15]* Indeed, recently a triamine-grafted PE MCM-41 (class 2) at a CO_2 partial pressure of 300 ppm under dry conditions was

measured to have a higher CO_2/N_2 selectivity than zeolites, mesoporous silica, MOFs, and carbon-based materials, as would be expected based on the heat of adsorption of these materials.*[146]*

Like the triamine-grafted PE MCM-41 adsorbent of Sayari, the HAS adsorbent can be prepared with large amine loadings that chemically adsorb CO_2, making them attractive candidates for the air capture application.*[146]* This chapter details the performance of the HAS varied loading adsorbent set (HAS-VLAS, described in Chapter 3, although renamed here for clarity) under dry and humid air capture conditions as well as the experimental challenges associated with these measurements.*[86]*

5.2. Experimental Section

5.2.1. Materials

Mesoporous SBA-15 silica was prepared following previously reported procedures.*[106, 107]* Specifically, P123 (Aldrich) was used as a structure directing agent to template the one-dimensional mesoporous structure. First, 17.9 g of this organic template was dissolved in 561 g of DI H_2O along with 99.4 g of hydrochloric acid (Fisher). The mixture solution was stirred overnight at room temperature before adding a silica source, i.e., 39.6 g of TEOS (Aldrich). After 5 minutes of vigorous stirring, the temperature of the precursor solution was elevated to 35 °C and maintained for 20 hours, producing a cloudy solution with a white precipitate. After subsequent heating at 80 °C for 24 hours, this solution was washed with DI H_2O and filtered to separate the precipitate. The resulting white solid was dried in an oven at 75 °C overnight before calcination. Calcination was performed with the following temperature protocol to remove the organic template: the sample was heated first to 200 °C at 1.2 °C/min rate and held for 1 hour, then heated at the same ramp rate to 550 °C and held for 6 hours.

Aziridine was also synthesized by the previously reported method to use a monomer for the preparation of hyperbranched aminopolymers.*[26]* A typical synthesis mixture was prepared by adding 34.5 g of 2-chloroethylamine hydrochloride (Aldrich) in an aqueous solution that comprises 34.1 g of potassium hydroxide (KOH, VWR) and 200 g of DI H_2O. After vigorous stirring at 50 °C for 2 hours, the solution was distilled under a partial static vacuum of 530 mm Hg to separate aziridine from water. Collected material was identified by ^1H NMR (400 MHz, D_2O) and stored at 0 °C until being used in the hybrid material synthesis. *Caution: aziridine is a highly toxic and reactive compound and appropriate precautions should be taken before working with the chemical.*

5.2.2. Adsorbent Preparation

The HAS adsorbents with different aminopolymer loadings were prepared based on a reported method by varying the initial amount of aziridine, as summarized in Table 5.1.*[26, 147]* Specifically, a desired amount of aziridine was added in the slurry containing a given quantity of SBA-15 in anhydrous toluene (Acros). Subsequently, polymerization of aziridine was carried out by adding a few drops of glacial acetic acid (Aldrich) to initiate the acid-catalyzed ring opening reaction. The mixture was further reacted overnight at room temperature in a glass pressure vessel. The resulting solid product was collected by successive filtration and washing with copious amounts of toluene, and then dried overnight at 50 °C under vacuum before further characterization.

A class 2 supported-amine adsorbent was prepared by functionalizing SBA-15 with N-(3-(trimethoxysilyl)propyl)ethane-1,2-diamine (AEAPTMS, Aldrich). Specifically, 2.0 g of AEAPTMS was added to 1.0 g of SBA-15 silica dispersed in anhydrous toluene, then stirred for 24 hours at room temperature under Ar atmosphere. The white product was filtered and washed with a copious amount of toluene, and then dried overnight at 50 °C under vacuum before further use, resulting in a supported amine

adsorbent containing both primary and secondary amine groups covalently bound to the silica support.

Table 5.1. HAS adsorbents with different aminopolymer loadings. The organic amount was identified by TGA and the amine loading was stoichiometrically estimated from this value. The pore diameter, pore volume, and the BET surface area were determined by the N_2 physisorption experiments.

Sample Name [a]	AFM Paper Sample Name [b]	Organic Content (wt%)	Amine Loading (mmol/g)	Aziridine to SBA-15 Ratio (w/w)	Pore Dia. (nm)	BET Surface Area (m^2/g)	Pore Volume (cc/g)
SBA	SBA2	0	0	0	6.2	840	0.78
HAS1	HAS14	9.9	2.29	0.13	6.3	579	0.69
HAS2	HAS10	12.3	2.87	0.33	6.4	314	0.51
HAS3	HAS13	15.9	3.69	0.53	5.9	278	0.49
HAS4	HAS11	22.9	5.33	5.01	5.4	234	0.39
HAS5	HAS2	36.1	8.39	2.03	5.0	71	0.15
HAS6	HAS1	42.5	9.88	2.65	4.9	45	0.11

[a] This sample name will be used for the discussion in Chapter 5.
[b] This is the corresponding sample name used in Chapter 3.*[86]*

5.2.3. Characterization of the Adsorbents

The hybrid adsorbents with different aminopolymer loadings were characterized by X-ray diffraction (XRD), transmission electron microscopy (TEM), N_2 physisorption, and TGA. XRD patterns were obtained from a PANalytical X'Pert Pro powder X-ray diffractometer and a PW3011 proportional detector with a parallel plate collimator (CuKα, λ=1.5418 Å). TEM images were obtained with a JEOL 100CX II TEM operating at 100kV. N_2 physisorption analyses were preformed on a Micromeritics ASAP 2010 apparatus at 77 K to determine the pore characteristics such as the BET surface area, the pore volume, and the pore diameter. Prior to the measurement, the adsorbents were degassed by heating at 100 °C under vacuum for 24 hours. The pore diameter was calculated by BdB-FHH method.*[95, 147]* The aminopolymer content was assessed by TGA measurement using a Netzsch STA409 by assigning the weight loss between 200 °C and 700 °C to organic species. About 20 mg of the samples were subjected to

continuous heating at a heating rate of 10 °C/min from room temperature to 900 °C under flowing air diluted by a nitrogen purge.

5.2.4. Adsorption Experiments

The CO_2 adsorption characteristics of the HAS adsorbents were characterized using a TA Q500 TGA and a Pfeiffer Vacuum QMS 200 Prisma Quadrupole MS, respectively. In typical TGA measurements, about 30 mg of the adsorbent was loaded in a platinum vessel and subjected to the following temperature protocols. First, the sample was desorbed by heating to 110 °C at 5 °C/min rate under Ar flow of a 100 ml/min and holding isothermally at 110 °C for 3 hours. After the desorption stage, the temperature was lowered to the ambient temperature (25 °C) and held for 1 hour at that temperature before introducing CO_2. Adsorption was then initiated by exposing the samples to the dry target gas of desired concentration (i.e., 400 ppm CO_2 or 10% CO_2 balanced with Ar, respectively) at a flow rate of 100 ml/min. The adsorption experiment was performed until the pseudo-equilibrium capacity was reached, which was determined to be the time when the weight gains from adsorbed CO_2 changed by less than 0.0001 %/min.

The CO_2 adsorption capacities of the HAS materials were determined under humid conditions using a fixed bed flow system coupled with a MS at 400 ppm and 10% CO_2 concentration, respectively. A detailed measurement procedure using this instrument has been reported elsewhere.*[26, 147]* The adsorption system was comprised of a Pfeiffer Vacuum QMS 200 Prisma Quadrupole MS coupled with a fixed-bed flow reactor. In a typical adsorption experiment, about 60 – 80 mg of the adsorbent sample was mixed with ~300 mg sieved sand (250 – 425 micron) and loaded in a pyrex tubular reactor. Before each experiment, the samples were desorbed under the same conditions as in the TGA experiment, i.e., 110 °C for 3 hours under Ar flow. The adsorption step was initiated by flowing humidified 400 ppm CO_2 with a flow rate of 20 ml/min at ambient conditions.

The amount of CO_2 captured by the adsorbent was calculated by monitoring the CO_2 concentration at the reactor outlet using the MS.*[147]*

5.3. Results and Discussion

5.3.1. Characterization of the Adsorbents

An in-depth analysis of the pore characteristics of these HAS materials via N_2 physisorption has been given in Chapter 3. The HAS materials and the inorganic support employed in this work were also characterized by XRD and electron microscopy, respectively. Figure 5.1 shows the diffraction patterns of SBA-15 and the HAS adsorbents with different amine loadings, along with a TEM image of the inorganic substrate, showing the presence of one dimensional mesoporous channels with a mean pore size of approximately 6.5 nm (Figure 5.1, inset). The diffraction pattern of the pure SBA-15 displays three characteristic peaks around 0.9, 1.5, and 1.8 within the 2θ ranges of 0.6 ~ 4.0 degrees, which can be indexed as the (100), (110), and (200) planes of SBA-15, respectively. These peaks are routinely used as an indication of the hexagonal mesoporous structure of SBA-15.*[148, 149]*

Diffraction patterns of the HAS adsorbents are consistent with structural changes associated with the aminopolymer integration into the pore space of the silica substrates. It is known that the intensity of the characteristic peaks decreases with the loading of organic substances, either by covalent immobilization or physical impregnation of amines, while the position of the peaks do not show significant changes compared to those of the mesoporous silica support.*[40, 150]* Similarly, the characteristic peak positions of pure SBA-15 and the HAS did not show significant differences, which reveals that the long-range ordered structure of SBA-15 was not influenced by incorporating aminopolymers via the hyperbranching polymerization of monomer units. On the other hand, it was observed that the intensity of the low-angle reflection peak

decreased as a result of the aminopolymer incorporation onto the mesoporous silica. The series of XRD patterns in Figure 5.1 illustrates that the (100) peak intensities were reduced as the aminopolymer loadings increased. Xu et al. reported that the PEI immobilized onto the outside of the MCM-41 pores did not cause considerable intensity changes of the characteristic peaks.*[40]* It suggests that at least a portion of aminopolymers in the HAS adsorbents are located in the mesoporous channels of the SBA-15 supports.

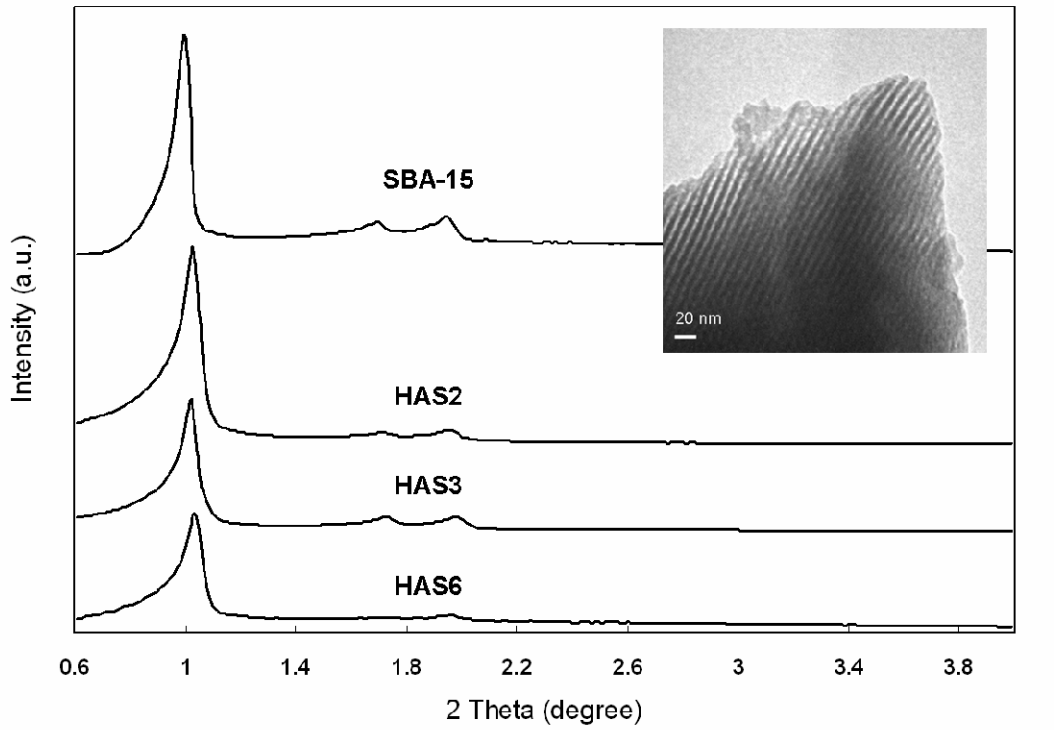

Figure 5.1. XRD patterns of SBA-15 and the HAS adsorbents with different aminopolymer loadings. The TEM image of SBA-15 mesoporous silica is also shown in the inset.

5.3.2. Air Capture Experimental Challenges

The adsorption of CO_2 by solid adsorbents is usually measured by either gravimetry or the integration of a transient concentration signal monitored by MS or gas

chromatography (GC). However, the ultra-low CO_2 concentration associated with air capture presents experimental challenges for both of these methods. For gravimetric methods, the sensitivity of the balance is crucial to measuring the small changes in weight associated with adsorption of CO_2 at low concentrations. In our gravimetric experiments, adsorption was monitored until the uptake rate was less than 0.0001 %/min. With a sample size of approximately 30 mg, a balance with a 0.1 μg sensitivity is required to achieve this resolution. Additionally, since some adsorbents may take several days to reach equilibrium, the gas delivery system and furnace of the balance must be stable over long periods of time to avoid fluctuation or drift of the mass signal. Initial attempts in our lab with a Netzsch STA409 typically used for determination of organic content via pyrolysis, were unsuccessful because the flow rate of test gas through the analysis chamber could not be held constant enough to avoid drift. However, after acquisition of a TA Q500 TGA, which was designed for adsorption experiments, we were able to quantitatively measure adsorption at these low concentrations. The balance in this instrument has a 0.1 μg sensitivity and is stable over several days because the flow rate of test gas is governed by a mass flow controller. Additionally, the test gas flows parallel to the sample pan, avoiding back-mixing that can result in dilution of the CO_2 concentration. In our experience, these features are crucial to the quantitative measurement of CO_2 adsorption kinetics and equilibrium capacities for the small mass changes associated with the adsorption from test gas with ultra-dilute CO_2 concentration.

Similar challenges exist for adsorption systems monitored by MS. These systems typically have an inline MS that samples from a capillary slip-stream connected to the outlet of the fixed-bed. Thus, the MS samples gas at atmospheric pressure through a valve that controls the ultra-low internal vacuum of the instrument (1e-9 torr). With a 10% CO_2 test gas, small variations in the MS internal pressure only cause small variations in the measured concentration. However, at 400 ppm CO_2, the same small variations in MS internal pressure cause much larger variations in measured

concentration, making instruments with poor vacuum control useless for this application. Another challenge for MS monitored air capture systems is the condensation of water in the MS capillary slip-stream and internal chambers. At the low concentration of 400 ppm, substantial quantities of CO_2 can be absorbed by contact with condensed water, significantly effecting the concentration measured downstream. For these reasons, it is imperative for the MS in an air capture adsorption system to have a computer-controlled internal pressure and heated sampling lines and internals.

5.3.3. CO_2 Adsorption Capacity: 400 ppm vs 10% CO_2

The steep initial slope of the CO_2 adsorption isotherm (Henry's Law regime) of most aminosilicas is caused by the relatively large heat of adsorption from the amine-CO_2 interaction. In this region, changes in CO_2 partial pressure can cause significant changes in the adsorption capacity of aminosilica adsorbents (see Chapter 2). The slope is so steep that even at the ambient air concentration of 400 ppm, aminosilicas, including the HAS adsorbent, should theoretically have substantial equilibrium capacities.

A fixed bed flow system coupled with a MS was employed to measure the equilibrium adsorption capacities of the HAS-VLAS at ambient temperature under simulated air capture conditions (400 ppm humidified CO_2). These capacities are compared to the capacities previously measured under flue gas conditions (10 % humidified CO_2, Chapter 3) in Figure 5.2. Impressively, the dramatic reduction in CO_2 concentration between the two conditions only resulted in modest reduction in capacities. For instance, despite a dilution in concentration by a factor of 250, the HAS6 adsorption capacity decreased by a factor of just 2.2, varying from 3.77 mmol/g to 1.72 mmol/g. These results suggests that HAS materials can capture considerable amounts of CO_2 from the ultra-dilute CO_2 sources, and thus could be a promising adsorbent for air capture applications.

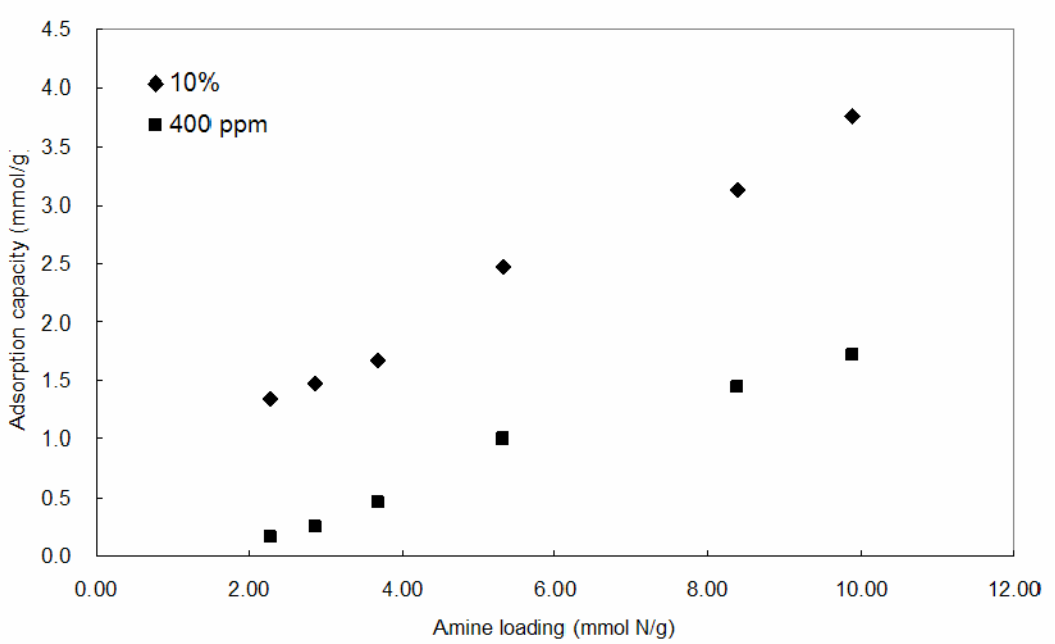

Figure 5.2. Comparison of the HAS equilibrium adsorption capacities at 400 ppm and 10% CO_2 measured by a fixed-bed adsorption system at room temperature under humid conditions.

As observed for the capacities measured at 10% CO_2, the air capture capacities of the HAS adsorbents presented in Figure 5.2 scale roughly linearly with their amine loading, increasing from 0.16 mmol/g to 1.72 mmol/g as the amine loading increased from 2.29 mmol/g (HAS1) to 9.88 mmol/g (HAS6).*[147]* Although the slope of this trend is similar to that observed for 10% CO_2, the trend does not seem to pass through the origin. This indicates that adsorption equilibrium was not reached in the 400 ppm measurements. It is also noteworthy that the HAS adsorbents with higher amine loadings were impacted less by CO_2 dilution in the feed. The adsorption capacity of the HAS6 (amine loading of 9.88 mmol/g) decreased by a factor of 2.2 (from 3.77 mmol/g to 1.72 mmol/g), while that of the HAS1 (amine loading of 2.29 mmol/g) decreased by a factor of 8.4 (from 1.34 mmol/g to 0.16 mmol/g) when the CO_2 concentration was changed from 10% to 400 ppm. It is known that the heat of adsorption of CO_2 on solid amine adsorbents decreases with surface coverage (meaning the magnitude of average heat of adsorption decreases as the CO_2 partial pressure increases),*[62]* and thus CO_2 adsorption

onto amine-grafted adsorbents is dominated by strong chemical adsorption at low CO_2 concentrations.*[151]* On the other hand, it is also known that, as amine loading decreases, the heat of adsorption of amine-functionalized silica decreases and becomes close to that of the unfunctionalized silica.*[55, 63]* Considering the relatively low amine content on the SBA-15 surface, the configuration of the HAS with low amine loadings seems to be closer to that of the silica support and thus the effect of the CO_2 dilution is more pronounced.*[66]* The relatively minor influence of the CO_2 dilution on the HAS materials with high amine loading may be attributed to the dominant impact of the chemical adsorption by hyperbranched amines at extremely low CO_2 partial pressures. In effect, this suggests that the adsorption capacity at the 10% CO_2 condition is elevated due to the presence of some physisorption under these conditions. These results show that HAS adsorbents with higher amine loadings may be more appropriate for air capture applications.

5.3.4. Adsorption Kinetics

The kinetics of adsorption and desorption are also important characteristics for the performance assessment of adsorbents for CO_2 capture. Many factors influence the adsorption kinetics of aminosilica adsorbents, including the type and density of grafted amines, amine accessibility, mass transfer through the pores to the adsorption sites, intrinsic chemical reaction rates, and other factors.*[147]* In Chapter 3, the apparent adsorption kinetics of the HAS-VLAS were characterized in a fixed-bed configuration under humid conditions. Here, the effect of increased amine loading among the HAS-VLAS was determined via gravimetry under dry conditions. These weight gain experiments allow the facile determination of adsorption kinetics. Specifically, the maximum adsorption rates were calculated from the linear slope of the CO_2 uptake curves, and the adsorption half times were determined as the time required to reach half

of the pseudo-equilibrium adsorption capacity (weight change of less than 0.0001 %/min).

Figure 5.3 shows the maximum adsorption rates and adsorption half times of the HAS-VLAS as a function of amine loading for the adsorption 400 ppm CO_2 balance argon. The maximum adsorption rate of the HAS-VLAS did not change much with varying amine loadings and was measured to be ~0.02 mmol/g*min. In contrast, the maximum adsorption rate of the HAS adsorbent for 10% CO_2 under dry conditions (not shown) was determined to be ~ 0.24 mmol/g*min. Clearly in this regime, CO_2 partial pressure has a significant impact on maximum adsorption rates. Unlike the maximum adsorption rates, the adsorption halftimes of the HAS-VLAS for adsorption of 400 ppm CO_2 increased drastically at higher amine loadings. The work in Chapter 3 showed that the highly loaded HAS adsorbents exhibited mass transfer limitations most likely due to pore blockages from polymerization.*[147]* These results at 400 ppm echo the observations in Chapter 3 and suggest that HAS materials have a key aminopolymer loading over which the adsorption kinetics are aggravated. Therefore, the composition of this hybrid should be carefully controlled to match the desired adsorption capacity and kinetics for air capture applications. A possible solution could be the use of pore-expanded mesoporous silicas as supports for aziridine polymerization as discussed in Chapter 4. Future work should examine the utility of these PEHAS adsorbents for the air capture application.*[152]*

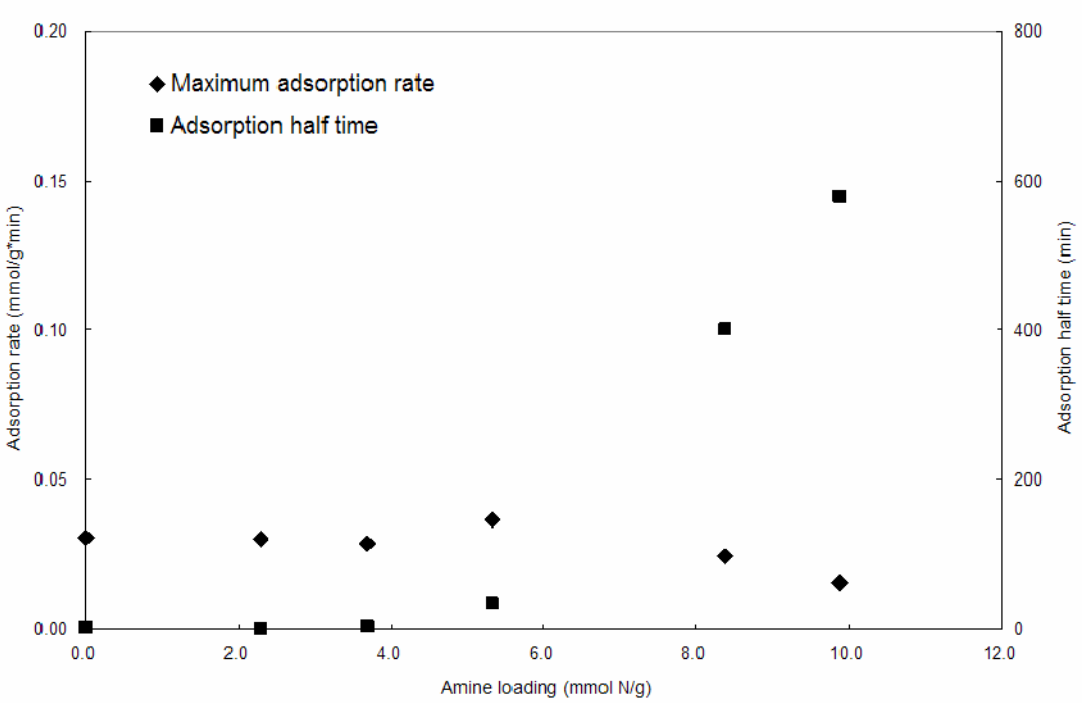

Figure 5.3. Maximum CO_2 adsorption rates and adsorption halftimes for the HAS-VLAS as functions of amine content. The maximum adsorption rate was calculated from the initial slope of 400 ppm CO_2 adsorption curves measured by TGA. The adsorption halftime represents half the time required for a given adsorbent to reach its pseudo-equilibrium capacity.

5.3.5. Regenerability of the Adsorbents

Adsorbent regenerability is another important parameter for practical air capture applications, as the adsorbent should retain stable CO_2 adsorption performance over many hundreds of adsorption/desorption cycles. The regenerability of the HAS adsorbent (HAS4) was assessed by measuring its working capacity over four adsorption (25 °C) and desorption (110 °C) cycles via gravimetry. Recurring measurement of the CO_2 uptake curves (Figure 5.4, inset) illustrated that the adsorptive performance of the HAS adsorbent was quite stable under the simulated air capture conditions, preserving its initial capacity without significant degradation. The regenerability of the HAS adsorbent was compared with that of a class 2 adsorbent prepared by grafting SBA-15 with di silane according to previously published methods, because class 2 adsorbents have been shown

to be very stable over many CO_2 adsorption/desorption cycles.*[26, 153]* The air capture capacities of both adsorbents over successive cycles are shown in Figure 5.4, and the results indicate that the HAS adsorbent exhibits similar regenerative stability to a typical class 2 adsorbent. This stability may be attributed to the fact that the aminopolymers in HAS are covalently bound to the silica support, preventing leaching.*[26, 147]* The good regenerative stability of HAS suggests that it is robust enough to allow repeated temperature swings without significant loss of amine contents, and thus can provide a stable air capture capacity during multiple adsorption/desorption cycles. The stability can be further enhanced by running under humidified conditions.*[142, 154]*

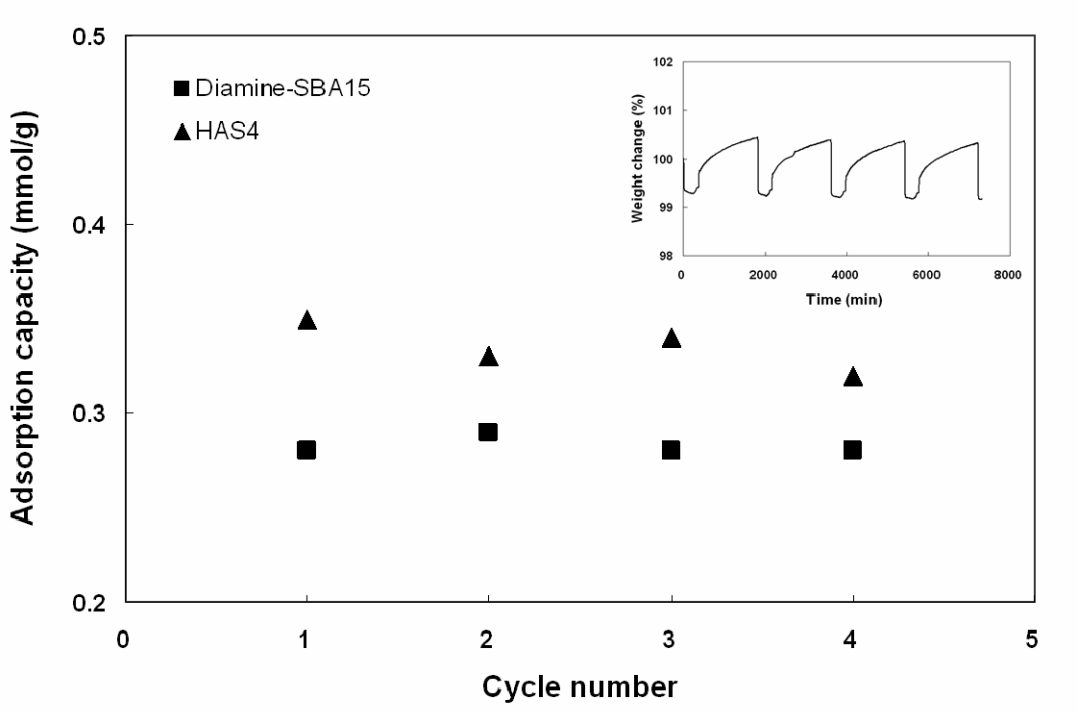

Figure 5.4. Adsorption working capacities of HAS4 adsorbent compared to a representative class 2 adsorbent (di silane functionalized SBA-15) measured via gravimetry over four adsorption/desorption cycles using dry 400 ppm CO_2 at ambient temperature. An example of the multicycle TGA adsorption curve of the HAS4 adsorbent is shown in the inset.

5.4. Conclusions

In comparison to the conventional CO_2 capture techniques targeting flue gases generated from large point sources, adsorptive CO_2 fixation from the ambient air provides a unique opportunity for a carbon negative technology, in that it can in principle reduce the actual CO_2 level in the atmosphere if applied on a large scale. In this work, the HAS adsorbent's ability to effectively capture CO_2 from ambient air was demonstrated. Several experimental challenges were overcome by acquiring analytical equipment with the proper sensitivity for measuring adsorption under these ultra-dilute conditions. The adsorption characteristics of the HAS adsorbents, including the adsorption capacity, apparent adsorption kinetics, and adsorbent regenerability, were investigated using ultra-dilute CO_2-containing gas mixtures that simulate the current atmospheric CO_2 concentration. An HAS material provided a higher adsorption capacity than a conventional class 2 adsorbent, while capturing CO_2 reversibly without significant degradation of performance in multicyclic operations. Materials of this type, if incorporated into appropriate, scalable processes, may one day be important components of practical air capture processes.

CHAPTER 6

EXPLORATION OF N-SUBSTITUTED-AZIRIDINES FOR THE SYNTHESIS OF SECOND GENERATION ADSORBENTS

6.1. Introduction

From the research done on the first generation HAS adsorbent, several conceptual improvements can be envisioned. The aminopolymer prepared from aziridine polymerization is hyperbranched and contains a substantial percentage of tertiary amines that can only capture CO_2 in the presence of water, and then only at high partial pressures. Thus, an adsorbent with linear aminopolymers that contain only primary and secondary amines would be preferable. Such a system can be synthesized by reaction with N-substituted-aziridines instead of through uncontrolled polymerization of unmodified aziridine, as N-substituted-aziridines only react with primary amines and, therefore, cannot self-polymerize. There are two types of N-substituted-aziridines that can be used in this strategy: N-alkylcarboxylate-protected aziridines that can be used in protection/deprotection functionalization schemes, and N-alkylaziridines that can be used as a "one-time" incremental growth of an alkylaminoethyl group. Both of these N-substituted-aziridine types have the added potential benefit of avoiding the pore-blocking phenomenon associated with aziridine polymerization that was described in previous chapters.

6.1.1. Introduction to N-alkylcarboxylate-protected Aziridines

The synthesis of linear poly(ethyleneimine) (LPEI) from a flat silica surface by step-wise polymerization was first reported by Park, et al.*[87]* The synthesis involved the ring-opening reaction of an N-carbobenzyloxy-protected aziridine (Cbz-aziridine) with a

primary amine to form a successive ethyleneimine unit. The ester protecting group was then cleaved by acid treatment (neat trifluoroacetic acid, TFA), yielding a terminal primary amine. Theoretically, this procedure could be applied to mesoporous silica and repeated a number of times to obtain low molecular weight LPEI polymers of tunable length, corresponding to an adsorbent with tunable capacity and amine efficiency. A generalized reaction scheme for the preparation of linear aminosilicas (LAS) with N-alkylcarboxylate-protected aziridine is given in Figure 6.1, where R = phenyl for the Cbz-aziridine.*[87]*

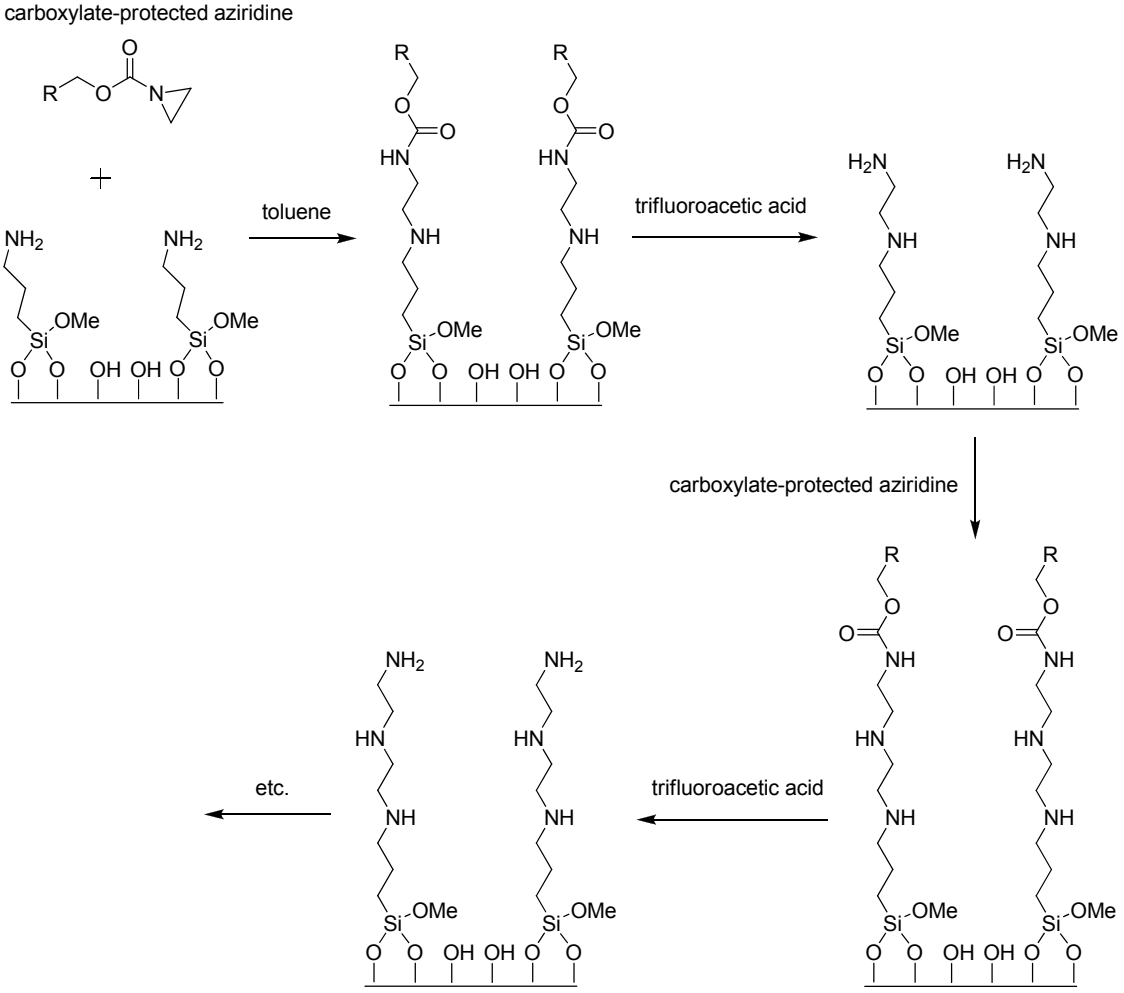

Figure 6.1. Reaction scheme for the step-wise polymerization of LPEI by reaction with carboxylate-protected aziridine and acid deprotection.*[87]*

While a variety of N-alkylcarboxylate-protected-azridines can be envisioned, their synthetic yields are not universal, and the strength of their protecting groups may require deprotection conditions that are too harsh to preserve the aminosilica structure. For these reasons, several N-alkylcarboxylate-protected-azridines were explored in parallel, in a search to find an easily synthesizable protected-aziridine that required only mild deprotection conditions.

6.1.2. N-alkylaziridines for the "One-time" Incremental Growth of Alkylaminoethyl Groups

N-alkylaziridines, such as N-methylaziridine, react with 1° amines by ring-opening to add alkylaminoethyl groups, converting the 1° amines to 2° amines. This reaction represents a simple and efficient way to add amine content to already-prepared aminosilica adsorbents, such as those prepared through aminosilane grafting (see Chapter 2). Figure 6.2 illustrates this idea by showing the reaction schemes for the reaction of mono, di, or tri silane grafted silica with N-alkylaziridine and the incremental increase of alkylaminoethyl groups in these materials. Of course, this strategy for increasing adsorbent amine loading could be applied to any 1° amine-containing aminosilicas.

In addition to increasing the amine content and, theoretically, CO_2 capacities of aminosilica adsorbents, N-alkyl-aziridine functionalization strategies create aminoalkyl moieties that contain only 2° amines. These structures could be used for the elucidation of the role and strength of dual-site adsorption in CO_2 capture. This is important because the best performing adsorbents in the literature are those with adjacent 1° and 2° amines (Sayari's tri silane functionalized silicas and HAS), however, no fundamental research has determined the importance of these sites on the adsorbed CO_2 structure and the corresponding heat of adsorption. To illustrate this point, Figure 6.3 shows the possible dual-site adsorption interactions for two types of diamine adsorbents: 1°-2° diamine materials synthesized via di silane and 2°-2° diamine materials synthesized via N-

alkylaziridine. Under dry conditions, two amines are required to capture one CO_2 molecule. Also, primary amines have higher heats of adsorption than secondary amines. Therefore, a single adsorption capacity measurement on 1°-2° diamine materials gives no information about the specific adsorbed species, because a number of dual-site interactions are possible. However, comparing the adsorption capacities and heats of adsorption for 1°-2° diamine materials with 2°-2° diamine materials, which only have 2°-2° interactions, could elucidate the importance of these interactions on adsorptive performance.

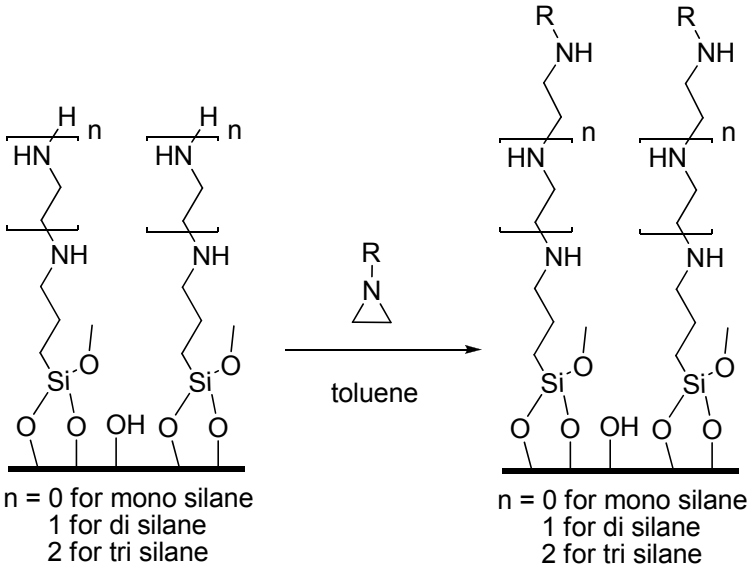

Figure 6.2. Reaction schemes for the reaction of mono, di, or tri silane grafted silica with N-alkylaziridine and the incremental increase of alkylaminoethyl groups.

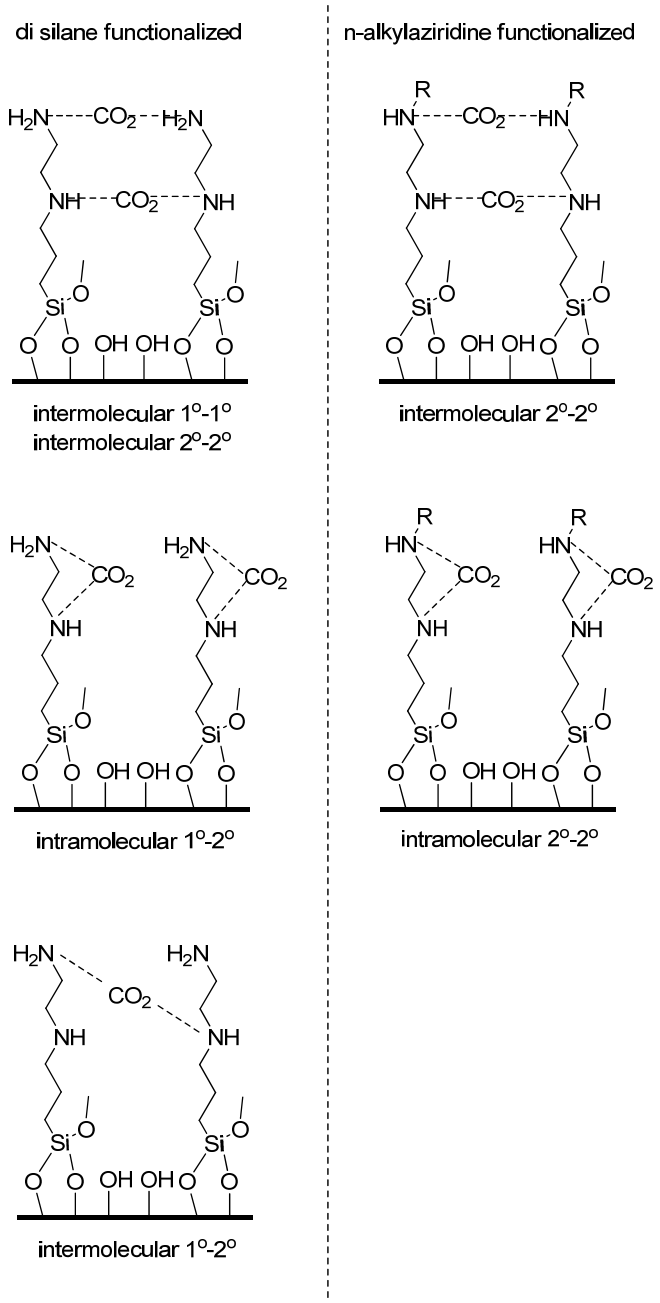

Figure 6.3. Possible dual-site interactions of 1°-2° diamine materials synthesized via di silane, and 2°-2° diamine materials synthesized via N-alkylaziridine. For clarity, dashed bonds denote interactions between amines and CO_2, and are not meant to represent bonds in actual adsorbed structures.

This chapter will describe the exploration of several strategies for the synthesis of N-substituted aziridines and their use in the preparation of linear aminosilicas for the

applications of increasing adsorbent amine loading and elucidating the role and strength of dual-site adsorption in CO_2 capture.

6.2. Exploration of the Synthesis and Utilization N-alkylcarboxylate-protected Aziridines

6.2.1. Carbobenzyloxy-protected Aziridine

The synthesis of linear poly(ethyleneimine) (LPEI) from a flat silica surface by step-wise polymerization was first reported by Park, et al.*[87]* The synthesis involved the ring-opening reaction of an N-carbobenzyloxy-protected aziridine (Cbz-aziridine) with a primary amine to form a successive ethyleneimine unit. The benzylester protecting group was then cleaved by acid treatment (neat trifluoroacetic acid, TFA), yielding a terminal primary amine. A generalized reaction scheme is given in Figure 6.1 where R = benzyl in this case.

The three-step synthesis of Cbz-aziridine was reported by Zinic, et al. (Figure 6.4).*[155]* In the first step, Cbz-ethanolamine (Figure 6.4, species 1) was produced from ethanolamine and benzyl acid chloride in the presence of sodium bicarbonate at 0 °C. After purification by distillation, the Cbz-ethanolamine (1) was tosylated by reaction with tosyl chloride in the presence of base (pyridine). After re-crystallization in acetone and then methanol, the clear white crystals of the tosylated intermediate (2) were determined to be 96% pure by ^{1}H NMR (Figure 6.5). Unfortunately, several attempts to cleanly synthesize Cbz-aziridine (3) from this tosylated intermediate (2) were unsuccessful. While aziridinyl protons were detected in the ^{1}H spectra at δ2.2 ppm, the two peaks at δ3.6 and 3.4 ppm revealed the presence of aminoethyl protons from non-ring-closed species (Figure 6.6). However, several attempts to separate the unconverted species (~85%) from the Cbz-aziridine (3) by column chromatography according to a published procedure were unsuccessful (Figure 6.7).*[155]* While the purification of Cbz-aziridine is

ultimately possible, the focus of this research was shifted to a different protected aziridine due to time constraints.

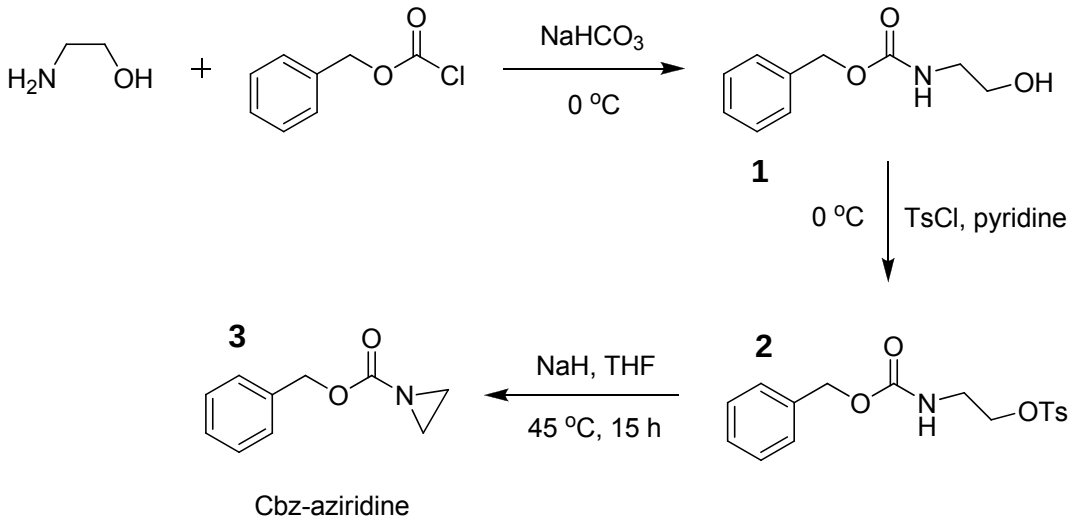

Figure 6.4. Reaction scheme for the three-step synthesis of Cbz-aziridine.

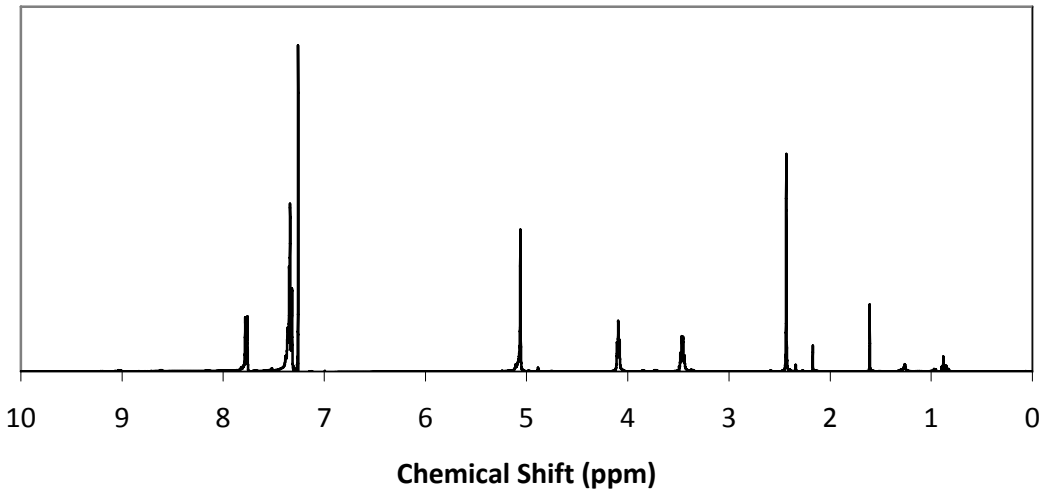

Figure 6.5. ^{1}H NMR spectrum of tosylated intermediate in the Cbz-aziridine synthesis. Appearance of shifts at δ7.8 and 2.4 ppm signify the addition of the tosylate group.

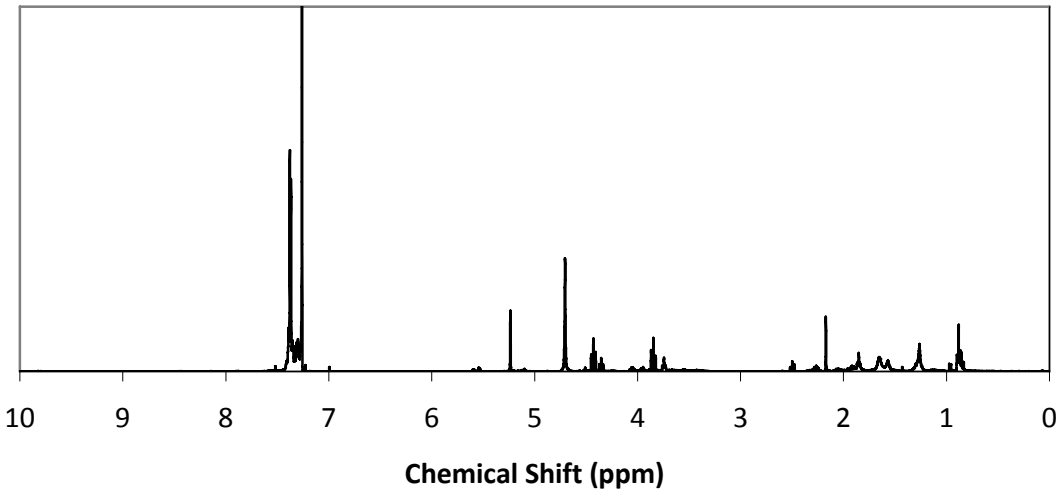

Figure 6.6. ^{1}H NMR spectrum of crude Cbz-aziridine (3) and unconverted species. Disappearance of shifts at δ7.8 and 2.4 ppm signify the loss of the tosylate group. Appearance of shift at δ2.2 ppm signifies closure of aziridinyl ring.

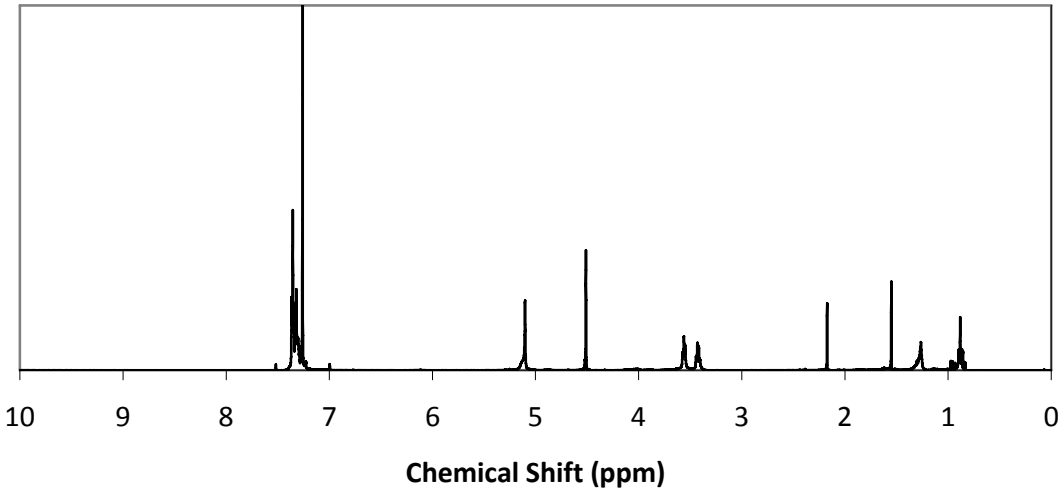

Figure 6.7. ^{1}H NMR spectrum of Cbz-aziridine (3) and unconverted species after purification by column chromatography. Disappearance of shifts at δ7.8 and 2.4 ppm signify the loss of the tosylate group. Appearance of shift at δ2.2 ppm signifies closure of aziridinyl ring. Shifts at δ3.6 and 3.4 ppm show the presence of non-ring-closed species.

6.2.2. Methylcarboxylate-protected Aziridine

As an alternative to the ring-closure of an aminoethyltosylate, protected aziridine was synthesized directly from an unfunctionalized aziridine small molecule. The reaction

of alkylchloroformate with aziridine in triethylamine was based on aziridine derivatizations published by Deyrup on a common theme (Figure 6.8).*[156]* The chloroformate reacts with aziridine and displaces HCl which quickly forms a salt with triethylamine and precipitates out of solution. Unfortunately, consistent with reported results, the equivalent reaction with benzylchloroformate (R = phenyl) resulted in poor yields.*[156]* In contrast, the reaction of aziridine with methylchloroformate (R = H) was accomplished in nearly quantitative yield. Thus, the step-wise procedure for synthesizing a LAS material was carried out instead with methylcarboxylate-protected aziridine.

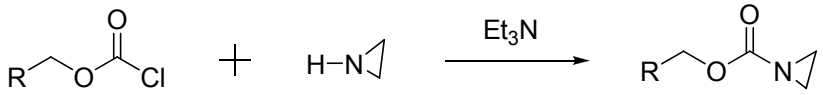

Figure 6.8. Reaction scheme for the formation of alkylcarboxylate-protected aziridines from alkylchloroformate and aziridine in the presence of triethylamine, adapted from a generalized scheme reported by Deyrup.*[156]*

Methylcarboxylate-protected aziridine was reacted with an aminosilica prepared by the functionalization of PE SBA-15 with aminopropyltrimethoxysilane according to a previously published procedure.*[106]* The amine loading of this starting aminopropyl functionalized silica was 1.73 mmol N/g SiO_2.

Three reactions were performed with this aminosilica and methylcarboxylate-protected aziridine at different reaction conditions to determine if temperature and acetic acid were essential to the reaction (Table 6.1). When reacted with protected aziridine at room temperature with no acid (LAS3), 0.57 mmol protected groups/g SiO_2 were added. In other words, a third of the amines initially present reacted with the protected aziridine, lengthening the aminopolymers by one unit. The LAS4 reaction was performed at toluene reflux without the presence of acid. This resulted in the addition of 2.28 mmol protected groups/g SiO_2, which is larger than the number of amines present in the original material. It is possible that the extra functionalization occurred on unfunctionalized silanol groups

on the surface of the silica or perhaps on residual silane methoxy groups that did not react with the silica surface during silane grafting. The LAS5 reaction was performed under toluene reflux in the presence of a catalytic amount of acetic acid. This resulted in a smaller loading of 1.27 mmol protected groups/g SiO_2 or two thirds of the initial amines reacted. It is unclear why the presence of acid resulted in a lower loading, but a possible explanation is that the acid catalyzed the homo-coupling of two protected aziridine molecules in solution, preventing functionalization of the solid.

Table 6.1. Materials synthesized from methylcarboxylate-protected aziridine and aminopropyl functionalized PE SBA-15 under different reaction conditions.

	Temperature	Catalytic Acid?	Organic Loading (g organic/ g SiO2)	Silane Loading (mmol silane/ g SiO2)	Prot. Az. Loading (mmol protected growth/ g SiO2)
PEmono1	25	No	0.13	1.73	0
LAS3	25	No	0.18	1.73	0.57
LAS4	110	No	0.36	1.73	2.28
LAS5	110	Yes	0.26	1.73	1.27

A series of experiments were conducted on the LAS4 material to investigate the next step in the step-wise polymerization scheme: deprotection of the secondary amine by acid cleavage. To probe the proper deprotection conditions, in two separate experiments two small amounts (~50 mg) of LAS4 were stirred overnight in ~ 20 ml of either neat TFA (LAS4d10%) or a 10% solution of TFA in DI H_2O (LAS4d100%). Table 6.2 shows that instead of losing organic content through cleavage of the methylcarboxylate group, the materials gained organic content after treatment with acid. This unexpected result could possibly be due to either TFA adsorption onto the aminosilica rather than cleavage of the methylcarboxylate group, or production of insoluble species after reaction with the methylcarboxylate group that deposited on the silica surface.

Table 6.2. Organic content of LAS4g1 material before and after attempted acidic cleavage.

Sample	Organic Content (g organic/g SiO_2)
LAS4	0.34
LAS4d100% [a]	0.42
LAS4d10% [b]	0.47

[a] Deprotected in neat TFA.
[b] Deprotected in 10% TFA in H_2O.

Figure 6.9 shows IR spectra of the PEmono1cap, LAS4, LAS4d10%, and LAS4d100% materials. The appearance of sharp CF_3 transitions in both deprotected samples (LAS4d10% and LAS4d100%) at 725 cm^{-1} confirmed the incorporation of TFA into the solid. Additionally, the C=O transition at 1650 cm^{-1} from the amide ester in LAS4, shifted to 1680 cm^{-1} and grew in intensity relative to the other transitions, indicating the incorporation of the carbonyl from the TFA into the solid. The CF_3 and C=O transitions of liquid TFA appear at 680 and 1780 cm^{-1}, respectively (Sigma Aldrich). These transitions are substantially different than those observed in the deprotected solids, thus it is unlikely that unreacted TFA was adsorbed in the solid. Regardless, the inability to deprotect the methylcarboxylate-protected amine provided motivation to pursue the use of a different protected aziridine to determine the importance of the protecting group.

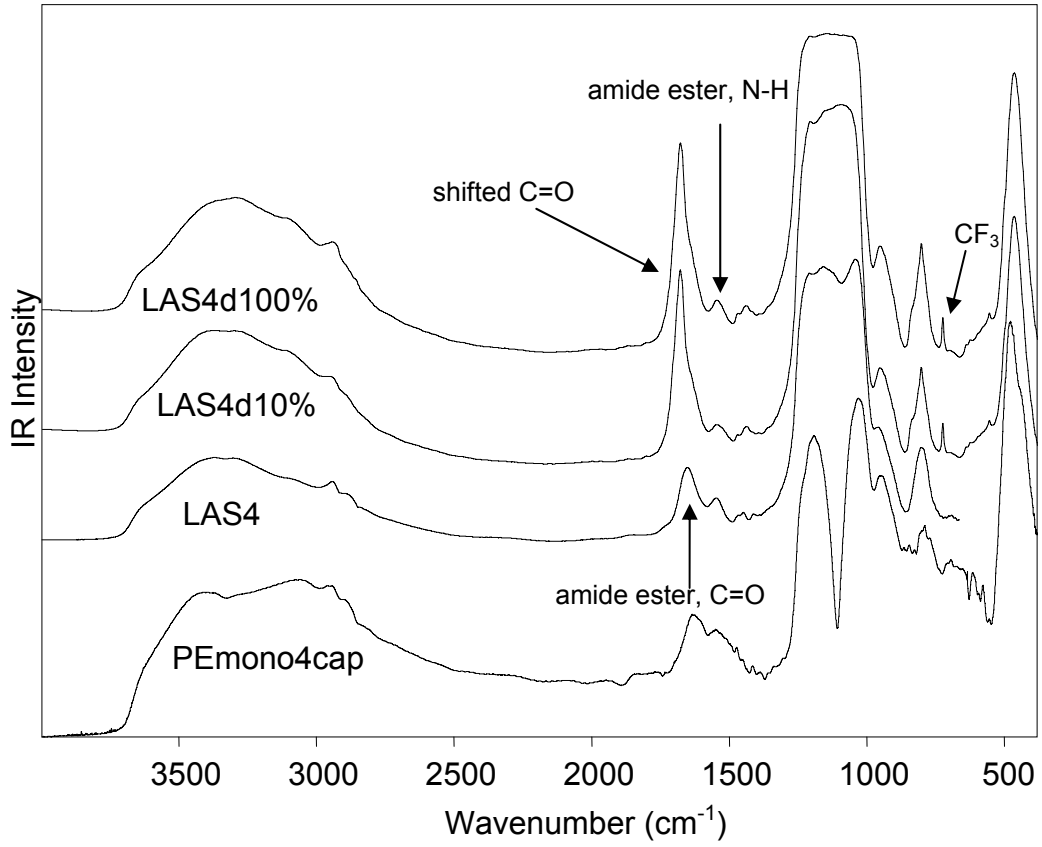

Figure 6.9. IR spectra of PEmono1cap, LAS4, LAS4d10%, and LAS4d100%.

6.2.3. Ethylcarboxylate-protected Aziridine

As discussed above, the synthesis of methylcarboxylate-protected aziridine was facile, however, the deprotection step of the step-wise polymerization was unsuccessful. To probe the effect of a larger protecting group, ethylcarboxylate-protected aziridine was synthesized in a similar manner to methylcarboxylate-protected aziridine. Culbertson and Dietz published a route to an ethylcarboxylate-protected aziridine through the reaction of ethylchloroformate with aziridine in the presence of triethylamine in benzene (Figure 6.10).*[157]* After reaction, the solution was allowed to warm to room temperature and then filtered to remove the triethylammonium chloride salts. The benzene and triethylamine were then removed in vacuo and the crude protected aziridine product was

recovered. After purification by distillation, ethylcarboxylate-protected aziridine was recovered in ~ 50% yield. Figure 6.11 shows the ^{1}H NMR spectrum of the purified product. The appearance of the aziridinyl peak at δ2.2 ppm and the two alkyl proton peaks at δ4.1 and 1.3 ppm show the formation of the protected aziridine product.

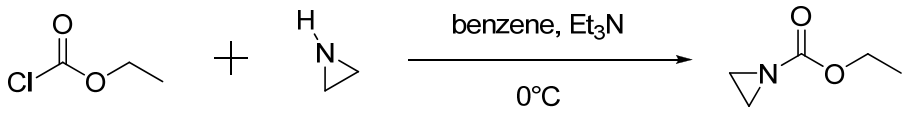

Figure 6.10. Reaction scheme for the synthesis of ethylcarboxylate-protected aziridine adapted from Culbertson and Dietz.*[157]*

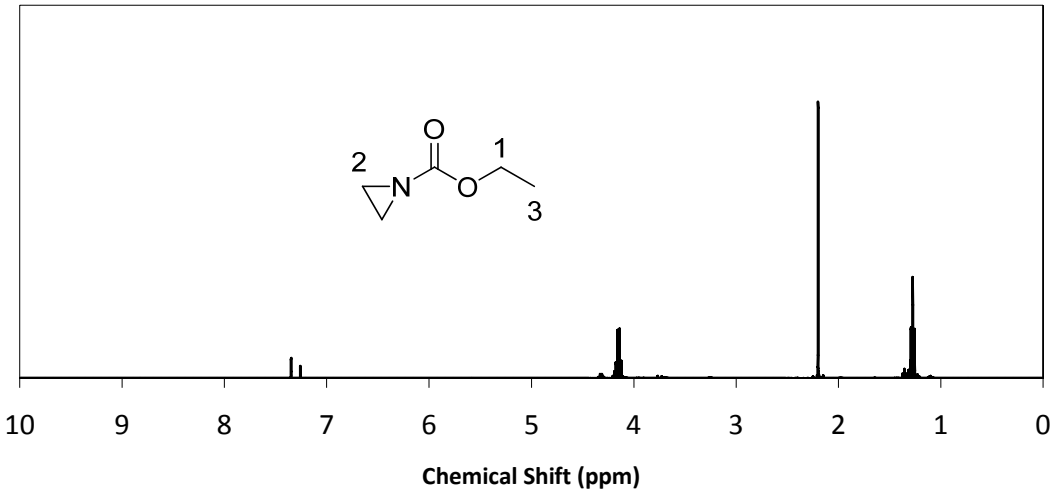

Figure 6.11. ^{1}H NMR spectrum of purified ethylcarboxylate-protected aziridine. Shifts at δ4.1, 2.2, and 1.3 ppm correspond to the protons at positions 1, 2, and 3, respectively.

To investigate the efficacy of the ethylcarboxylate-protected aziridine, a parent aminosilica was prepared by the reaction of an aminopropylsilane with PE SBA-15. The silane loading (equimolar to amine loading) for the parent aminosilica (sample ID of PEmono4) was 1.51 mmol/g SiO_2 (Table 6.3). Additionally, the parent aminosilica was reacted with 1,1,1,3,3,3-hexamethyldisilazane (HMDS) to "cap" any unreacted silanol groups with trimethylsilyl groups, creating an additional loading of 0.0142 g trimethylsilyl/g SiO_2. Three protected aziridine functionalizations (LAS9 through

LAS11) were then carried out with different reaction temperatures and reactant concentrations (Table 6.3). LAS9 was prepared with a protected aziridine to supported amine molar ratio of 1.6 at 80ºC. By TGA, about a third (0.53 mmol protected growth/ g SiO_2) of the primary amines in the parent aminosilica were functionalized with a new protected aminoethyl group. When the reaction temperature was increased to toluene reflux and the reactant ratio increased to 6.3 mol protected aziridine/mol supported amine for the LAS10 material, the generational growth increased to 1.27 mmol protected growth/g SiO_2. Finally, at toluene reflux and a reactant ratio of 10.29 mol protected aziridine/mol supported amine for the LAS11 material, the generational growth increased to 1.57 mmol protected growth/g SiO_2, suggesting complete reaction with the aminopropyl groups of the parent aminosilica.

Table 6.3. Reaction conditions and compositions of aminosilica materials from step-wise polymerization scheme.

Sample	Silane Loading (mmol silane/ g SiO_2)	Cap Loading (g cap/ g SiO_2)	PA Reaction Temperature (ºC) [a]	Reactant Ratio (mmol PA/ mmol silane) [b]	Protected Growth (mmol protected growth/ g SiO_2) [c]
PEmono4	1.51	n/a	n/a	n/a	n/a
PEmono4cap	1.51	0.0142	n/a	n/a	n/a
LAS9	1.51	0.0142	80	1.6	0.53
LAS10	1.51	0.0142	110	6.3	1.27
LAS11	1.51	0.0142	110	10.29	1.57

[a] PA = protected aziridine.
[b] Molar ratio of protected aziridine to silane loading of aminosilica added to the reaction environment.
[c] Calculated by subtracting the silane and cap loading from the total organic loading determined by TGA, then multiplying by the molecular weight of ethylcarboxylate-protected aziridine.

In order to verify the presence of the ethylcarboxylate protecting group in the LAS9 and LAS10 materials, FT-IR spectra were measured using the KBr method (Figure 6.12). The amide ester carbonyl transition around 1700 cm^{-1} appears in the LAS9 spectrum accompanied by the reduction of the primary amine signal at 1600 cm^{-1}. Additionally, the appearance of a new transition at ~1525 cm^{-1} indicates the presence of

the protected secondary amine. These effects are much more prominent in the spectrum for LAS10, which has a higher degree of functionalization.

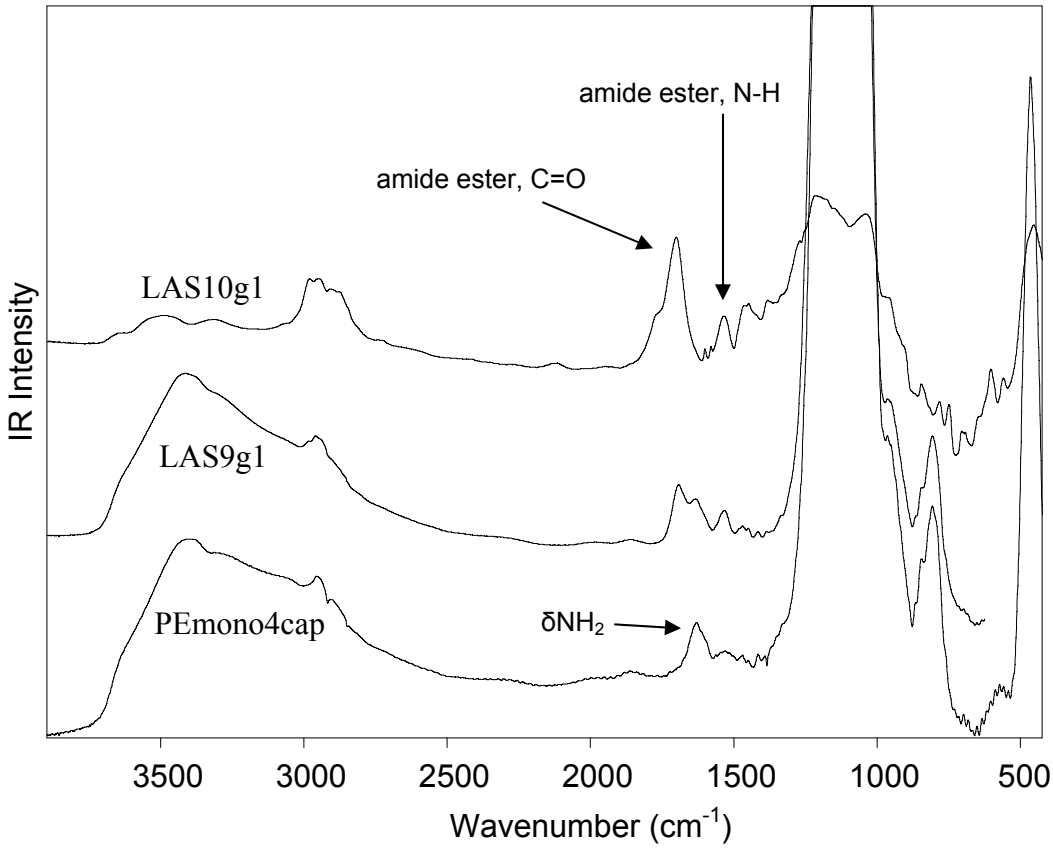

Figure 6.12. FT-IR spectra of aminopropyl silica and two linear aminosilicas prepared by reaction with protected aziridine (LAS9 and LAS10).

Several attempts at deprotecting the ring-opened species in LAS10 and LAS11 were made by treatment with acid. These deprotection experiments are described in Table 6.4. The first deprotection attempt (LAS10d1) was adapted from a deprotection method reported for Cbz-aziridine where the aminosilica was stirred in neat TFA overnight at room temperature.*[87]* After the solid was filtered, washed with methanol, and dried, TGA showed that the sample actually gained about 1% organic content. A second deprotection attempt (LAS10d2) was done in a 1:1 TFA:MeOH solution at 60 ºC

overnight, but the sample gained even more organic content. It was then hypothesized that the product formed during the deprotection reaction was insoluble in methanol, so the solid was then washed consecutively with water, toluene, hexane, ethanol, and chloroform, and dried under vacuum at 75 ºC. The TGA of this washed solid showed about a 50% removal of the protecting groups.

With these results in mind, additional deprotection reactions were performed in an attempt to find conditions that would result in complete deprotection. The LAS11 material and another ethylcarboxylate-protected aziridine treated aminosilica (LAS12, prepared similarly to LAS10 and LAS11) were subjected to several deprotection strategies that are described in Table 6.4. After each deprotection treatment, the solids were all filtered, washed with consecutively with water, toluene, hexane, ethanol, and chloroform, and dried under vacuum at 75 ºC. Unfortunately, only deprotection at 75 ºC in 1:1:1 MeOH:chloroform:TFA resulted in a decrease in organic content of the solids, but this weight loss corresponded to the deprotection of only 35% of the ethylcarboxylate groups. These results indicate that acidic treatment of the ethylcarboxylate-protected amine may not result in complete deprotection, regardless of the solvent combination used. Indeed, as described above, deprotection in neat TFA only resulted in 50% removal of protecting groups. To eliminate the possible formation of insoluble deprotection products by combination with the trifluoroacetate ion, similar deprotection experiments were performed with HCl, however, these experiments also failed to remove the ethylcarboxylate protecting groups.

Table 6.4. Conditions and percent deprotected for protected-aziridine deprotection reactions.

Deprot. Run	Change in Organic Content (g/g SiO_2) [b]	Deprot. Time (h)	Deprot. Temp. (°C) [c]	Deprotection Solution [d]
LAS10d1	0.022	overnight	rt	TFA
LAS10d2	0.084	overnight	60	1:1 TFA:MeOH
LAS11d1	-0.040	overnight	75	1:1:1 MeOH:chloroform:TFA
LAS11d2	0.017	overnight	110	1:1:1 toluene:MeOH:TFA
LAS12d1	0.027	overnight	80	1:1 TFA:toluene
LAS12d2	0.010	overnight	80	
LAS12d3	dissolved the solid	1.5	200	3 g ethylene glycol, 0.3 g KOH, 0.05 g hydrazine hydrate

[a] Deprot. = Deprotection
[b] Calculated by the change in organic content determined by TGA. A negative value represents a decrease in the organic content of the solid and indicates that species were deprotected.
[c] rt = room temperature
[d] Makeup of solution used for deprotection. A large excess of solvent was used for each experiment.

Figures 13 and 14 show the Raman and IR spectra, respectively, of PEmono4cap parent aminosilica, LAS11, and two deprotection attempts, LAS11d1 and LAS11d2. Figures 15 and 16 show the Raman and IR spectra, respectively, of PEmono4cap parent aminosilica, LAS12, and two deprotection attempts, LAS12d1 and LAS12d2. Unfortunately, the Raman spectra (Figures 13 and 15) for the deprotected samples suffered from severe fluorescence, most likely due to the introduction of trace metal impurities during the washing steps.*[158]* However, the IR spectra in Figures 14 and 16 reveal that the C=O and N-H transitions at 1700 and 1535 cm^{-1}, respectively, associated with the protected amide ester, were largely unchanged after each deprotection attempt. There is a slight increase in intensity of the shoulder at 1630 cm^{-1} in the LAS11d1 (Figure 14) material corresponding to the 1° amine N-H transition, and confirming the successful deprotection of a fraction of the primary amines, as inferred from TGA analysis.

Interestingly, the CF_3 transitions observed in the deprotected methylcarboxylate materials discussed in the previous section (LAS4d10% and LAS4d100%) were absent in Figures 14 and 16 for the deprotected LAS11 and LAS12 materials. It appears that whatever insoluble products formed from the trifluoroacetate ions in the LAS4

deprotection attempts were successfully washed away in the LAS11 and LAS12 deprotection attempts and thus, were not the cause of the observed weight increases. While the exact nature of this observed weight increase is uncertain, these results eliminate the possibilities of adsorbed TFA or CF_3-containing insoluble deprotection products as contributors.

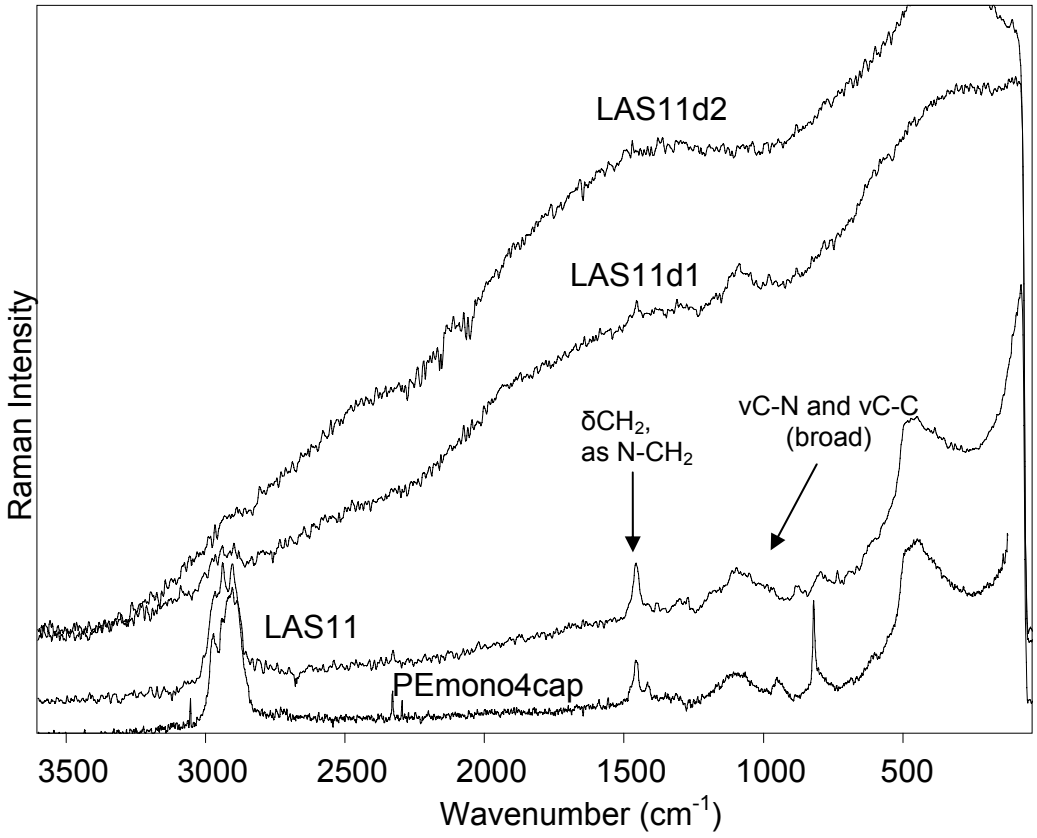

Figure 6.13. Raman spectra of PEmono4cap, LAS11, LAS11d1, LAS11d2.

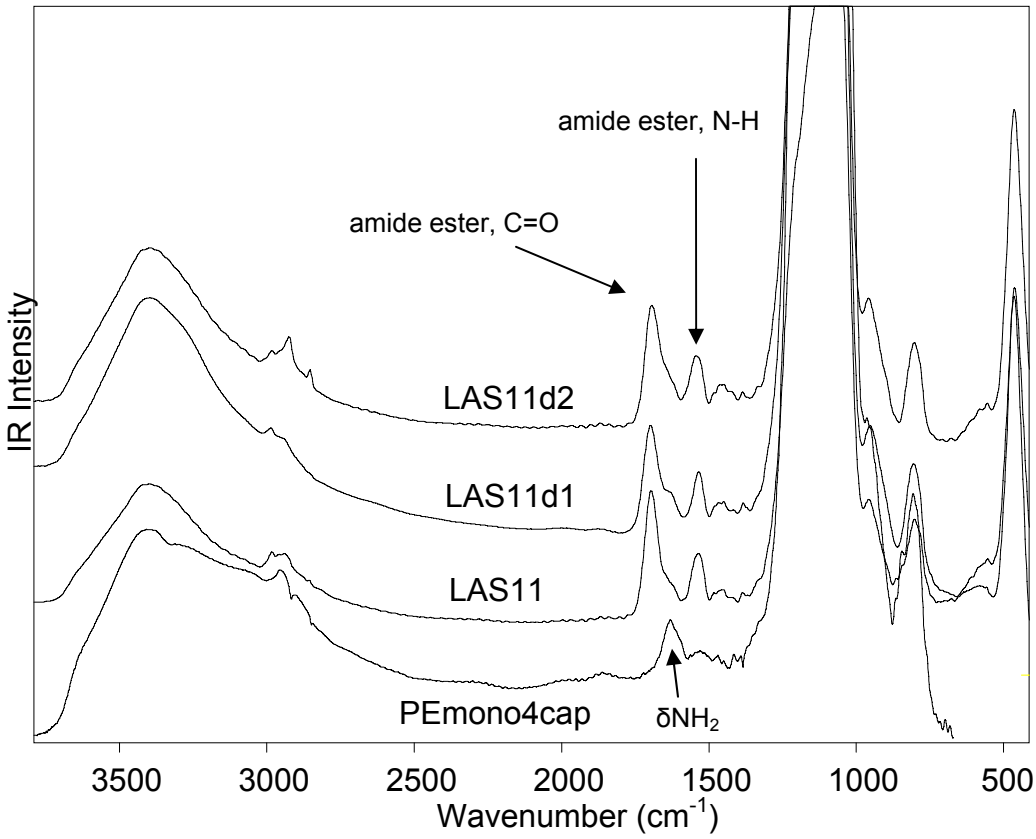

Figure 6.14. IR spectra of PEmono4cap, LAS11, LAS11d1, LAS11d2.

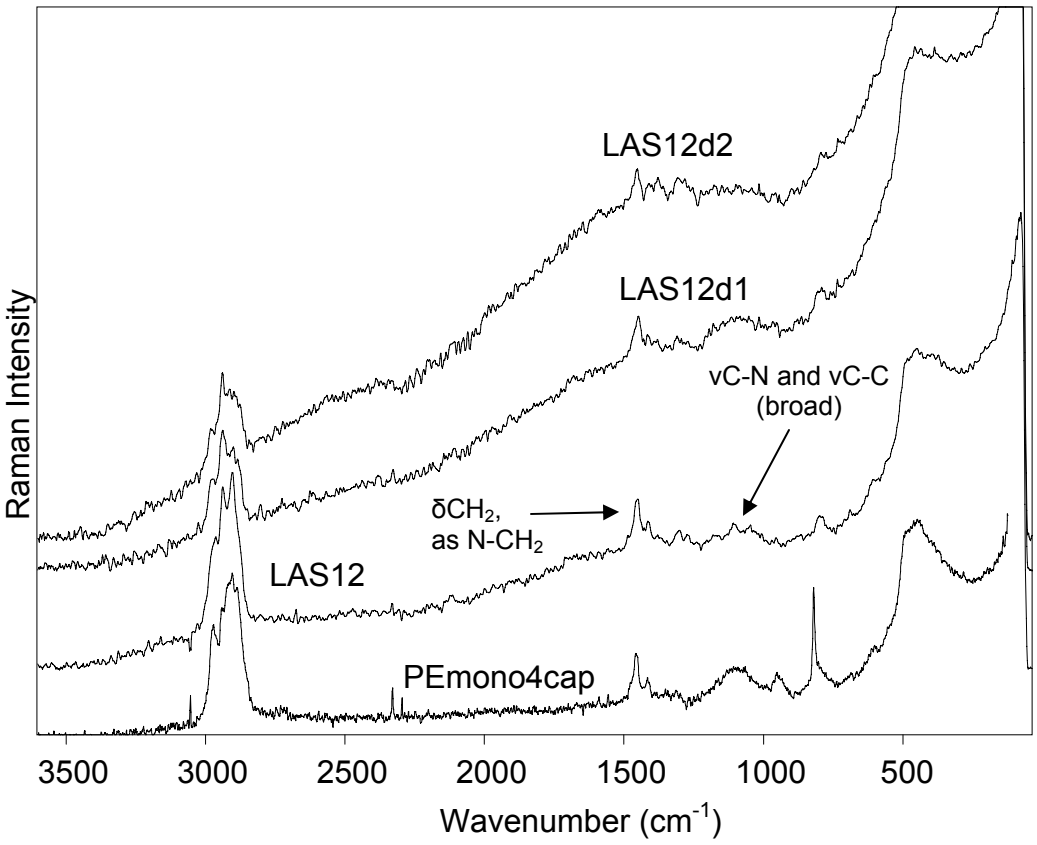

Figure 6.15. Raman spectra of PEmono4cap, LAS12, LAS12d1 and LAS12d2.

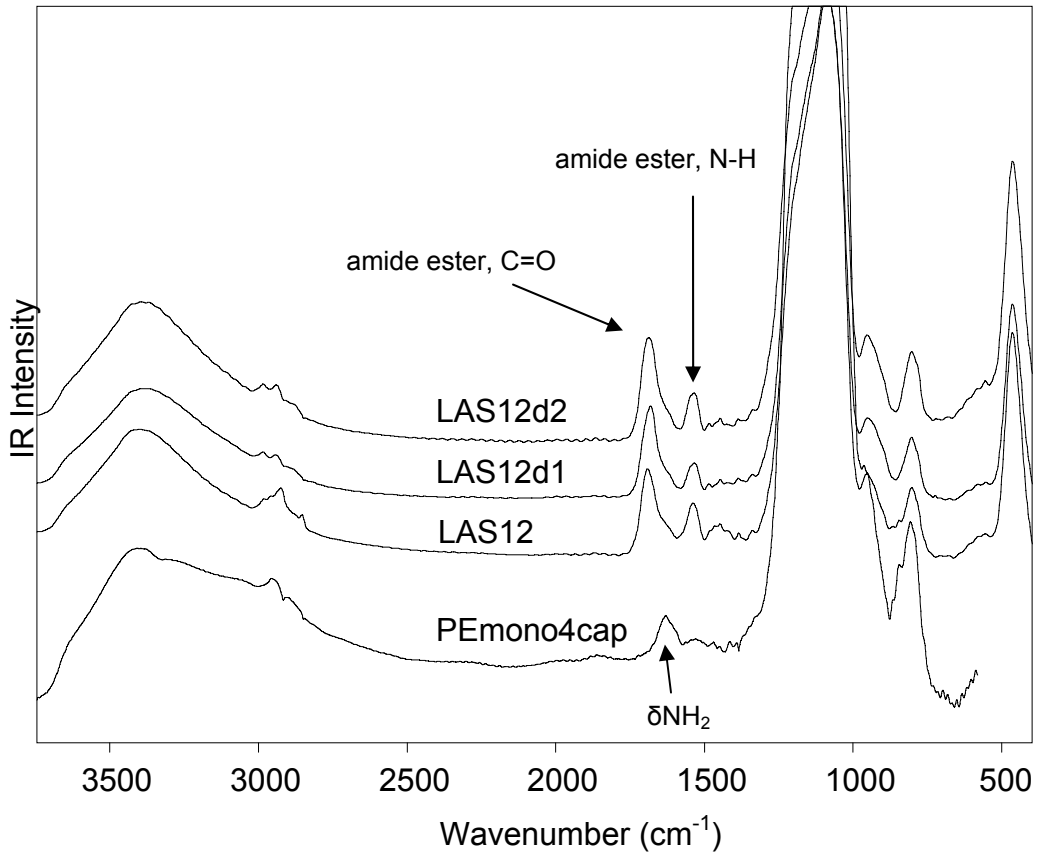

Figure 6.16. IR spectra of PEmono4cap, LAS12, LAS12d1 and LAS12d2.

An alternative to acidic deprotection was also attempted by adaptation of a deprotection strategy for carboxylate-protected pyrrolidines, where LAS12 was treated with a mixture of ethylene glycol, KOH, and hydrazine hydrate at 200 ºC for 1.5 hours (LAS12d3, Table 6.4).*[159]* However, upon filtration it was discovered that the deprotection mixture dissolved the mesoporous silica support. This highlights a particular problem with applying common protection/deprotection chemical techniques to porous aminosilicas. Often, the conditions necessary to cleave a certain protecting group require strongly acidic or basic environments at high temperatures (> 100 ºC), but these conditions can also disrupt the SiO_2 framework or the Si-C bonds that link the organic groups to the silica support. Thus, we have been unable to discover ethylcarboxylate-

protected amine deprotection conditions that are sufficiently strong to completely convert to the deprotected species without degrading or dissolving the silica support in the process.

6.3. Simplified Route to LAS Materials Via N-alkylaziridines: Methylaziridine

The experiments described above highlight the challenges associated with synthesizing protected aziridines and successfully accomplishing the deprotection step after ring-opening. Unfortunately, these challenges make the step-wise polymerization scheme to create LAS materials experimentally difficult. As alternatives, N-alkylaziridines, the other type of N-substituted-aziridines discussed in the introduction of this chapter, could react with a primary amine-terminated aminopolymer to incrementally increase the amine content by one alkylaminoethyl unit. This process is shown in Figure 6.17 where an aminosilica is prepared through reaction with mono silane (according to a previously published method *[106]*) and then reacted with methylaziridine to form a 2°-2° diamine functionalized silica. As with the other N-substituted aziridines, methylaziridine only reacts with primary amines so the functionalization terminates after the diamine is formed.

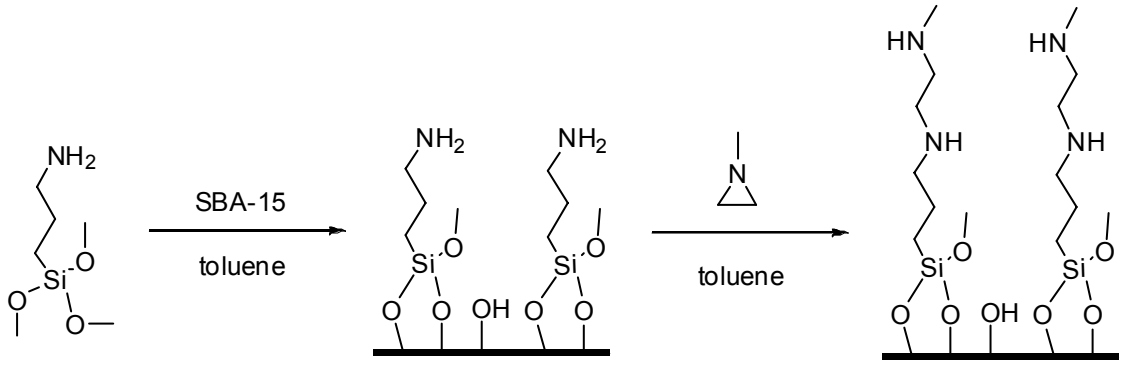

Figure 6.17. Reaction scheme for the synthesis of a 2°-2° diamine functionalized silica through the reaction of methylaziridine with an aminopropyl functionalized silica.

6.3.1. Synthesis of Methylaziridine

Methylaziridine was synthesized according to a procedure adapted from Smith, et al., with ~ 50% yield.*[160]* Figure 6.18 shows this reaction scheme, where the first step is the conversion of the alcohol in 2-(methylamino)ethanol to the chloro species at 0 °C. After purification by vacuum distillation at 150 °C, the solid residue was dissolved in strong base, closing the aziridinyl ring. Methylaziridine was then recovered by distillation. The vapor pressure of pure methylaziridine at room temperature is very high, as its boiling point is 25 °C. Thus, methylaziridine was stored in an equal weight of THF to solvate the molecule and reduce its vapor pressure. Formation of the methylaziridine product was verified by ^{1}H NMR (Figure 6.19). Interestingly, because the methyl group forces the aziridinyl nitrogen into an sp^3 hybridization, two sets of aziridinyl protons were observed at δ1.02 and 1.71 ppm, due to the differences in proximity of the aziridinyl protons above and below the aziridinyl plane to the protons of the methyl group.*[160]*

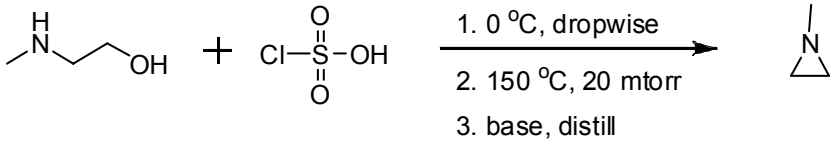

Figure 6.18. Reaction scheme for the synthesis of methylaziridine adapted from the strategy reported by Smith, et al.*[160]*

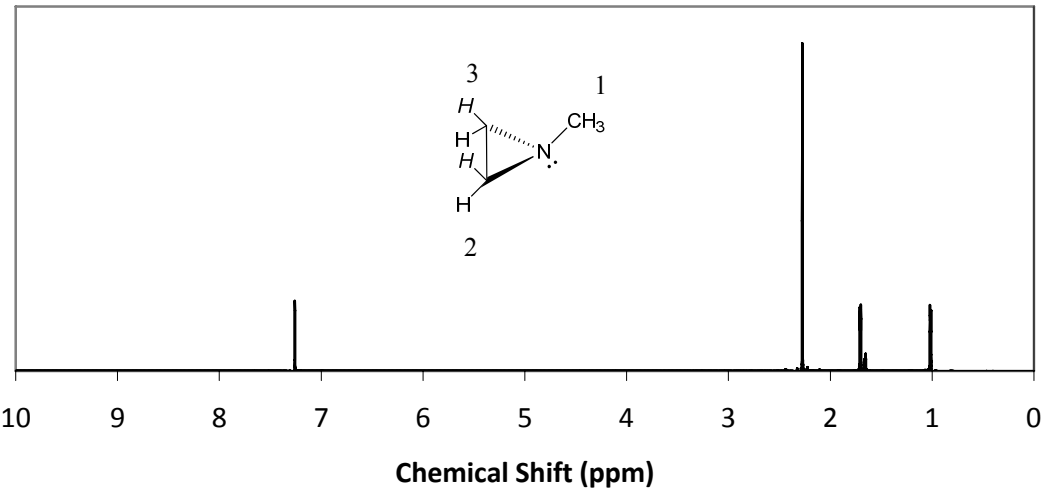

Figure 6.19. ^{1}H NMR spectrum of methylaziridine. Shifts at δ2.2, 1.7, and 1 ppm correspond to the protons at positions 1, 2, and 3, respectively.

6.3.2. Reaction of Methylaziridine with Unfunctionalized SBA-15

To provide a baseline for the functionalization of aminosilicas with methylaziridine and determine the reactivity of methylaziridine with silica silanol groups, excess methylaziridine was reacted with unfunctionalized mesoporous silica (non-pore-expanded SBA-15) (methazsilica, Scheme shown in Figure 6.20). Interestingly, the amine loading of the resulting aminosilica was 3.87 mmol N/g, which is quite high compared to the loading of 2.16 mmol N/g achieved through the corresponding silane chemistry to create 2° amine-functionalized silica (i.e., reaction with 3-(methylaminopropyl)trimethoxysilane) by Zelenak, et al.*[60]* Intuitively, the higher loading from reaction with methylaziridine could be explained by the realization that methylaziridine reacts with the silica surface through only one silanol group, while silanes typically react with at least two silanol groups.*[107]* Additionally, the size of the methylaminoethyl group is sufficiently small enough to not interfere with reaction at neighboring silanol groups. Thus, it is possible to synthesize aminosilicas with

moderately high amine loadings solely through reaction with N-alkylaziridines due to their substantial reactivity with silica silanol groups.

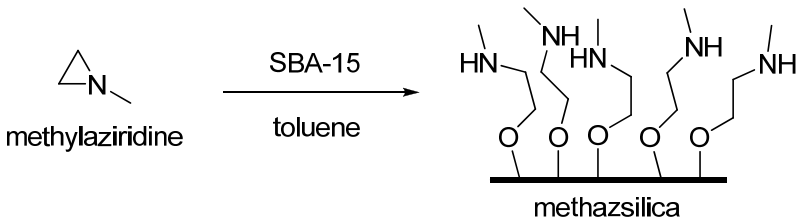

Figure 6.20. Reaction scheme for the functionalization of unfunctionalized SBA-15 with methylaziridine.

For verification of the addition of methylaminoethyl groups, IR and Raman spectra were measured for the methazsilica material (Figures 21 and 22, respectively). The appearance of transitions at 2820 cm^{-1} corresponding to C-H bonds in the terminal aminomethyl groups, along with intense CH_2 as N-CH_2 transitions at 1460 cm^{-1}, signified the addition of methylaminoethyl groups in methazsilica.

6.3.3. Synthesis of 2°-2° Diamine Materials Via Reaction with Methylaziridine

Two aminosilicas prepared by functionalization with mono silane and subsequently capped with HMDS (PEmono4cap and PEmono5cap), were used as parent materials for reaction with methylaziridine. Table 6.5 gives the amine loadings of two 2°-2° diamine materials prepared by reaction of methylaziridine with these parent aminosilicas. After reaction at a reactant ratio of 3.33 g methylaziridine/g PEmono5cap, the amine loading of the 2°-2° diamine material (mono_methaz1) increased from 1.64 to 2.45 mmol N/g SiO_2, corresponding to the conversion of 49% of the primary amines in the parent aminosilica.

In an attempt to increase this conversion, the PEmono4cap parent aminosilica was washed with a 1:1 NH_4OH:H_2O solution prior to reaction with methylaziridine to ensure

all of the primary amines were deprotonated. After reaction at a reactant ratio of 6 g methylaziridine/g PEmono4cap, the amine loading of the 2°-2° diamine material (mono_methaz2) increased from 1.51 to 3.56 mmol N/g. These results suggest that the ammonium hydroxide washing step created additional sites accessible to reaction with methylaziridine, because more than 100% conversion of the parent primary amines was observed. Since high amine loadings were achieved by the reaction of methylaziridine with silanol groups alone in the methazsilica material, it is very possible that in the mono_methaz2 material, methylaziridine reacted with primary amine and silanol sites. While it is clear that the aminosilica's amine content was drastically increased by reaction with methylaziridine, care must be taken to remove residual silanol groups through reaction with HMDS before methylaziridine treatment.

Table 6.5. Amine loadings of mono silane functionalized silicas before and after reaction with methylaziridine.

Sample	Silane Loading [a] (mmol silane/g SiO_2)	Amine Loading After Methylaziridine Reaction [b] (mmol N/g SiO_2)
PEmono5cap	1.64	n/a
mono_methaz1	1.64	2.45
PEmono4cap	1.51	n/a
mono_methaz2	1.51	3.56

[a] Calculated by a stoichiometric conversion of the weight loss determined by TGA.
[b] Calculated by subtracting the organic loading per weight of silica determined for the starting aminosilica from the total mass loss measured by TGA and then stoichiometrically converting the remaining mass loss per weight of silica by the molecular weight of methylaziridine. This amine loading was then added to the amine loading per weight of silica determined for the starting aminosilica (e.g. 1.64 mmol N/g SiO_2 in the case of the PEmono5cap material.

To verify this addition of methylaminoethyl groups, IR and Raman spectra of the PEmono5cap, mono_methaz1, PEmono4cap, PEmono4capwash (PEmono4cap after washing with 1:1 NH_4OH:H_2O), mono_methaz2, and methazsilica (see section 6.3.2) materials (Figures 6.21 and 6.22, respectively). The appearance of transitions at 2820 cm^{-1} corresponding to C-H bonds in the terminal aminomethyl groups, along with the

increases in intensity of the CH_2 as N-CH_2 transitions at 1460 cm^{-1}, signified the addition of methylaminoethyl groups in the mono_methaz1, and mono_methaz2 materials.

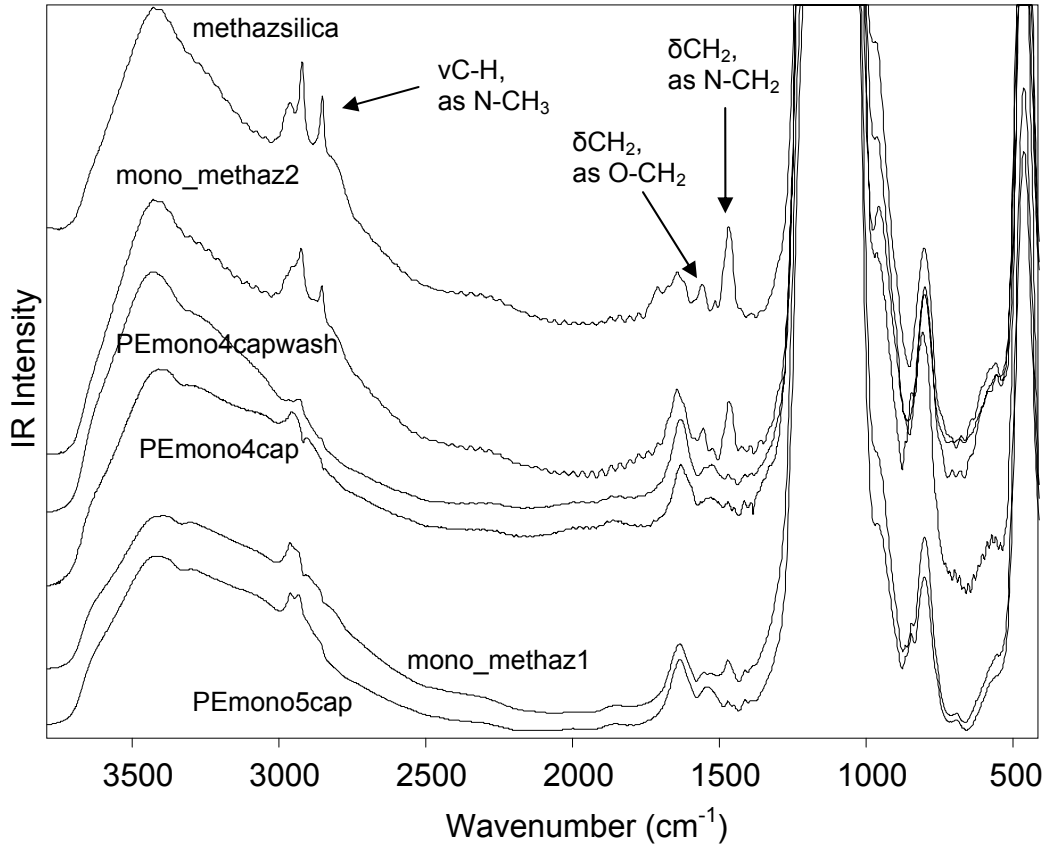

Figure 6.21. IR spectra of PEmono5cap, mono_methaz1, PEmono4cap, PEmono4capwash, mono_methaz2, and methazsilica (unfunctionalized SBA-15 reacted with methylaziridine).

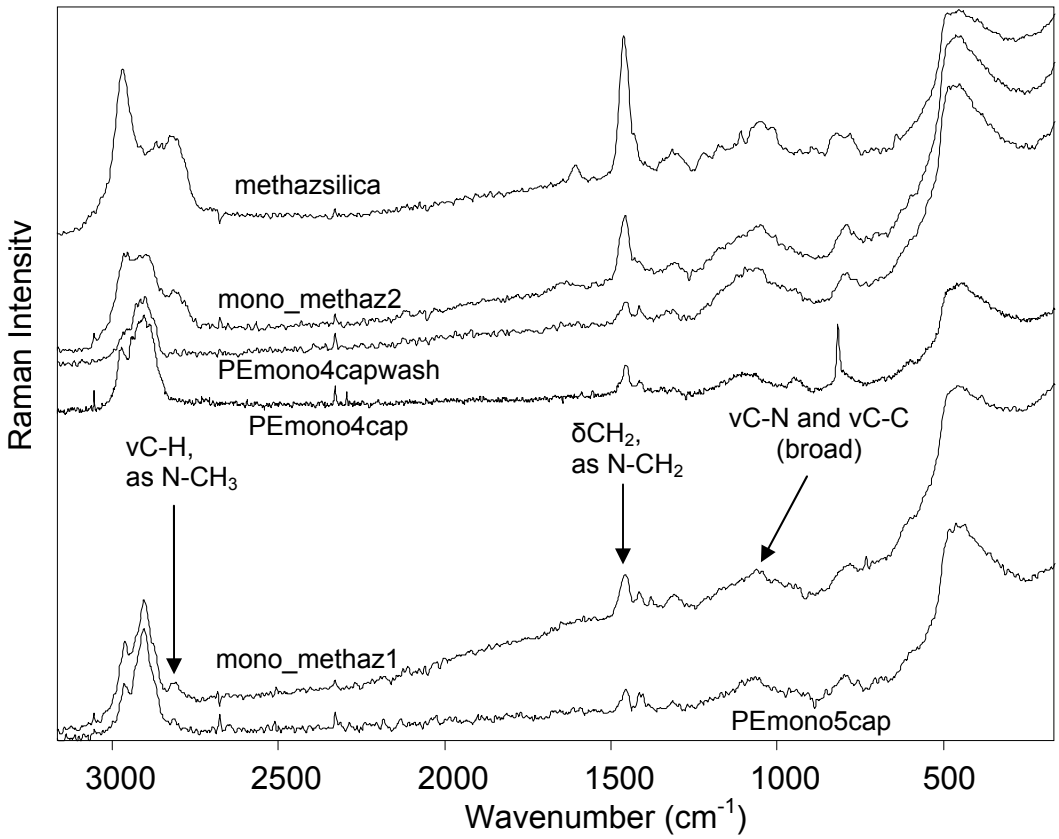

Figure 6.22. Raman spectra of PEmono5cap, mono_methaz1, PEmono4cap, PEmono4capwash, mono_methaz2, and methazsilica (unfunctionalized SBA-15 reacted with methylaziridine).

It was theorized that the washing the PEmono4cap material with a 1:1 NH_4OH:H_2O solution created additional (likely silanol) sites accessible to reaction with methylaziridine, resulting in an amine loading greater than that required to completely react with all of the 1° amines in the parent aminosilica. Theoretically, this additional functionalization with methylaziridine could occur on silanol sites possibly produced in the ammonium hydroxide washing step. In this case, some ring-opened methylaminoethyl groups would be attached to the silica surface through an Si-O-C bond series, similar to the groups in the methazsilica material (Figure 6.21). Although the assignment of CH_2 as O-CH_2 transitions is difficult in these types of materials, a tentative assignment can be made at 1560 cm^{-1}. Fitting with this hypothesis, this transition appears in the IR spectra

of methazsilica and mono_methaz2, but not in the parent aminosilica of mono_methaz2 or in the lower-loaded mono_methaz1 (Figure 6.21). Although this determination is tenuous at best, the reaction of methylaziridine with silica silanols is certainly a distinct possibility, and should be considered when preparing aminosilicas in this fashion.

The 2°-2° diamine structures of the mono_methaz1 and mono_methaz2 materials are unique from the perspective that similar materials cannot be prepared via silane chemistry (without modification of existing silanes) because no commercial 2°-2° diamine silanes exist. As described in the introduction to this chapter, adsorption experiments with these materials could provide important information on the intramolecular interactions of two amines during CO_2 capture. Comparing the heats of adsorption for 2°-2° diamine materials with those of 1°-2° diamine materials could elucidate whether intramolecular adsorption affects the heat of adsorption and whether the degree of the amine is important. Future adsorption experiments in this fashion with a Calvet calorimeter (Setaram, newly acquired by our group) should provide important fundamental information on the affinities of these materials for CO_2.

6.3.4. Reaction with Protected-aziridines as a Tool for Adsorbent Tailoring

Unfortunately, the step-wise polymerization of LPEI from a protection/deprotection strategy involving alkylcarboxylate-protected aziridines ultimately failed because of the inability to deprotect the terminal amine after ring-opening. Exploration of this strategy was abandoned for the more straightforward incremental functionalization with N-substituted aziridines. While not a polymerization, this method was shown to substantially increase the amine loading of aminosilicas prepared through silane grafting, adding methylaminoethyl groups to each primary amine termini.

The largest amine content among commercial silanes is three amines per molecule for the 3-[2-(2-aminoethyl)aminoethyl]aminopropyltrimethoxysilane. However, reaction with methylaziridine can be used as a tool to increase the amine content of each silane moiety attached to the silica surface, effectively increasing a triamine silane to a tetramine silane, the important difference being the conversion of a moiety containing one 1° and two 2° amines to a moiety containing four 2° amines (Figure 6.23). While this difference may have consequences on adsorbent stability, the increased amine loading should result in a substantial increase in adsorption capacity (theoretically, 25% increase for the triamine and 50% for the monoamine). Indeed, initial experiments were done on two tri silane functionalized silicas to show a proof of concept. Table 6.6 shows that the amine loading of an aminosilica prepared by tri silane functionalization (tri) was increased from 4.53 to 6.41 mmol N/g SiO_2 by reaction with methylaziridine in toluene (tri_methaz). Similarly, the amine loading of an aminosilica prepared by water-aided functionalization by tri silane according to methods reported by Sayari, et al. (tri_wa), was increased from 10.75 to 13.27 mmol N/g SiO_2 by reaction with methylaziridine in toluene (tri_wa_methaz). While the amine loading of the tri_wa_methaz material was not increased by the theoretical 25%, a substantial increase of 2.52 mmol N/g SiO_2 was still achieved. The less than theoretical loading may be due to inaccessibility of terminal primary amines created through the water-aided grafting process.*[71]* Future work will have to confirm that these increases in adsorbent amine loading result in increases in adsorption capacity.

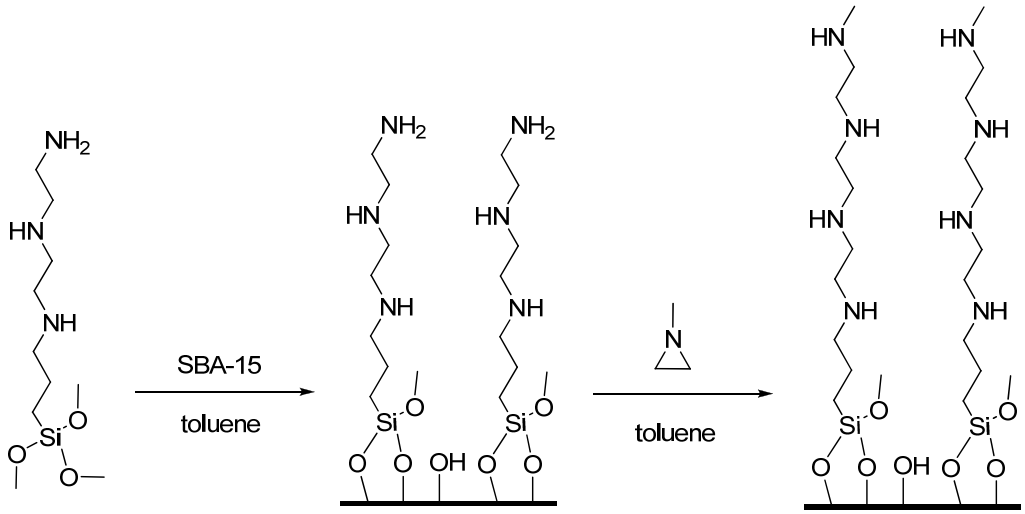

Figure 6.23. Reaction scheme for the modification of a tri silane functionalized silica with methylaziridine to prepare a tetraamine-functionalized silica.

Table 6.6. Amine loadings of tri silane functionalized silicas before and after reaction with methylaziridine.

Sample	Silane Loading [c] (mmol silane/g SiO_2)	Amine Loading from Silane [c] (mmol N/g SiO_2)	Amine Loading After Methylaziridine Reaction [d] (mmol N/g SiO_2)
tri [a]	1.51	4.53	4.53
tri_methaz [b]	1.51	4.53	6.41
tri_wa	3.58	10.75	10.75
tri_wa_methaz	3.58	10.75	13.27

[a] Aminosilica prepared by reaction of tri silane with SBA-15 in the absence of water.
[b] Aminosilica prepared by reaction of tri silane with PE SBA-15 in the presence of 0.3 mL H_2O/ g PESBA.
[c] Calculated by a stoichiometric conversion of the weight loss determined by TGA.
[d] Calculated by subtracting the organic loading per weight of silica determined for the starting aminosilica from the total mass loss measured by TGA and then stoichiometrically converting the remaining mass loss per weight of silica by the molecular weight of methylaziridine. This amine loading was then added to the amine loading per weight of silica determined for the starting aminosilica (e.g. 4.53 mmol N/g SiO_2 in the case of the tri material.

To verify the addition of methylaminoethyl groups after reaction with methylaziridine, IR and Raman spectra were measured for the tri, tri_methaz, tri_wa, and tri_wa_methaz materials (Figures 6.24 and 6.25, respectively). The appearance of transitions at 2820 cm^{-1} corresponding to C-H bonds in the terminal aminomethyl groups, along with the increases in intensity of the N-H and CH_2 as N-CH_2 transitions at 1660

and 1460 cm^{-1}, respectively, signified the addition of methylaminoethyl groups in these materials.

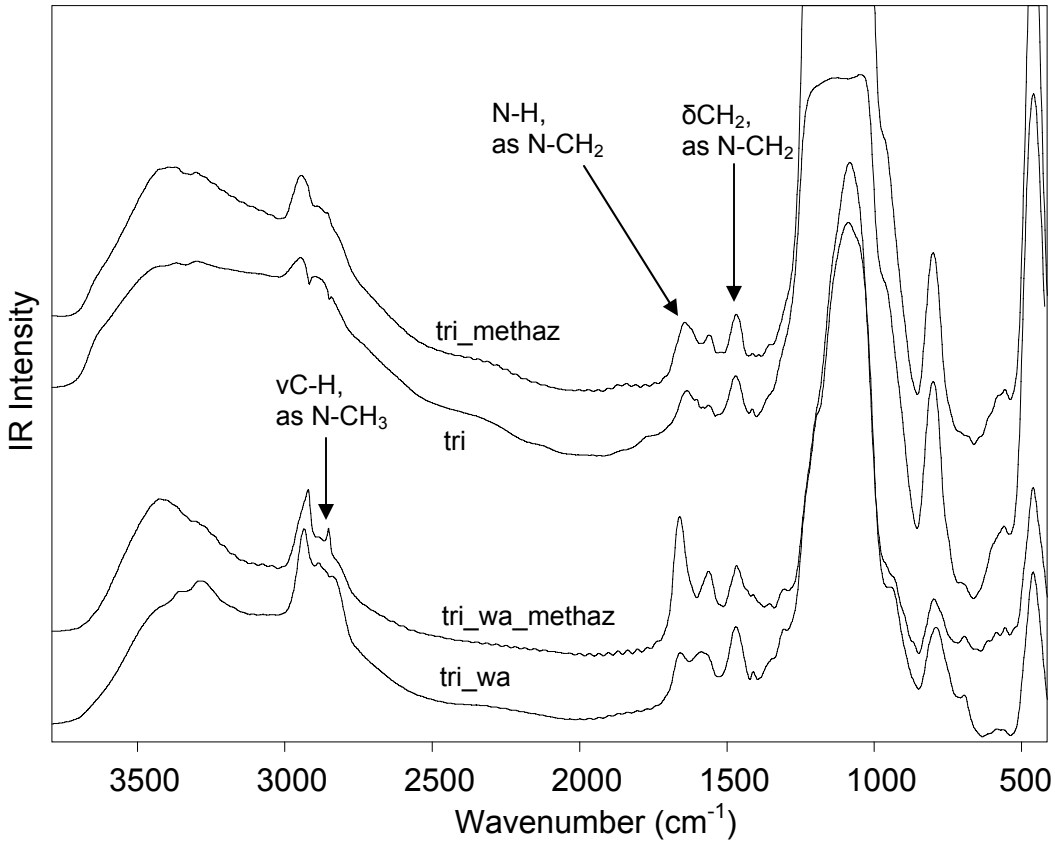

Figure 6.24. IR spectra of tri_wa, tri_wa_methaz, tri, and tri_methaz,.

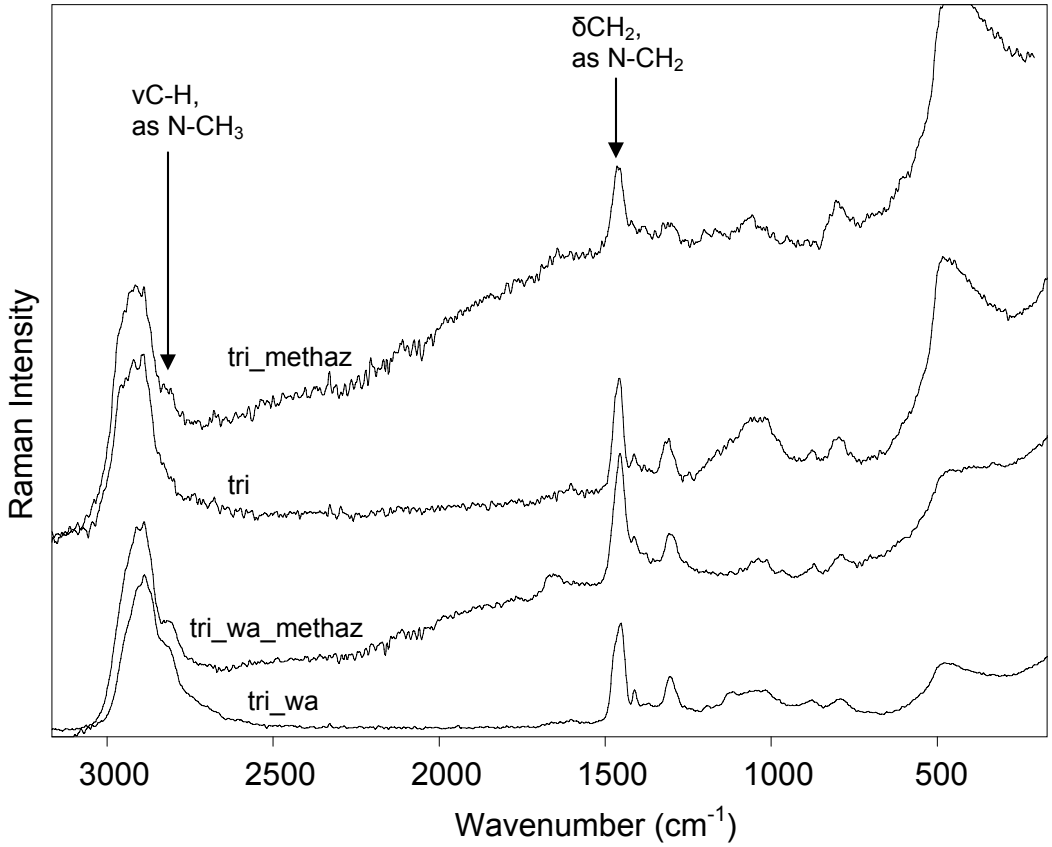

Figure 6.25. Raman spectra of tri_wa, tri_wa_methaz, tri, and tri_methaz.

6.4. Conclusion

In this chapter, the potential use of several N-substituted-aziridines for the synthesis of linear aminosilicas was explored. In parallel, benzylcarboxylate, methylcarboxylate, and ethylcarboxylate-protected aziridines were synthesized according to various methods adapted from literature. Experimental challenges were encountered in the purification of benzylcarboxylate-protected aziridine, so focus was shifted to the exploration of the methylcarboxylate and ethylcarboxylate-protected aziridines due to time constraints. Through trial and error, the proper conditions for the step-wise reaction of mono silane functionalized silica with both methylcarboxylate- and ethylcarboxylate-protected aziridines were determined. However, deprotection of the alkylcarboxylate

groups via acid cleavage were largely unsuccessful. Spectroscopic investigation revealed the formation of insoluble deprotection products associated with the CF_3 group of the trifluoroacetate ion. It was discovered that these insoluble products could be removed by applying solvent washing steps, but still no successful acidic cleavage conditions were found that resulted in complete deprotection of the alkylcarboxylate groups. Spectroscopic investigation confirmed this incomplete deproctection.

While exploration of N-alkylcarboxylate-protected aziridines did not result in the successful preparation of linear aminosilicas, investigation in tandem of N-methylaziridine resulted in the successful preparation of three types of linear aminosilicas. Methylaziridine was reacted with unfunctionalized mesoporous silica to functionalize the silica surface with methylaminoethyl groups. Methylaziridine had a strong affinity for the silica surface silanols, as amine loadings 79% higher than experienced via the corresponding silane chemistry were achieved in this material.

The second type of aminosilica was prepared through the reaction of methylaziridine with mono silane functionalized silica to create 2°-2° diamine aminosilicas. These materials are interesting from the perspective of fundamental investigation of the role and strength of dual-site adsorption in aminosilica CO_2 adsorbents. Future adsorption and calorimetry experiments with these 2°-2° diamine aminosilicas could elucidate the effect of dual-site adsorption on the heats of adsorption of specific amine types.

The third application of methylaziridine was the incremental increase in amine loading of two tri silane functionalized silicas. These experiments highlight the role of methylaziridine as an aminosilica adsorbent tailoring agent, where theoretically, the amine loading of any 1° amine-containing adsorbent can be increased by the conversion of each 1° amine to two 2° amines. Future experiments should confirm that this increase in amine loading results in a corresponding increase in adsorption capacity.

6.5. Experimental

All chemicals were purchased from Sigma-Aldrich and used without modification. Single component gases were purchased from Airgas, Inc. Custom gas mixtures were purchased from Matheson Tri-Gas, Inc.

6.5.1. SBA-15 Synthesis

Mesoporous SBA-15 was synthesized similar to previously reported methods.*[106-108]* In a typical synthesis, 17.9 g Pluronic 123 (EO-PO-EO block copolymer), 99.4 g HCl, and 561 g H_2O were stirred overnight in a 1 L Erlenmeyer flask. To the micellular solution, 39.6 g TEOS was added and stirred for 5 minutes. The solution was transferred to an oven and stirred at 35 ºC for 20 h. Stirring was then terminated and the solution was post-treated at 80 ºC for 24 h. The white solid was filtered and washed with copious amounts of DI H_2O and dried overnight at 75 ºC. The organic template was removed by calcination using the following temperature program: (1) ramping the temperature to 200 ºC at a rate of 1.2 ºC $min.^{-1}$, (2) holding at 200 ºC for 1 h., (3) ramping the temperature to 550 ºC at a rate of 1.2 ºC $min.^{-1}$, (4) holding at 550 ºC for 6 h. The calcined SBA-15 was then dried at 200 ºC under vacuum overnight.

6.5.2. Pore-expanded SBA-15 Synthesis

The synthesis of mesoporous PE SBA-15 was adapted from a previously reported method. In a typical synthesis, 13.2 g Pluronic 123 (EO-PO-EO block copolymer), 79.4 g HCl, and 343.7 g DI H_2O were stirred in a 1 L Erlenmeyer flask at room temperature. After 5 min, 13.2 g TMB was added to the solution as a swelling agent. After an hour of stirring, 28.3 g TEOS was added to the micellular solution and stirred for another 5 minutes. The solution was transferred to a sealed autoclave and stirred at 35 ºC for 24 h. Stirring was then terminated and the solution was post-treated at the desired temperature (100, 110, or 120 ºC) for 72 h. The white solid was filtered, washed with copious

amounts of DI H_2O, and dried overnight at 75 ºC. The organic template was removed by calcination in air using the following temperature program: (1) ramping the temperature to 200 ºC at a rate of 1.2 ºC $min.^{-1}$, (2) holding at 200 ºC for 1 h., (3) ramping the temperature to 550 ºC at a rate of 1.2 ºC $min.^{-1}$, (4) holding at 550 ºC for 6 h. The calcined SBA-15 was then dried at 200 ºC under vacuum overnight.

6.5.3. Aziridine Synthesis

Aziridine was synthesized and purified similar to reported methods.*[26, 87]* In a typical synthesis, 34.5 g 2-chloroethylamine hydrochloride was added to a solution of 34.1 g KOH in 200 g DI H_2O. The solution was stirred at 50 ºC for 2 h. Aziridine was then distilled from solution under a partial static vacuum of 530 mm Hg and collected in a cold trap. The collection flask was sealed and then stored at 0 ºC. ^{1}H NMR (400 MHz, D_2O, δ): 1.56 (s); ^{13}C NMR (400 MHz, CD_2Cl_2, δ): 18.1. Aziridine is toxic if swallowed, inhaled, or absorbed through the skin. *Caution: Aziridine is a carcinogen and reproductive hazard. Use extreme caution when handling aziridine. Only handle aziridine in a ventilated fume hood and always wear proper personal protection equipment.*

6.5.4. Synthesis of Cbz-aziridine

The synthesis of Cbz-protected aziridine was adapted from a previously published method.*[155]* In a typical synthesis, 8.1 g benzyl *N*-(2-hydroxyethyl)carbamate (commonly, N-Z-ethanolamine), 25.3 g pyridine, and 6.1 g tosyl chloride were added to a 250 mL flask and stirred at 0 °C for 2 h. The tosylated compound was precipitated by addition of ~400 mL of ice water, and recovered by extraction with three 200 mL portions of diethyl ether. The ether was then removed in vacuo, and the tosylated compound was recrystallized from acetone and then methanol. Under a N_2 atmosphere, 4.9 g of the recrystallized tosylated intermediate was dissolved in 12.3 g THF and added

dropwise over a 2 hour period to a solution of 1.91 g NaH (60 wt% in mineral oil) in 52 g THF at 45 ºC. The crude product was recovered after filtering through a column of celite and removal of solvent in vacuo.

6.5.5. Synthesis of Alkylcarboxylate-protected Aziridine

The synthesis of alkylcarboxylate-protected aziridine was based on aziridine derivatizations published by Deyrup on a common them.*[156]* In a typical synthesis, 185 mmol of alkylchloroformate (20 g in the case of ethylchloroformate) was dissolved in 125 g benzene and a solution of 8.9 g aziridine, 24.1 g triethylamine, and 50 g benzene was added dropwise at 0 ºC. After stirring for 30 min., the white triethylammonium chloride salt was removed by filtration and washed with 30 mL of benzene. The alkylcarboxylate-protected aziridine was recovered from the filtrate after removal of solvent and unreacted aziridine in vacuo.

6.5.6. Synthesis of Methylaziridine

The synthesis of methylaziridine was adapted from a procedure adapted from Smith, et al.*[160]* In a typical reaction, 17.4 g chlorosulfonic acid was added dropwise at 0 ºC to a 250 mL flask containing 11.2 g 2-(methylamino)ethanol while stirring. The dark-brown viscous mixture was heated at 145 ºC for 2 h in vacuo. This residue was dissolved in a solution of 40 g KOH in 40 mL DI H_2O. Methylaziridine was recovered from this mixture by distillation at 100 ºC.

6.5.7. Reaction of Solids with Methylaziridine

The particular reaction conditions of solids with methylaziridine are described in the text for each specific material where appropriate. In a general reaction, a small amount of solid (< 1 g) was dispersed in toluene in a 75 mL glass pressure vessel. An excess amount of methylaziridine was added, the vessel was capped, and the mixture was stirred at moderate temperature (50-75 ºC) overnight. The solid was recovered by

filtration, washed with copious toluene, methanol and hexanes, and dried at 75 ºC in vacuo.

6.5.8. Characterization

Amine loadings were determined by TGA using a Netzsch STA409. Total organic loading was estimated as the weight loss from 160 to 760 °C. Molar loadings were then calculated by stoichiometric conversion. FT-IR spectroscopy using KBr pellets and FT-Raman spectroscopy were obtained on a Bruker Vertex 80v optical bench with a RAMII Raman module. ^{1}H solution NMR experiments were conducted on a Varian Mercury Vx 400.

CHAPTER 7

SUMMARY

Initial work by our research group resulted in the synthesis of a new aminosilica by the ring-opening polymerization of aziridine from an SBA-15 mesoporous silica support.*[26]* The large obtainable amine loading in this HAS material made it an attractive candidate for CO_2 adsorption from dilute sources where membrane separation and other technologies are inefficient. The capability of the HAS material for CO_2 adsorption was demonstrated in our first publication on the subject in JACS.*[26]* The main goal of this thesis was to develop an understanding of the role of HAS adsorbent composition and structure on adsorptive performance, and apply this knowledge towards improving performance through molecular design of the adsorbent.

The first stage of this understanding was accomplished through the publication of a review of the solid CO_2 adsorbent literature, focusing on the relationships between composition/structure and adsorptive performance. With this knowledge as a framework, the limitations of the HAS adsorbent were found by creating a set of adsorbents with different amine loadings by changing the aziridine to silica reactant ratio.*[86]* It was discovered that at high amine loadings, the aziridine polymerization blocks the pore openings, creating inaccessible adsorption sites and retarding the mass transfer of gas through the pores. While still maintaining some of the largest observed CO_2 capacities in the literature, these highly loaded HAS materials suffered from reduced amine efficiencies and retarded adsorption kinetics. In an attempt to relieve this limitation, the use of several different pore-expanded mesoporous silicas as supports for the aziridine polymerization was investigated. Unfortunately, it was determined that the polymerizations in these materials terminated well before filling the pore spaces,

resulting in adsorbents with only moderate amine loadings. Furthermore, it was determined that when normalized by amine loading, the adsorption kinetics of these PEHAS materials were fairly universal and were similar to non-pore-expanded HAS materials with low to moderate amine loadings.

The application of the HAS adsorbent to capturing CO_2 from ambient air was also investigated. The large heat of adsorption for the amine-CO_2 interaction affords aminosilicas a unique advantage at these ultra-low CO_2 concentrations, because of their capacities' sharp dependence on CO_2 partial pressure at or near the Henry's Law regime. Indeed, in both humid and dry conditions, the HAS adsorbent was found to have a surprisingly large CO_2 capacity in light of the 250-fold reduction in CO_2 partial pressure from 10% CO_2 (flue gas application) to 400 ppm CO_2 (air capture application).

Finally, a series of experiments with N-substituted-aziridines were conducted in an attempt to impose molecular-level control on adsorbent amine density through the step-wise polymerization of LPEI by a protection/deprotection strategy. Experimental difficulties in the synthesis and purification of N-alkylcarboxylate-protected aziridines, as well as the inability to completely deprotect the amine after ring-opening, led to the abandonment of the step-wise polymerization strategy. An alternative method to controllably increase adsorbent amine loading was demonstrated by the functionalization of existing aminosilicas with methylaziridine. This "one-time" treatment reacts with existing primary amines or silanol groups to incrementally form a linear growth of methylaminoethyl groups. Hopefully, the future application of methylaziridine functionalization will lead to the increased control of adsorbent amine loadings and their associated adsorption capacities.

APPENDIX A

CHAPTER 3 SUPPLEMENTARY INFORMATION

A.1. Characterization of HAS: IR Spectroscopy

IR spectra of the HAS-VLAS were measured by the KBr method and compared to the spectrum of unmodified SBA-15 (Figure A.1). Generally, the relative signals at 2960, 2850, 1570, 1480, and 1410 cm^{-1} increased as the amine loading of the HAS material increased. These signals correspond to aliphatic amines and the formation of CO_2 – amine adducts. This information is expected, as the organic loading increases due to the aziridine polymerization and the materials were stored under atmospheric conditions.

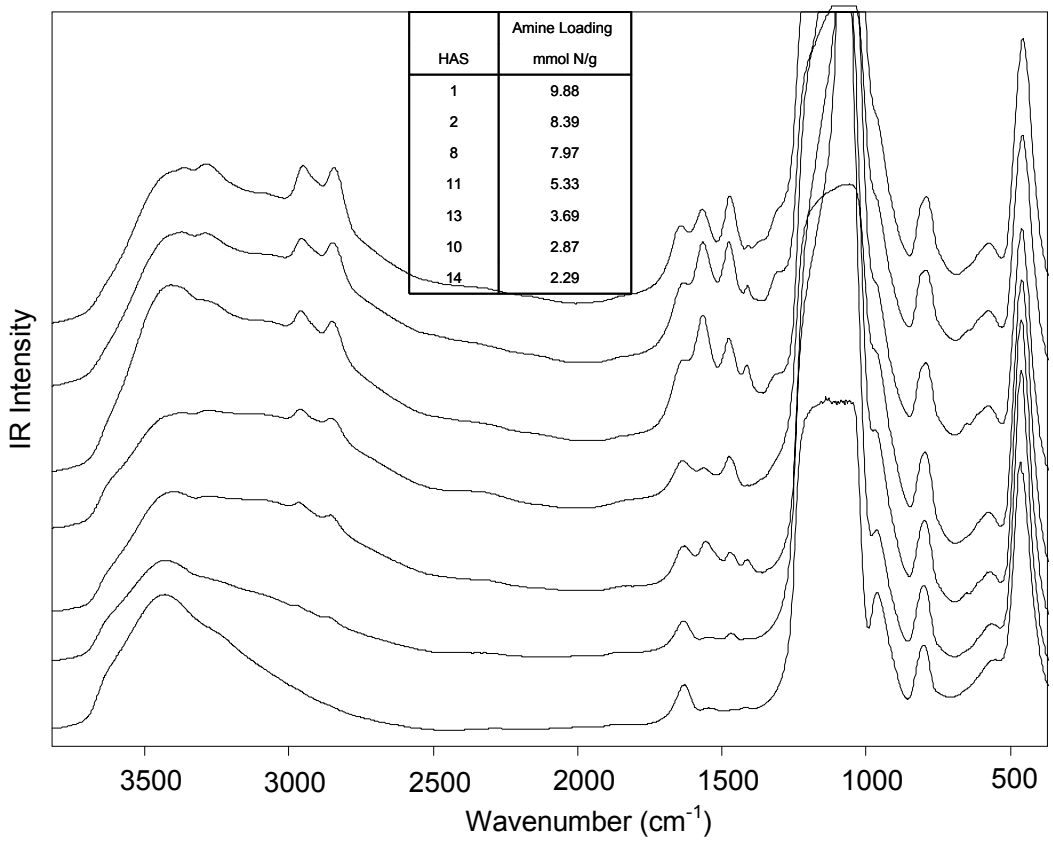

Figure A.1. IR spectra of the HAS-VLAS and unfunctionalized SBA-15.

A.2. Characterization of HAS: Inversely-Gated ^{13}C NMR

A ^{13}C NMR spectrum of commercial low molecular weight PEI is shown in Figure A.2 and definitions of the eight unique carbon environments are given in Figure A.3. The peaks, designated 1 through 8, appear at 57.5, 54.5, 52.5, 52, 49, 47, 41 and 39 ppm respectively.*[109]* The ratio of 1°:2°:3° amines is based on the summation of peak integrations given by.*[38]*

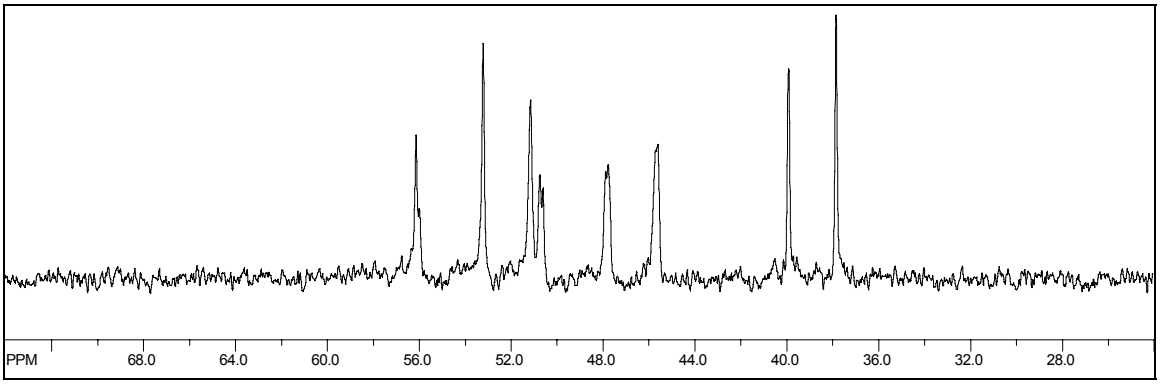

Figure A.2. Inversely-gated ^{13}C NMR spectrum of commercial low molecular weight PEI.

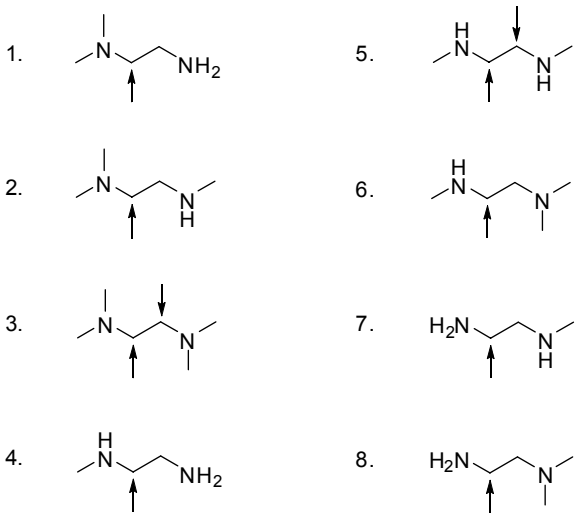

Figure A.3. Definitions of the eight different carbon environments in PEI.

Equation A.1. Formula for amine ratio determination.

$$1° : 2° : 3° = (A_7 + A_8) : \frac{(A_4 + A_5 + A_6)}{2} : \frac{(A_1 + A_2 + A_3)}{3}$$

A.3. Adsorption Capacity Calculations

In a previous work,*[26]* CO_2 capacities were calculated from the detection of the first CO_2 signal until the end of the 200 minute experiment. This process is depicted in Figure A.4, where the step signal marks the detection of the first CO_2 signal, the blank area between the curves represents the subtracted background due to dilution effects, and the shaded area represents the calculated capacity. This method assumes that all adsorbents will have the same breakthrough time (time from the introduction of test gas until the detection of CO_2). However, as the amine loadings of adsorbents are varied, and thus their CO_2 capacities, it is likely that breakthrough times will also change. To account for this change, CO_2 capacities were calculated from the time-point that the inlet valve was switched from the inert purge gas to the test gas. Backgrounds with inert sample were also measured using this method and subtracted from each run to account for dilution effects caused by the switching of gas flows. This process is depicted in Figure A.5, where the step signal marks the introduction of test gas, the blank area between the curves represents the subtracted background due to dilution effects, and the shaded area represents the calculated capacity.

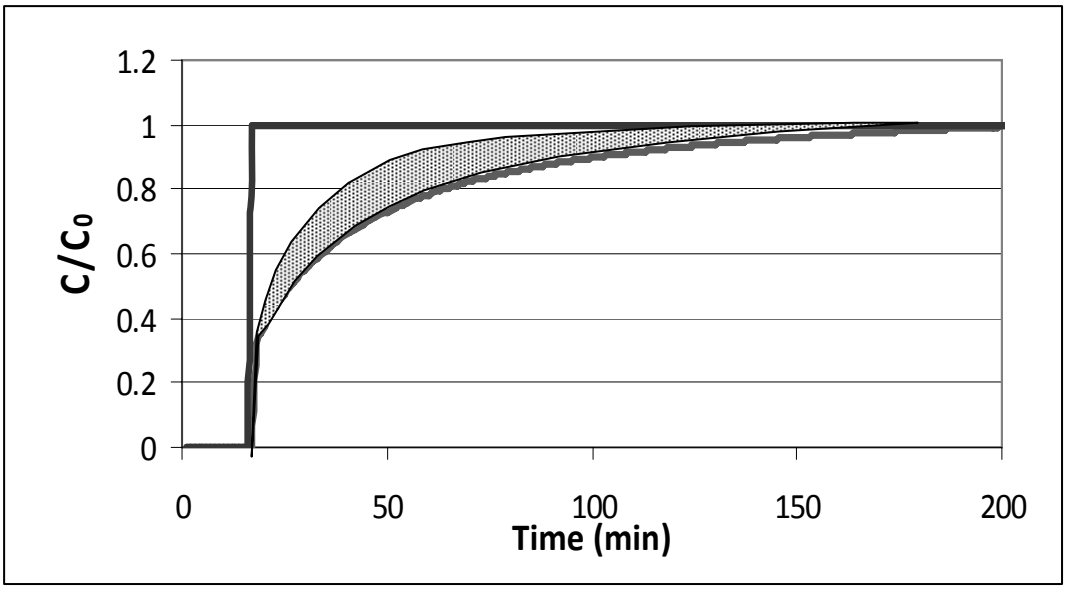

Figure A.4. Calculation of CO_2 capacity from the detection of first CO_2 signal.

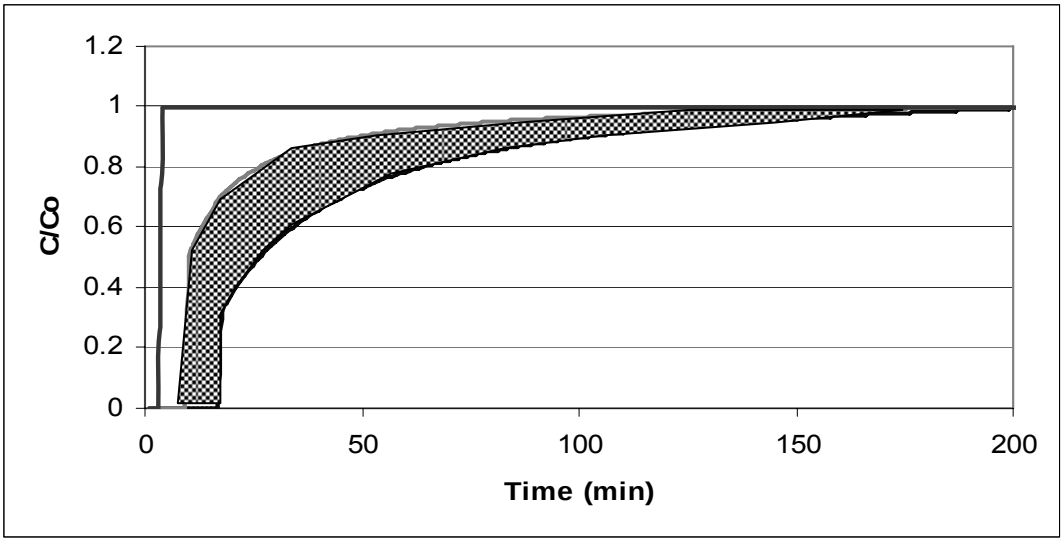

Figure A.5. Calculation of CO_2 capacity from the introduction of test gas.

A.4. Adsorption Kinetics Uptake Plots

The adsorption kinetics of the HAS-VLAS at 25 and 75 ºC are shown in the form of uptake plots in Figures A.6 and A.7, respectively.

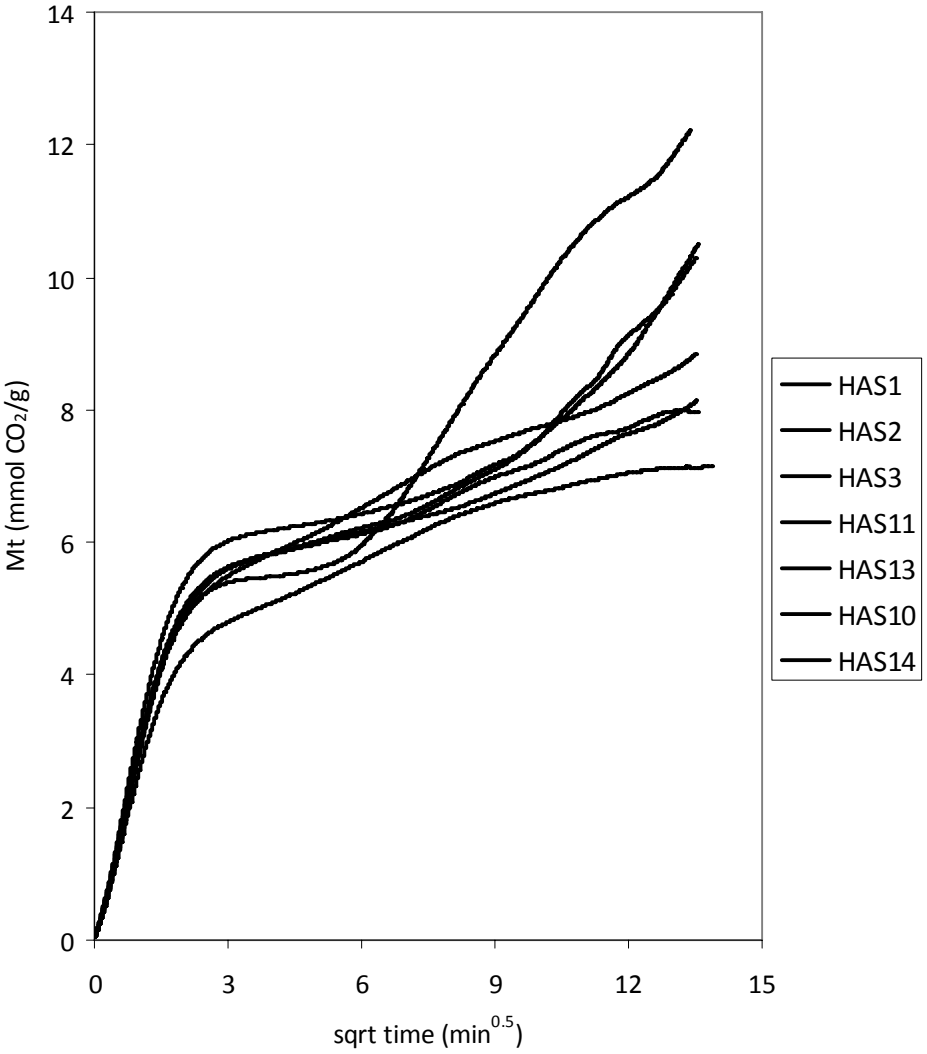

Figure A.6. Uptake plot of HAS materials set at 22 ºC. Curves are ordered according to legend: top to bottom.

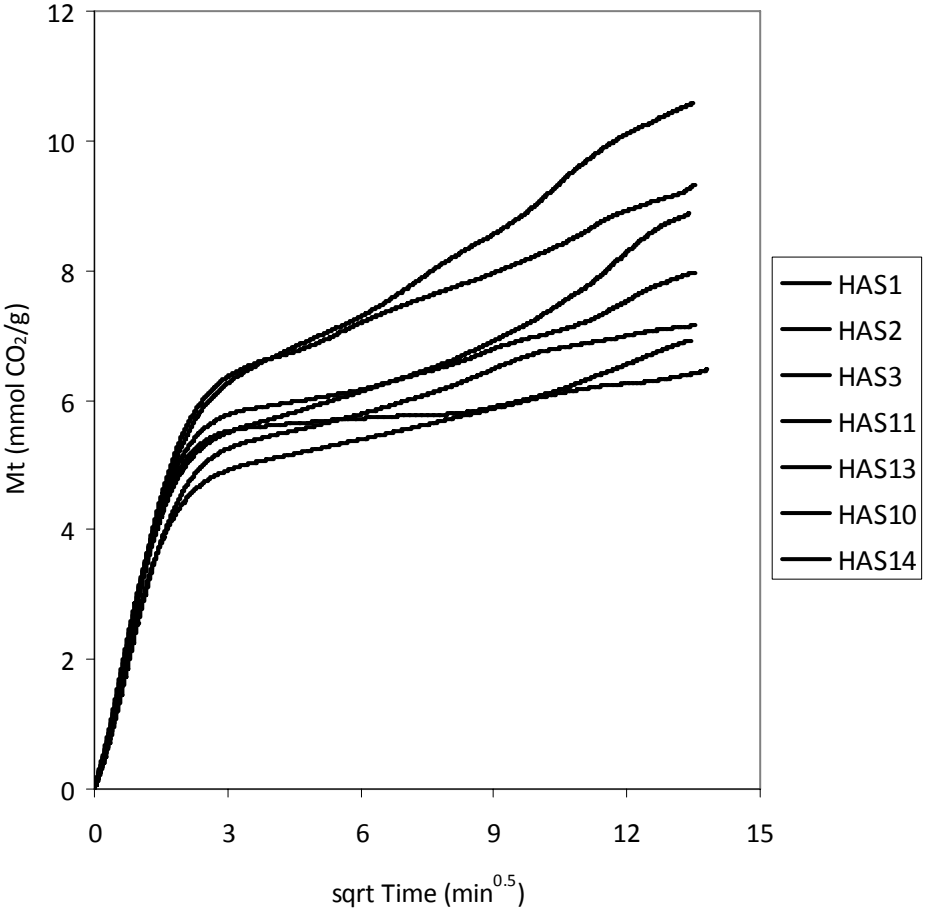

Figure A.7. Uptake plots of HAS material set at 75 ºC. Curves are ordered according to legend: top to bottom.

A.5. N_2 Adsorption Isotherms of the HAS-VLAS at 77 K

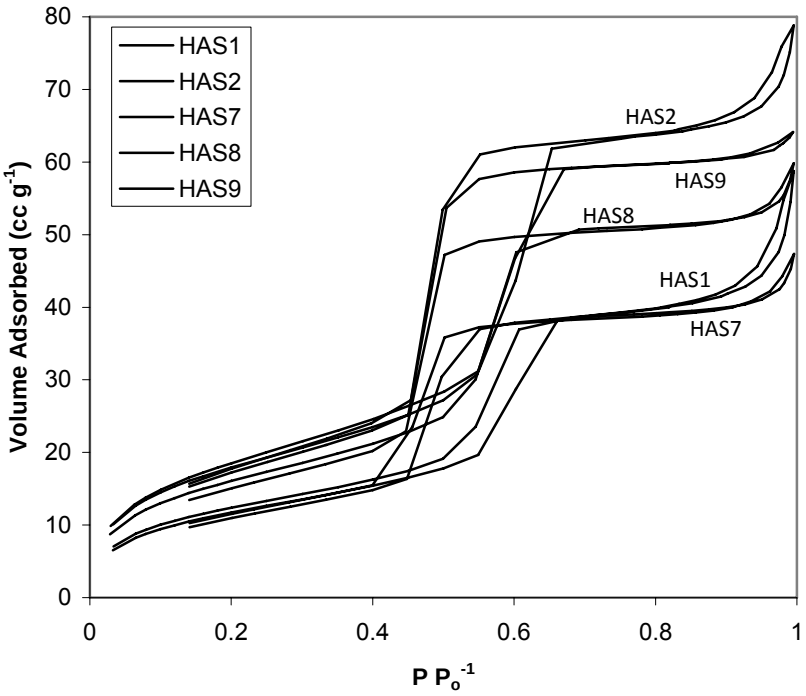

Figure A.8. N_2 adsorption isotherms at 77 K for several HAS adsorbents.

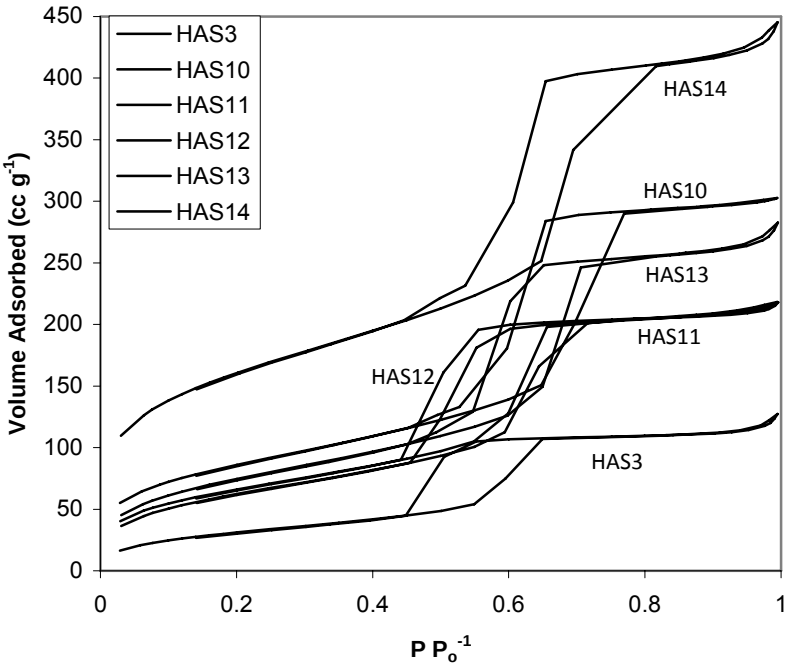

Figure A.9. N_2 adsorption isotherms at 77 K for several HAS adsorbents.

A.6. Calibration Curve for Determination of Aminopolymer Molecular Weight by ASEC

A calibration curve (Figure A.10) for the molecular weights of HAS aminopolymers was assembled from the measured retention times of several commercial PEI samples (Table A.1).

Table A.1. Average molecular weights and retention times of five commercial PEI samples.

Standard	Avg. Mw [Daltons]	Retention Time [min]
PEIST1	600	43.76
PEIST2	1200	43.58
PEIST3	1600	43.25
PEIST4	1800	43.12
PEIST5	10000	40.41

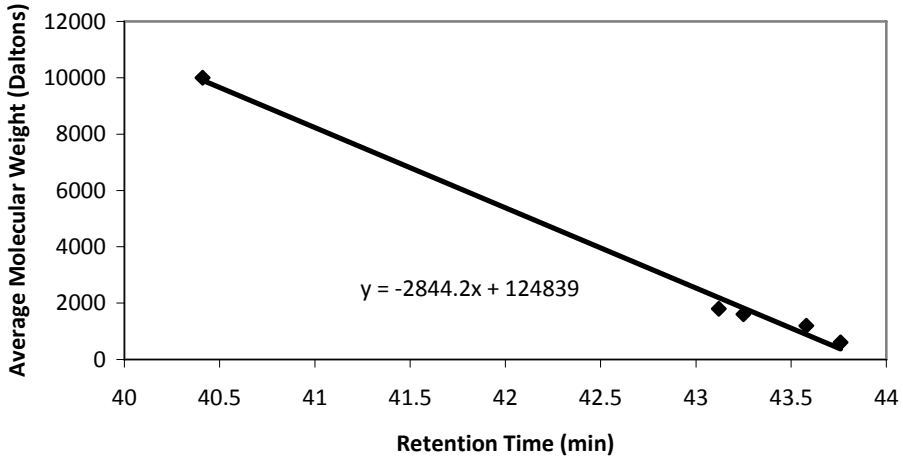

Figure A.10. Calibration curve for aminpolymer molecular weight.

A.7. Scanning Electron Microscopy (SEM) of HAS Adsorbents with High Amine Loadings

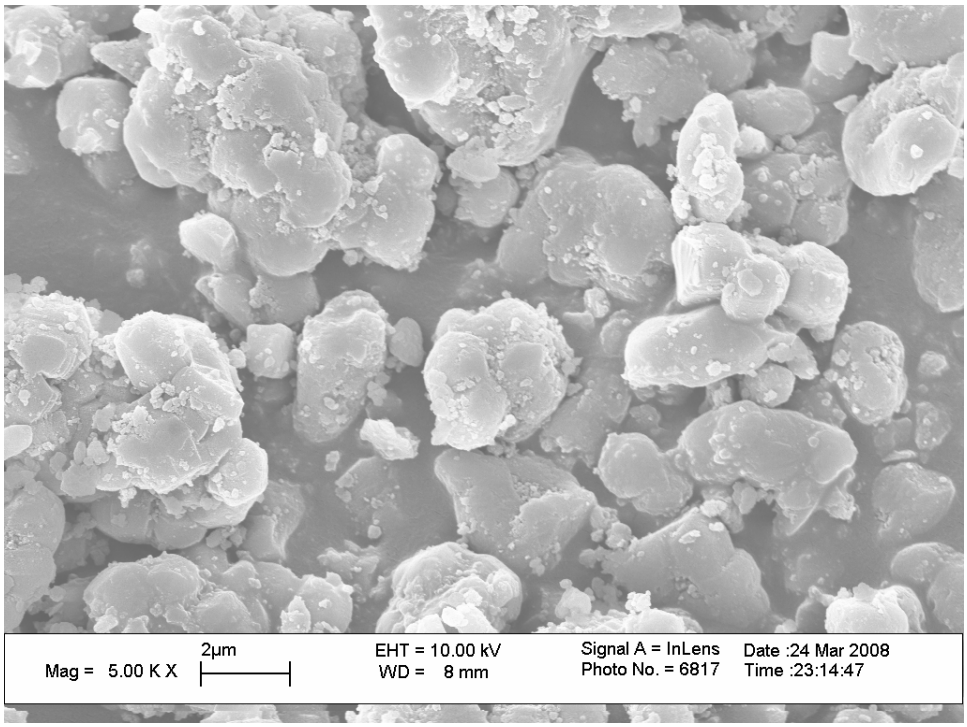

Figure A.11. SEM image of HAS1.

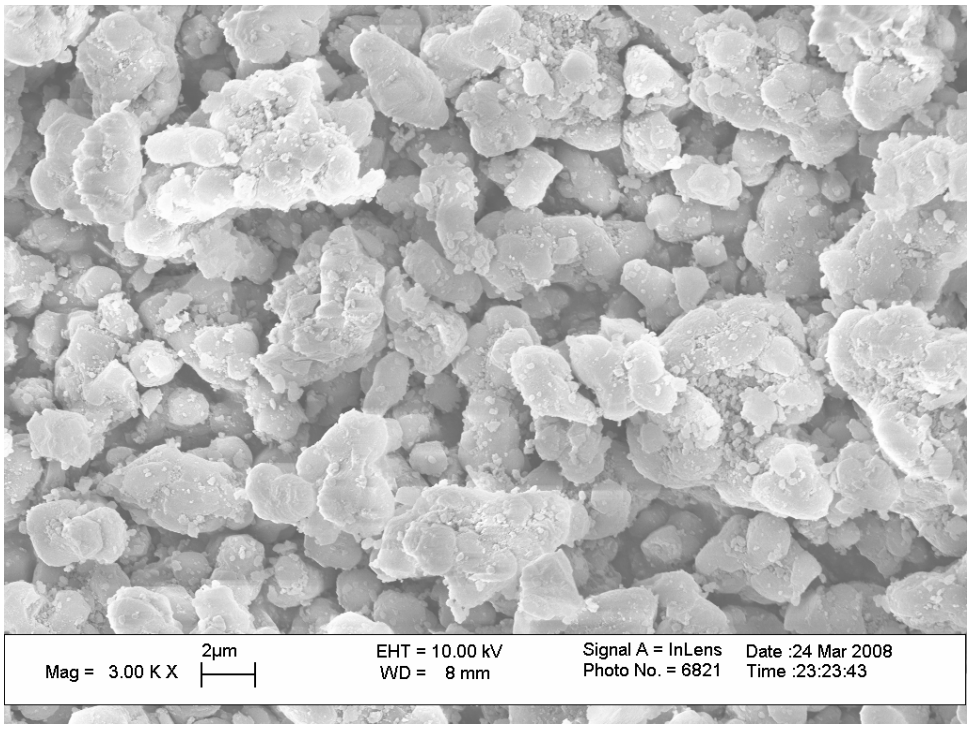

Figure A.12. SEM image of HAS2.

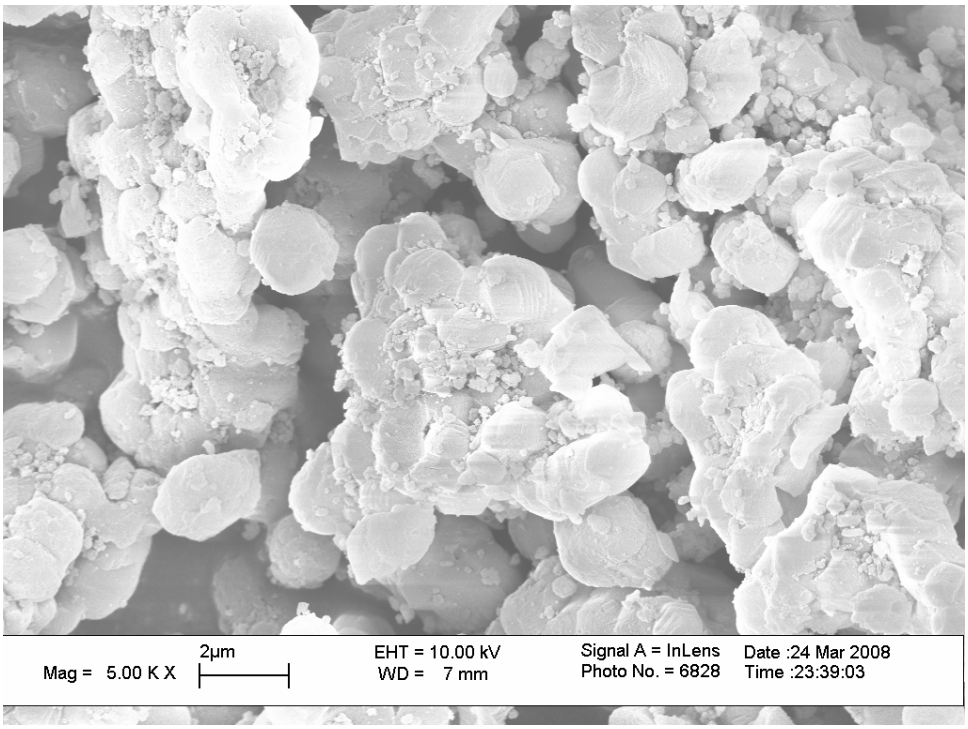

Figure A.13. SEM image of HAS3.

APPENDIX B

CHAPTER 4 SUPPLEMENTARY INFORMATION

B.1. N_2 Physisorption Isotherms

Figures B.1 through B.5 show the N_2 physisorption isotherms measured at 77 K for each unfunctionalized pore-expanded support and the PEHAS materials synthesized with the respective silica support.

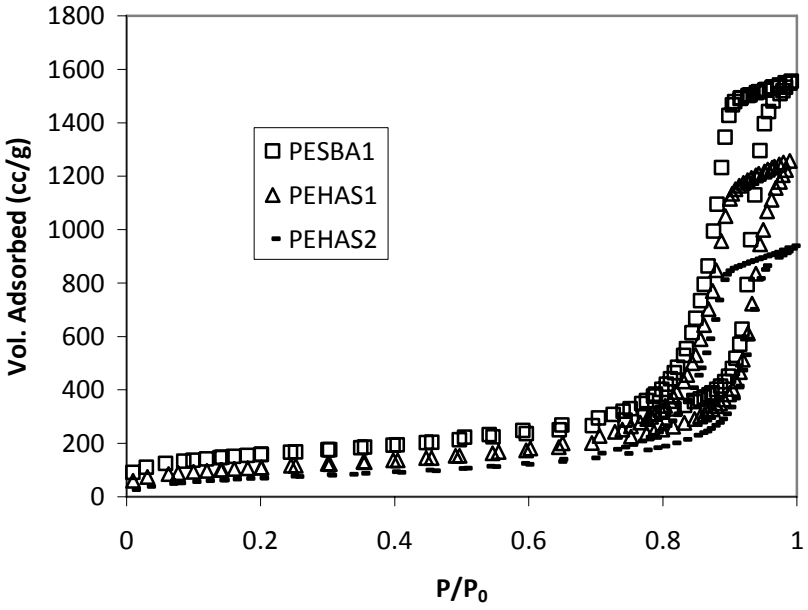

Figure B.1. N_2 physisorption isotherms at 77 K for PESBA1, PEHAS1, and PEHAS2.

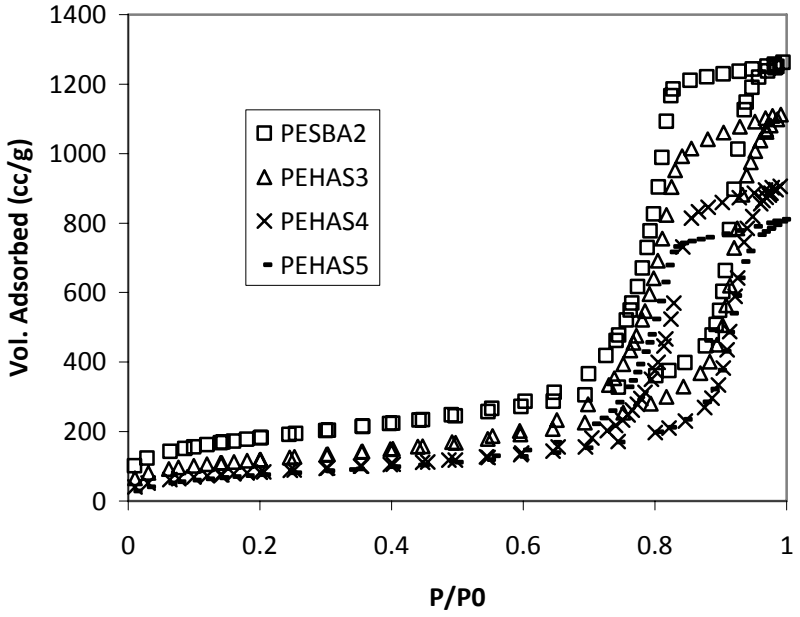

Figure B.2. N_2 physisorption isotherms at 77 K for PESBA2, PEHAS3, PEHAS4, and PEHAS5.

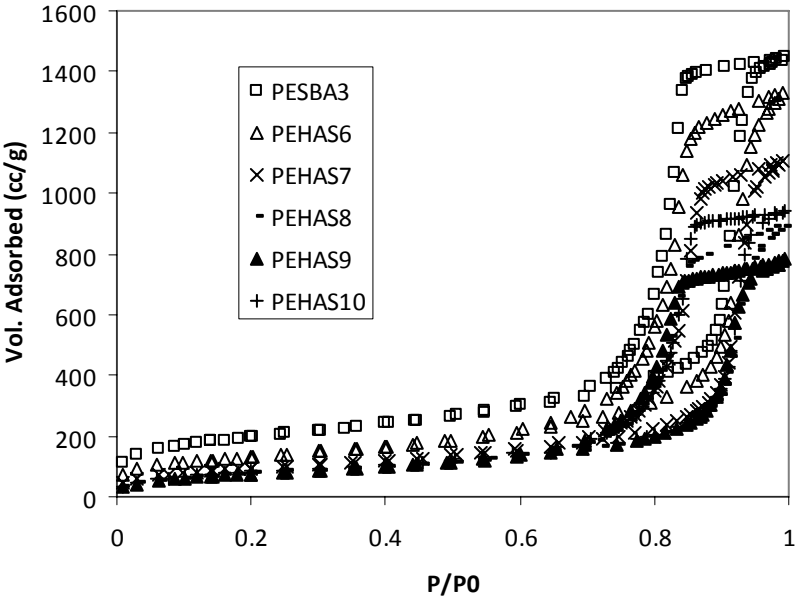

Figure B.3. N_2 physisorption isotherms at 77 K for PESBA3, PEHAS6, PEHAS7, PEHAS8, PEHAS9, and PEHAS10.

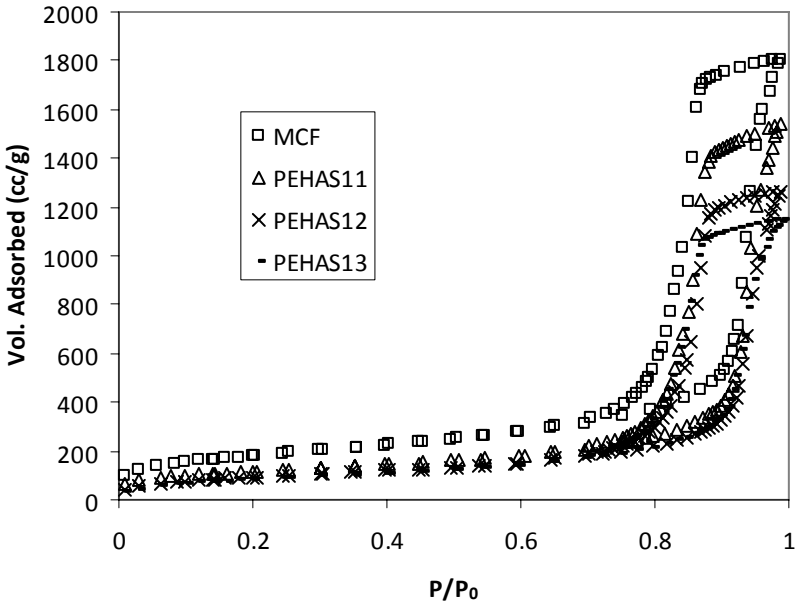

Figure B.4. N_2 physisorption isotherms at 77 K for MCF, PEHAS11, PEHAS12, and PEHAS13.

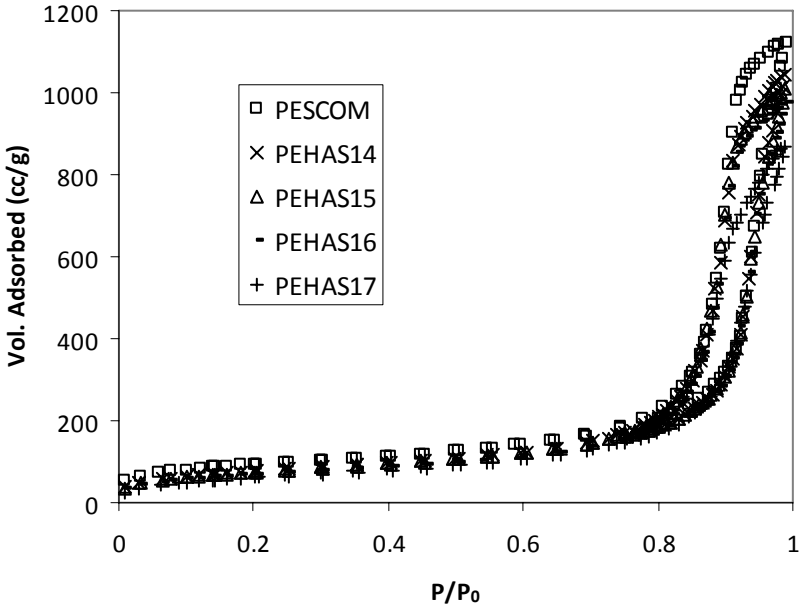

Figure B.5. N_2 physisorption isotherms at 77 K for PESCOM, PEHAS14, PEHAS15, PEHAS16, and PEHAS17.

B.2. SEM of Pore-expanded Silica Supports

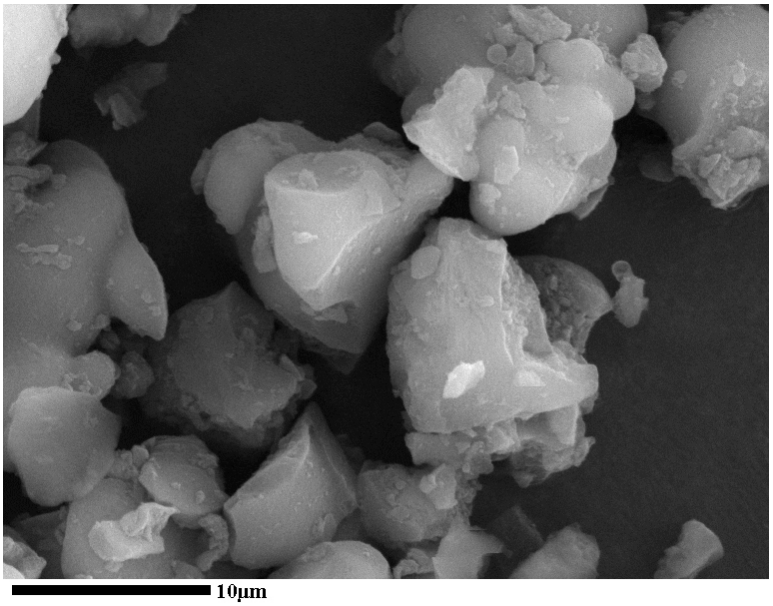

Figure B.6. SEM image of PESBA1.

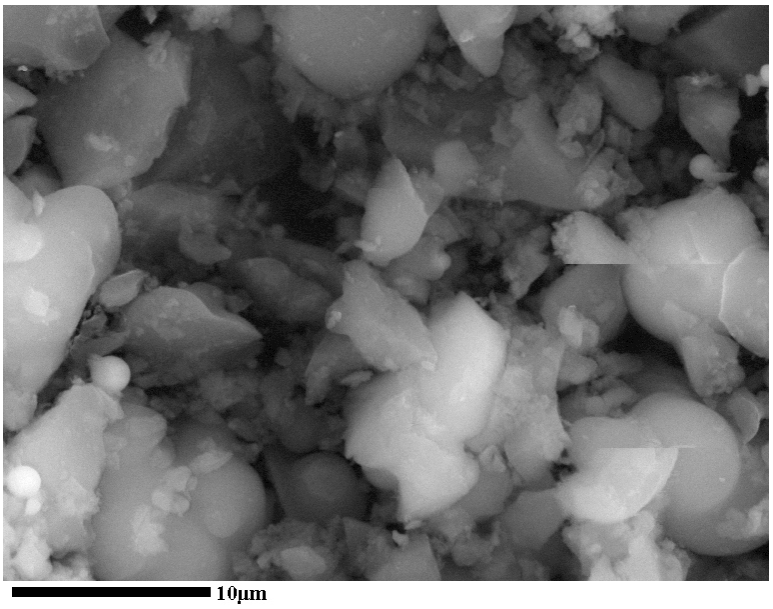

Figure B.7. SEM image of PESBA2.

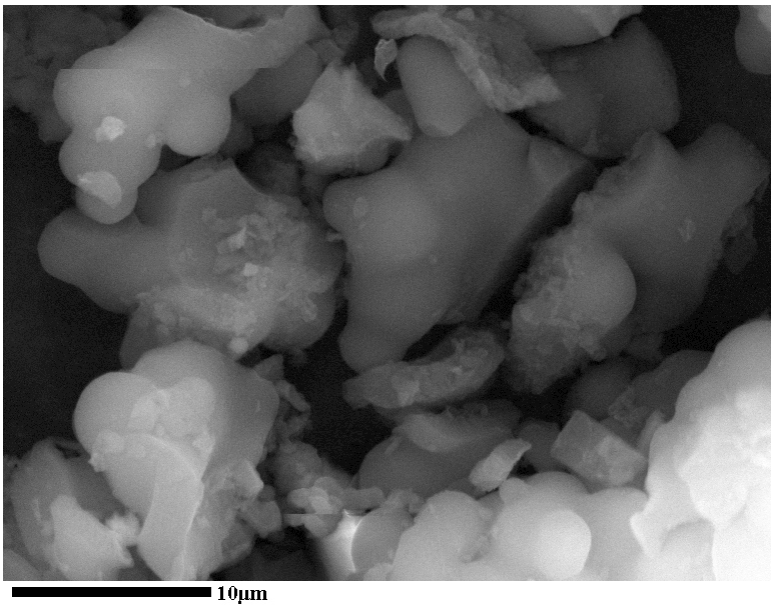

Figure B.8. SEM image of PESBA3.

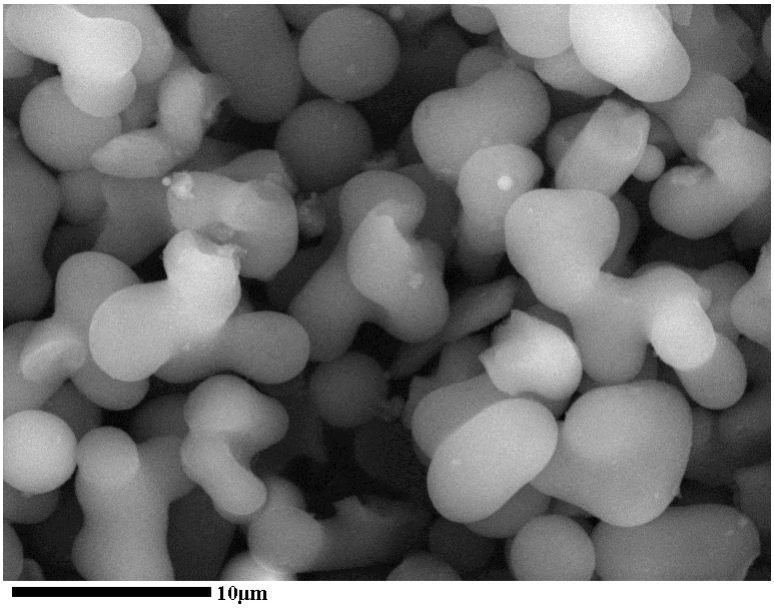

Figure B.9. SEM image of MCF.

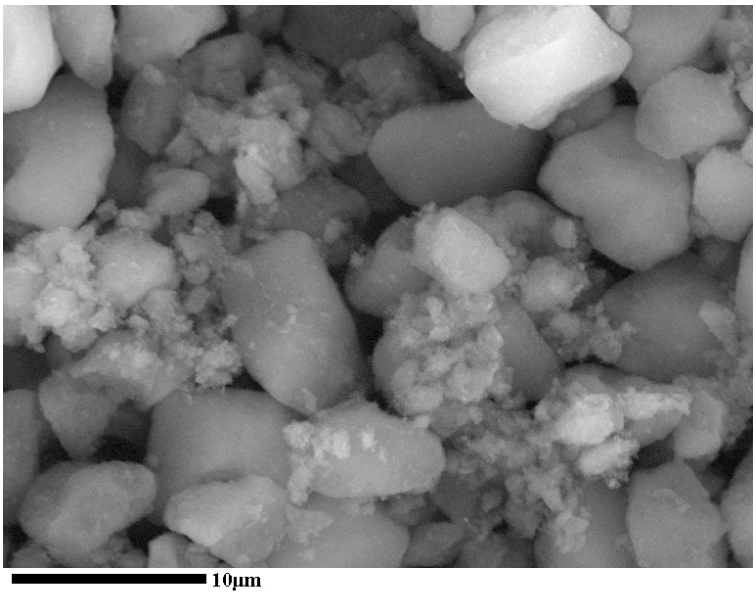

Figure B.10. SEM image of PESCOM.

B.3. FT-Raman Spectra of PEHAS Materials

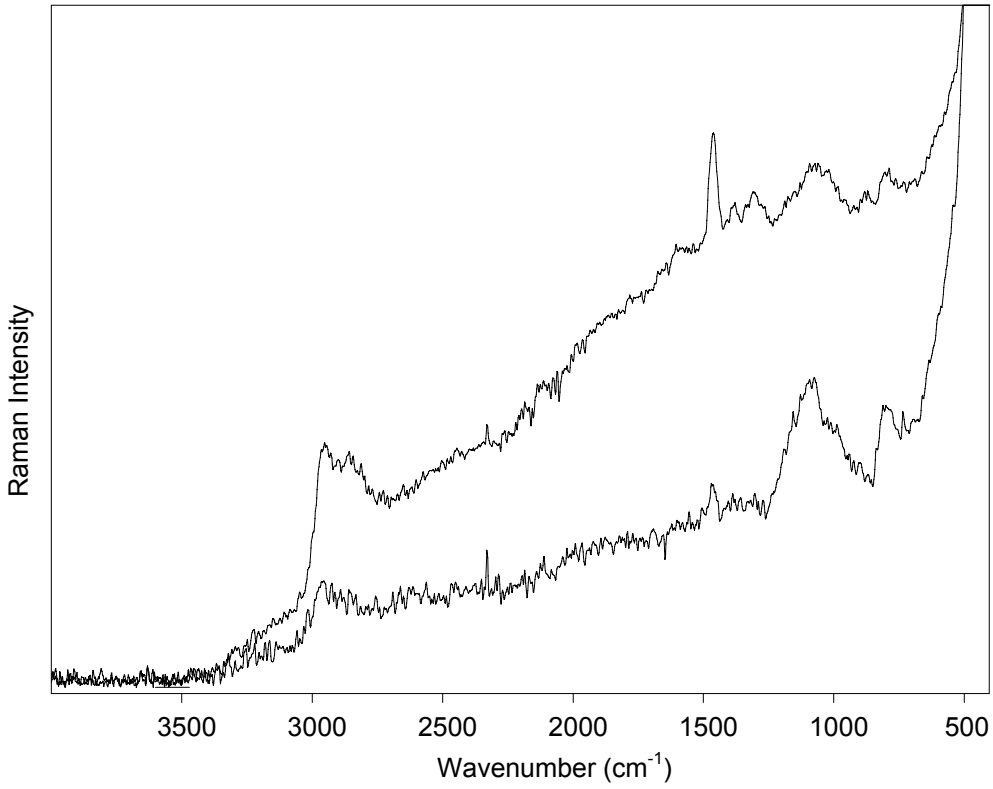

Figure B.11. FT-Raman spectra of PEHAS1 (bottom) and PEHAS2 (top).

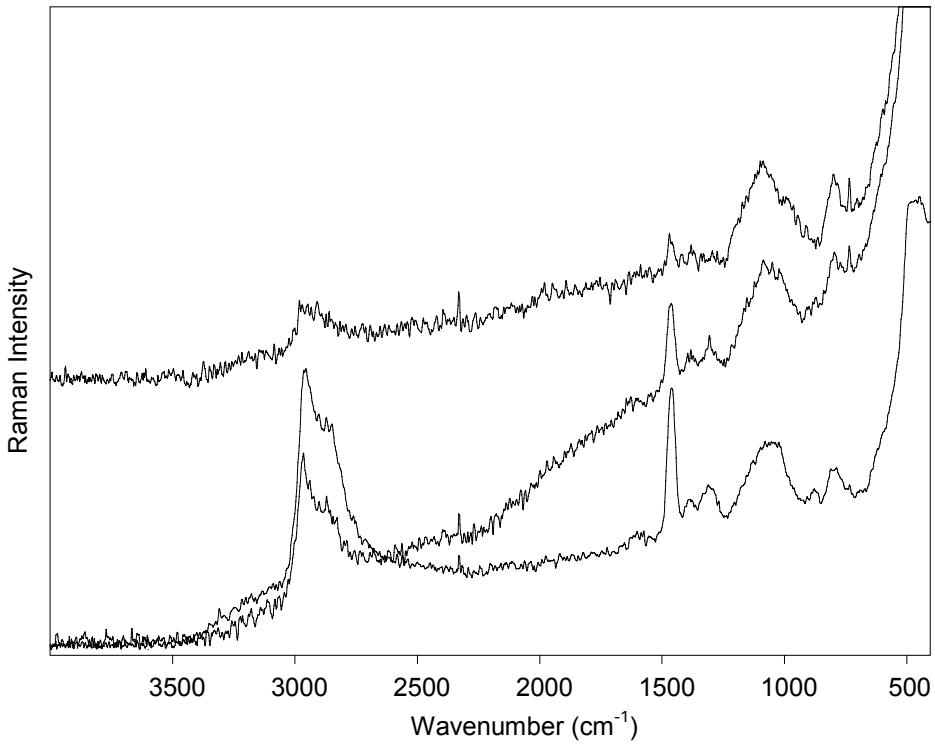

Figure B.12. FT-Raman spectra of PEHAS3, PEHAS4, and PEHAS5 (top to bottom).

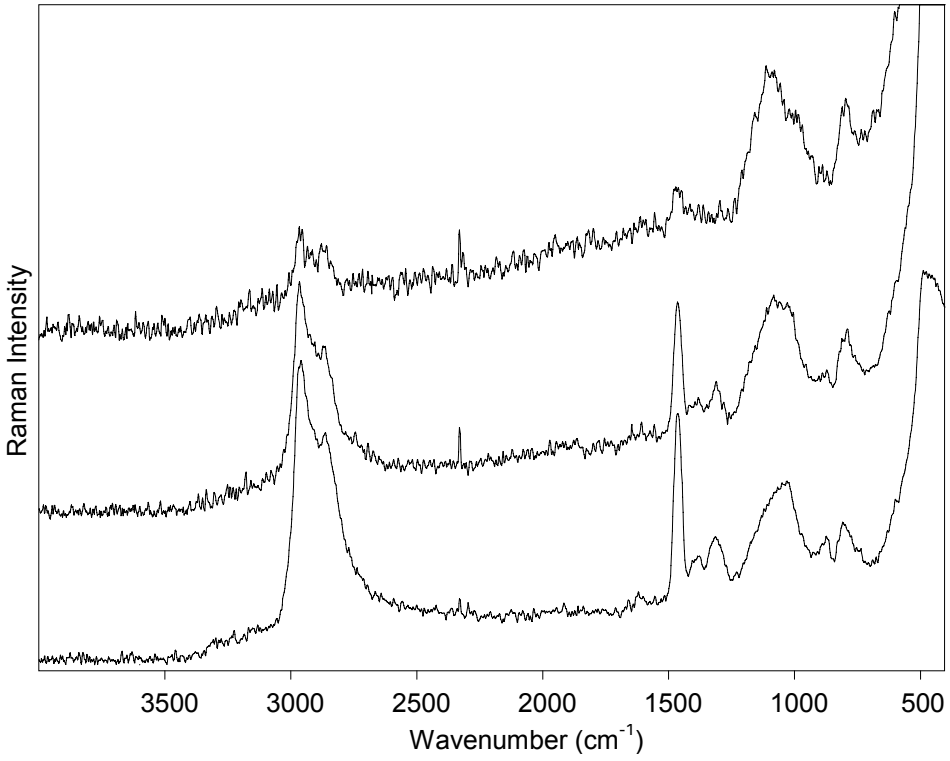

Figure B.13. FT-Raman spectra of PEHAS6, PEHAS7, and PEHAS8 (top to bottom).

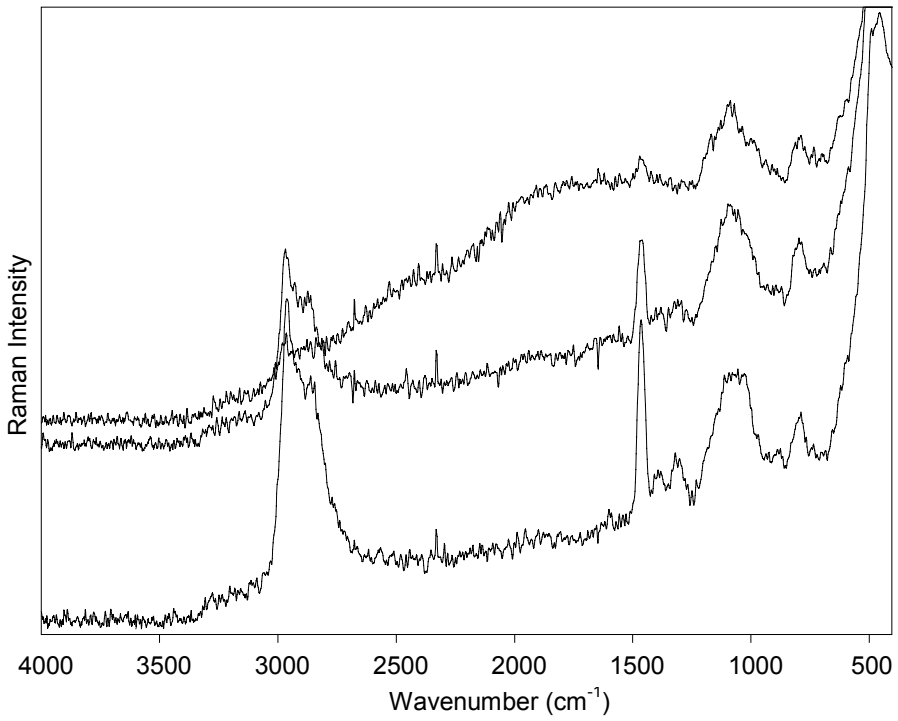

Figure B.14. FT-Raman spectra of PEHAS11, PEHAS12, and PEHAS13 (top to bottom).

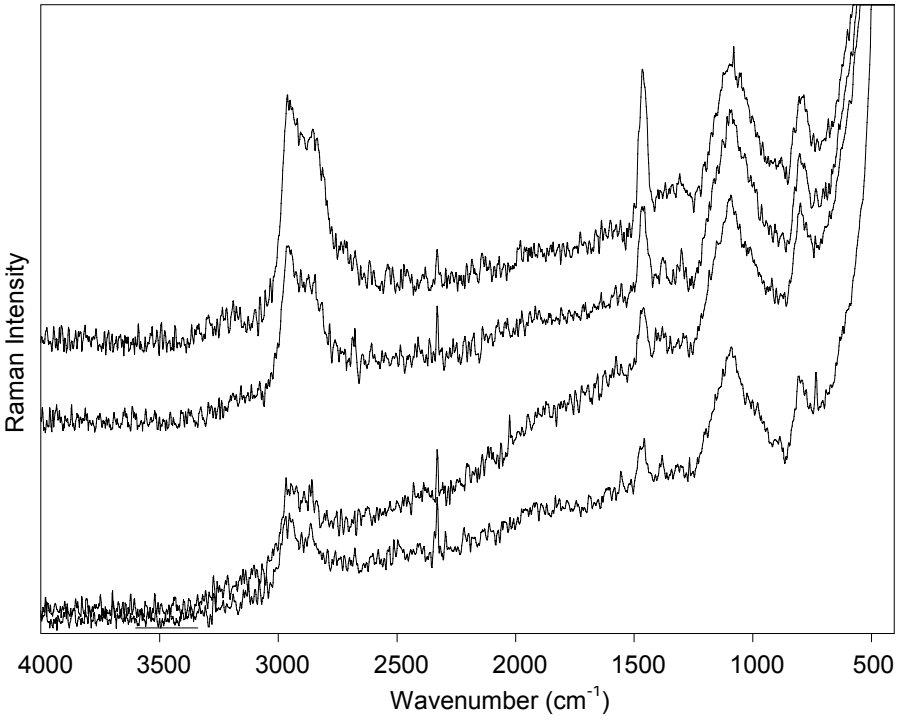

Figure B.15. FT-Raman spectra of PEHAS14, PEHAS15, PEHAS16, and PEHAS17 (bottom to top).

B.4. Physical Characteristics of HAS Adsorbents (Reported Elsewhere)*[86]*

Table B.1. Synthesis parameters, amine loadings, and pore characteristics of HAS adsorbents prepared from non-pore-expanded SBA-15 mesoporous silica.

Material	Silica Support	Aziridine to Silica Ratio	Amine Loading (mmol N/g)	Pore Dia. (nm)	Pore Vol. (cc/g)	Surf. Area (m^2/g)	Norm. Pore Vol.	Norm. Surf. Area
HAS1	SBA-15	0.13	2.29	6.4	0.66	579	0.96	0.72
HAS2	SBA-15	0.33	2.87	6.4	0.49	261	0.72	0.33
HAS3	SBA-15	0.53	3.69	6.0	0.47	278	0.68	0.35
HAS4	SBA-15	5.00	5.33	5.1	0.38	234	0.55	0.29
HAS5	SBA-15	1.33	7.33	4.9	0.24	119	0.34	0.15
HAS6	SBA-15	2.03	8.39	4.9	0.14	71	0.21	0.09
HAS7	SBA-15	2.65	9.88	4.9	0.11	45	0.16	0.06

B.5. Effect of Acetic Acid on PEHAS Materials

Three PEHAS materials were synthesized with different quantities of acetic acid as catalyst. The acetic acid was added to the reaction vessel immediately after the addition of aziridine. Table B.2 shows the amine loadings of the synthesized materials as well as the amine loading of the equivalent PEHAS material prepared with no acetic acid.

Table B.2. Synthesis parameters and amine loadings of PEHAS materials prepared by modified synthesis methods.

Sample	Silica Support	Aziridine to Silica Ratio	Acetic Acid (mL)	Amine Loading (mmol N/g)
PEHAS8	PESBA3	2.65	0	4.63
PEHAS18	PESBA3	2.65	0.1	5.04
PEHAS20	PESBA3	2.65	0.4	3.56
PEHAS19	PESBA3	2.65	0.8	5.17
PEHAS21	PESBA3	2.65[a]	5[a]	3.31
PEHAS22	PESBA3	3.00[b]	0	4.73
PEHAS23	PESBA3	5.30[c]	8 drops (~0.2 mL)	5.68

[a] The silica support was pretreated with a solution of 5 mL of acetic acid in toluene. The solid was filtered and washed once with toluene, then redispersed in fresh toluene and the reaction with aziridine was carried out without further addition of acetic acid.
[b] Aziridine added to reaction in 6 equal aliquots at 0, 30, 60, 85, 105, and 120 minutes after start of reaction.
[c] Aziridine and acetic acid were added to reaction in 2 equal aliquots at 0 and 12 hours after start of reaction.

B.6. Alternate Analysis of Adsorption Kinetics

The adsorption kinetics of PEHAS and HAS adsorbents were alternatively determined by calculating the amount of CO_2 adsorbed (Uptake2) when the CO_2 outlet concentration of the breakthrough curve reached 95% of the CO_2 feed concentration (Tables B.2 and B.3, respectively).

Figure B.16 shows the amount of CO_2 adsorbed by the PEHAS and HAS materials with different amine loadings. The amounts of CO_2 adsorbed by pore-expanded and non-pore-expanded HAS materials follow essentially the same linear trend with increasing amine loading. There is no clear trend in the amine efficiencies of the PEHAS adsorbents in terms of the different pore-expanded silica supports used in the synthesis, simply a slight decrease with increasing amine loading.

Figure B.17 shows the 98% uptake times for the PEHAS and HAS materials. All of the adsorbents, except for three HAS materials shown previously to have blocked pores, had nearly the same uptake times (from 9.6 to10.8 min), showing that near the end of breakthrough, the pore-expanded materials do not show the hindered diffusion effects seen in the highly loaded HAS materials with blocked pores.*[86]*

Table B.3. Amounts of CO_2 adsorbed, amine efficiencies, and uptake kinetics for PEHAS adsorbents. Completion of uptake measurement determined when outlet CO_2 concentration reached 95% of feed concentration (Uptake2).

Material	Silica Support	CO_2 Uptake2 (mmol CO_2/g)	Amine Efficiency (mol CO_2/mol N)	95% of Feed CO_2 Concentration	
				50% Uptake (min)	98% Uptake (min)
PEHAS1	PESBA1	0.29	0.12	2.3	10.1
PEHAS2	PESBA1	0.44	0.10	2.4	10.6
PEHAS3	PESBA2	0.34	0.13	2.3	10.1
PEHAS4	PESBA2	0.37	0.13	2.4	10.5
PEHAS5	PESBA2	0.45	0.09	2.5	10.3
PEHAS6	PESBA3	0.32	0.21	2.3	9.6
PEHAS7	PESBA3	0.48	0.12	2.4	9.9
PEHAS8	PESBA3	0.51	0.11	2.5	10.6
PEHAS11	MCF	0.25	0.14	2.3	9.9
PEHAS12	MCF	0.32	0.09	2.4	10.1
PEHAS13	MCF	0.56	0.12	2.5	10.2
PEHAS14	PESCOM	0.23	0.13	2.5	10.8
PEHAS15	PESCOM	0.20	0.11	2.3	9.9
PEHAS16	PESCOM	0.26	0.11	2.4	10.1
PEHAS17	PESCOM	0.30	0.10	2.5	10.5
class 2	SBA-15	0.62	0.17	2.6	11.3
class 1	MCM-41	0.36	0.06	2.5	11.4

Table B.4. Adsorption uptakes, amine efficiencies, and uptake kinetics for HAS adsorbents prepared from non-pore-expanded SBA-15 mesoporous silica (reported elsewhere*[86]*). Completion of uptake measurement determined when outlet CO_2 concentration reached 95% of feed concentration (Uptake2).

Material	Silica Support	CO_2 Uptake2 (mmol CO2/g)	Amine Efficiency (mol CO_2/mol N)	95% of Feed CO_2 Concentration	
				50% Uptake (min)	98% Uptake (min)
HAS1	SBA-15	0.08	0.04	2.3	9.9
HAS2	SBA-15	0.58	0.16	2.5	10.4
HAS3	SBA-15	0.56	0.20	2.4	9.9
HAS4	SBA-15	0.74	0.14	2.3	9.9
HAS5	SBA-15	0.92	0.13	2.4	11.0
HAS6	SBA-15	1.27	0.15	2.8	11.5
HAS7	SBA-15	1.36	0.14	2.9	12.7

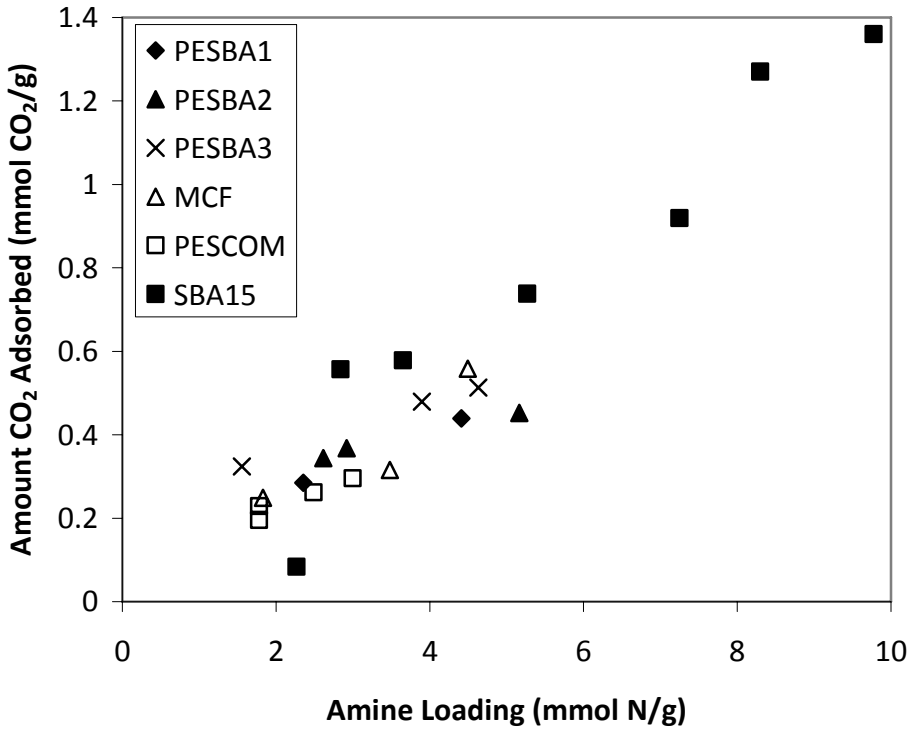

Figure B.16. Amounts of CO_2 adsorbed by PEHAS and HAS adsorbents prepared with different amine loadings. Completion of uptake measurement determined by the Uptake2 method. SBA-15 HAS materials were previously reported elsewhere.*[86]*

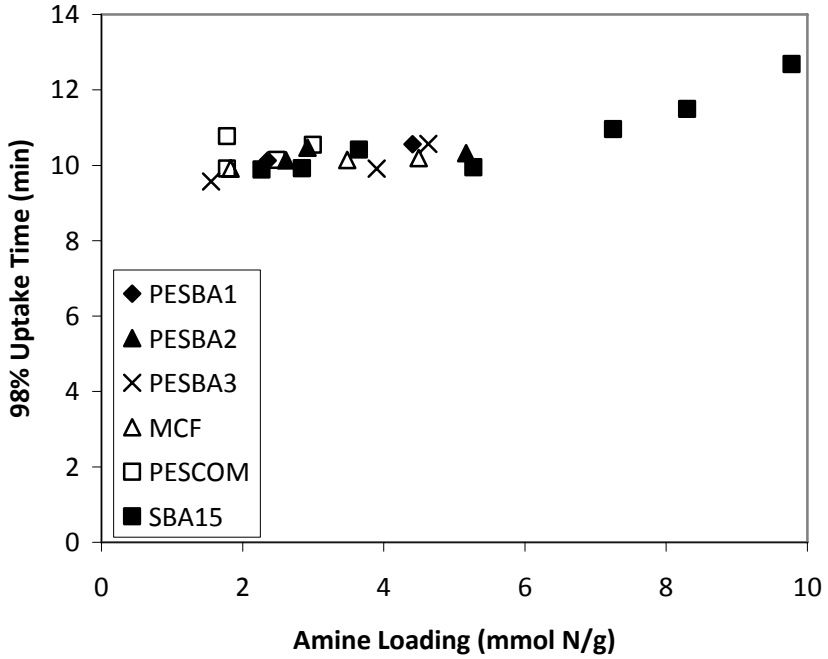

Figure B.17. 98% uptake times for PEHAS and HAS adsorbents with different amine loadings. Completion of adsorption measurement determined by the Uptake2 method. SBA-15 HAS materials were previously reported elsewhere.*[86]*

B.7. Adsorption Performance of HAS Adsorbents

Table B.5. Adsorption uptakes, amine efficiencies, and uptake kinetics for HAS adsorbents prepared from non-pore-expanded SBA-15 mesoporous silica (reported elsewhere*[86]*). Completion of uptake measurement determined when differential uptake was less than 0.0002 mmol CO_2/min.

Material	Silica Support	CO_2 Uptake (mmol CO2/g)	Amine Efficiency (mol CO_2/mol N)	mmol CO_2/min = 0.0002	
				50% Uptake (min)	98% Uptake (min)
HAS1	SBA-15	0.35	0.15	2.4	15.8
HAS2	SBA-15	0.84	0.23	2.6	15.2
HAS3	SBA-15	0.82	0.29	2.5	14.4
HAS4	SBA-15	1.26	0.24	2.6	37.4
HAS5	SBA-15	1.84	0.25	2.9	45.0
HAS6	SBA-15	2.08	0.25	3.2	48.0
HAS7	SBA-15	2.62	0.27	3.8	79.0

REFERENCES

[1] http://www.earthpolicy.org/Indicators/CO2/2008_data3.htm (accessed 10/1/2009).
[2] S. Solomon, D. Qin, M. Manning, Z. Chen, M. Marquis, K. B. Averyt, M. Tignor, H. L. Miller, Cambridge, United Kingdom and New York, NY, USA **2007**.
[3] X. L. Shan, N. J. Guan, X. Zeng, J. X. Chen, S. H. Xiang, *Chinese Journal of Catalysis* **2001**, *22*, 237.
[4] R. Steeneveldt, B. Berger, T. A. Torp, *Chemical Engineering Research & Design* **2006**, *84*, 739.
[5] J. Davison, *Energy* **2007**, *32*, 1163.
[6] J. W. Dijkstra, D. Jansen, *Energy* **2004**, *29*, 1249.
[7] P. V. Danckwerts, *Chem. Eng. Sci.* **1979**, *34*, 443.
[8] P. V. Danckwerts, M. M. Sharma, *The Chemical Engineer* **1966**, *CE*, 244.
[9] S. Bishnoi, G. T. Rochelle, *Chem. Eng. Sci.* **2000**, *55*, 5531.
[10] D. A. Glasscock, J. E. Critchfield, G. T. Rochelle, *Chem. Eng. Sci.* **1991**, *46*, 2829.
[11] G. F. Versteeg, L. A. J. Van Dijck, W. P. M. Van Swaaij, *Chem. Eng. Commun.* **1996**, *144*, 113.
[12] S. Sircar, *Ind. Eng. Chem. Res.* **2006**, *45*, 5435.
[13] R. T. Yang, *Gas Separation by Adsorption Processes*, Imperial College Press, London **1997**.
[14] R. Bredesen, T. A. Peters, in *Membrane Technology*, Vol. 2 (Eds: K.-V. Peinemann, S. Pereira Nunes), Wiley-VCH Verlag GmbH & Co. KGaA, Weinheim **2008**, 217.
[15] S. Choi, J. H. Drese, C. W. Jones, *ChemSusChem* **2009**, *2*, 796.
[16] F. Brandani, D. M. Ruthven, *Ind. Eng. Chem. Res.* **2004**, *43*, 8339.
[17] Y. X. Wang, Y. P. Zhou, C. M. Liu, L. Zhou, *Colloids and Surfaces a-Physicochemical and Engineering Aspects* **2008**, *322*, 14.
[18] R. Barker, *Journal of Applied Chemistry and Biotechnology* **1973**, *23*, 733.
[19] J. R. Hufton, S. Mayorga, S. Sircar, *Aiche J.* **1999**, *45*, 248.
[20] J. Ida, R. Xiong, Y. S. Lin, *Sep Purif Technol* **2004**, *36*, 41.
[21] R. A. Khatri, S. S. C. Chuang, Y. Soong, M. Gray, *Energy Fuels* **2006**, *20*, 1514.
[22] X. C. Xu, C. S. Song, B. G. Miller, A. W. Scaroni, *Fuel Processing Technology* **2005**, *86*, 1457.
[23] B. Arstad, H. Fjellvag, K. O. Kongshaug, O. Swang, R. Blom, *Adsorption* **2008**, *14*, 755.
[24] L. Pan, K. M. Adams, H. E. Hernandez, X. T. Wang, C. Zheng, Y. Hattori, K. Kaneko, *J. Am. Chem. Soc.* **2003**, *125*, 3062.
[25] A. R. Millward, O. M. Yaghi, *J. Am. Chem. Soc.* **2005**, *127*, 17998.
[26] J. C. Hicks, J. H. Drese, D. J. Fauth, M. L. Gray, G. G. Qi, C. W. Jones, *J. Am. Chem. Soc.* **2008**, *130*, 2902.
[27] V. V. Mahajani, J. B. Joshi, *Gas Separation & Purification* **1988**, *2*, 50.

[28] G. F. Versteeg, L. A. J. van Dijck, W. P. M. van Swaaij, *Chem. Eng. Commun.* **1996**, *144*, 113.
[29] P. D. Vaidya, E. Y. Kenig, *Chemical Engineering & Technology* **2007**, *30*, 1467.
[30] M. Caplow, *Journal of the American Chemical Society* **1968**, *90*, 6795.
[31] G. Sartori, D. W. Savage, *Industrial & Engineering Chemistry Fundamentals* **1983**, *22*, 239.
[32] T. L. Donaldson, Y. N. Nguyen, *Industrial & Engineering Chemistry Fundamentals* **1980**, *19*, 260.
[33] R. A. Khatri, S. S. C. Chuang, Y. Soong, M. Gray, *Industrial & Engineering Chemistry Research* **2005**, *44*, 3702.
[34] T. Tsuda, T. Fujiwara, Y. Taketani, T. Saegusa, *Chemistry Letters* **1992**, 2161.
[35] T. Tsuda, T. Fujiwara, *Journal of the Chemical Society-Chemical Communications* **1992**, 1659.
[36] O. B. Leal, Carmelo; Ovalles, Cesar; Garcia, Juan Jose; Espidel, Youssef, *Inorganica Chimica Acta* **1995**, *240*, 183.
[37] X. C. Xu, C. S. Song, J. M. Andresen, B. G. Miller, A. W. Scaroni, *Energy & Fuels* **2002**, *16*, 1463.
[38] A. von Harpe, H. Petersen, Y. X. Li, T. Kissel, *Journal of Controlled Release* **2000**, *69*, 309.
[39] X. C. Xu, C. S. Song, B. G. Miller, A. W. Scaroni, *Ind. Eng. Chem. Res.* **2005**, *44*, 8113.
[40] X. C. Xu, C. S. Song, J. M. Andresen, B. G. Miller, A. W. Scaroni, *Microporous and Mesoporous Materials* **2003**, *62*, 29.
[41] W. J. Son, J. S. Choi, W. S. Ahn, *Microporous Mesoporous Mater.* **2008**, *113*, 31.
[42] T. C. Drage, A. Arenillas, K. M. Smith, C. E. Snape, *Microporous Mesoporous Mater.* **2008**, *116*, 504.
[43] M. B. Yue, Y. Chun, Y. Cao, X. Dong, J. H. Zhu, *Advanced Functional Materials* **2006**, *16*, 1717.
[44] M. B. Yue, L. B. Sun, Y. Cao, Y. Wang, Z. J. Wang, J. H. Zhu, *Chemistry-a European Journal* **2008**, *14*, 3442.
[45] M. B. Yue, L. B. Sun, Y. Cao, Z. J. Wang, Y. Wang, Q. Yu, J. H. Zhu, *Microporous and Mesoporous Materials* **2008**, *114*, 74.
[46] R. S. Franchi, P. J. E. Harlick, A. Sayari, *Ind. Eng. Chem. Res.* **2005**, *44*, 8007.
[47] G. J. D. Soler-illia, C. Sanchez, B. Lebeau, J. Patarin, *Chemical Reviews* **2002**, *102*, 4093.
[48] S. Satyapal, T. Filburn, J. Trela, J. Strange, *Energy & Fuels* **2001**, *15*, 250.
[49] M. B. Yue, L. B. Sun, Y. Cao, Y. Wang, Z. J. Wang, J. H. Zhu, *Chem.--Eur. J.* **2008**, *14*, 3442.
[50] C. J. Brinker, G. W. Scherer, *Sol-Gel Science: The Physics and Chemistry of Sol-Gel Processing*, Academic Press, Inc., San Diego **1990**.
[51] M. L. Gray, Y. Soong, K. J. Champagne, H. Pennline, J. Baltrus, *International Journal of Environmental Technology and Management* **2004**, *4*, 82.
[52] M. L. Gray, Y. Soong, K. J. Champagne, H. Pennline, J. P. Baltrus, R. W. Stevens, R. Khatri, S. S. C. Chuang, T. Filburn, *Fuel Processing Technology* **2005**, *86*, 1449.

[53] N. Hiyoshi, K. Yogo, T. Yashima, *Microporous and Mesoporous Materials* **2005**, *84*, 357.
[54] R. Serna-Guerrero, E. Da'na, A. Sayari, *Industrial & Engineering Chemistry Research* **2008**.
[55] G. P. Knowles, S. W. Delaney, A. L. Chaffee, *Industrial & Engineering Chemistry Research* **2006**, *45*, 2626.
[56] G. P. Knowles, J. V. Graham, S. W. Delaney, A. L. Chaffee, *Fuel Processing Technology* **2005**, *86*, 1435.
[57] H. Y. Huang, R. T. Yang, D. Chinn, C. L. Munson, *Industrial & Engineering Chemistry Research* **2003**, *42*, 2427.
[58] A. C. C. Chang, S. S. C. Chuang, M. Gray, Y. Soong, *Energy & Fuels* **2003**, *17*, 468.
[59] N. Hiyoshi, K. Yogo, T. Yashima, *Chemistry Letters* **2004**, *33*, 510.
[60] V. Zelenak, D. Halamova, L. Gaberova, E. Bloch, P. Llewellyn, *Microporous Mesoporous Mater.* **2008**, *116*, 358.
[61] S. Kim, J. Ida, V. V. Guliants, J. Y. S. Lin, *Journal of Physical Chemistry B* **2005**, *109*, 6287.
[62] C. Knofel, J. Descarpentries, A. Benzaouia, V. Zelenak, S. Mornet, P. L. Llewellyn, V. Hornebecq, *Microporous and Mesoporous Materials* **2007**, *99*, 79.
[63] J. Wei, J. Shi, H. Pan, W. Zhao, Q. Ye, Y. Shi, *Microporous and Mesoporous Materials* **2008**, *116*, 394.
[64] F. Zheng, D. N. Tran, B. J. Busche, G. E. Fryxell, R. S. Addleman, T. S. Zemanian, C. L. Aardahl, *Industrial & Engineering Chemistry Research* **2005**, *44*, 3099.
[65] P. J. E. Harlick, A. Sayari, *Industrial & Engineering Chemistry Research* **2007**, *46*, 446.
[66] P. J. E. Harlick, A. Sayari, *Industrial & Engineering Chemistry Research* **2006**, *45*, 3248.
[67] P. Van der Voort, I. Gillis-D'Hamers, K. C. Vracken, E. F. Vansant, *J. Chem. Soc. Faraday Trans.* **1991**, *87*, 3899.
[68] Z. Liang, B. Fadhel, C. J. Schneider, A. L. Chaffee, *Microporous and Mesoporous Materials* **2008**, *111*, 536.
[69] E. J. Acosta, C. S. Carr, E. E. Simanek, D. F. Shantz, *Adv. Mater.* **2004**, *16*, 985.
[70] N. Hiyoshi, K. Yogo, T. Yashima, *Journal of the Japan Petroleum Institute* **2005**, *48*, 29.
[71] R. Serna-Guerrero, E. Da'na, A. Sayari, *Ind. Eng. Chem. Res.* **2008**, *47*, 9406.
[72] Y. D. Tang, K. Landskron, *Journal of Physical Chemistry C* **2010**, *114*, 2494.
[73] A. Kohl, R. Nielsen, *Gas Purification, 5th ed.*, Gulf Publishing Co., Houston **1997**.
[74] E. Tzimas, A. Mercier, C. C. Cormos, S. D. Peteves, *Energy Policy* **2007**, *35*, 3991.
[75] M. G. Plaza, C. Pevida, A. Arenillas, F. Rubiera, J. J. Pis, *Fuel* **2007**, *86*, 2204.
[76] E. P. Dillon, C. A. Crouse, A. R. Barron, *Acs Nano* **2008**, *2*, 156.
[77] M. L. Gray, Y. Soong, K. J. Champagne, J. Baltrus, R. W. Stevens, P. Toochinda, S. S. C. Chuang, *Separation and Purification Technology* **2004**, *35*, 31.
[78] M. J. Schladt, T. P. Filburn, J. J. Helble, *Industrial & Engineering Chemistry Research* **2007**, *46*, 1590.

[79] Z. W. Chen, M. Chanda, *Journal of Polymer Materials* **2002**, *19*, 381.
[80] P. Y. Li, B. Q. Ge, S. J. Zhang, S. X. Chen, Q. K. Zhang, Y. N. Zhao, *Langmuir* **2008**, *24*, 6567.
[81] A. Diaf, J. L. Garcia, E. J. Beckman, *Journal of Applied Polymer Science* **1994**, *53*, 857.
[82] A. Diaf, E. J. Beckman, *Reactive & Functional Polymers* **1995**, *27*, 45.
[83] B. Ochiai, K. Yokota, A. Fujii, D. Nagai, T. Endo, *Macromolecules* **2008**, *41*, 1229.
[84] T. C. Drage, A. Arenillas, K. M. Smith, C. Pevida, S. Piippo, C. E. Snape, *Fuel* **2007**, *86*, 22.
[85] M. G. Plaza, C. Pevida, A. Arenillas, F. Rubiera, J. J. Pis, "CO2 capture by adsorption with nitrogen enriched carbons", **2007**.
[86] J. H. Drese, S. Choi, R. P. Lively, W. J. Koros, D. J. Fauth, M. L. Gray, C. W. Jones, *Adv. Funct. Mater.* **2009**, *19*, 3821.
[87] H. J. Kim, J. H. Moon, J. W. Park, *Journal of Colloid and Interface Science* **2000**, *227*, 247.
[88] L. Bergman, J. Rosenholm, A. B. Ost, A. Duchanoy, P. Kankaanpaa, J. Heino, M. Linden, *Journal of Nanomaterials* **2008**.
[89] J. M. Rosenholm, A. Duchanoy, M. Linden, *Chemistry of Materials* **2008**, *20*, 1126.
[90] J. M. Rosenholm, M. Linden, *Chemistry of Materials* **2007**, *19*, 5023.
[91] J. M. Rosenholm, M. Linden, *Journal of Controlled Release* **2008**, *128*, 157.
[92] J. M. Rosenholm, A. Penninkangas, M. Linden, *Chemical Communications* **2006**, 3909.
[93] J. S. Beck, J. C. Vartuli, W. J. Roth, M. E. Leonowicz, C. T. Kresge, K. D. Schmitt, C. T. W. Chu, D. H. Olson, E. W. Sheppard, S. B. Mccullen, J. B. Higgins, J. L. Schlenker, *Journal of the American Chemical Society* **1992**, *114*, 10834.
[94] G.-J. Kim, J.-H. Shin, *Tetrahedron Letters* **1999**, *40*, 6827.
[95] W. W. Lukens, P. Schmidt-Winkel, D. Y. Zhao, J. L. Feng, G. D. Stucky, *Langmuir* **1999**, *15*, 5403.
[96] E. P. Barrett, L. G. Joyner, P. P. Halenda, *J. Am. Chem. Soc.* **1951**, *73*, 373.
[97] J. C. P. Broekhoff, J. H. de Boer, *Journal of Catalysis* **1967**, *9*, 8.
[98] T. L. Hill, *Adv Catal* **1952**, *4*, 211.
[99] G. Halsey, *J Chem Phys* **1948**, *16*, 931.
[100] G. D. Halsey, *Adv Catal* **1952**, *4*, 259.
[101] B. S. Tian, C. Yang, *Journal of Physical Chemistry C* **2009**, *113*, 4925.
[102] W. G. Barb, *Journal of the Chemical Society* **1955**, 2564.
[103] D. D. Do, *Adsorption Analysis: Equilibria and Kinetics*, Vol. 2, Imperial College Press, London **1998**.
[104] T. L. Donaldson, J. A. Quinn, *Proceedings of the National Academy of Sciences of the United States of America* **1974**, *71*, 4995.
[105] R. P. Lively, R. R. Chance, J. H. Drese, C. W. Jones, W. J. Koros, *under review* **2009**.
[106] J. C. Hicks, R. Dabestani, A. C. Buchanan, C. W. Jones, *Chem. Mater.* **2006**, *18*, 5022.
[107] J. C. Hicks, C. W. Jones, *Langmuir* **2006**, *22*, 2676.

[108] D. Y. Zhao, Q. S. Huo, J. L. Feng, B. F. Chmelka, G. D. Stucky, *Journal of the American Chemical Society* **1998**, *120*, 6024.
[109] T. S. Pierre, M. Geckle, *Journal of Macromolecular Science-Chemistry* **1985**, *A22*, 877.
[110] J. H. Drese, S. Choi, S. A. Didas, P. Bollini, M. L. Gray, C. W. Jones, **2010**, *manuscript in preparation*.
[111] D. M. Ford, E. E. Simanek, D. F. Shantz, *Nanotechnology* **2005**, *16*, S458.
[112] J. D. Lunn, D. F. Shantz, *Chem. Mater.* **2009**, *21*, 3638.
[113] J. C. Vartuli, K. D. Schmitt, C. T. Kresge, W. J. Roth, M. E. Leonowicz, S. B. Mccullen, S. D. Hellring, J. S. Beck, J. L. Schlenker, D. H. Olson, E. W. Sheppard, *Chem. Mater.* **1994**, *6*, 2317.
[114] P. Schmidt-Winkel, W. W. Lukens, D. Y. Zhao, P. D. Yang, B. F. Chmelka, G. D. Stucky, *J. Am. Chem. Soc.* **1999**, *121*, 254.
[115] T. W. Kim, F. Kleitz, B. Paul, R. Ryoo, *J. Am. Chem. Soc.* **2005**, *127*, 7601.
[116] W. Li, S. Choi, J. Drese, M. Hornbostel, G. Krishnan, P. Eisenberger, C. Jones, *ChemSusChem* **2010**, *3*, 899.
[117] E. W. Ping, R. Wallace, J. Pierson, T. F. Fuller, C. W. Jones, *Microporous Mesoporous Mater.* **2010**, *132*, 174.
[118] Y. Han, S. S. Lee, J. Y. Ying, *Chem. Mater.* **2007**, *19*, 2292.
[119] A. Katiyar, L. Ji, P. Smirniotis, N. G. Pinto, *J. Chromatogr., A* **2005**, *1069*, 119.
[120] www.eia.doe.gov.
[121] K. S. Lackner, H. Ziock, P. Grimes, "Carbon dioxide extraction from air: Is it an option?", presented at *The 24th International Conference on Coal Utilization & Fuel Systems*, Clearwater, Florida, **1999**.
[122] K. S. Lackner, P. Grimes, H. Ziock, "Carbon dioxide extraction from air?", presented at *Los Alamos National Laboratory, LAUR-99-5113*, Los Alamos, NM, 1999, **1999**.
[123] D. W. Keith, M. Ha-Duong, J. K. Stolaroff, *Clim. Change* **2006**, *74*, 17.
[124] J. B. Tebe, B. F. Dodge, *Trans. Am. Inst. Chem. Eng.* **1943**, *39*, 255.
[125] D. W. Keith, *Science* **2009**, *325*, 1654.
[126] M. Steinberg, V. D. Dang, *Energy Conversion* **1977**, *17*, 97.
[127] V. D. Dang, M. Steinberg, *Energy Conversion* **1977**, *17*, 133.
[128] S. Stucki, A. Schuler, M. Constantinescu, *Int. J. Hydrog. Energy* **1995**, *20*, 653.
[129] F. S. Zeman, K. S. Lackner, *World Res. Rev.* **2004**, *16*, 157.
[130] V. Nikulshina, N. Ayesa, M. E. Galvez, A. Steinfeld, *Chem. Eng. J.* **2008**, *140*, 62.
[131] V. Nikulshina, C. Gebald, A. Steinfeld, *Chem. Eng. J.* **2009**, *146*, 244.
[132] V. Nikulshina, D. Hirsch, M. Mazzotti, A. Steinfeld, *Energy* **2006**, *31*, 1715.
[133] R. Baciocchi, G. Storti, M. Mazzotti, *Chem. Eng. Process.* **2006**, *45*, 1047.
[134] F. Zeman, *Environmental Science & Technology* **2007**, *41*, 7558.
[135] F. Zeman, *Aiche J.* **2008**, *54*, 1396.
[136] J. K. Stolaroff, D. W. Keith, G. V. Lowry, *Environmental Science & Technology* **2008**, *42*, 2728.
[137] K. S. Lackner, S. Brennan, *Clim. Change* **2009**, *96*, 357.
[138] K. S. Lackner, *Eur. Phys. J. Spec. Top.* **2009**, *176*, 93.
[139] R. A. Pielke, *Environ. Sci. Policy* **2009**, *12*, 216.

[140] M. Mahmoudkhani, D. W. Keith, *Int. J. Greenhouse Gas Control* **2009**, *3*, 376.
[141] F. S. Zeman, D. W. Keith, *Philos. Trans. R. Soc. London, Ser. A* **2008**, *366*, 3901.
[142] Y. Belmabkhout, R. Serna-Guerrero, A. Sayari, *Chem. Eng. Sci.* **2010**, *65*, 3695.
[143] P. M. Eisenberger, R. W. Cohen, G. Chichilnisky, N. M. Eisenberger, R. R. Chance, C. W. Jones, *Energy Environ.* **2009**, *20*, 973.
[144] S. Choi, J. H. Drese, P. M. Eisenberger, C. W. Jones, "A new paradigm of anthropogenic CO_2 reduction: Adsorptive fixation of CO_2 from the ambient air as a carbon negative technology", presented at *AIChE Annual Meeting*, Nashville, Tennessee, **2009**.
[145] A. Iwan, H. Stephenson, W. C. Ketchie, A. A. Lapkin, *Chem. Eng. J.* **2009**, *146*, 249.
[146] Y. Belmabkhout, R. Serna-Guerrero, A. Sayari, *Ind. Eng. Chem. Res.* **2010**, *49*, 359.
[147] J. H. Drese, S. Choi, R. Lively, M. Gray, D. J. Fauth, C. W. Jones, *Adv. Funct. Mater.* **2009**, *19*, 3821.
[148] D. Y. Zhao, J. L. Feng, Q. S. Huo, N. Melosh, G. H. Fredrickson, B. F. Chmelka, G. D. Stucky, *Science* **1998**, *279*, 548.
[149] D. Margolese, J. A. Melero, S. C. Christiansen, B. F. Chmelka, G. D. Stucky, *Chem. Mat.* **2000**, *12*, 2448.
[150] L. Li, J. Shi, J. Yan, X. Zhao, H. Chen, *Appl. Catal., A* **2004**, *263*, 213.
[151] Y. Belmabkhout, A. Sayari, *Adsorption* **2009**, *15*, 318.
[152] J. H. C. Drese, S.; Didas, S. A.; Bollini, P.; Gray, M. L.; Jones, C. W.;, *in prep.* **2010**.
[153] A. Sayari, Y. Belmabkhout, *J. Am. Chem. Soc.*, *132*, 6312.
[154] W. Li, S. Choi, J. H. Drese, M. Hornbostel, G. Krishnan, P. M. Eisenberger, C. W. Jones, *ChemSusChem* **2010**, *in press*, DOI: 10.1002/cssc.201000131.
[155] M. Zinic, S. Alihodzic, V. Skaric, *J. Chem. Soc.-Perkin Trans. 1* **1993**, 21.
[156] J. A. Deyrup, *Chemistry of Heterocyclic Compounds-a Series of Monographs* **1983**, *42*, 1.
[157] Culberts.Bm, S. Dietz, *Canadian Journal of Chemistry* **1968**, *46*, 3399.
[158] H. L. Baranska, Anna; Terpinski, Jacek;, *Laser Raman Spectroscopy: analytical applications*, Ellis Horwood Limited, Chichester, UK **1987**.
[159] T. Shono, Y. Matsumura, K. Uchida, K. Tsubata, A. Makino, *J Org Chem* **1984**, *49*, 300.
[160] R. H. Smith, B. D. Wladkowski, J. E. Taylor, E. J. Thompson, B. Pruski, J. R. Klose, A. W. Andrews, C. J. Michejda, *J Org Chem* **1993**, *58*, 2097.